Mechanisms Of Alpha]-synuclein-induced Neurodegenertaion In Parkinson's Disease And Stroke

2011

Cherine Belal
University of Central Florida

MECHANISMS OF α-SYNUCLEIN-INDUCED NEURODEGENERATION IN PARKINSON'S DISEASE AND STROKE

by

CHERINE BELAL
B.S. University of Central Florida, 2005
M.S. University of Central Florida, 2009

A dissertation submitted in partial fulfillment of the requirements
for the degree of Doctor of Philosophy in Biomedical Sciences
in the Burnett School of Biomedical Sciences
in the College of Graduate Studies
at the University of Central Florida
Orlando, Florida

Fall Term
2011

Major Professor: Sic L. Chan

ABSTRACT

Parkinson's disease (PD) is a debilitating neurodegenerative disorder affecting one million Americans. Despite its social and economic impact, the pathological cascades that lead to neuron dysfunction and degeneration in PD are poorly understood. Endoplasmic reticulum (ER) stress has been implicated as an initiator or contributing factor in neurodegenerative diseases including PD. The ER is an organelle central to protein folding and intracellular Ca^{2+} homeostasis. Perturbations of these functions result in ER stress and upregulation of ER stress proteins, of which some have been implicated in counteracting ER stress-induced cell death. The mechanisms that lead to ER stress and how ER stress proteins contribute to the degenerative cascades remain unclear but their understanding is critical to devising effective therapies for PD. Both the accumulation of mutant α-synuclein (αSyn), which causes an inherited form of PD, and the inhibition of mitochondrial complex I function by PD-inducing neurotoxin lead to ER stress. The critical involvement of ER stress in experimental models of PD supports its potential relevance to PD pathogenesis and led us to test the hypothesis whether the homocysteine-inducible ER protein (Herp), an ubiquitin-like domain (UBD) containing ER-resident protein, can counteract mutant αSyn- and neurotoxin- induced pathological cascades.

In the first part of my study I showed that knockdown of Herp aggravates ER stress-mediated cell death induced by PD-linked mutant αSyn. Functionally, Herp plays

a role in maintaining ER homeostasis by facilitating proteasome-mediated degradation of ER-resident Ca^{2+} release channels in a neuronal-like cell line expressing the mutant A53T-αSyn. Deletion of UBD or pharmacological inhibition of the proteasomes abolishes the Herp-mediated stabilization of ER Ca^{2+} homeostasis. Furthermore, knockdown or pharmacological inhibition of ER Ca^{2+} release channels ameliorates ER stress suggesting that impaired homeostatic regulation of Ca^{2+} channels promotes a protracted ER stress with the consequent activation of ER stress-associated cell death pathways. Interestingly, sustained upregulation of ER stress markers and aberrant accumulation of ER Ca^{2+} release channels were detected in transgenic mutant A53T-αSyn mice. These data establish a causative link between impaired ER Ca^{2+} homeostasis and chronic ER stress in the degenerative cascades induced by mutant A53T-αSyn and suggest that Herp is essential for the resolution of ER stress through maintenance of ER Ca^{2+} homeostasis.

Because oxidants and mitochondria-derived free radicals can target ER-based Ca^{2+} regulatory proteins and cause uncontrolled Ca^{2+} release that may contribute to protracted ER stress resulting in cell death, I next determined the impact of the PD causing neurotoxin, 1-methyl-4-phenyl-1,2,3,6-tetrahydropyridine (MPTP), the precursor of 1-methyl-4-phenylpyridinium (MPP^+) on ER functions. I demonstrated that knockdown of Herp renders dopaminergic cells vulnerable to MPP^+-induced toxicity by a mechanism involving upregulation of CCAAT/enhancer binding protein homologous protein (CHOP) and depletion of the ER Ca^{2+} store. Conversely, ectopic expression of Herp confers protection by blocking MPP^+ -induced CHOP upregulation, ER Ca^{2+} store depletion and mitochondrial Ca^{2+} accumulation in a manner dependent on a functional

ubiquitin-proteasomal protein degradation pathway. Deletion of the UBD or treatment with a proteasomal inhibitor abolished the central function of Herp in ER Ca^{2+} homeostasis. Collectively, our findings suggest that approaches that aim to increase Herp levels or its ER Ca^{2+}-stabilizing action may prevent or ameliorate neuronal loss in PD.

Though abnormal protein aggregates are characteristic features of the slowly progressive neurodegenerative disorders, they are also found in acute pathological states such as cerebral ischemia. The role of protein aggregation in neuronal pathology after brain ischemia is not clear. In the last part of my work, I show that transient focal ischemia induces the continuous accumulation of insoluble αSyn and DJ-1, two proteins linked to early-onset PD, in vulnerable neurons from the onset of reperfusion until delayed neuronal death. Double immunocytochemical analysis reveals that αSyn and DJ-1 are co-localized in inclusion-like structures in the vulnerable neurons of the lesioned cortices suggesting that DJ-1 is recruited into the αSyn-containing inclusions and thereby precludes this neuroprotective protein from exercising its anti-oxidant and chaperone-like activities. Supporting this notion, knockdown of DJ-1 promotes αSyn insolubility and renders neurons vulnerable to an ischemic insult whereas ectopic expression of DJ-1 ameliorates αSyn -induced degenerative cascades and reverses ischemic neuronal injury. Furthermore, mice deficient in αSyn exhibit significantly smaller infarcts and improved behavioral recovery after ischemia compared to non-transgenic mice. Ablation of αSyn ameliorates the accumulation of insoluble DJ-1 and the ensuing oxidative damage following an ischemic insult. Taken together, our data show that aberrant accumulation of αSyn plays a precipitating role in ischemic neuronal

injury and suggest that PD-causing mutations in αSyn and DJ-1 can worsen ischemic brain damage.

In conclusion, these studies provide insights into the molecular cascade of αSyn-induced degeneration and may uncover novel therapeutic strategies for PD and stroke.

To my beloved Grandfather, Mohamed Kehal (1927–2003), whose wisdom and guidance have been the source of my strength…

ACKNOWLEDGMENTS

I would like to convey my sincere respect and gratitude to Dr. Sic L. Chan: “Thank you BOSS, you have been an excellent mentor and guide for me!” So many special thanks are owed to the entire Chan lab, for the personal and professional guidance, friendship, and comic relief over the years. I would like to communicate these words of enlightenment to our undergraduate students, “*Insanity: doing the same thing over and over again and expecting different results.*” AND “*If we knew what it was we were doing, it would not be called research, would it*?”--Albert Einstein**.** I also would like to sincerely thank my committee members Dr. Steven Ebert, Dr. William Self, and Dr. Kenneth Teter for their constructive guidance and invaluable advice.

Above all, I am eternally grateful to my beloved family, to my father Nour-eddine, my mother Soraya, my grandmother Fatima, my drôle brother BMW, and my little sister Jehane for their unlimited love, unwavering faith, and endless support. Last but not least, I offer a special thank you to my friends in Orlando, Paris, and Algeria for their generous support and encouragement. Here I will conclude this dedication with words of wisdom.

“*Success is the ability to go from one failure to another with no loss of enthusiasm*.”--Winston Churchill

TABLE OF CONTENTS

LIST OF FIGURES

LIST OF TABLES

LIST OF ABBREVIATIONS

αSyn	α-synuclein
18S rRNA	18S ribosomal RNA
A30P	alanine 30 proline
A53T	alanine 53 threonine
AD	Alzheimer's disease
AHA	American Heart Association
AMPA	α-amino-3-hydroxy-5methyl-4-isoxazole propionic acid
ANOVA	analysis of variance
ATP	adenosine triphosphate
AUC	area under the curve
BAPTA-AM	1,2-*Bis*(2-aminophenoxy)ethane-*N*,*N*,*N*',*N*'-tetraacetic acid tetrakis(acetoxymethyl ester)
BBB	blood-brain barrier
Bcl2	B-cell lymphoma 2
BK	bradykinin
Ca^{2+}	calcium
Casp12	caspase-12
cDNA	complementary deoxyribonucleic acid
CHOP	CCAAT/enhancer binding protein homologous protein

CICR	Ca^{2+}-induced Ca^{2+} release
CNS	central nervous system
CYT C	cytochrome C
DA	dopamine
DAPI	4',6-diamidino-2-phenylindole
DAT	dopamine transporter
DMEM	Dulbecco's modified Eagle medium
DMSO	dimethyl sulfoxide
DNA	deoxyribonucleic acid
ECL	enhanced chemiluminescence
eiF2α	eukaryotic initiation factor 2α
ER	endoplasmic reticulum
ERAD	ER-associated protein degradation
ERK	extracellular signal-regulated kinase
FBS	fetal bovine serum
FITC	fluorescein isothiocyanate
Fluo4-AM	fluo4- acetoxymethyl ester
Fura2-AM	fura2-acetoxymethyl ester
GADPH	glyceraldehyde 3-phosphate dehydrogenase
GFAP	glial fibrillary acidic protein
GFP	green fluorescent protein
Grp	glucose regulated protein
GST	glutathione ***S***-transferase

HD	Huntington's disease
HEK 293	human embryonic kidney 293
Herp	homocysteine-inducible ER stress protein
HRP	horseradish peroxidase
Hsp70	heat shock protein 70
IP	immunoprecipitation
I/R	ischemia-reperfusion
Iba1	ionized calcium binding adaptor molecule 1
IgG	immunoglobulin G
IP_3R	inositol triphosphate receptor
JNK	c-Jun N-terminal kinase
KRH	Krebs–Ringer-Hepes
LB	Lewy bodies
LDH	lactate dehydrogenase
MCA	middle cerebral artery
MPP^+	1-methyl-4 phenylpyridinium
MPTP	1-methyl-4-phenyl-1,2,3,6-tetrahydropyridine
mRNA	messenger ribonucleic acid
NMDA	N-methyl-D-aspartate
Non-Tg	non-transgenic
Nrf2	nuclear factor erythroid 2-related factor 2
nSyn	nitrated α-synuclein
OGD	oxygen glucose deprivation

PARP	poly (ADP-ribose) polymerase
PC12	pheochromocytoma 12
PCR	polymerase chain reaction
PD	Parkinson’s disease
PDGF-β	platelet-derived growth factor–β
P-fraction	detergent insoluble pellet
PIM	proteasome-interacting motif
PS1	presenilin1
qRT-PCR	quantitative real time-PCR
rAAV	adeno-associated virus
RNA	ribonucleic acid
RNAi	RNA interference
ROS	reactive oxygen species
RT	reverse transcription
RT-PCR	semi-quantitative reverse transcriptase polymerase chain reaction
RyR	ryanodine receptor
Sal	salubrinal
SDS-PAGE	sodium dodecyl sulfate polyacrylamide gel electrophoresis
SEM	standard error of the mean
S-Fraction	detergent soluble
siRNA	small interference RNA
SN	substantia nigra
SNCA	synuclein, alpha (non A4 component of amyloid precursor)

SNP	single nucleotide polymorphism
SOD1	superoxide dismutase 1
Tet	tetracycline
TFs	transcription factors
Thap	thapsigargin
TTC	2,3,5-triphenyltetrazoliun chloride monohydrate.
Tuni	tunicamycin
UBL	ubiquitin-like
UPP	ubiquitin-proteasomal pathway
UPR	unfolded protein response
VT	vector
WT	wild-type

CHAPTER ONE: GENERAL INTRODUCTION

Part I

Being one of the most common debilitating neurodegenerative disorders, Parkinson's disease (PD) presents an enormous medical, social, financial and scientific problem. PD is a progressive movement disorder that stems predominantly from the degeneration of dopaminergic neurons (DA) in the substantia nigra pars compacta (SNpc) (1). It is second only to Alzheimer's disease as the most common age-associated neurodegenerative disorder with an estimated incidence of 20/100,000 and a prevalence of 150/100,000 (2). One main neuropathological hallmark of PD is the presence of lewy bodies (LB) and lewy neurites in DA neurons (**Figure 1**). These are intracellular aggregates of αSyn that were initially characterized by eosin staining (2, 3).

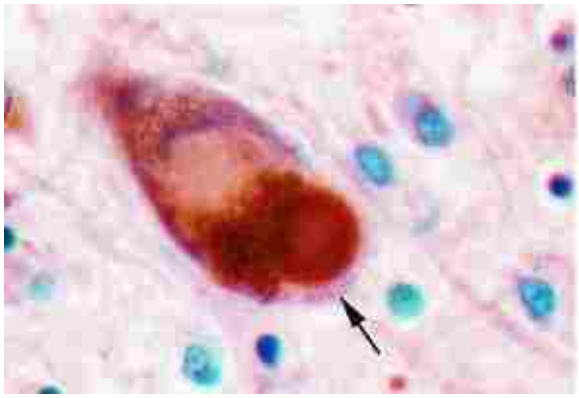

Figure 1-1. A mature lewy body in neuron of the substantia nigra pars compacta (3)

Though PD has been known since ancient times, it was first described by James Parkinson in 1817 in his detailed medical essay entitled, 'An Essay of the Shaking Palsy'. Clinical manifestations of PD include motor impairments such as resting tremor,

rigidity, bradykinesia, gait disturbances and postural instability. These result from the inhibition of the nigrostriatal motor pathway due to loss of 70-80% of striatal dopamine (4). While the motor symptoms of PD prevail the clinical picture and even define the parkinsonism syndrome, many PD patients also experience non-motoric symptoms like autonomic, cognitive and psychiatric problems (**Table 1**). To date, there is no known prevention or cure for PD. Although the motor symptoms are treatable, the benefit of the drugs frequently diminishes or become less consistent over time. A major hurdle in the development of effective neuroprotective agents is the limited understanding of the disease process leading to death of DA neurons.

Table 1-1. Clinical Features of PD

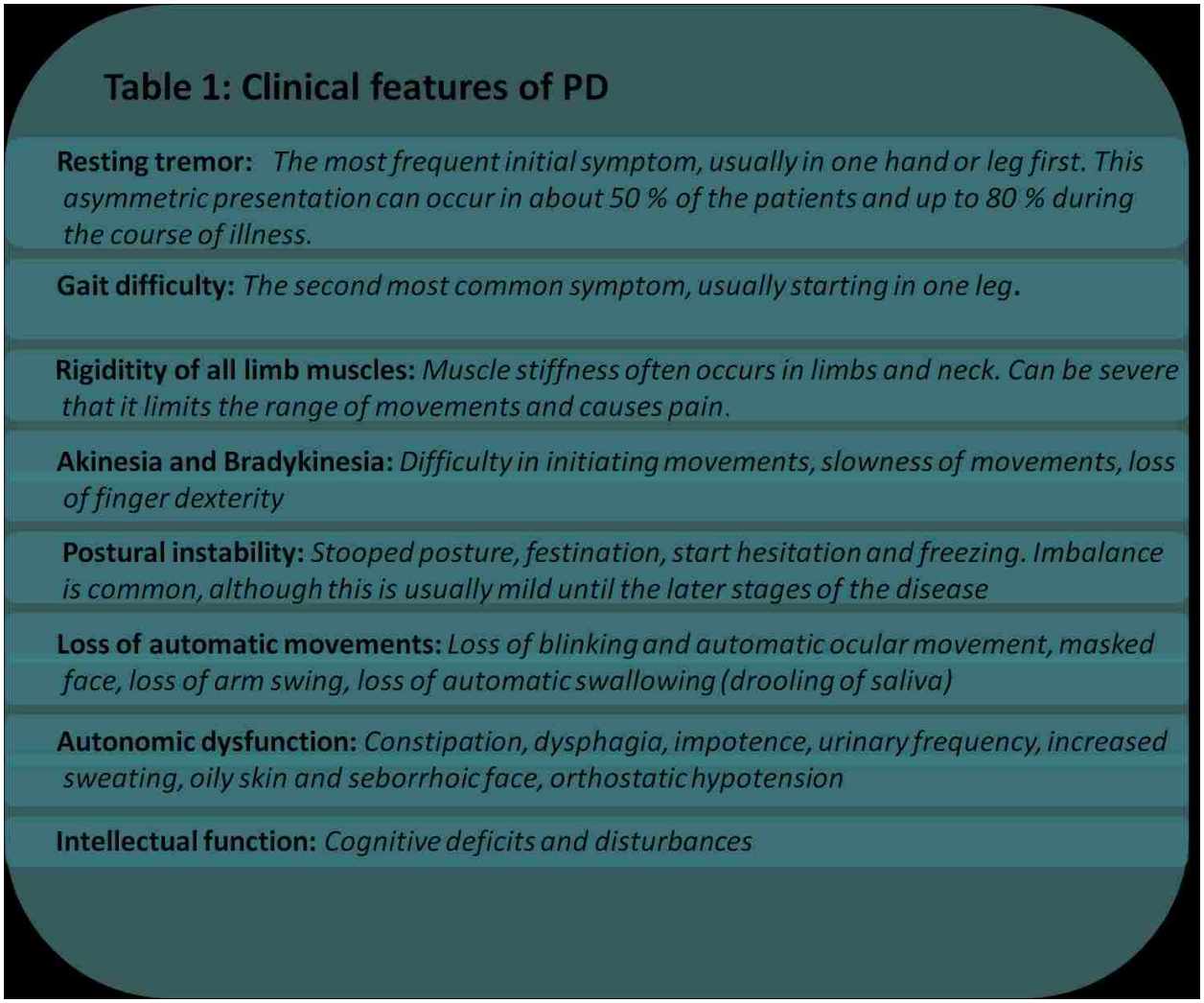

The specific etiology of PD is incompletely understood, but it is believed that a combination of genetic susceptibilities (**Table 2**) and environmental factors, herbicides and pesticides, seem to play a critical role (6). While the majority of cases are sporadic, epidemiological studies unveil that < 10% of PD has a strict familial etiology. The discovery of at least 10 distinct genetic loci accountable for rare Mendelian forms of PD (**Table 2**) have established the role of heredity in the development of PD and granted imperative cues to understanding the molecular pathogenesis of the more common sporadic forms of this disease (4). Studies on the genetics, epidemiology, and

neuropathology of PD, in addition to the development of new experimental models revealed new concepts on disease mechanisms that are guiding researchers to develop treatments to prevent neurodegeneration and halt the progressive course of PD.

Table 1-2. Several gene loci identified for PD

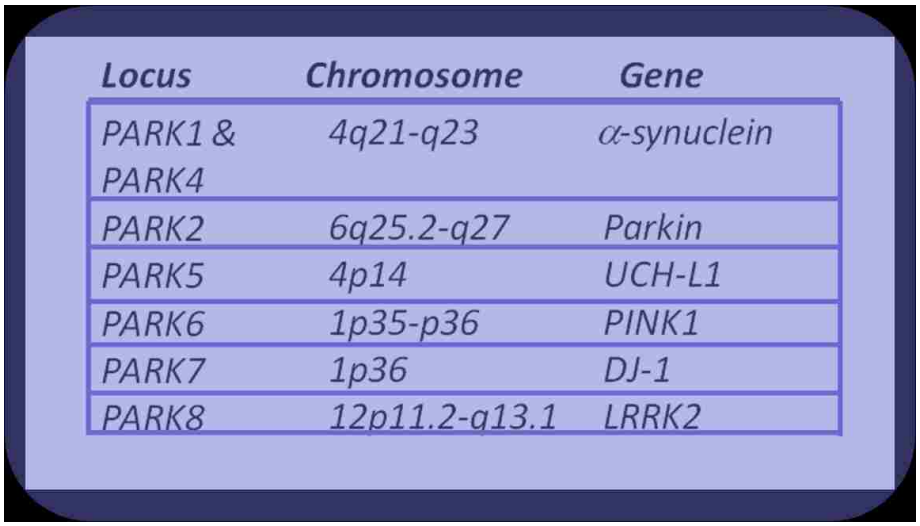

Locus	Chromosome	Gene
PARK1 & PARK4	4q21-q23	α-synuclein
PARK2	6q25.2-q27	Parkin
PARK5	4p14	UCH-L1
PARK6	1p35-p36	PINK1
PARK7	1p36	DJ-1
PARK8	12p11.2-q13.1	LRRK2

Animal and cell culture models are essential tools to identify disease mechanisms, novel therapeutic targets, and assess potential therapies. Two experimental models of PD include the engineered genetic model (**Chapter 2**) and the neurotoxin model (**Chapter 3**).

1) **The Neurotoxin Model**. Among the neurotoxins, (1-methyl-4-phenyl-1,2,3,6-tetrahydropyridine), MPTP, is the best studied and widely used to model environmental cause of PD in non-human primates and rodents. MPTP is lipid-soluble and readily penetrates the blood-brain barrier, BBB and brain cells. MPTP is converted by monoamine oxidase B in astrocytes to the toxic MPP^+ which then enters the DA neurons via the dopamine transporter (DAT)

and inhibits mitochondrial complex I resulting in ATP depletion, oxidative injury and death of DA neurons (5, 6) (**Figure 2**).

2) **Engineered models.** Pathological αSyn is linked mechanistically to both familial and sporadic PD. Therefore, to elucidate the pathophysiology of PD various transgenic mice overexpressing the PD-linked mutant αSyn were developed. As transgenic mice expressing mutant A53T αSyn exhibit more severe effects than the other αSyn mutations, we employed the A53T αSyn mice under the regulatory control of the prion promoter (7).These mice develop severe movement disorder, paralysis and synucleinopathy and show an extensive loss and degeneration in brainstem neurons and spinal cord motor neurons. However, they do not completely recapitulate the disease process as there was no evidence of DA degeneration in the substantia nigra (8-12). However, Dr. Masliah's Lab has developed a transgenic model that exhibits DA neuronal loss. This was achieved by overexpressing αSyn under the control of the platelet-derived growth factor–β (PDGF-β) promoter (12). In addition, overexpression and knockout experiments of the other familial PD genes in mice have also been created. These experimental animal models have improved our understanding of disease development of the more common sporadic form of PD.

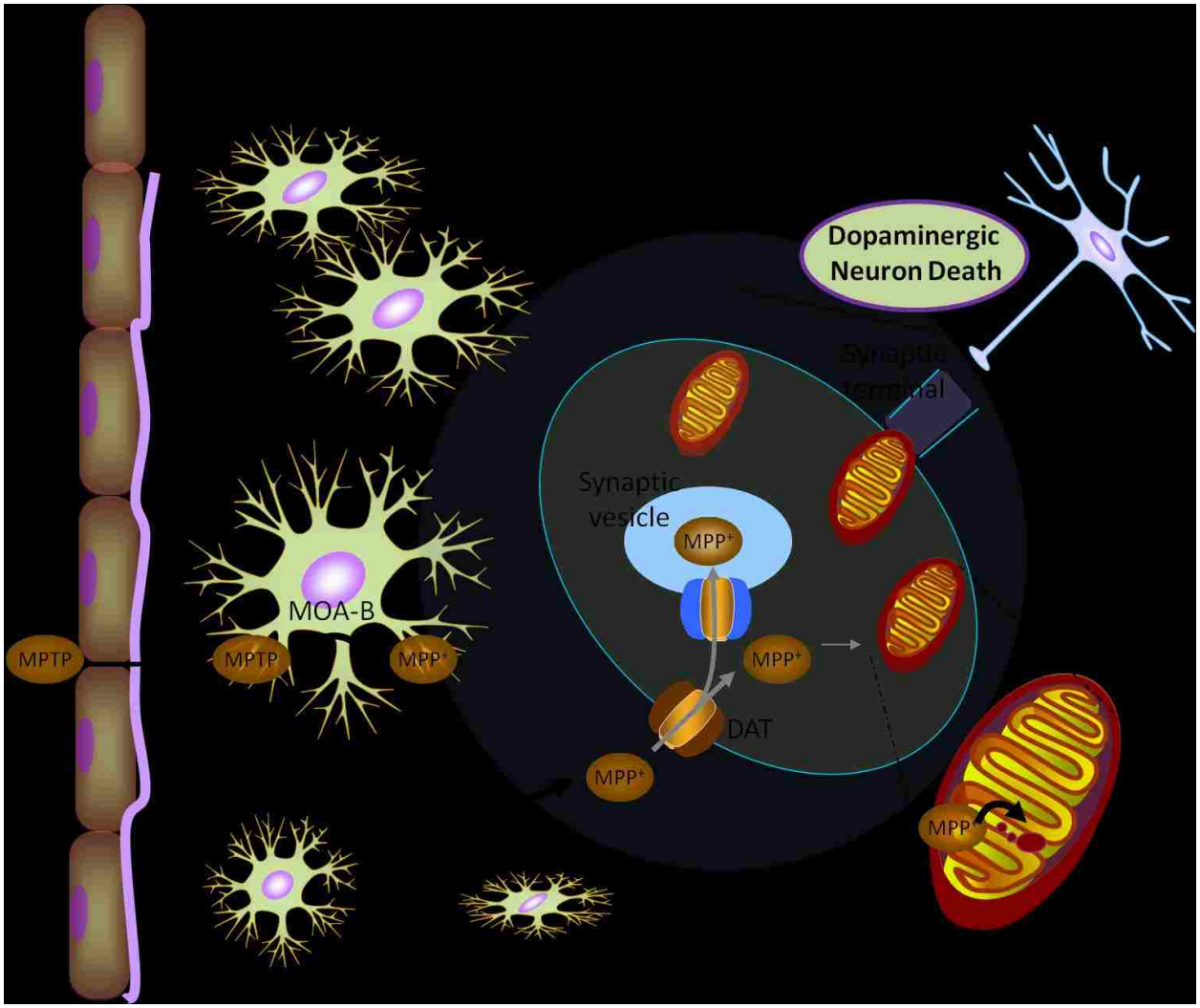

Figure 1-2. Schematic illustration of the mechanisms involved in toxicity of MPTP

The mechanisms responsible for the preferential degeneration of DA neurons in PD have been debated for decades. The principal molecular pathways that commonly underlie the pathogenesis of both sporadic and familial forms of PD are depicted in (**Figure 4**). These include the production of free radicals and oxidative stress, mitochondrial damage, dysfunction of the ubiquitin-proteasome system (UPS), aberrant protein degradation and aggregation.

Recent studies have demonstrated hallmarks of endoplasmic reticulum (ER) stress in experimental models of PD (13-16).The ER is an essential intracellular organelle implicated in the regulation of intracellular Ca^{2+} homeostasis and in the folding and processing of proteins. Conditions that compromise ER functions induce ER stress (17, 18) (**Figure 3**). ER stress triggers the unfolded protein response (UPR) that consists of a series of interconnected control mechanisms that diminish cell damage caused from protein buildup in the ER (19-21). These include the attenuation of general protein synthesis, the transcriptional activation of the genes encoding ER-resident chaperones to relieve disturbances of the ER, and molecules involved in ER-associated degradation (ERAD). ERAD functions in cellular 'quality control' and regulation of ER-resident proteins, and is crucial for the disposal of accumulated unfolded proteins (22, 23). Severe and prolonged ER stress inevitably leads to cell death (17).

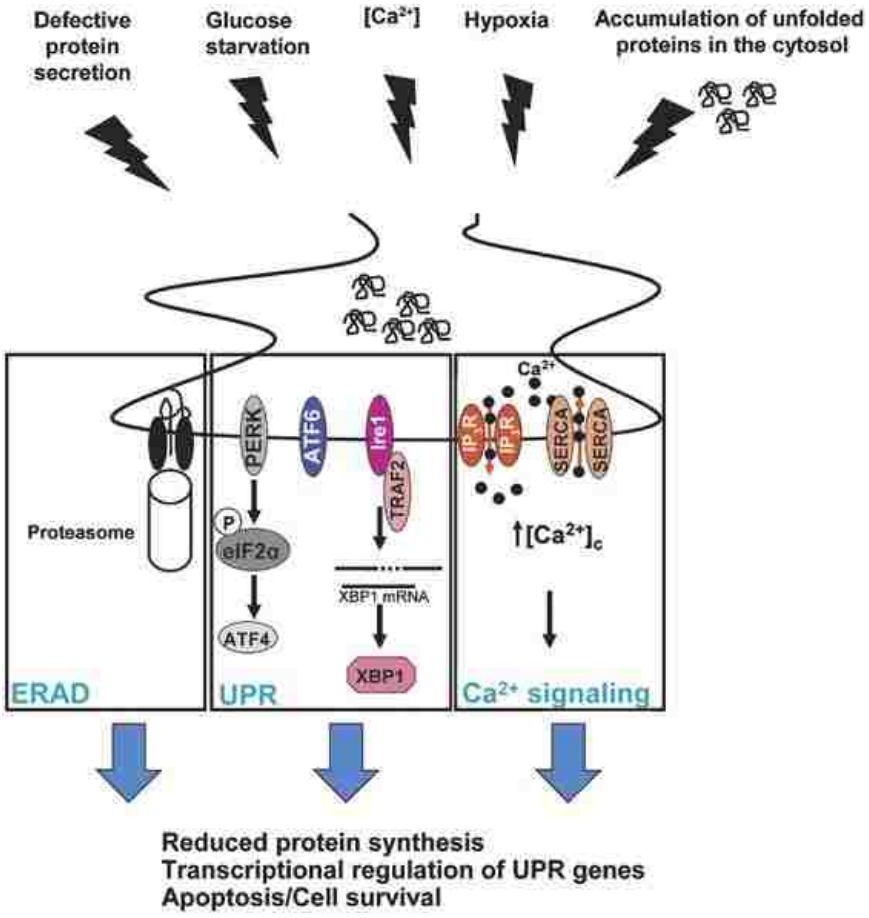

Figure 1-3. ER stress elicits UPR, ERAD and Ca^{2+} signaling (24)

Though ER stress is closely associated with PD, it is yet not clear whether and how ER stress contributes to the degenerative cascades in PD. Characteristic of UPR have been demonstrated in several experimental models of PD (13-15). Particularly, induction of mutant A53TαSyn in PC12 cells causes ER stress (15). Parkin, a protein ubiquitin E3 ligase that is involved in the degradation of unfolded proteins is the most commonly mutated gene known to result in familial PD (25, 26). Loss of function mutations in parkin are implicated in abnormal protein degradation by the UPS thus inducing ER stress (26, 27). Formation of LB together with the accumulation of oxidatively damaged and aggregated proteins in the SNpc of sporadic PD patients are indicative of aberrant proteolytic degradation (28). UPR is also upregulated in the

neurotoxin-induced cell death model of PD (13, 14, 29) suggesting that ER stress may symbolize a common molecular pathway contributing to the neuronal degeneration in familial and sporadic PD.

Cell fate after ER stress is believed to be regulated by the balance between pro-apoptotic and survival signals (30) (**Figure 3**). Important mediators of ER stress-associated cell death include activation of procaspase 12 (in mouse) or procaspase 4 (in human) and increased expression of the pro-apoptotic transcription factor CCAAT/enhancer-binding protein homologous protein (CHOP) (31, 32). For instance, the expression of mutant A53T PD-linked αSyn results in reduction of proteasomal activity, elevation of CHOP and Grp78/Bip expression, induction of caspase-12 activation and ultimately in ER-mediated cell death (15). CHOP has been identified as a critical mediator of apoptotic death in the SNpc dopamine neurons in an *in vivo* neurotoxin model of PD (33) and in ischemic stroke (34). Its critical role in ER-stress-induced cell death has been demonstrated using CHOP knockout mice (34, 35). Moreover, upregulation of ER stress proteins during the ER stress response is important to restore ER homeostasis and enhance cell survival (**Figure 3**). Specifically, Grp78/Bip a fundamental regulator of ER homeostasis owing to its copious functions in protein folding, ER calcium binding, and controlling of the activation of the transmembrane ER stress sensor; its induction during ER stress represents a prosurvival arm of the UPR (36-38). Another positive regulator of ER stress is the homocysteine-inducible ER stress protein (Herp), an ER membrane-bound, ubiquitin-like protein with both its N- and C- termini facing the cytoplasm (39, 40). Its N-terminal contains a proteasome-interacting motif (PIM) (40, 41) and interacts with Hrd1, a

membrane anchored E3 ligase (42). These findings have led to the supposition that Herp may interact with the proteasome during UPR to facilitate ERAD and thus alleviate ER stress. Studies have demonstrated that Herp expression is rapidly upregulated in cultured primary neurons and astrocytes exposed to proteasomal inhibitors or pharmacological agents that selectively induce ER dysfunction (43, 44). Increased Herp transcripts were also observed in the peri-ischemic regions in rat brains after ischemic stroke (44). Significantly, studies using Herp null cells revealed enhanced vulnerability to ER stress-mediated cell death (44). Reduction of Herp expression by RNA interference (RNAi) enhances susceptibility to ER stress-induced cell death whereas its overexpression promotes neuronal survival (43). Herp has also been shown to preserve ER Ca^{2+} homeostasis and mitochondrial function, and inhibits caspase-12 activation in neuronal cells subjected to ER stress (43). Therefore, the ability of Herp to alleviate ER stress and cellular death is suggested to be coupled with its capacity to stabilize cellular Ca^{2+} homeostasis.

Several reports implicate deregulated ER Ca^{2+} release in the pathophysiology of numerous neurodegenerative diseases including, Alzheimer's, Huntington, and prion disease as well as acute disorders such as stroke (16, 45-47). Yet, very little is known about the ER Ca^{2+} homeostatic response during ER stress and whether its dysregulation leads to sustained ER stress and activation of ER stress-mediated cell death pathways. As the major intracellular Ca^{2+} store, the ER controls several vital neuronal activities such as transmitter release, gene transcription and synaptic plasticity (46, 48, 49). It contains two main types of Ca^{2+} release channels, the inositol 1,4,5-triphosphate receptors (IP3R) and the ryanodine receptors (RyR). RyRs are stimulated

to release further Ca^{2+} by Ca^{2+} itself, a process termed Ca^{2+}-induced Ca^{2+} release (CICR) (46, 50, 51). The IP3R's on the other hand are activated by the second messenger IP3. Large increases in the expression of IP3R are reported to accompany apoptosis in several cell types (50, 51). Several lines of evidence suggest that the increased level of RyR is associated with enhanced Ca^{2+} response to the RyR agonist caffeine (52-54) and increased neuronal vulnerability to excitotoxic and oxidative insults (52, 53, 55). Both prion (PrP106-126) and Aβ peptides enhance oxidative stress, caspase 12 activation, and apoptotic cells death by a mechanism that involves the exaggerated ER Ca^{2+} release through IP3R and RYR (45, 52, 56, 57). Ca^{2+} release from the ER also appears instrumental in ischemic cell injury and trauma (47). Thus, the importance of ER Ca^{2+} release and its central involvement in ER stress-associated cell death is demonstrated in studies showing that blockers of IP3Rs and RyR can protect neurons against cell death induced by glutamate excitotoxicity, Aβ and prion peptides (52, 56, 58). Uncontrolled Ca^{2+} release from the ER via RyR and IP3R may also be involved in the pathogenesis of PD, but a detailed mechanism of their contribution is yet to be determined (**Chapter 2**).

ER stress increases ER Ca^{2+} fluxes that can activate apoptosis via mitochondrial dependent and/or independent mechanisms (32, 59). Ca^{2+} released from the ER could activate caspase 12 but may also function as a positive amplifying loop for the mitochodrial-dependent apoptotic pathway (60, 61). A plethora of studies have established that loss of ER Ca^{2+} and concomitant Ca^{2+} uptake by mitochodria can lead to the collapse of mitochondria membrane potential, opening of mitochodrial transition pore and release of proapoptotic factors (62-64). Ca^{2+} uptake by mitochondira leads to

increased reactive oxygen species (ROS) production which instigate a vicious postivie feed back cycle involving ROS-induced deregulated Ca^{2+} release from ER stores, destabilization of mitochodrial Ca^{2+} handling and more ROS generation (62). ROS has been shown to directly modulate the gating or RyR (65) and IP3R (66) suggesting that oxidative stress can facilitate RyR and IP3R-induced apoptosis (66) in which deregulated Ca^{2+} release leads to increased mitochondrial Ca^{2+} loading. Hence, disruption of ER Ca^{2+} homeostasis is a common denominator of pathological processes resulting in neuronal injury in various neurodegenerative diseases.

To date, dopamine replacment therapy using (L-DOPA) is the most prowerful treatment for PD, however, it is not a cure nor it can halt the progerssion of this disorder. Additional efforts are still required in order to further characterize the common mechanisms involved in the demise of dopaminergic neurons both in the sporadic and the genetic forms of PD. This will ultimatly provide vital advances in our understanding of the disease and will broaden our horizon in better designing targeted and more specific therapies.

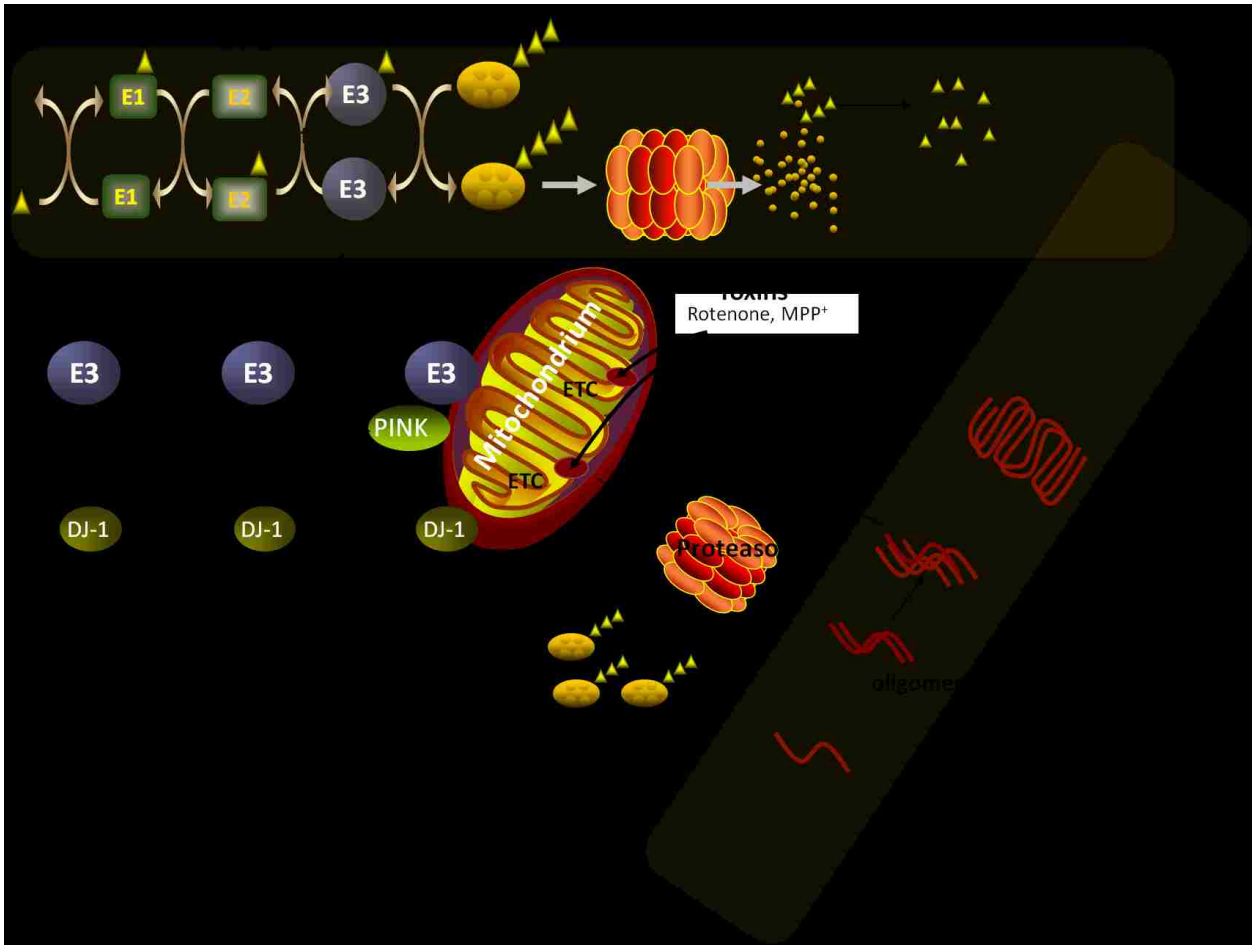

Figure 1-4. Schematic representation of the mechanisms involved in neurodegeneration in PD

Part II

Ischemic stroke is the commonest acute neurodegenerative disease; it represents 87% of all strokes (67) (**Figure 5**). It is considered to be the third leading cause of death in the US after diseases of the heart and cancers in addition to being the second worldwide (68-70). To convey the gravity and the burden that this disease imposes on society, the AHA estimated that 6 400 000 Americans over the age of 20 years have already experienced a stroke, and that approximately 795 000 people each year have a stroke (69, 70). Stroke causes substantial morbidity and mortality, the AHA group states that on average someone dies of a stroke every 4 minutes and that someone in the US has a stroke every 40 seconds (AHA computation based on latest available data). The total costs of stroke are colossal and it was estimated that 73.7 billions of dollars were spent in 2010 (69, 70), unfortunately, we still have limitations in stroke therapy.

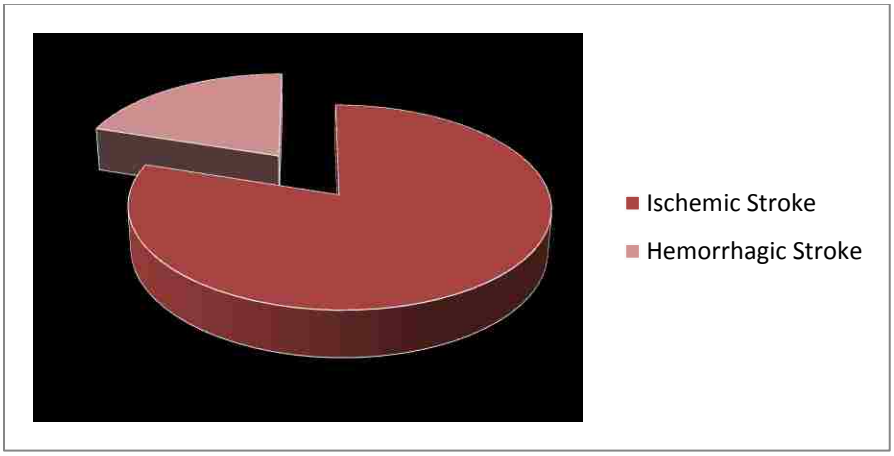

Figure 1-5. Causes of Stroke: > 80% are ischemic and ~20% are hemorrhagic

As in PD, the incidence of stroke also increases with aging. The prevalence of stroke is higher in women as it represents an important health concern especially for postmenopausal women; however, its incidence seems to be the reverse, whereby

younger men are at higher risks than younger females (68-70). Situations like, hypertension, high cholesterol, diabetes, obesity and cigarette smoke as well as decreased physical activity predominantly play a causative role and increases the risks for stroke episode (68, 70). It has been known for decades that genetics is a contributing element and thus play a role as a risk factor for stroke. To this end, an elegant genome wide association studies published in the New England journal of medicine identified two genes, namely *WNK1* and *NINJ2* that may be strongly implicated in ischemic stroke (71). Wnk1 is a large cytoplasmic serine-threonine kinase, expressed in the developing nervous system, kidneys and heart (72, 73). Being an ion homeostasis regulator (74), mutations in Wnk1 have been associated with familial hyperkalemic hypertension (75) and the severity in hypertension (73, 76, 77) further suggesting its implication in ischemic stroke. Ninj 2 is a homophilic cell adhesion molecule (78), also known as “nerve-injury-induced protein” as its name clearly states it; Ninj2 plays a role in nerve regeneration and neurite outgrowth (78). A recent study further shows the link between polymorphism in Ninj2 and its association with ischemia in a Chinese Han population (79, 80) this further supports the notion and confirms that genetic variations influence the risks of stroke.

Ischemic stroke occurs when a blood vessel supplying blood to the brain is obstructed as shown in (**Figure 6**).

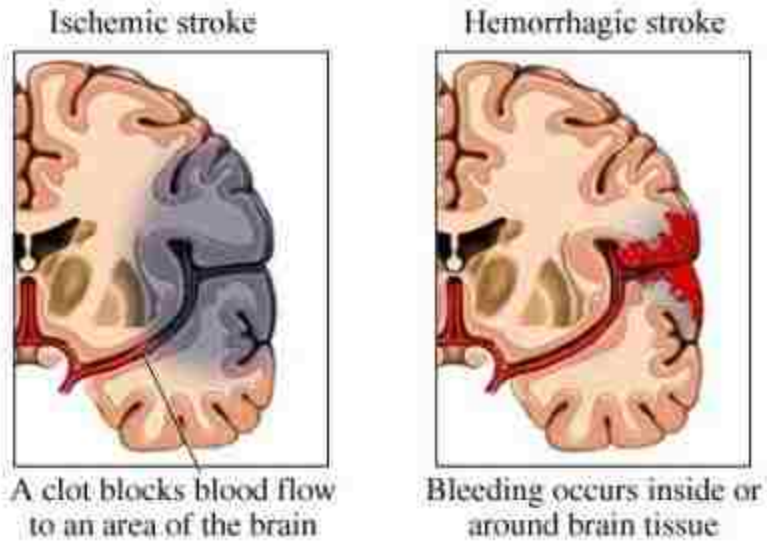

Figure 1-6. Types of stroke

Immediately following ischemia synaptic transmission is disrupted, glutamate accumulates at synapses, resulting in overactivation and desensitization of its receptors that can eventually be neurotoxic (81, 82). Glutamate is the major excitatory neurotransmitter in the mammalian central nervous system (CNS) (83). This amino acid is implicated in several neuronal processes such as neural development, excitatory synaptic transmission and plasticity (83-85). Glutamate activates three classes of ionophore-linked postsynaptic receptors, namely, N-methyl-D-aspartate (NMDA), α-amino-3-hydroxy-5methyl-4-isoxazole propionic acid (AMPA) and Kainate receptors (83). NMDA receptor-mediated toxicity is dependent on Ca^{2+} entry directly through this receptor-gated ion channel (81, 86). As most AMPA receptor channels have poor Ca^{2+} permeability neuronal injury may result primarily from indirect Ca^{2+} entry through voltage –gated Ca^{2+} channels (87), or Ca^{2+} permeable acid sensing ion channels (88). The combination of ischemia reperfusion I/R and Ca^{2+} overload trigger several downstream

lethal reactions including nitrosative and oxidative stress and mitochondrial dysfunction (81, 89), as summarized in (**Figure 7**). Furthermore, a plethora of transcription factors (TFs) are activated immediately after an ischemic insult. These TFs have been shown to contribute in the post-ischemic inflammation and ischemic neuronal death (90, 91), specifically, the transcription factor p53 (92). Though, p53 is best known for its tumor suppression functions (93), it also plays a key role in I/R induced cell death (92, 94). Consistent with this notion, pharmacological inhibition of p53 improved neuronal survival after ischemic injury (95). As noted, the overstimulation of glutamate receptors trigger intracellular event that induces neuronal death after ischemic stroke. Thus, synaptic glutamate receptor channels have been considered as a promising target for stroke therapy (96). Alas, all clinical stroke trials targeting glutamate receptors (AMPA or NMDA) have failed, conceivably because these receptor antagonists interfere with the physiological functions of glutamate as well (97, 98).

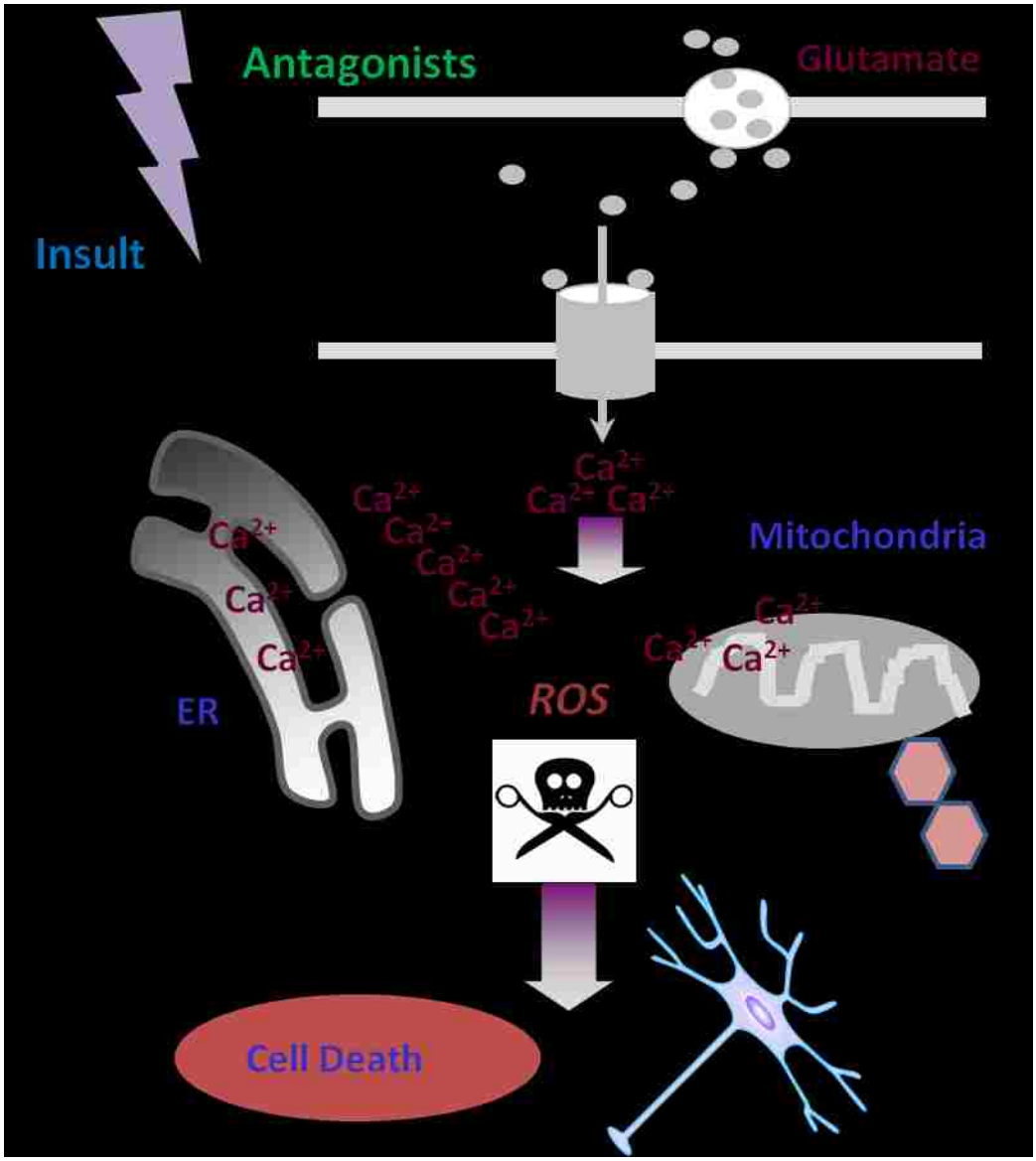

Figure 1-7. Schematic diagram summarizing glutamate excitotoxicity in ischemic neuronal degeneration

Stroke has been classified as an epidemiologic risk factor for Alzheimer's disease and may play a pivotal role in the initiation or acceleration process of neurodegenerative events (99). Yet, whether ischemia is implicated in increasing the risk of developing PD is still questionable. Like in PD, protein aggregation is also a feature of acute neurodegenerative disease. Abnormal buildup of protein aggregates

also develops post ischemic stroke and has been detected in vulnerable neurons from the onset of I/R until delayed neuronal death (100, 101). Both the nature and the role of the protein aggregates found in ischemic brains have not been established yet. Several studies support the critical role of oxidative and nitrative stress in neuronal demise after I/R and demonstrate that oxidation modified proteins accumulate and participate in the generation of protein aggregates (102, 103).

αSyn accumulates in neurons with age (104); moreover, its toxicity is generally considered a consequence of its aggregation (25). αSyn is the first gene discovered whose mutations cause autosomal dominant forms of familial PD (105) (**Table 2**). It is a small 140 amino acid abundant synaptic protein whose physiological functions are still being deciphered. αSyn is a natively unfolded protein that becomes structured upon binding to lipid membranes (106, 107). It is thought to play a role in regulating synaptic plasticity, vesicle release and trafficking (108, 109). Cell culture studies have shown that overexpression, impaired turnover and mutations lead to αSyn aggregation, block the activity of the ubiquitin-proteasomal system (UPS) and ultimately to neuronal cell death (110, 111) (**Figure 4**). Biochemical studies have shown that αSyn forms amyloid fibrils and that all three missense mutations in αSyn accelerate the aggregation of the protein (112, 113). Furthermore, exposure to oxidizing conditions, specifically nitration of αSyn has been shown to increase its propensity to aggregate (11). Of much greater significance is the finding that overexpression of wild-type αSyn also causes autosomal-dominant PD demonstrating that abnormal accumulation of the normal αSyn protein is sufficient to cause disease (114). At higher doses, αSyn is deleterious to neurons and this has further been confirmed in a study showing that MPTP treatment increases αSyn

expression and hastens dopaminergic neuronal death (115). Conversely, αSyn $^{-/-}$ mice are resistant to MPTP-induced toxicity (116). Furthermore, the endangering consequences of αSyn following traumatic brain injury were also prevented in αSyn $^{-/-}$ mice (117). Hence, αSyn accumulation and aggregation has proven to be associated in the pathological cascades leading to neuronal loss in both acute and chronic neurodegenerative disorders.

DJ-1 is another PD gene linked to early onset disease with autosomal recessive inheritance (118) (**Table 2**). DJ-1 is a small 189 amino acid protein (119) that is profusely found in most mammalian tissues, including the brain, where it is localized to both neurons and glia (120). The physiological function of DJ-1 remains mostly unknown although many lines of evidence suggest that DJ-1 may function as an anti-oxidant protein or as a sensor of oxidative stress (121). DJ-1 oxidizes itself to remove hydrogen peroxide *in vitro,* suggesting that it may function in part as a direct scavenger of ROS (121, 122). Other proposed functions include transcriptional co-activator and chaperone activity (123, 124). Its noticeable antioxidant activity emerges from the ability of DJ-1 to stabilize Nrf2 (nuclear factor erythroid 2-related factor), a key transcriptional regulator of the oxidant response (123). DJ-1 also functions as a redox-regulated chaperone to inhibit aggregation and toxicity of αSyn during oxidative stress (124). Moreover, eleven different mutations have been found in the *DJ-1* gene (118, 125), of which the L166P and C106A missense mutations (126) shown to cause loss of function and exacerbate neuronal death under stress conditions (118, 127). Consistent with this notion, DJ-1 knockdown cells and DJ-1 $^{-/-}$ mice or flies are exceedingly susceptible to PD-inducing neurotoxins such as, MPTP, paraquat, rotenone, and 6-hydroxydopamine

(128-130). DJ-1 $^{-/-}$ mice also display larger infarcts post I/R as compared to their wild-type counterparts (131); however, its overexpression *in vivo* confers neuroprotection against I/R induced injury (132) (**Figure 8**).

Several studies point to the interaction between DJ-1 and αSyn and its pathological accumulation in brain tissues from PD patients (133), in *in vitro* settings (134) as well as other related disorders such as Alzheimer's disease, Pick's Disease and corticobasal degeneration (135). Reduced DJ-1 solubility has been verified in PD brain tissues and thereby hinders it from performing its cellular anti-oxidant responses (133). Supporting this notion, DJ-1 has been shown to translocate to mitochondria where it plays a role in maintaining mitochondrial integrity (128, 136). Loss of DJ-1 function renders mitochondria more sensitive to oxidative stress and aggravates ROS production (129). This in part, results in the activation of redox-regulated TFs, p53 (137). Under normal conditions, p53 exists in the cells at very low levels, but its expression rapidly increases in response to diverse insults including oxidative stress and DNA damage (138). The Jun N-terminal kinase 1/2 (JNK1/2) is known to be activated by oxidative stress and increases p53 stability by phosphorylation (139). P53 propagates death responses to oxidative stress and has been shown play a pivotal role in I/R induced cell death (92, 94, 95, 138). Its importance has been shown in both PD and ischemic models whereby DJ-1 deficiency leads to the activation of the p53 pathway (95, 137). P53$^{-/-}$ mice or treatments with pifithrin-α, a p53 inhibitor renders neurons more resistant to MPTP toxicity (140, 141). Furthermore, chemical inhibition of p53 has been shown rescue vulnerable neurons from ischemic insults both *in vivo* and *in vitro* (95, 138). Parkin, another PD-associated gene (**Table 2**) has also been shown

to play a role in neuronal degeneration post ischemic injury (142). I/R contribute to the reduction of parkin protein which results in the accumulation and aggregation of ubiquitylated proteins and thus enhancing vulnerability to ER-stress induced cell death. Recently, it has been shown that parkin alleviates αSyn-induced neuronal cell death in animal and cell culture models (143). These findings suggest a functional relationship between these PD-associated proteins.

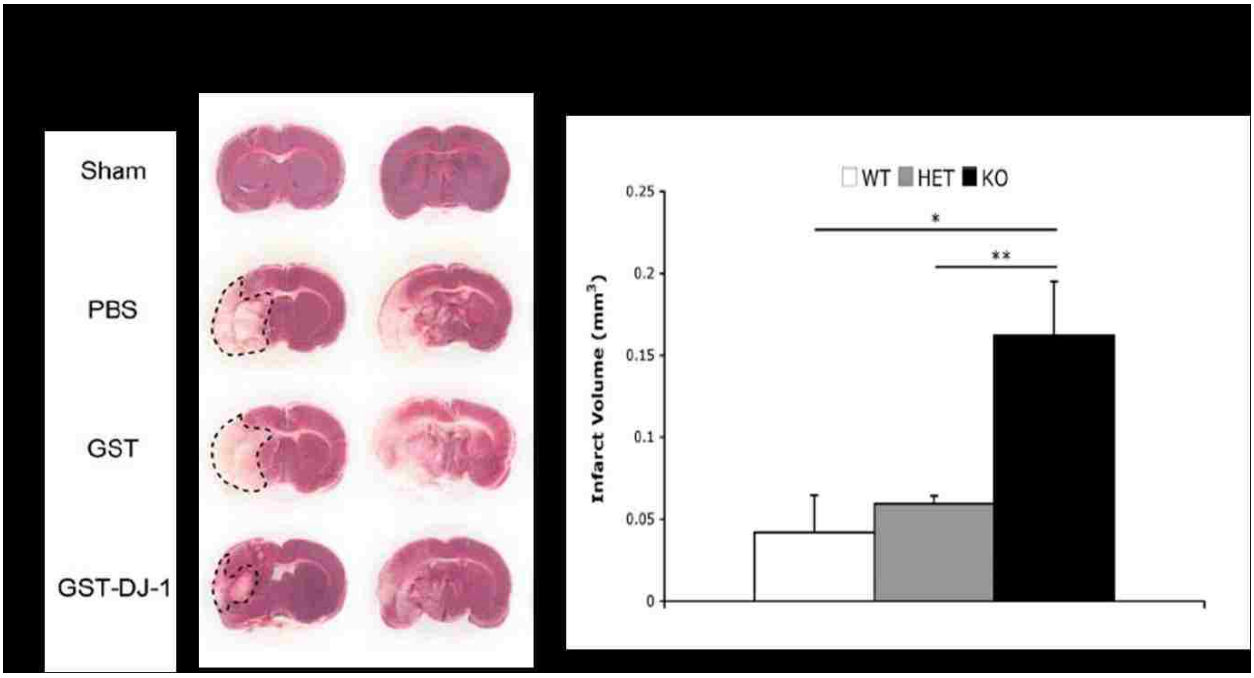

Figure 1-8. DJ-1 reduces infarct size after Ischemia-reperfusion
(A) Intrastriatally injected rats with Glutathione ***S***-transferase tagged DJ-1, GST-DJ-1 (132). (B) DJ-1 wild-type (WT), HET (heterozygous), KO (knockout) mice (131).

In conclusion, the development of effective neuroprotective therapies is of paramount importance. Over the years, a great number of animal and cellular models have been developed to mimic human stroke. These models have helped scientists understand the complexity of the pathological mechanisms involved in ischemic injury. Despite all these efforts, we still do not have a preventative remedy for stroke. It is

noteworthy to point that the mechanisms involved in neuronal death in stroke and chronic neurodegenerative diseases are usually investigated independently. Consequently, it is of imperative endeavor to thoroughly decipher the overlapping interrelated pathophysiological processes associated with chronic and acute neurodegenerative disease to help develop powerful and successful therapies.

References

1. Braak H, Del Tredici K, Rub U, de Vos RA, Jansen Steur EN, Braak E. Staging of brain pathology related to sporadic Parkinson's disease. Neurobiol Aging. 2003;24(2):197-211.

2. Schapira AH. Science, medicine, and the future: Parkinson's disease. BMJ. 1999;318(7179):311-4. PMCID: 1114782.

3. Chu CT, Caruso JL, Cummings TJ, Ervin J, Rosenberg C, Hulette CM. Ubiquitin immunochemistry as a diagnostic aid for community pathologists evaluating patients who have dementia. Mod Pathol. 2000;13(4):420-6.

4. Moore DJ, West AB, Dawson VL, Dawson TM. Molecular pathophysiology of Parkinson's disease. Annu Rev Neurosci. 2005;28:57-87.

5. Eberhardt O, Schulz JB. Apoptotic mechanisms and antiapoptotic therapy in the MPTP model of Parkinson's disease. Toxicol Lett. 2003;139(2-3):135-51.

6. Sedelis M, Schwarting RK, Huston JP. Behavioral phenotyping of the MPTP mouse model of Parkinson's disease. Behav Brain Res. 2001;125(1-2):109-25.

7. Giasson BI, Duda JE, Quinn SM, Zhang B, Trojanowski JQ, Lee VM. Neuronal alpha-synucleinopathy with severe movement disorder in mice expressing A53T human alpha-synuclein. Neuron. 2002;34(4):521-33.

8. Cabin DE, Gispert-Sanchez S, Murphy D, Auburger G, Myers RR, Nussbaum RL. Exacerbated synucleinopathy in mice expressing A53T SNCA on a Snca null background. Neurobiol Aging. 2005;26(1):25-35.

9. Martin LJ, Pan Y, Price AC, Sterling W, Copeland NG, Jenkins NA, et al. Parkinson's disease alpha-synuclein transgenic mice develop neuronal mitochondrial degeneration and cell death. J Neurosci. 2006;26(1):41-50.

10. van der Putten H, Wiederhold KH, Probst A, Barbieri S, Mistl C, Danner S, et al. Neuropathology in mice expressing human alpha-synuclein. J Neurosci. 2000;20(16):6021-9.

11. Giasson BI, Duda JE, Murray IV, Chen Q, Souza JM, Hurtig HI, et al. Oxidative damage linked to neurodegeneration by selective alpha-synuclein nitration in synucleinopathy lesions. Science. 2000;290(5493):985-9.

12. Masliah E, Rockenstein E, Veinbergs I, Mallory M, Hashimoto M, Takeda A, et al. Dopaminergic loss and inclusion body formation in alpha-synuclein mice: implications for neurodegenerative disorders. Science. 2000;287(5456):1265-9.

13. Holtz WA, O'Malley KL. Parkinsonian mimetics induce aspects of unfolded protein response in death of dopaminergic neurons. J Biol Chem. 2003;278(21):19367-77.

14. Ryu EJ, Harding HP, Angelastro JM, Vitolo OV, Ron D, Greene LA. Endoplasmic reticulum stress and the unfolded protein response in cellular models of Parkinson's disease. J Neurosci. 2002;22(24):10690-8.

15. Smith WW, Jiang H, Pei Z, Tanaka Y, Morita H, Sawa A, et al. Endoplasmic reticulum stress and mitochondrial cell death pathways mediate A53T mutant alpha-synuclein-induced toxicity. Hum Mol Genet. 2005;14(24):3801-11.

16. Lindholm D, Wootz H, Korhonen L. ER stress and neurodegenerative diseases. Cell Death Differ. 2006;13(3):385-92.

17. Paschen W, Mengesdorf T. Endoplasmic reticulum stress response and neurodegeneration. Cell Calcium. 2005;38(3-4):409-15.

18. Xu C, Bailly-Maitre B, Reed JC. Endoplasmic reticulum stress: cell life and death decisions. J Clin Invest. 2005;115(10):2656-64. PMCID: 1236697.

19. Harding HP, Calfon M, Urano F, Novoa I, Ron D. Transcriptional and translational control in the Mammalian unfolded protein response. Annu Rev Cell Dev Biol. 2002;18:575-99.

20. Kaufman RJ. Stress signaling from the lumen of the endoplasmic reticulum: coordination of gene transcriptional and translational controls. Genes Dev. 1999;13(10):1211-33.

21. Patil C, Walter P. Intracellular signaling from the endoplasmic reticulum to the nucleus: the unfolded protein response in yeast and mammals. Curr Opin Cell Biol. 2001;13(3):349-55.

22. Meusser B, Hirsch C, Jarosch E, Sommer T. ERAD: the long road to destruction. Nat Cell Biol. 2005;7(8):766-72.

23. McCracken AA, Brodsky JL. Recognition and delivery of ERAD substrates to the proteasome and alternative paths for cell survival. Curr Top Microbiol Immunol. 2005;300:17-40.

24. Hoyer-Hansen M, Jaattela M. Connecting endoplasmic reticulum stress to autophagy by unfolded protein response and calcium. Cell Death Differ. 2007;14(9):1576-82.

25. Cookson MR. The biochemistry of Parkinson's disease. Annu Rev Biochem. 2005;74:29-52.

26. Shimura H, Hattori N, Kubo S, Mizuno Y, Asakawa S, Minoshima S, et al. Familial Parkinson disease gene product, parkin, is a ubiquitin-protein ligase. Nat Genet. 2000;25(3):302-5.

27. Kitada T, Asakawa S, Hattori N, Matsumine H, Yamamura Y, Minoshima S, et al. Mutations in the parkin gene cause autosomal recessive juvenile parkinsonism. Nature. 1998;392(6676):605-8.

28. Wooten MW, Hu X, Babu JR, Seibenhener ML, Geetha T, Paine MG, et al. Signaling, polyubiquitination, trafficking, and inclusions: sequestosome 1/p62's role in neurodegenerative disease. J Biomed Biotechnol. 2006;2006(3):62079. PMCID: 1559922.

29. Yamamuro A, Yoshioka Y, Ogita K, Maeda S. Involvement of endoplasmic reticulum stress on the cell death induced by 6-hydroxydopamine in human neuroblastoma SH-SY5Y cells. Neurochem Res. 2006;31(5):657-64.

30. Welihinda AA, Tirasophon W, Kaufman RJ. The cellular response to protein misfolding in the endoplasmic reticulum. Gene Expr. 1999;7(4-6):293-300.

31. Szegezdi E, Fitzgerald U, Samali A. Caspase-12 and ER-stress-mediated apoptosis: the story so far. Ann N Y Acad Sci. 2003;1010:186-94.

32. Breckenridge DG, Germain M, Mathai JP, Nguyen M, Shore GC. Regulation of apoptosis by endoplasmic reticulum pathways. Oncogene. 2003;22(53):8608-18.

33. Silva RM, Ries V, Oo TF, Yarygina O, Jackson-Lewis V, Ryu EJ, et al. CHOP/GADD153 is a mediator of apoptotic death in substantia nigra dopamine neurons in an in vivo neurotoxin model of parkinsonism. J Neurochem. 2005;95(4):974-86. PMCID: 3082498.

34. Tajiri S, Oyadomari S, Yano S, Morioka M, Gotoh T, Hamada JI, et al. Ischemia-induced neuronal cell death is mediated by the endoplasmic reticulum stress pathway involving CHOP. Cell Death Differ. 2004;11(4):403-15.

35. Oyadomari S, Mori M. Roles of CHOP/GADD153 in endoplasmic reticulum stress. Cell Death Differ. 2004;11(4):381-9.

36. Lee AS. The ER chaperone and signaling regulator GRP78/BiP as a monitor of endoplasmic reticulum stress. Methods. 2005;35(4):373-81.

37. Li J, Ni M, Lee B, Barron E, Hinton DR, Lee AS. The unfolded protein response regulator GRP78/BiP is required for endoplasmic reticulum integrity and stress-induced autophagy in mammalian cells. Cell Death Differ. 2008;15(9):1460-71. PMCID: 2758056.

38. Rao RV, Peel A, Logvinova A, del Rio G, Hermel E, Yokota T, et al. Coupling endoplasmic reticulum stress to the cell death program: role of the ER chaperone GRP78. FEBS Lett. 2002;514(2-3):122-8.

39. van Laar T, Schouten T, Hoogervorst E, van Eck M, van der Eb AJ, Terleth C. The novel MMS-inducible gene Mif1/KIAA0025 is a target of the unfolded protein response pathway. FEBS Lett. 2000;469(1):123-31.

40. Kokame K, Agarwala KL, Kato H, Miyata T. Herp, a new ubiquitin-like membrane protein induced by endoplasmic reticulum stress. J Biol Chem. 2000;275(42):32846-53.

41. Upadhya SC, Hegde AN. A potential proteasome-interacting motif within the ubiquitin-like domain of parkin and other proteins. Trends Biochem Sci. 2003;28(6):280-3.

42. Schulze A, Standera S, Buerger E, Kikkert M, van Voorden S, Wiertz E, et al. The ubiquitin-domain protein HERP forms a complex with components of the endoplasmic reticulum associated degradation pathway. J Mol Biol. 2005;354(5):1021-7.

43. Chan SL, Fu W, Zhang P, Cheng A, Lee J, Kokame K, et al. Herp stabilizes neuronal Ca2+ homeostasis and mitochondrial function during endoplasmic reticulum stress. J Biol Chem. 2004;279(27):28733-43.

44. Hori O, Ichinoda F, Yamaguchi A, Tamatani T, Taniguchi M, Koyama Y, et al. Role of Herp in the endoplasmic reticulum stress response. Genes Cells. 2004;9(5):457-69.

45. Hetz C, Russelakis-Carneiro M, Maundrell K, Castilla J, Soto C. Caspase-12 and endoplasmic reticulum stress mediate neurotoxicity of pathological prion protein. EMBO J. 2003;22(20):5435-45. PMCID: 213791.

46. Mattson MP, LaFerla FM, Chan SL, Leissring MA, Shepel PN, Geiger JD. Calcium signaling in the ER: its role in neuronal plasticity and neurodegenerative disorders. Trends Neurosci. 2000;23(5):222-9.

47. Paschen W, Gissel C, Linden T, Althausen S, Doutheil J. Activation of gadd153 expression through transient cerebral ischemia: evidence that ischemia causes endoplasmic reticulum dysfunction. Brain Res Mol Brain Res. 1998;60(1):115-22.

48. Berridge MJ. The endoplasmic reticulum: a multifunctional signaling organelle. Cell Calcium. 2002;32(5-6):235-49.

49. Berridge MJ. Neuronal calcium signaling. Neuron. 1998;21(1):13-26.

50. Hajnoczky G, Davies E, Madesh M. Calcium signaling and apoptosis. Biochem Biophys Res Commun. 2003;304(3):445-54.

51. Hajnoczky G, Csordas G, Madesh M, Pacher P. Control of apoptosis by IP(3) and ryanodine receptor driven calcium signals. Cell Calcium. 2000;28(5-6):349-63.

52. Chan SL, Mayne M, Holden CP, Geiger JD, Mattson MP. Presenilin-1 mutations increase levels of ryanodine receptors and calcium release in PC12 cells and cortical neurons. J Biol Chem. 2000;275(24):18195-200.

53. Lee SY, Hwang DY, Kim YK, Lee JW, Shin IC, Oh KW, et al. PS2 mutation increases neuronal cell vulnerability to neurotoxicants through activation of caspase-3 by enhancing of ryanodine receptor-mediated calcium release. FASEB J. 2006;20(1):151-3.

54. Smith IF, Hitt B, Green KN, Oddo S, LaFerla FM. Enhanced caffeine-induced Ca2+ release in the 3xTg-AD mouse model of Alzheimer's disease. J Neurochem. 2005;94(6):1711-8.

55. Mori F, Okada M, Tomiyama M, Kaneko S, Wakabayashi K. Effects of ryanodine receptor activation on neurotransmitter release and neuronal cell death following kainic acid-induced status epilepticus. Epilepsy Res. 2005;65(1-2):59-70.

56. Ferreiro E, Resende R, Costa R, Oliveira CR, Pereira CM. An endoplasmic-reticulum-specific apoptotic pathway is involved in prion and amyloid-beta peptides neurotoxicity. Neurobiol Dis. 2006;23(3):669-78.

57. Guo Q, Sopher BL, Furukawa K, Pham DG, Robinson N, Martin GM, et al. Alzheimer's presenilin mutation sensitizes neural cells to apoptosis induced by trophic factor withdrawal and amyloid beta-peptide: involvement of calcium and oxyradicals. J Neurosci. 1997;17(11):4212-22.

58. Mattson MP. Calcium and neurodegeneration. Aging Cell. 2007;6(3):337-50.

59. Ferri KF, Kroemer G. Organelle-specific initiation of cell death pathways. Nat Cell Biol. 2001;3(11):E255-63.

60. Nakagawa T, Yuan J. Cross-talk between two cysteine protease families. Activation of caspase-12 by calpain in apoptosis. J Cell Biol. 2000;150(4):887-94. PMCID: 2175271.

61. Nakagawa T, Zhu H, Morishima N, Li E, Xu J, Yankner BA, et al. Caspase-12 mediates endoplasmic-reticulum-specific apoptosis and cytotoxicity by amyloid-beta. Nature. 2000;403(6765):98-103.

62. Jacobson J, Duchen MR. Mitochondrial oxidative stress and cell death in astrocytes--requirement for stored Ca2+ and sustained opening of the permeability transition pore. J Cell Sci. 2002;115(Pt 6):1175-88.

63. Nutt LK, Chandra J, Pataer A, Fang B, Roth JA, Swisher SG, et al. Bax-mediated Ca2+ mobilization promotes cytochrome c release during apoptosis. J Biol Chem. 2002;277(23):20301-8.

64. Scorrano L, Oakes SA, Opferman JT, Cheng EH, Sorcinelli MD, Pozzan T, et al. BAX and BAK regulation of endoplasmic reticulum Ca2+: a control point for apoptosis. Science. 2003;300(5616):135-9.

65. Boraso A, Williams AJ. Modification of the gating of the cardiac sarcoplasmic reticulum Ca(2+)-release channel by H2O2 and dithiothreitol. Am J Physiol. 1994;267(3 Pt 2):H1010-6.

66. Madesh M, Hawkins BJ, Milovanova T, Bhanumathy CD, Joseph SK, Ramachandrarao SP, et al. Selective role for superoxide in InsP3 receptor-mediated mitochondrial dysfunction and endothelial apoptosis. J Cell Biol. 2005;170(7):1079-90. PMCID: 2171541.

67. Ayala C, Greenlund KJ, Croft JB, Keenan NL, Donehoo RS, Giles WH, et al. Racial/ethnic disparities in mortality by stroke subtype in the United States, 1995-1998. Am J Epidemiol. 2001;154(11):1057-63.

68. Ingall T. Stroke--incidence, mortality, morbidity and risk. J Insur Med. 2004;36(2):143-52.

69. Lloyd-Jones D, Adams RJ, Brown TM, Carnethon M, Dai S, De Simone G, et al. Executive summary: heart disease and stroke statistics--2010 update: a report from the American Heart Association. Circulation. 2010;121(7):948-54.

70. Lloyd-Jones D, Adams RJ, Brown TM, Carnethon M, Dai S, De Simone G, et al. Heart disease and stroke statistics--2010 update: a report from the American Heart Association. Circulation. 2010;121(7):e46-e215.

71. Ikram MA, Seshadri S, Bis JC, Fornage M, DeStefano AL, Aulchenko YS, et al. Genomewide association studies of stroke. N Engl J Med. 2009;360(17):1718-28. PMCID: 2768348.

72. Delaloy C, Hadchouel J, Imbert-Teboul M, Clemessy M, Houot AM, Jeunemaitre X. Cardiovascular expression of the mouse WNK1 gene during development and adulthood revealed by a BAC reporter assay. Am J Pathol. 2006;169(1):105-18. PMCID: 1698764.

73. Newhouse S, Farrall M, Wallace C, Hoti M, Burke B, Howard P, et al. Polymorphisms in the WNK1 gene are associated with blood pressure variation and urinary potassium excretion. PLoS One. 2009;4(4):e5003. PMCID: 2661139.

74. Eladari D, Chambrey R. WNKs: new concepts in the regulation of NaCl and K+ balance. J Nephrol. 2007;20(3):260-4.

75. O'Reilly M, Marshall E, Macgillivray T, Mittal M, Xue W, Kenyon CJ, et al. Dietary electrolyte-driven responses in the renal WNK kinase pathway in vivo. J Am Soc Nephrol. 2006;17(9):2402-13.

76. Tobin MD, Raleigh SM, Newhouse S, Braund P, Bodycote C, Ogleby J, et al. Association of WNK1 gene polymorphisms and haplotypes with ambulatory blood pressure in the general population. Circulation. 2005;112(22):3423-9.

77. Newhouse SJ, Wallace C, Dobson R, Mein C, Pembroke J, Farrall M, et al. Haplotypes of the WNK1 gene associate with blood pressure variation in a severely hypertensive population from the British Genetics of Hypertension study. Hum Mol Genet. 2005;14(13):1805-14.

78. Araki T, Milbrandt J. Ninjurin2, a novel homophilic adhesion molecule, is expressed in mature sensory and enteric neurons and promotes neurite outgrowth. J Neurosci. 2000;20(1):187-95.

79. Wan XH, Li SJ, Cheng P, Zhang Q, Yang XC, Zhong GZ, et al. NINJ2 polymorphism is associated with ischemic stroke in Chinese Han population. J Neurol Sci. 2011;308(1-2):67-71.

80. Chen K, Xiao ZS, Hou SQ, Zhao RT, Liu YF, Dou HD, et al. [Strong association between the NINJ2 gene polymorphism and the susceptibility of stroke in Chinese Han population in Fangshan district]. Beijing Da Xue Xue Bao. 2010;42(5):498-502.

81. Lipton P. Ischemic cell death in brain neurons. Physiol Rev. 1999;79(4):1431-568.

82. Benveniste H, Drejer J, Schousboe A, Diemer NH. Elevation of the extracellular concentrations of glutamate and aspartate in rat hippocampus during transient cerebral ischemia monitored by intracerebral microdialysis. J Neurochem. 1984;43(5):1369-74.

83. Meldrum BS. Glutamate as a neurotransmitter in the brain: review of physiology and pathology. J Nutr. 2000;130(4S Suppl):1007S-15S.

84. Carroll RC, Zukin RS. NMDA-receptor trafficking and targeting: implications for synaptic transmission and plasticity. Trends Neurosci. 2002;25(11):571-7.

85. Kwon HB, Sabatini BL. Glutamate induces de novo growth of functional spines in developing cortex. Nature. 2011;474(7349):100-4. PMCID: 3107907.

86. Choi DW. Calcium: still center-stage in hypoxic-ischemic neuronal death. Trends Neurosci. 1995;18(2):58-60.

87. Weiss JH, Hartley DM, Koh J, Choi DW. The calcium channel blocker nifedipine attenuates slow excitatory amino acid neurotoxicity. Science. 1990;247(4949 Pt 1):1474-7.

88. Xiong ZG, Zhu XM, Chu XP, Minami M, Hey J, Wei WL, et al. Neuroprotection in ischemia: blocking calcium-permeable acid-sensing ion channels. Cell. 2004;118(6):687-98.

89. Fiskum G, Murphy AN, Beal MF. Mitochondria in neurodegeneration: acute ischemia and chronic neurodegenerative diseases. J Cereb Blood Flow Metab. 1999;19(4):351-69.

90. Yi JH, Park SW, Kapadia R, Vemuganti R. Role of transcription factors in mediating post-ischemic cerebral inflammation and brain damage. Neurochem Int. 2007;50(7-8):1014-27. PMCID: 2040388.

91. Stephenson D, Yin T, Smalstig EB, Hsu MA, Panetta J, Little S, et al. Transcription factor nuclear factor-kappa B is activated in neurons after focal cerebral ischemia. J Cereb Blood Flow Metab. 2000;20(3):592-603.

92. Hong LZ, Zhao XY, Zhang HL. p53-mediated neuronal cell death in ischemic brain injury. Neurosci Bull. 2010;26(3):232-40.

93. Levine AJ. p53, the cellular gatekeeper for growth and division. Cell. 1997;88(3):323-31.

94. Li Y, Chopp M, Zhang ZG, Zaloga C, Niewenhuis L, Gautam S. p53-immunoreactive protein and p53 mRNA expression after transient middle cerebral artery occlusion in rats. Stroke. 1994;25(4):849-55; discussion 55-6.

95. Culmsee C, Zhu X, Yu QS, Chan SL, Camandola S, Guo Z, et al. A synthetic inhibitor of p53 protects neurons against death induced by ischemic and excitotoxic insults, and amyloid beta-peptide. J Neurochem. 2001;77(1):220-8.

96. Simon RP, Swan JH, Griffiths T, Meldrum BS. Blockade of N-methyl-D-aspartate receptors may protect against ischemic damage in the brain. Science. 1984;226(4676):850-2.

97. Morris GF, Bullock R, Marshall SB, Marmarou A, Maas A, Marshall LF. Failure of the competitive N-methyl-D-aspartate antagonist Selfotel (CGS 19755) in the treatment of severe head injury: results of two phase III clinical trials. The Selfotel Investigators. J Neurosurg. 1999;91(5):737-43.

98. Ikonomidou C, Turski L. Why did NMDA receptor antagonists fail clinical trials for stroke and traumatic brain injury? Lancet Neurol. 2002;1(6):383-6.

99. Qiu C, Xu W, Winblad B, Fratiglioni L. Vascular risk profiles for dementia and Alzheimer's disease in very old people: a population-based longitudinal study. J Alzheimers Dis. 2010;20(1):293-300.

100. Hu BR, Janelidze S, Ginsberg MD, Busto R, Perez-Pinzon M, Sick TJ, et al. Protein aggregation after focal brain ischemia and reperfusion. J Cereb Blood Flow Metab. 2001;21(7):865-75.

101. Hu BR, Martone ME, Jones YZ, Liu CL. Protein aggregation after transient cerebral ischemia. J Neurosci. 2000;20(9):3191-9.

102. Piantadosi CA, Zhang J. Mitochondrial generation of reactive oxygen species after brain ischemia in the rat. Stroke. 1996;27(2):327-31; discussion 32.

103. Giasson BI, Ischiropoulos H, Lee VM, Trojanowski JQ. The relationship between oxidative/nitrative stress and pathological inclusions in Alzheimer's and Parkinson's diseases. Free Radic Biol Med. 2002;32(12):1264-75.

104. Xuan Q, Xu SL, Lu DH, Yu S, Zhou M, Ueda K, et al. Increase expression of alpha-synuclein in aged human brain associated with neuromelanin accumulation. J Neural Transm. 2011.

105. Polymeropoulos MH, Lavedan C, Leroy E, Ide SE, Dehejia A, Dutra A, et al. Mutation in the alpha-synuclein gene identified in families with Parkinson's disease. Science. 1997;276(5321):2045-7.

106. Jo E, McLaurin J, Yip CM, St George-Hyslop P, Fraser PE. alpha-Synuclein membrane interactions and lipid specificity. J Biol Chem. 2000;275(44):34328-34.

107. Davidson WS, Jonas A, Clayton DF, George JM. Stabilization of alpha-synuclein secondary structure upon binding to synthetic membranes. J Biol Chem. 1998;273(16):9443-9.

108. Cabin DE, Shimazu K, Murphy D, Cole NB, Gottschalk W, McIlwain KL, et al. Synaptic vesicle depletion correlates with attenuated synaptic responses to prolonged repetitive stimulation in mice lacking alpha-synuclein. J Neurosci. 2002;22(20):8797-807.

109. Cookson MR. alpha-Synuclein and neuronal cell death. Mol Neurodegener. 2009;4:9. PMCID: 2646729.

110. Betarbet R, Sherer TB, Greenamyre JT. Ubiquitin-proteasome system and Parkinson's diseases. Exp Neurol. 2005;191 Suppl 1:S17-27.

111. Zhou W, Hurlbert MS, Schaack J, Prasad KN, Freed CR. Overexpression of human alpha-synuclein causes dopamine neuron death in rat primary culture and immortalized mesencephalon-derived cells. Brain Res. 2000;866(1-2):33-43.

112. Conway KA, Lee SJ, Rochet JC, Ding TT, Williamson RE, Lansbury PT, Jr. Acceleration of oligomerization, not fibrillization, is a shared property of both alpha-synuclein mutations linked to early-onset Parkinson's disease: implications for pathogenesis and therapy. Proc Natl Acad Sci U S A. 2000;97(2):571-6. PMCID: 15371.

113. Conway KA, Harper JD, Lansbury PT. Accelerated in vitro fibril formation by a mutant alpha-synuclein linked to early-onset Parkinson disease. Nat Med. 1998;4(11):1318-20.

114. Mata IF, Shi M, Agarwal P, Chung KA, Edwards KL, Factor SA, et al. SNCA variant associated with Parkinson disease and plasma alpha-synuclein level. Arch Neurol. 2010;67(11):1350-6. PMCID: 3010848.

115. Vila M, Vukosavic S, Jackson-Lewis V, Neystat M, Jakowec M, Przedborski S. Alpha-synuclein up-regulation in substantia nigra dopaminergic neurons following administration of the parkinsonian toxin MPTP. J Neurochem. 2000;74(2):721-9.

116. Dauer W, Kholodilov N, Vila M, Trillat AC, Goodchild R, Larsen KE, et al. Resistance of alpha -synuclein null mice to the parkinsonian neurotoxin MPTP. Proc Natl Acad Sci U S A. 2002;99(22):14524-9. PMCID: 137916.

117. Uryu K, Giasson BI, Longhi L, Martinez D, Murray I, Conte V, et al. Age-dependent synuclein pathology following traumatic brain injury in mice. Exp Neurol. 2003;184(1):214-24.

118. Bonifati V, Rizzu P, van Baren MJ, Schaap O, Breedveld GJ, Krieger E, et al. Mutations in the DJ-1 gene associated with autosomal recessive early-onset parkinsonism. Science. 2003;299(5604):256-9.

119. Bonifati V, Rizzu P, Squitieri F, Krieger E, Vanacore N, van Swieten JC, et al. DJ-1(PARK7), a novel gene for autosomal recessive, early onset parkinsonism. Neurol Sci. 2003;24(3):159-60.

120. Bandopadhyay R, Kingsbury AE, Cookson MR, Reid AR, Evans IM, Hope AD, et al. The expression of DJ-1 (PARK7) in normal human CNS and idiopathic Parkinson's disease. Brain. 2004;127(Pt 2):420-30.

121. Taira T, Saito Y, Niki T, Iguchi-Ariga SM, Takahashi K, Ariga H. DJ-1 has a role in antioxidative stress to prevent cell death. EMBO Rep. 2004;5(2):213-8. PMCID: 1298985.

122. Mitsumoto A, Nakagawa Y. DJ-1 is an indicator for endogenous reactive oxygen species elicited by endotoxin. Free Radic Res. 2001;35(6):885-93.

123. Clements CM, McNally RS, Conti BJ, Mak TW, Ting JP. DJ-1, a cancer- and Parkinson's disease-associated protein, stabilizes the antioxidant transcriptional

master regulator Nrf2. Proc Natl Acad Sci U S A. 2006;103(41):15091-6. PMCID: 1586179.

124. Shendelman S, Jonason A, Martinat C, Leete T, Abeliovich A. DJ-1 is a redox-dependent molecular chaperone that inhibits alpha-synuclein aggregate formation. PLoS Biol. 2004;2(11):e362. PMCID: 521177.

125. Vila M, Przedborski S. Genetic clues to the pathogenesis of Parkinson's disease. Nat Med. 2004;10 Suppl:S58-62.

126. Moore DJ, Zhang L, Dawson TM, Dawson VL. A missense mutation (L166P) in DJ-1, linked to familial Parkinson's disease, confers reduced protein stability and impairs homo-oligomerization. J Neurochem. 2003;87(6):1558-67.

127. Yokota T, Sugawara K, Ito K, Takahashi R, Ariga H, Mizusawa H. Down regulation of DJ-1 enhances cell death by oxidative stress, ER stress, and proteasome inhibition. Biochem Biophys Res Commun. 2003;312(4):1342-8.

128. Canet-Aviles RM, Wilson MA, Miller DW, Ahmad R, McLendon C, Bandyopadhyay S, et al. The Parkinson's disease protein DJ-1 is neuroprotective due to cysteine-sulfinic acid-driven mitochondrial localization. Proc Natl Acad Sci U S A. 2004;101(24):9103-8. PMCID: 428480.

129. Kim RH, Smith PD, Aleyasin H, Hayley S, Mount MP, Pownall S, et al. Hypersensitivity of DJ-1-deficient mice to 1-methyl-4-phenyl-1,2,3,6-tetrahydropyrindine (MPTP) and oxidative stress. Proc Natl Acad Sci U S A. 2005;102(14):5215-20. PMCID: 555037.

130. Martinat C, Shendelman S, Jonason A, Leete T, Beal MF, Yang L, et al. Sensitivity to oxidative stress in DJ-1-deficient dopamine neurons: an ES-derived cell model of primary Parkinsonism. PLoS Biol. 2004;2(11):e327. PMCID: 521171.

131. Aleyasin H, Rousseaux MW, Phillips M, Kim RH, Bland RJ, Callaghan S, et al. The Parkinson's disease gene DJ-1 is also a key regulator of stroke-induced damage. Proc Natl Acad Sci U S A. 2007;104(47):18748-53. PMCID: 2141848.

132. Yanagisawa D, Kitamura Y, Inden M, Takata K, Taniguchi T, Morikawa S, et al. DJ-1 protects against neurodegeneration caused by focal cerebral ischemia and reperfusion in rats. J Cereb Blood Flow Metab. 2008;28(3):563-78.

133. Meulener MC, Graves CL, Sampathu DM, Armstrong-Gold CE, Bonini NM, Giasson BI. DJ-1 is present in a large molecular complex in human brain tissue and interacts with alpha-synuclein. J Neurochem. 2005;93(6):1524-32.

134. Zhou W, Zhu M, Wilson MA, Petsko GA, Fink AL. The oxidation state of DJ-1 regulates its chaperone activity toward alpha-synuclein. J Mol Biol. 2006;356(4):1036-48.

135. Neumann M, Muller V, Gorner K, Kretzschmar HA, Haass C, Kahle PJ. Pathological properties of the Parkinson's disease-associated protein DJ-1 in alpha-synucleinopathies and tauopathies: relevance for multiple system atrophy and Pick's disease. Acta Neuropathol. 2004;107(6):489-96.

136. McCoy MK, Cookson MR. DJ-1 regulation of mitochondrial function and autophagy through oxidative stress. Autophagy. 2011;7(5):531-2. PMCID: 3127213.

137. Bretaud S, Allen C, Ingham PW, Bandmann O. p53-dependent neuronal cell death in a DJ-1-deficient zebrafish model of Parkinson's disease. J Neurochem. 2007;100(6):1626-35.

138. Culmsee C, Mattson MP. p53 in neuronal apoptosis. Biochem Biophys Res Commun. 2005;331(3):761-77.

139. Milne DM, Campbell LE, Campbell DG, Meek DW. p53 is phosphorylated in vitro and in vivo by an ultraviolet radiation-induced protein kinase characteristic of the c-Jun kinase, JNK1. J Biol Chem. 1995;270(10):5511-8.

140. Trimmer PA, Smith TS, Jung AB, Bennett JP, Jr. Dopamine neurons from transgenic mice with a knockout of the p53 gene resist MPTP neurotoxicity. Neurodegeneration. 1996;5(3):233-9.

141. Duan W, Zhu X, Ladenheim B, Yu QS, Guo Z, Oyler J, et al. p53 inhibitors preserve dopamine neurons and motor function in experimental parkinsonism. Ann Neurol. 2002;52(5):597-606.

142. Mengesdorf T, Jensen PH, Mies G, Aufenberg C, Paschen W. Down-regulation of parkin protein in transient focal cerebral ischemia: A link between stroke and degenerative disease? Proc Natl Acad Sci U S A. 2002;99(23):15042-7. PMCID: 137541.

143. Petrucelli L, O'Farrell C, Lockhart PJ, Baptista M, Kehoe K, Vink L, et al. Parkin protects against the toxicity associated with mutant alpha-synuclein: proteasome dysfunction selectively affects catecholaminergic neurons. Neuron. 2002;36(6):1007-19.

CHAPTER TWO: THE HOMOCYSTEINE-INDUCIBLE ENDOPLASMIC RETICULUM (ER) STRESS PROTEIN HERP COUNTERACTS MUTANT A-SYNUCLEIN-INDUCED ER STRESS VIA HOMEOSTATIC REGULATION OF ER-RESIDENT CALCIUM RELREASE CHANNEL PROTEINS

Human Molecular Genetics (IN PRESS), published by Oxford University Press

Introduction

Parkinson's disease (PD) is a progressive neurodegenerative movement disorder that results from the degeneration of dopaminergic (DA) neurons in the substantia nigra (1). A common pathological feature of PD is the aggregation of α-synuclein (αSyn) into cytoplasmic inclusions called Lewy bodies in the degenerating dopaminergic neurons (1). Cell culture studies have shown that overexpression, impaired turnover, and mutations lead to αSyn aggregation (2). Two missense mutations (Ala53Thr and Ala30Pro) in αSyn that cause early-onset, autosomal dominant forms of PD enhance the aggregation and toxicity of the protein (2). Duplication or triplication of the *αSyn* gene was also found to cause early onset PD suggesting that elevated levels of wild-type αSyn can also lead to neurotoxicity (3). It is not yet clear how αSyn aggregation induces the degenerative cascades leading to PD.

Recent studies have demonstrated that mutant αSyn may exert its pathological effects in parts by inactivating the Grp78/Bip chaperone function (4) or impeding endoplasmic reticulum (ER) to Golgi vesicular transport (5) leading to abnormal accumulation of proteins within the ER and induction of ER stress. Cells respond to ER

stress by activating the unfolded protein response (UPR) aimed at inducing translational repression and expression of ER-resident chaperones to enhance protein folding, processing and degradation of misfolded proteins, thus relieving cells from ER stress (6). Prolonged or unmitigated ER stress associated with insufficient degradation of misfolded proteins or deranged Ca^{2+} homeostasis would subsequently activate ER stress-associated apoptotic pathways (7).

Hallmarks of ER stress are detected in several experimental models of PD (8, 9) and in nigral dopaminergic neurons of PD subjects (10). Expression of PD-linked mutant αSyn elevates CCAAT/enhancer binding protein (C/EBP) homologous protein (CHOP) (11), an ER stress-induced apoptotic mediator (12). CHOP is also elevated in neurotoxin models of PD (8, 9) and is a critical mediator of apoptotic death in substantia nigra dopamine neurons (13). Salubrinal, a neuroprotective agent that acts to inhibit ER stress protects cells from death induced by overexpression of mutant αSyn (11). Furthermore, ER stress is closely associated with the aggregation of αSyn in dopaminergic neurons (10). Though these studies suggest that ER stress is of pathophysiological relevance in PD, the underlying mechanisms of ER stress-mediated degenerative cascades and the specific roles of the various UPR proteins in PD pathogenesis remain unknown.

Herp (Homocysteine-inducible ER stress protein) is an ER integral membrane protein with the N-terminal ubiquitin-like domain projecting into the cytosol (14). Upregulation of Herp is essential for neuronal survival as Herp knockdown enhances vulnerability to ER stress-induced apoptosis (15, 16). How Herp contributes to the restoration of ER homeostasis remains unclear. Herp appears to stabilize ER Ca^{2+}

homeostasis and mitochondrial function in neural cells subjected to ER stress (16). Herp may also play an essential role in ER-associated protein degradation (ERAD), the primary mechanism of misfolded protein degradation, as its knockdown results in the selective accumulation of ERAD substrates (17). Recent studies demonstrated that Herp is induced in PD substantia nigra and is present in the core of Lewy bodies (18). The roles of Herp in PD remain unknown. Because Herp was shown to be critical for survival adaptation in the neurotoxin models of PD (19), we investigated whether Herp may counteract the neurodegenerative cascades caused by induced expression of mutant αSyn. We found that Herp plays an essential role in suppressing mutant αSyn-induced activation of ER stress-associated apoptosis signaling by inhibiting the deregulated ER Ca^{2+} release associated with the aberrant accumulation of ER resident Ca^{2+} release channels.

Materials and Methods

Cells, Plasmid and Reagents

Pheochromocytoma 12 (PC12) and human embryonic kidney 293 (HEK293) cells were purchased from ATTC. PC12 cells were selected because they are dopaminergic and have been extensively studied as models of neuronal degeneration. The pcDNA3.1 plasmids containing the c-myc-tagged full-length or loss-of-function deletion of human Herp cDNA have been described previously (16, 19). Xestospongin C (Tocris), dantrolene (Sigma), bradykinin (Sigma) were prepared as concentrated 1000x stocks in dimethylsulfoxide (DMSO; Sigma) or Lock's solution (mM): NaCl, 154; KCl, 5.6; $CaCl_2$, 2.3; $MgCl_2$, 1.0; $NaHCO_3$, 3.6; glucose, 10; Hepes buffer, 5 (pH 7.2). Salubrinal was

purchased from Santa Cruz. The dose of each drug was selected based on previously published studies (11, 20). Caffeine (Sigma) was freshly prepared in water. Additional reagents included: Lipofectamine 2000, TRIzol, Opti-MEM, priopidium iodide, and protein A beads (Invitrogen), MG-132 (BioMol), Trypan blue solution (0.4%; VWR), and tunicamycin (Sigma).

Cell Culture, Transduction, and Electroporations

PC12 and HEK293 cells were maintained in a humidified 5% CO_2 and 95% air atmosphere at 37 °C in Dulbecco's Modified Eagle Medium (DMEM) high glucose medium supplemented with 10% heat-inactivated horse serum, 5% heat-inactivated fetal bovine serum, 50 units/ml penicillin, and 0.05 mg/ml streptomycin (16, 20). PC12 cell lines expressing the human wild-type and mutant αSyn were generated using a tetracycline (Tet)-on system. For the induction of αSyn expression, culture medium was replaced every other day with DMEM containing 1% horse and 0.5% fetal bovine sera (InVitrogen), 100 ng/ml nerve growth factor (Upstate) and Tet (2 µM; Sigma). In some studies, non-induced clones were transduced with recombinant adeno-associated viral (rAAV) particles prior to induction with Tet. Transient transfection was carried out using the Neon transfection system according to the manufacture's instructions (Invitrogen). PC12 cells (1-2 x 10^7/ ml) were transfected by electroporation with 4-8 µg of empty vector, wild-type αSyn, or mutant αSyn (gift from Dr. R.G. Perez, Department of Neurology, University of Pittsburgh) using the following optimized conditions: 1400 V, 20 ms and 1 pulse. The transfection efficiency following electroporation with wild-type αSyn-GFP was ~70%.

Ectopic Expression of Herp

The Herp and ΔUBL-Herp constructs have been inserted into a rAAV expression construct (GenDetect). The resulting cDNAs were cloned into the HindIII/BamHI site of the pAd-YC2 shuttle vector. For homologous recombination, the shuttle vector (5 μg) and rescue vector pJM17 (5 μg) were co-transfected into HEK293 cells. To amplify the recombinants, cell culture supernantant was serially diluted into serum-free media and incubated with HEK293 cells. The recombinants were purified from supernatants by ultracentrifugation. The band containing mature viral particles were collected and desalted against phosphate-buffered saline (PBS) in a Vivaspin column (Vivascience AG), and titers were determined by counting the number of plaques. Cells were infected with the virus at a MOI of 500 in medium containing 2% FBS for 4 h, after which DMEM containing 10% FBS was added. Analysis of rAAV-GFP expression indicated an infection rate of ~85-90%.

Experimental Treatments

To induce ER stress, cultures of PC12 cells were treated with 20 μg/ml Tuni. In some studies, the proteasomal inhibitor MG-132 (0.1-10 μM) or salubrinal (75 μM) were added prior to Tuni. These drugs were prepared in DMSO immediately before applying them to the cultures. When DMSO was used as the solvent, their final concentration did not exceed 0.1%. At the end of each treatment, the cultures were processed for immunoblotting and evaluating cell viability.

RNA interference (RNAi)

Cells were transfected with Mission predesigned siRNA duplexes (Sigma) targeting Herp, IP3R1, RYR1, and RYR3, or a control siRNA (siRNA-Con; Ambion) using Lipofectamine 2000 (Invitrogen) in Opti-MEM according to manufacturer's protocol. The target sequences of each siRNA are listed in **Supplemental Tables 1S**. Results of quantitative RT-PCR analysis of total RNA from PC12 cells and tissue samples revealed expression of IP3R2, IP3R3 and RYR2 below the limit of detection of the qRT-PCR assay method (Ct values >35). The optimized siRNA concentrations are 100 nM of siRNA-Herp, 250 nM of siRNA- IP3R1, and 100 nM of each siRNA-RYR1 and siRNA-RYR3 added in combination. After 4 h of transfection, the medium was replaced, and 24-48 h later, the indicated experiments were conducted. To monitor knockdown, cells were harvested and processed for qRT-PCR and Western blot analyses. The transfection efficiency of siRNA-Con-FITC (Santa Cruz) in PC12 cells was greater than 95% (data not shown).

Assessment of Cell Death

Cell death was assessed by either trypan blue exclusion or propidium iodide staining as described previously (16, 20). Trypan blue and propidium iodide (50 μg/ml) stain only the cells with disrupted plasma membrane integrity so these cells were considered dead. The PI was excited with the 568-nm yellow line of a confocal microscope (Leica), and the acquisition of PI labeling images was performed at the wavelength higher than 600 nm via a photomultiplier through a band-pass filter centered at 605 nm. Dead cells were counted in four microscopic fields per dish, with a minimum of 100 cells per field and results were expressed as a percentage of the total number of

cells. All of the experiments were repeated at least three times without knowledge of treatment history.

Immunoprecipitation

Cells and tissues were solubilized in binding buffer containing 50 mM Tris–HCl (pH 7.4), 150 mM NaCl, 1 mM EDTA, 1 mM DTT, 0.2 mM phenylmethanesulfonyl fluoride, and 1.0% NP-40 as described previously (21). The homogenate was centrifuged at 20,000 × g for 10 min. Solubilized proteins were adjusted to 0.1% NP-40 and incubated for 12 h at 4 °C with a polyclonal antibody to anti-Herp (BioMol), IP3R1 (Millipore) or pan-RyR (Santa Cruz). After an additional incubation with protein A conjugated beads, the immune complexes were then recovered by low speed centrifugation and washed extensively with the binding buffer containing 0.1% NP-40. Immunoprecipitated proteins were eluted by boiling in SDS-PAGE sampling buffer and analyzed by immunoblotting.

Immunoblotting

Protein lysates were centrifuged at 20,000 g and equal amounts of the proteins were loaded into each well of a SDS-PAGE. After electrophoretic separation and transfer to nitrocellulose membranes (Bio-rad), blots were incubated in blocking solution (5% milk in TBS-T) for 1 h at RT, followed by an overnight incubation with primary the following antibodies diluted in blocking buffer: α-Syn [human specific antibody (Abcam) or cross-reactive with human, rat, and mouse (Santa Cruz)], KDEL (Santa Cruz), actin (Sigma), ERK1 (Cell Signaling), caspase-12 (Abcam), Herp [polyclonal antibody (Biomol) and monoconal antibody (Santa Cruz)], CHOP (Abcam), IP3R1 (Millipore),

pan-RyR (Santa Cruz), S5a (Cell Signaling) and presenilin 1 (Abcam). Membranes were then incubated for 1 h in secondary antibody conjugated to horseradish peroxidase (HRP), and bands were visualized by enhanced chemiluminescence (ECL, Thermo-Scientific). Membranes were stripped and re-probed with either the actin or ERK1 antibody to normalize protein loading. The intensity of the signals obtained was quantified by densitometric scanning using Scion (NIH Image).

Immunostaining

Spinal cords were removed after perfusion with heparinized saline (0.9% NaCl) transcardially followed by 4% buffered paraformaldehyde (PFA) and post-fixed overnight in PFA. Serial sections of the lumbar region were sectioned at 30 µm with a freezing microtome (Microm HM 505 N) and collected on slides. Cultured cells plated on coverslips were fixed for 20 min with 4% paraformaldehyde in PBS following experimental treatments. Cells were then incubated for 5 min in a solution of 0.2% Triton X-100 in PBS and for 1 h in blocking solution (0.02% Triton X-100, 5% normal horse or goat serum in PBS). Tissue sections and coverslips were processed for immunofluorescence staining as described (16, 21) with the following primary antibodies: αSyn (Abcam), nitro-αSyn (Abcam), Herp (Santa Cruz); CHOP (Cell Signaling); KDEL (Santa Cruz); pan-RyR (Santa Cruz), IP3R1 (Millipore), and NeuN (Millipore). All antibodies were diluted in blocking solution and used within the concentration ranges recommended by the manufacturer. To test for nonspecific staining by the secondary antibodies, additional sections or coverslips were processed in a similar fashion without the primary antibodies or with adsorbed antibodies. After three washes, sections or coverslips were incubated with fluorescein isothiocyanate

(FITC)-conjugated anti-rabbit and Cy3-conjugated anti-mouse secondary antibodies and then mounted. To stain the nuclei, sections or coverslips were further incubated with the nucleic acid stain 4',6-diamidino-2-phenylindole (DAPI) in PBS containing 1% RNase and 0.2% Triton X-100 for 10 min, and then mounted in FluorSave aqueous mounting medium (Calbiochem). Immunofluorescence staining was examined by using a NIKON 80i fluorescent microscope equipped with a x60 oil immersion objective lens. For quantification, digitized images of immunostained sections were obtained with Qimaging Retiga 2000 SVGA FAST 1394 cooled digital camera system mounted on the microscope and then analyzed with IP lab software (BD Biosciences- Bio-imaging). Total area of pixel intensity was measured with the automated measurement tools in IP lab software. The total density was averaged and expressed as normalized, corrected values.

Measurement of [Ca^{2+}]i

PC12 cells were plated at a density of $1x10^6$ cells / 35mm glass bottom MatTek dish (Ashland) the day before the experiment. Cells were loaded with 2 μM Fura-2 acetoxymethyl ester in Krebs–Ringer-Hepes (KRH) buffer [129mM NaCl, 5mM $NaHCO_3$, 4.8mM KCl, 1.2mM KH_2PO_4, 1mM $CaCl_2$, 1.2mM $MgCl_2$, 10 mM glucose and 10mM Hepes (pH7.4)], for 20 minutes and then washed twice with KRH and incubated for additional 30 minutes at 37°C. Dishes were placed into a heated chamber mounted on the stage of an inverted fluorescence microscope (Nikon Eclipse TiE with perfect focus and DG-5 Xenon excitation) and perfused with Ca^{2+}-deficient KRH at a rate of 1.5 ml/ minute. Baseline was established for 6 minutes before stimulation. Measurements were continued for 4-5 min after Ca^{2+} peak was recorded. Fura-2 dual excitation images

were captured through a Nikon S Fluor 20X objective (NA 0.75) with a Photometrics QuantEM 16bit EMCCD camera using 340 nm and 380 nm excitation filters and a 470-550nm emission filter. Data were acquired and analyzed using Nikon Elements software. Background fluorescence signals were collected at the same rate for the same wavelengths and were subtracted from the corresponding fluorescence images. The fluorescence intensities of 10-20 cells / dish were expressed as ratio of excitation 340/380 nm and area under the curve (AUC).

RT-PCR and Quantitative Real Time-PCR (qRT-PCR)

Total RNA was isolated with TRIzol (Invitrogen). To prevent genomic DNA contamination, the isolated total RNA samples were treated with DNAse. 2 µg of total RNA was reverse transcribed with Superscript II reverse transcriptase and an oligo(dT) primer (Invitrogen). RT-PCR products were resolved on agorose gels stained with ethidium bromide. Relative quantification of gene expression was performed by normalizing the fluorescence intensities of each band to those of actin. qRT-PCR was performed as previously described (22). The integrity of the RT-PCR products was confirmed by melting curve analysis. Melting curves for all reaction showed one specific peak. We used 18 S rRNA as an endogenous control to normalize variations in RNA extraction and variability in RT efficiency. mRNA levels were quantified with the comparative C_t method (22). The pairs of primers used for RT-PCR and qRT-PCR are listed in Supplemental **Tables 2** and **3**, respectively.

Animals

Mice transgenic for human A53Tα-Syn (THY1-SNCA-A53T; Jackson) have been characterized in a previous study (30). All animal experimental procedures were performed in accordance with the guidelines of the NIH and approved by the Institutional Animal Care and Use Committee at University of Central Florida.

Statistical analysis

Comparison between two groups was performed using Student's *t* test, whereas multiple comparisons between more than two groups was analyzed by one-way ANOVA and post hoc tests by least significant difference. Data evaluated for the effects of two variables was analyzed using two-way ANOVA (Prism 4 version 4.03; GraphPad Software, Inc.). Results are presented as means ± SEM. For all analyses, statistical significance is defined as a p value of ≤ 0.05.

Supplementary Methods

Calcium imaging

PC12 cells were plated on 35-mm glass bottom dishes (Matek) and loaded with 4 µM Fluo-4 acetoxymethyl ester (Invitrogen) in Lock's buffer at 37 °C for 30 min. The cells were then washed twice with and incubated in Lock's buffer for an additional 30 min, and then mounted on the stage of an inverted confocal microscope (Carl Zeiss) equipped with a 40× objective. To trigger ER Ca^{2+} release, 10 µM bradykinin was added directly to the cell solution. Cells were excited using the 488-nm laser line, and images were acquired at 5-s intervals under time-lapse mode.

Immunoprecipitation

Cell lysates and tissue homogenates were incubated with an antibody to Herp (BioMol), c-myc (Sigma), S5a (Cell Signaling), IP3R1 (Millipore), pan-RyR (Santa Cruz) or αSyn (Abcam and Santa Cruz) antibody in binding buffer containing 50 mM Tris–HCl (pH 7.4), 150 mM NaCl, 1 mM EDTA, 1 mM DTT, 0.2 mM phenylmethanesulfonyl fluoride, and 1.0% NP-40. Antigen-antibody complexes were precipitated with immobilized protein A, washed three times in immunoprecipitation buffer, and solubilized by heating in Laemmli buffer containing 2-mercaptoethanol at 100 °C for 4 min. The solubilized proteins were separated by electrophoresis and analyzed by immunoblotting.

Results

Expression of Mutant αSyn Evokes a Sustained ER Stress Response

Previous studies provide evidence that mutant αSyn triggers a cell death program that involves activation of the ER stress response (11). It is yet not clear which and how ER stress proteins contribute to mutant αSyn-induced cell death. To investigate the role of Herp in the mutant αSyn-induced degenerative process, we generated Tet-inducible PC12 cells. Time course analysis indicated that αSyn protein level reaches a plateau 48 h after induction (**Fig. 1A**). Concurrently, mRNA and protein levels of the ER stress markers Grp78 and Herp were markedly elevated in the PC12 cells expressing mutant αSyn, especially those expressing A53TαSyn (PC12-A53TαSyn), when compared to PC12 cells expressing wild-type αSyn (PC12-WTαSyn) (**Fig. 1B**). Levels of CHOP were also markedly higher in PC12-A53TαSyn (**Fig. 1B**)

suggesting, that at this expression level, there was a selective deleterious effect of A53TαSyn but not WTαSyn. Similar results were obtained in PC12 cells transiently expressing A53TαSyn and WTαSyn (**Fig. 1C**).

Herp Protects Against Mutant αSyn-Induced Cell Death

Compared to PC12 cells stably expressing the empty vector (PC12-VT), PC12-WTαSyn and PC12-A30PαSyn, PC12-A53TαSyn exhibits significantly higher baseline cell death (**Fig. 2A**) which correlated with increased CHOP protein level and caspase-12 activation (**Fig. 2B**). Because A53TαSyn enhances activation of ER stress-related apoptosis signaling, we utilized PC12-A53TαSyn in subsequent knockdown studies. PC12-A53TαSyn treated with a small interference RNA (siRNA) targeting Herp (siRNA-Herp) but not a non-silencing control siRNA (siRNA-Con) exhibited higher basal rate of cell death (**Fig. 2C**). In contrast, ectopic expression of Herp, but not the dominant-negative mutant ΔUBL-Herp that lacks the UBL domain (**Fig 2D**), significantly improved the viability of PC12-A53TαSyn (**Fig. 2E**). Notably, ΔUBL-Herp appeared to potentiate A53TαSyn-induced cell death consistent with a dominant-negative action of ΔUBL-Herp as reported previously (19).

Mutant αSyn Perturbs ER Ca^{2+} Homeostasis During ER Stress

Given that Herp protects from A53TαSyn-induced death (**Figs 2C, E**) and that Herp plays a crucial role in stabilizing ER Ca^{2+} homeostasis in ER-stressed PC12 cells (16), we next determined whether A53T-αSyn may perturb ER Ca^{2+} regulation by altering the activity of the two main classes of ER-resident Ca^{2+} release channels, IP_3R

(inositol triphosphate receptor) and RYR (ryanodine receptor) which can be activated by their respective agonists, bradykinin and caffeine (20-22). The average peak amplitude of bradykinin-evoked Ca^{2+} release in the absence of extracellular Ca^{2+} was significantly larger in PC12-A53TαSyn when compared to PC12-WTαSyn and PC12-VT (**Fig 3A**) indicating that A53TαSyn enhances ER Ca^{2+} release. No significant difference was observed in thapsigargin-induced depletion of ER Ca^{2+} store (**Supplementary Fig 1A**) suggesting that the ER stress–induced perturbation of intracellular Ca^{2+} level ($[Ca^{2+}]i$) in PC12-A53TαSyn cannot be explained by higher ER lumenal Ca^{2+} but rather is caused by a higher fraction of ER Ca^{2+} being released via IP_3R.

Tunicamycin (Tuni) is a classical ER stressor that induces a sustained increase of ER stress proteins (**Supplementary Fig 1B, C**). The magnitude of the bradykinin-evoked Ca^{2+} release was also higher in PC12 cells treated with Tuni (PC12-Tuni) when compared to control cells that were left untreated or treated with vehicle (data not shown; 16,19). Consequently, treatment with BAPTA-AM, a cell permeable Ca^{2+} chelator, markedly improves the viability of both PC12-A53TαSyn and PC12-Tuni (**Fig 3B**) suggesting that Tuni and A53TαSyn increase susceptibility to ER stress-induced death by enhancing ER Ca^{2+} release.

Mutant αSyn-Induced ER Stress Perturbs Homeostatic Regulation of ER-Resident Ca^{2+} Release Channels

Next, we determined whether the heightened cytosolic Ca^{2+} level in PC12-Tuni and PC12-A53TαSyn results from altered homeostatic regulation of ER-resident Ca^{2+} release channels. Three distinct types of IP_3Rs (types 1–3) have been cloned in mammals and each type shows distinct properties in terms of their IP_3 sensitivity,

modulation by cytoplasmic Ca^{2+} concentration, and unique tissue distribution (23,24). Among them, the type 1 IP_3R (IP_3R1) is highly expressed in the central nervous system (24). qRT-PCR analysis showed that IP_3R1 is the major IP_3R isoform expressed in PC12 cells (unpublished data). PC12 cells also express RYR1 and RYR3 (pan-RyR) (20, 21). Levels of IP_3R2, IP_3R3, and RYR2 mRNAs were not assessed due to their low abundance in PC12 cells. PC12-Tuni exhibit marked accumulation of IP_3R1 and pan-RyR protein (**Fig 3D; Suppl Fig 1C**) consistent with the notion that Tuni-induced ER stress leads to disruption of ER Ca^{2+} homeostasis (16). Expression of A53TαSyn also induces a marked increase in the protein levels of IP_3R1 (**Fig 3E**) and pan-RyR (**Fig 3F**) suggesting that the aberrant accumulation of ER Ca^{2+} release channels was likely mediated through a common ER stress-related mechanism. Consistent with the elevated pan-RYR protein levels, PC12-Tuni and PC12-A53TαSyn were more vulnerable to cell death in the presence of caffeine when compared to their respective controls (**Supplementary Fig 1D**). By contrast, level of presenilin1 (PS1) which functions as a passive ER Ca^{2+} leak channel (25), was not markedly altered by ER stress (**Fig 3D, E**). It is worth noting that unlike the increase of ER stress proteins which is mediated by a transcriptional mechanism (6, 7), the ER stress-associated accumulation of IP_3R1 and pan-RYR was independent of transcription (**Supplementary Fig 1E,F**).

Inhibition of Deregulated ER Ca^{2+} Release Ameliorates ER Stress-Mediated Cell Death and αSyn Aggregation

Because ER-released cytosolic Ca^{2+} plays a critical role in the activation of several death effector pathways (16), we next determined whether blockade of ER Ca^{2+}

release may ameliorate ER stress-induced cell death. Xestospongin C (a blocker of IP_3R) and dantrolene (a RyR blocker) at doses that did not cause robust death within 24 h substantially improved the viability of PC12-Tuni (**Fig 4A**) and PC12-A53TαSyn (**Fig 4B**). Neither IP_3R nor RyR inhibition altered the expression of αSyn (data not shown), thereby confirming that inhibition of ER Ca^{2+} release rather than reduced expression of A53T-αSyn contributes to cell protection.

To further determine whether these ER-resident Ca^{2+} release channels are responsible for the heightened sensitivity of PC12-A53TαSyn to ER stress-mediated cell death, we knocked down each channel protein at a time by using either siRNA-IP_3R1 or siRNA-RYR1 and siRNA-RYR3 in combination (**Fig 4C**). The non-silencing control siRNA (siRNA-Con) alone did not alter IP3R1 nor RYR1/RYR3 expression (not shown). A close correlation between protein levels of these ER Ca^{2+} release channels and the ER stress-induced apoptotic mediator CHOP (**Supplementary Fig 2**) was observed in PC12-Tuni (**Fig. 4D**) and PC12-A53TαSyn (**Fig 4E**). CHOP which is known to be upregulated following a severe or prolonged ER stress, was markedly suppressed along with Herp and Grp94/78 in PC12-Tuni transfected with the silencing siRNAs (**Supplementary Fig 2**). These data suggest that impaired homeostatic regulation of ER-resident Ca^{2+} release channels might underlie chronic activation of ER stress and associated apoptosis signaling.

Because ER-released cytosolic Ca^{2+} plays a role in promoting αSyn aggregation (26), we next examined αSyn inclusion formation in PC12 cells transiently transfected with either WTαSyn or A53TαSyn tagged to green fluorescent protein (GFP) by fluorescence microscopy. Xestospongin C substantially reduces not only the fraction of

cells bearing cytoplasmic αSyn inclusions but also the size of the inclusions (**Supplementary Fig 3**). These fluorescent aggregates were not detected in PC12 cells transfected with GFP alone (data not shown).

Salubrinal Inhibits ER Stress-mediated Cell Death by Preventing the Aberrant Accumulation of ER-Resident Ca^{2+} Release Channels

Next, we asked the question whether salubrinal, a compound that has been shown to ameliorate A53TαSyn-induced cell death (11), may counteract prolonged ER stress through the homeostatic regulation of ER-resident Ca^{2+} release channels. Salubrinal at a dose that inhibits the cellular phosphatase complexes that dephosphorylate eiF2α (**Supplementary Fig 4**) not only blocks the ER stress-associated increase of IP_3R and pan-RYR but also dramatically reduces protein levels of Herp, Grp94/78 and CHOP in both PC12-Tuni (**Fig 5A**) and PC12- A53TαSyn (**Fig 5B**) suggesting that this compound likely ameliorates ER stress by improving the homeostatic regulation of ER Ca^{2+} release channels through a mechanism that is independent of transcription (**Fig 5C**). By contrast, salubrinal did not alter PS1 protein level in PC12-Tuni (**Fig 5A**) and PC12-A53TαSyn (**Fig 5B**). The salubrinal-mediated decrease of ER Ca^{2+} release channels was accompanied by a substantial reduction in the bradykinin-evoked Ca^{2+} transients in both PC12-Tuni (**Supplementary Fig 5A**) and PC12-αA53TSyn (**Supplementary Fig 5B**). Consequently, salubrinal also significantly ameliorates the Ca^{2+} dependent aggregation of A53TαSyn-GFP in the cytosol (**Supplementary Fig 3**).

Herp Counteracts ER Stress Through the Homeostatic Regulation of ER-Resident Ca^{2+} Release Channels

Because Herp counteracts Tuni-induced cell death through the stabilization of ER Ca^{2+} homeostasis (16), we next determined whether Herp protects PC12-A53TαSyn (**Fig 2C, D**) by a similar mechanism. Knockdown of Herp substantially increases the amplitude of the bradykinin (BK)- induced Ca^{2+} transients (**Fig 6A**) that result from the marked accumulation of IP_3R1 (**Fig 6B; Supplementary Fig 6A**). Levels of pan-RYR but not PS1 proteins were also affected by Herp knockdown (**Fig 6B; Supplementary Fig 6A**). Consequently, the deficits in Herp-dependent homeostatic regulation of ER Ca^{2+} release channels is also accompanied by increased levels of the ER stress markers Grp94/78 and CHOP (**Fig 6B; Supplementary Fig 6A**) and enhanced vulnerability to αSyn-induced death (**Fig 6C**). Conversely, ectopic expression of Herp suppresses the aberrant accumulation of IP_3R1 and pan-RYR but not PS1 proteins (**Fig 6D; Supplementary Fig 6B**). Neither knockdown nor ectopic expression of Herp alters mRNA levels of IP_3R1 and pan-RYR (**Supplementary Fig 6C, D**) suggesting that, analogously to salubrinal, Herp promotes the homeostatic regulation of these ER-resident Ca^{2+} release channels through a mechanism that is independent of transcription.

Knockdown of Herp also increases basal (**Fig 6E, F**) and stress-induced accumulation (**Fig 6E, G**) of both IP_3R1 and pan-RYR proteins independently of transcription (**Fig 6H**) in PC12-Tuni. Consistent with the notion that Herp counteracts Tuni-induced death (19), knockdown of Herp results in a significant increase of CHOP protein by transcriptional regulation (**Fig 6 E, H**).

Herp Promotes Degradation of ER-Resident Ca^{2+} Release Channels Through ERAD

Because Herp has been shown to bind to and target protein substrates for ERAD (17), we next tested whether Herp modulates the levels of IP_3R1 and/or pan-RYR proteins by a similar mechanism. Immunoprecipitation with an anti-Herp antibody followed by immunoblotting with antibodies to each ER Ca^{2+} release channel demonstrated that a greater fraction of Herp forms a complex with IP_3R1 and pan-RYR in PC12-Tuni when compared to vehicle-treated control cells (**Fig 7A**). The specificity of the interaction was confirmed by immunoblotting the Herp-containing protein complex with an antibody to Grp78 (**Supplementary Fig 7A**) and by performing the co-immunoprecipitation assay using lysates from HEK293 expressing c-myc-tagged Herp (**Supplementary Fig 7B**). Neither the pre-immune normal IgG nor Grp78 antibody forms a protein complex with Herp. Double immunofluorescence labeling confirmed Herp colocalization with each ER Ca^{2+} release channel protein in PC12-Tuni (**Supplementary Fig 7C**). Herp also interacts with A53TαSyn (**Supplementary Fig 7D, E**) suggesting that this interaction could possibly interfere with the protective role of Herp (see discussion).

To determine whether binding of Herp to IP_3R1 and pan-RYR results in proteasome-mediated protein degradation of these Ca^{2+} release channel proteins, PC12 cells were treated with the proteasome inhibitor MG-132. Consistent with the notion that the degradation of IP_3R1 and pan-RYR proteins is mediated by the proteasomes (27, 28), MG-132 markedly increases steady-state protein levels of these ER-resident Ca^{2+} release channels (**Fig 7B; Supplementary Fig 8A**). Ectopic expression of Herp results in a significant reduction of IP_3R1 and pan-RYR protein

levels (**Fig 7C**) that can be reversed upon inhibition of proteasome activity (**Fig 7D, Supplementary Fig 8B**). Note that MG-132 also increases Herp protein levels (**Fig 7B, D**) suggesting that Herp itself is a proteasome substrate (29). In support for this notion, Herp interacts and co-localizes with the ubiquitin-interacting S5a subunit of the proteasome in PC12-Tuni (**Supplementary Fig 9A, B**). Increased co-localization of S5a with the Grp78-labeled ER was also detected in PC12 cells transfected with Herp (**Suppl Fig 9B**). Though S5a protein level was not markedly altered in PC12-Tuni (**Supplementary Fig 9C**), knockdown of Herp substantially reduces S5a co-localization with the ER in PC12-Tuni suggesting that ER stress-induced upregulation of Herp but not S5a is sufficient for the recruitment of proteasomes to the ER (**Supplementary Fig 9D**). Collectively, our data indicate that aberrant accumulation of IP_3R and pan-RYR perturbs ER Ca^{2+} homeostasis in ER stressed cells and that Herp prevents aberrant ER Ca^{2+} release by targeting these ER-resident Ca^{2+} release channels for ERAD.

Accumulation of ER Stress Markers and ER-Resident Ca^{2+} Channels in A53TαSyn Transgenic Mice

Next, we explored whether A53TαSyn-induced ER stress markers and ER Ca^{2+} channels were detected *in vivo*. Transgenic mice overexpressing A53TαSyn (A53T mice) develop motor abnormalities associated with the accumulation of αSyn inclusions in spinal cord motor neurons (30). Immunoblotting reveals marked upregulation of Herp and Grp78/Bip proteins in spinal cords of $\geq$8 months old A53T mice (symptomatic) when compared to 2 months old A53T mice (pre-symptomatic) and non-transgenic (Non-Tg) mice (**Fig 8A, B**). CHOP protein was low in Non-Tg mice but was readily detected in A53T mice (**Fig 8A, B**). Immunohistochemistry indicates a marked

increase of nitrated αSyn in NeuN-labeled spinal cord neurons and further confirms the increase of ER stress markers and ER-resident Ca^{2+} release channels in 13-15 months old (symptomatic) when compared to 5 months old (pre-symptomatic) A53T mice (**Supplementary Fig 10 A**). By contrast to the ER stress markers, the upregulation of ER-resident Ca^{2+} release channels was not attributed to increased expression (**Supplementary Fig 10 B**). The amounts of IP_3R1 and pan-RYR in the spinal cord homogenates that form a protein complex with Herp were also markedly higher in A53T compared to Non-Tg mice (**Fig 8C**) consistent with the notion that ERAD may contribute to the homeostatic regulation of ER Ca^{2+} release channel proteins in spinal cord motor neurons. The interaction between Herp and A53TαSyn was also confirmed in spinal cords of symptomatic transgenic mice (**Supplementary Fig 10 C**) suggesting that this interaction may impair the ability of Herp to prevent the aberrant accumulation of ER-resident Ca^{2+} release channels and, hence, its ER Ca^{2+} -stabilizing action in ER stressed motor neurons. These findings link aberrant ER Ca^{2+} regulation and chronic ER stress to motor neuron dysfunction and death in the pathophysiology of synucleinopathies.

Discussion

Neuronal loss in both familial and sporadic forms of neurodegenerative disorders is accompanied by formation of protein inclusions or fibrillar aggregates composed of misfolded proteins that can induce ER stress. The accumulation of evidence that ER stress is critically involved in the pathogenesis of neurodegenerative disorders suggests that approaches that aim to halt ER stress may prevent the pathological cascades induced by protein inclusions. There is growing evidence that the ER can play pivotal

roles in regulating cell survival and apoptosis in a variety of cell types including neurons (30, 31), but the mechanisms linking ER stress to apoptosis are incompletely understood. The identification of conditions that slow ER stress may reveal novel strategies for counteracting ER stress-mediated cell death.

The ER is the major intracellular store of Ca^{2+} and aberrant regulation of luminal ER Ca^{2+} is thought to play critical roles in many apoptotic cascades (31). Deregulated ER Ca^{2+} homeostasis has also been implicated in the pathophysiology of chronic neurodegenerative diseases such as prion disorders, Huntington's and Alzheimer's (32-34). Here we showed that A53TαSyn evokes ER stress and that the attendant disturbances in ER Ca^{2+} homeostasis contributes to a higher sensitivity to ER stress-induced cell death. We demonstrate that Herp counteracts A53TαSyn-induced cell death by stabilizing ER Ca^{2+} homeostasis. Ectopic expression of Herp markedly reduced A53TαSyn-induced toxicity whereas knockdown of Herp exacerbates or prolongs ER stress leading to a significant augmentation of toxicity. Hence, a better understanding of the function of Herp is therefore of high significance to elucidate the functional link between the ER stress and ER Ca^{2+} homeostasis and to develop mechanism-based neuroprotective strategies for PD and related neurodegenerative diseases.

The underlying molecular mechanism(s) whereby Herp modulates ER Ca^{2+} homeostasis remains poorly understood. Knockdown of Herp leads to the accumulation of IP_3R1 and pan-RyR proteins in PC12 cells and, consequently, promotes aberrant ER Ca^{2+} release that in turn may decrease the threshold for the activation of ER stress-related cell death pathways. Consistent with this notion, gene knockdown and

pharmacological inhibition of ER Ca^{2+} release channels ameliorates ER stress and protects PC12- A53TαSyn and PC12-Tuni against ER stress-induced cell death (**Fig 4**). Conversely, overexpression of Herp stabilizes ER Ca^{2+} homeostasis and inhibits ER stress-induced cell death by preventing the accumulation of ER Ca^{2+} release channel proteins in PC12-A53TαSyn. It is noteworthy that the accumulation of IP_3R1 and pan-RyR proteins was partially suppressed in spite of the elevated level of endogenous Herp in PC12-A53TαSyn suggesting that binding of Herp to A53TαSyn (**Supplementary Fig 7D**) and its accumulation in the core of Lewy bodies (18) may interfere with its protective function and that ectopically expressed Herp can overcome this A53TαSyn-mediated inhibition.

Mechanistically, Herp interacts with and facilitates the degradation of ER Ca^{2+} release channel proteins by ERAD. Several recent studies support a role for Herp in ERAD (17) based on the notion that Herp is rapidly degraded in a proteasome-dependent fashion (29) and that knockdown of Herp leads to the accumulation of several established ERAD substrates (17). Herp has been shown to interact with Hrd1p, a membrane-anchored E3 ligase that is required for ERAD (17), and with ubiquilin, a shuttle protein that delivers ubiquitinated substrates to the proteasome for degradation (35). We found that Herp knockdown in ER stressed cells leads to the accumulation of both IP_3R1 and pan-RYR. Conversely, ectopic expression of Herp prevents the accumulation of these ER Ca^{2+} release channels. Treatment with MG-132 not only elevates the basal level of IP_3R1 and pan-RYR proteins but also prevents the ability of Herp to inhibit their accumulation in ER stressed cells (**Fig 7D**) suggesting the critical involvement of ERAD in the homeostatic regulation of these ER Ca^{2+} release channels.

Deletion and function analyses further support the involvement of ERAD in Herp-mediated cell protection via the stabilization of ER Ca^{2+} homeostasis. Ectopic expression of Herp lacking the UBL-domain which functions as a proteasome-interacting domain (17, 43) fails not only to stabilize ER Ca^{2+} homeostasis but also to protect PC12-Tuni (16) and PC12-A53TαSyn from ER stress-induced death (**Fig 2E**). Notably, salubrinal appears to modulate the vulnerability of PC12 cells to ER stress-induced cell death by preventing the accumulation of ER Ca^{2+} channels (**Fig 6**). How this eIF2α dephosphorylation inhibitor impacts the homeostatic regulation of ER Ca^{2+} channels remains to be investigated.

Our data provide the first evidence that ER stress is regulated by the activity of ER-resident Ca^{2+} release channels. We found that pharmacological inhibition or knockdown of ER Ca^{2+} release proteins ameliorates ER stress-induced cell death suggesting that aberrant ER Ca^{2+} release is associated with higher susceptibility to chronic enhancement of ER stress. Though the detailed mechanisms underlying Ca^{2+}-dependent cell death in PC12-A53TαSyn was not investigated in the present study, it is likely that accumulation of ER Ca^{2+} release channels leads to enhanced ER to mitochondria Ca^{2+} flow that triggers the loss of mitochondrial membrane potential and increased generation of reactive oxygen species (ROS) (16). Previous studies demonstrate that ROS-induced damage to the ER may amplify Ca^{2+} release via a mechanism involving oxidation-induced activation of RYR and IP_3R (36). Ectopic expression of Herp has been shown to counteract this deleterious positive feedback loop by inhibiting the proapoptotic Ca^{2+} flow from the ER to mitochondria in PC12 cells exposed to the PD-inducing toxin 1-methyl-4-phenylpyridinium (MPP^+) (19). The

increase of CHOP detected in PC12-Tuni, PC12-A53TαSyn and siRNA-Herp treated PC12 cells likely results from the depletion of ER Ca^{2+} store associated with the aberrant accumulation of IP_3R1 and pan-RYR as ectopic expression of Herp counteracts CHOP upregulation by promoting the homeostatic regulation of these ER Ca^{2+} channel proteins.

It is noteworthy that chronic enhancement of ER stress resulting from the disruption of ER Ca^{2+} homeostasis could trigger αSyn protein aggregation in the cytosol and that blockade of ER Ca^{2+} release channels (**Supplementary Fig 2**) ameliorates αSyn inclusion formation suggesting a causative link between chronic ER stress and αSyn oligomer formation. Consistent with this notion, sustained ER Ca^{2+} release triggered by thapsigargin accelerates the formation of potentially cytotoxic oligomers in αSyn-GFP transfected cells (26). Tuni at doses that induce chronic stress associated with sustained ER Ca^{2+} release (16, 37) has also been shown to promote the accumulation of αSyn oligomers (38). Because Sal ameliorates ER stress and protects PC12- Tuni and PC12-A53TαSyn, it is conceivable that its neuroprotective action may be due to improved regulation of ER Ca^{2+} homeostasis. In support of this notion, Sal inhibits the aberrant accumulation of ER-resident Ca^{2+} release channels (**Fig 6**) and prevents αSyn aggregation (**Supplementary Fig 5**).

Consistent with the findings in PC12-A53T cells, we detected higher levels of several ER stress markers including the ER stress-induced apoptotic mediator CHOP, and ER-resident Ca^{2+} release channels in the spinal cords of symptomatic A53T mice when compared to Non-Tg and pre-symptomatic A53T mice suggesting that accumulation of A53TαSyn promotes motor neuron degeneration in part by a

mechanism involving chronic ER stress associated with the deregulation of ER Ca^{2+} homeostasis. In addition to the elevation of Herp protein, we detected increased interaction of Herp with A53TαSyn in spinal cord homogenates of symptomatic A53T mice which further supports the notion that Herp-dependent ERAD of ER-resident Ca^{2+} release channels may be impaired in vulnerable motor neurons.

Dopaminergic neurons appear to be relatively resistant to degeneration in A53T mice (30, 39) and express relatively high levels of the Ca^{2+}-binding protein calbindin (39). By contrast, spinal cord motor neurons are characterized by low cytosolic Ca^{2+} buffering capacities (40) and, hence, may be more susceptible to chronic ER stress induced by A53TαSyn and associated degenerative processes triggered by the aberrant ER Ca^{2+} release. Future studies will determine whether direct modulation of Herp expression *in vivo* may impact the levels of ER-resident Ca^{2+} release channel proteins, αSyn inclusion formation, disease manifestations and progression. Because ER stress elicited by the aggregation of amyotrophic lateral sclerosis-linked mutant superoxide dismutase 1 (SOD1) has been implicated in motor neuron death (41) and because salubrinal delays the disease process and extends the lifespan of mutant G93A-SOD1 mice (42), elucidation of the cellular and molecular mechanisms that promote or prevent disturbances in ER Ca^{2+} homeostasis may lead to novel approaches for therapeutic intervention for synucleinopathies and motor neuron diseases.

Funding

This work was supported by the American Federation on Aging Research [to S.L.C.]; National Institutes of Health [NIH 1R21NS066265-01 to S. L.C]; and the

National Institute on Aging Intramural Research Program of the National Institute of Health [to M.P.M].

Figures

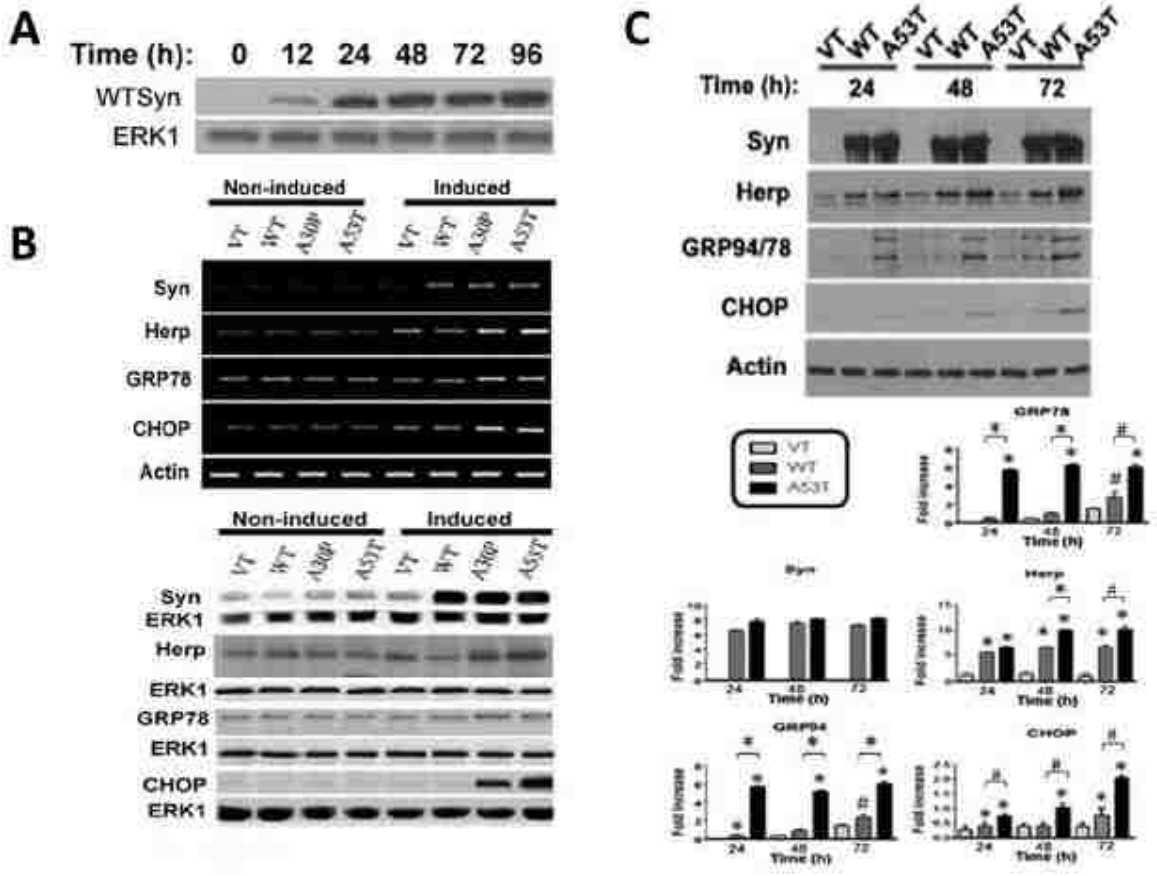

Figure 2-1. Expression of mutant αSyn induces a heightened ER stress response

(A) A representative immunoblot showing the time course of wild-type (WT) human αSyn protein level after the addition of Tet. The antibody used was specific for human αSyn. (B) Representative gel images *(top)* and immunoblots *(bottom)* of WT and mutant (A30P and A53T) αSyn, Herp, Grp94/78, and CHOP mRNA and protein levels, respectively, in PC12 cells 72 h after the addition of Tet (induced) or vehicle (non-

induced). PCR products amplified were separated on ethidium bromide stained agarose gels. Blots were reprobed with ERK1 to confirm equality of total protein loading. (C) Representative immunoblots (top) and results of densitometric analysis (bottom) of Herp, Grp94/78, and CHOP protein levels in PC12 cells at the indicated time points following transient transfection with either WT or mutant (A53T) αSyn. Control cells were transfected with the empty vector (VT). The antibody used was specific for human αSyn. Values are the mean ± SEM of three independent experiments. #p<0.05; *p<0.01, compared to PC12-VT and PC12-WTα-Syn and between the indicated groups.

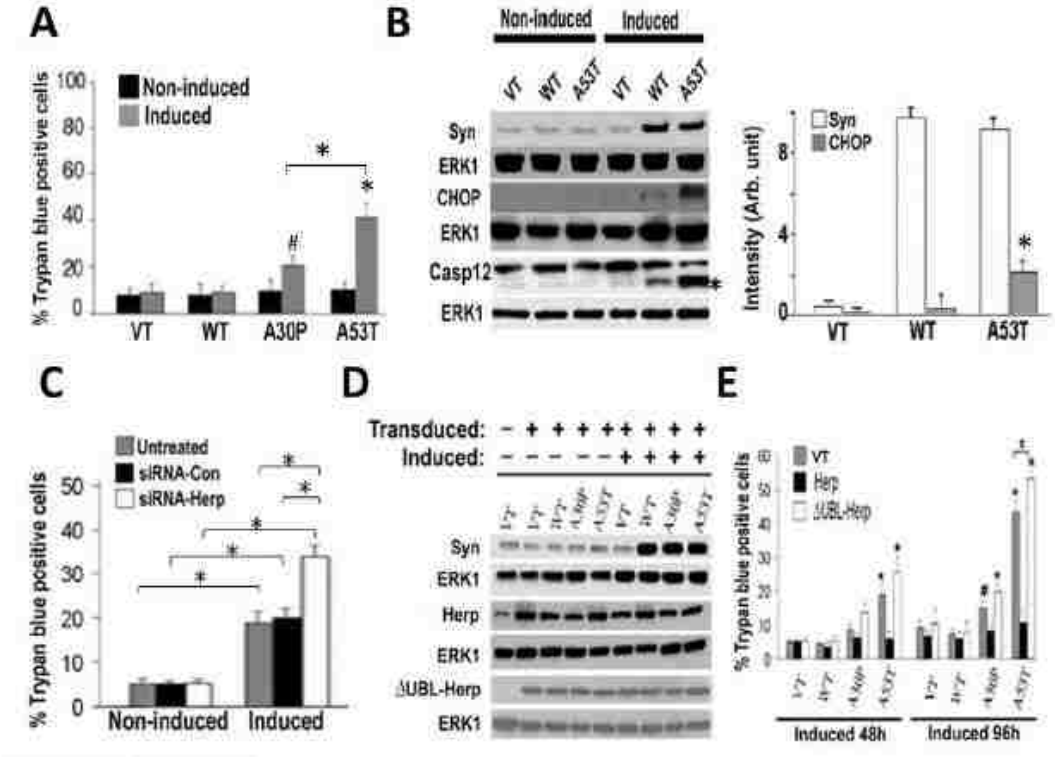

Figure 2-2. Herp protects from mutant αSyn-induced cell death

(A) Trypan blue exclusion was used to determine the viability of the indicated PC12 clones at 96 h under induced or non-induced conditions. Data represent the mean ± SEM of three separate experiments. $^{\#}p<0.05$,*$p<0.01$, compared to PC12-WTαSyn and PC12-VT under non-induced and induced conditions; *$p<0.01$, between the indicated clones expressing mutant αSyn. (B) Representative immunoblots of protein levels of αSyn and CHOP and caspase-12 (Casp12) processing in the indicated PC12 cells 72 h after the addition of Tet (induced) or vehicle (non-induced). Appearance of the active proteolytic fragment of Casp12 is indicated by an asterisk. ERK is used as an internal control of protein loading. Histogram shows densitometric analysis of CHOP protein. $^{\#}P<0.05$, versus the PC12-WTαSyn and PC12-VT under non-induced and induced conditions; (C) Histograms show the viability of the PC12-A53T after transfection with siRNA-Con and siRNA-Herp (100 nM). One day after transfection, Tet was added to the cultures and cell viability was determined 48 h after by trypan blue exclusion. Values represent the mean ± SEM of three separate experiments. $^{\#}p<0.05$, *$p<0.01$ compared to respective non-induced and between the indicated induced PC12 cells. (D) Representative immunoblots of αSyn, Herp and ΔUBL-Herp protein levels in the indicated PC12 cells under non-induced (-) or induced (+) conditions for 48 h. PC12 cells were transduced with viral particles expressing empty vector or vector containing Herp or ΔUBL-Herp construct 48 h prior to induction. ERK is used as an internal control of protein loading. (E) Histograms show the viability of the indicated PC12 cells after ectopic expression of Herp and ΔUBL-Herp. Trypan blue exclusion was used to determine cell viability 48 and 96 h after induction. Values represent the mean ± SEM of

three separate experiments. $^{\#}p<0.05$, *$p<0.01$, compared to groups transduced with the empty vector or Herp and between the indicated transduced groups.

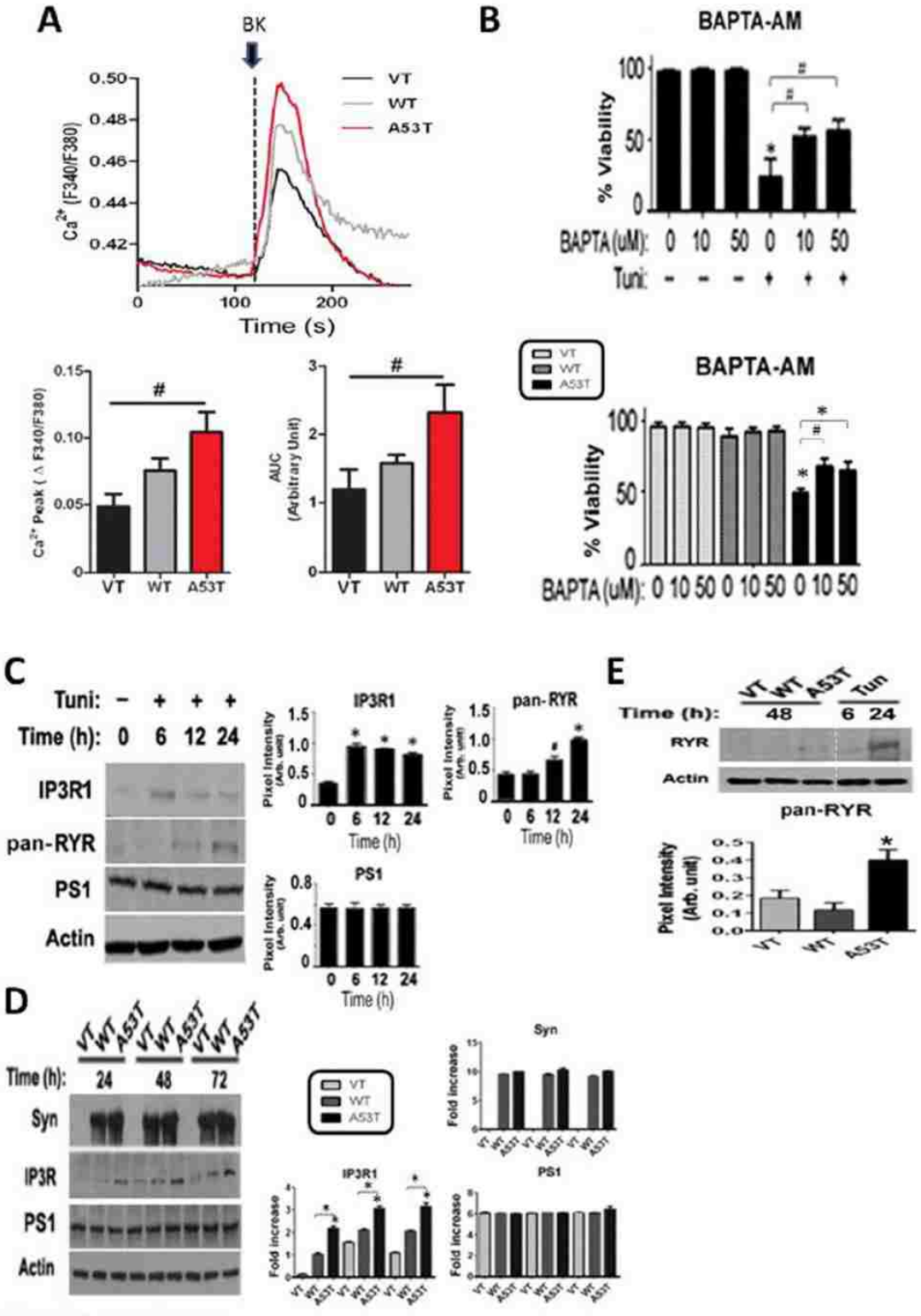

Figure 2-3. ER stress-induced by tunicamycin and mutant α-Syn perturbs ER Ca^{2+} homeostasis through the aberrant accumulation of ER-resident Ca^{2+} release channels

(A) Representative recordings of the bradykinin (BK; 10 μM)-induced elevation of intracellular Ca^{2+} ($[Ca^{2+}]i$) in PC12 cells 48 h after expression of wild-type (WT) and mutant (A53T) αSyn. PC12 cells transfected with empty vector (VT) were included as controls. Cells were loaded with fura-2 and $[Ca^{2+}]_i$ was recorded in Ca^{2+} free medium as described under "Materials and Methods". Arrow indicates time of BK addition. Histograms show Ca^{2+} peak values (change from baseline) and AUC (area under the curve). Values are the mean ± SEM of determinations made in 4 to 6 separate cultures (15-20 cells assessed/culture). $^{\#}p<0.05$, compared to VT. (B) Histograms show the percent of viable cells after treatment of PC12-Tuni *(top)* and PC12-A53TαSyn *(bottom)* with the indicated doses of BAPTA-AM. PC12 cells were pretreated with BAPTA-AM 2 h prior to either exposure to Tuni (20 μg/mL) or expression of VT, WT and A53T. Cell viability was determined 24 h after by Trypan blue exclusion. Values represent the mean ± SEM of three separate experiments. $*p<0.01$, $^{\#}p<0.05$, compared to vehicle or VT at each time point and between the indicated groups. (C) Representative immunoblots *(left)* and results of densitometric analyses *(right)* of IP3R1, pan-RYR and PS1 protein levels in PC12-Tuni at the indicated time points. Values represent the mean ± SEM of three independent experiments. $*p<0.01$, $^{\#}p<0.05$ compared to the untreated group. (D) Representative immunoblots *(left)* and results of densitometric analyses *(right)* of α-Syn, IP3R1 and PS1 protein levels in PC12 cells at the indicated time points after expression of VT, WT or A53T. Values represent the mean ± SEM of three separate experiments. $^{\#}p<0.05$, $*p< 0.01$, compared to VT and WTαSyn. (E) A representative immunoblot *(top)* and results of densitometric analysis *(bottom)* of pan-RYR protein in PC12 cells at the indicated time points after expression of VT, WT or

A53T. The Tuni-treated samples were included as positive controls for ER stress-induced increase of pan-RyR protein level. *p<0.01, compared to VT and WT. Equal protein loading in the immunoblots shown in *C-E* was confirmed after reprobing the membranes for actin.

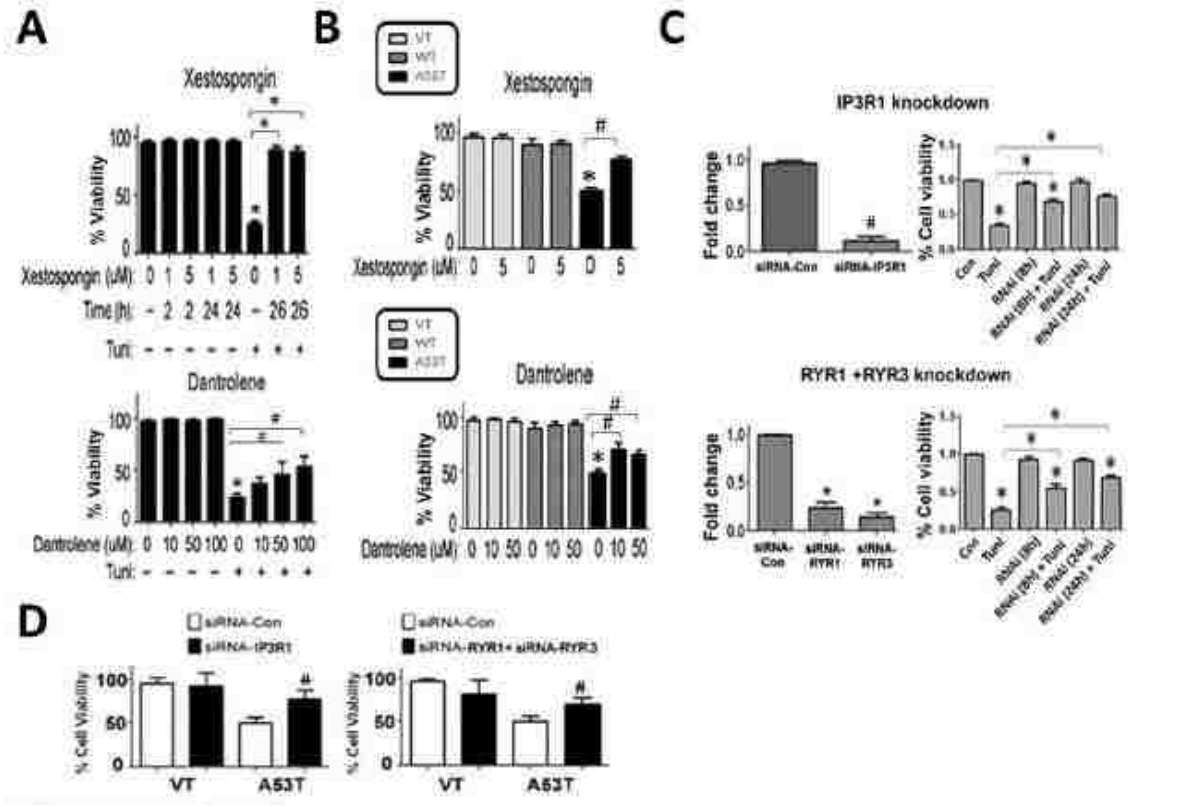

Figure 2-4. Pharmacological inhibition or gene knockdown of ER-resident Ca^{2+} release channels ameliorates ER stress-induced cell death

(A) Histograms show the percent of viable PC12 cells after treatment with tunicamycin (Tuni; 20 μg/ml) (+) or vehicle (-) for 24 h in the absence or presence of the indicated doses of xestospongin C (an IP3R blocker) or dantrolene (a RyR blocker). Both drugs were added 2 h prior to Tuni. Values are the mean ± SEM of three independent experiments. #p<0.05; *p< 0.01, compared to vehicle control and between the indicated

groups. (B) Histograms show the percent of viable PC12 cells expressing empty vector (VT), wild-type (WT) and mutant (A53T) α-Syn. Xestospongin C (5 μM) or dantrolene (50 μM) were added 24 h after induction. Values are the mean ± SEM of three independent experiments. #p<0.05; *p< 0.01, compared to VT and WTα-Syn and between the indicated groups. (C) Histograms show the fold change of the indicated ER Ca^{2+} release channel, IP3R1 (top) or RYR1/RYR3 (bottom), in PC12 cells 24 h after transfection with the respective siRNAs *(left panels)* and the percent of viable transfected PC12 cells at the indicated time points after exposure to Tuni or vehicle (Con) *(right panels).* The siRNAs were added either 8 or 24 h (denoted by asterisk) prior to Tuni exposure. Values represent the mean ± SEM of three independent experiments. #p<0.05;*p< 0.01, compared to Con and between the indicated groups. (D) Histograms show the viability of the indicated PC12 cells in the presence of siRNA-IP3R1 *(top)* or siRNA-RYR1 and siRNA-RYR3 combined *(bottom).* Values represent the mean ± SEM of three independent experiments. #p<0.05; *p<0.01, compared to siRNA-Con.

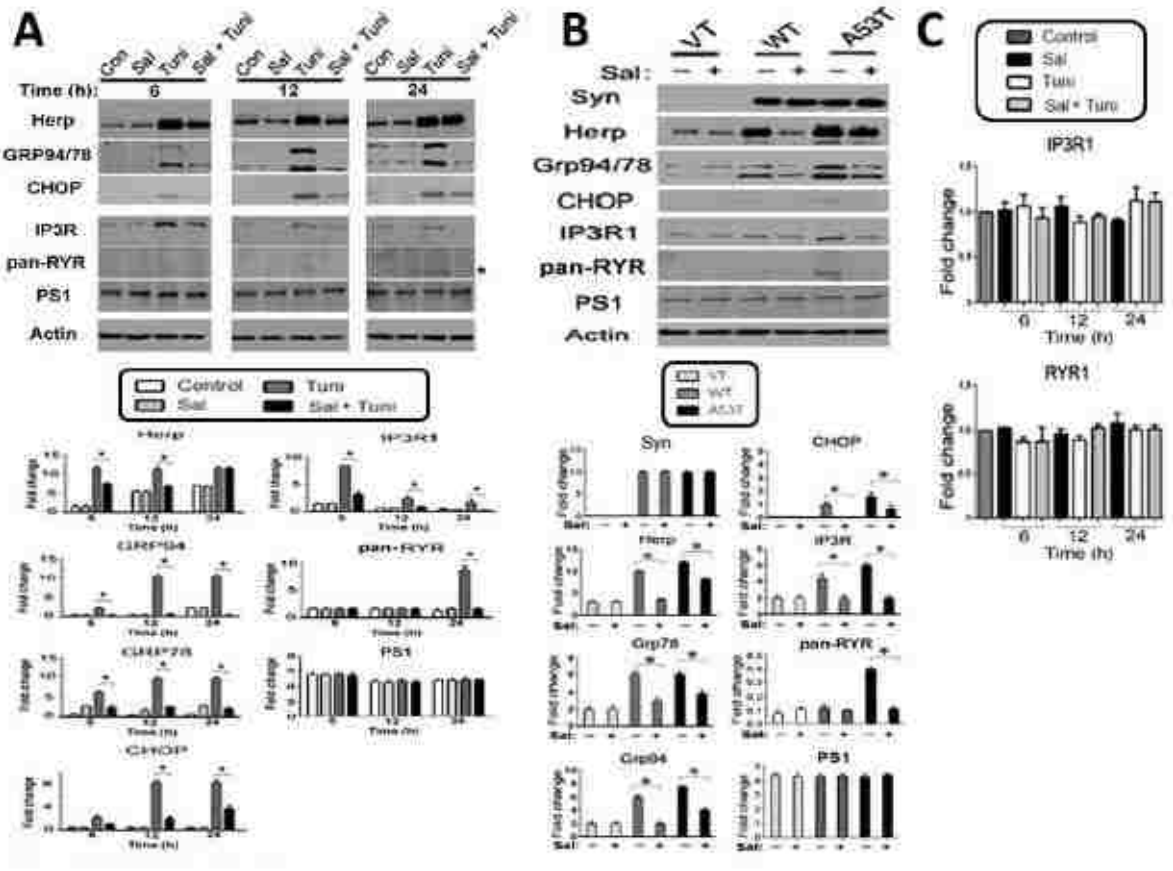

Figure 2-5. Salubrinal ameloriates the induction of ER stress markers and levels of ER-resident Ca^{2+} release channels

(A) Representative immunoblots *(top)* and results of densitometric analysis *(bottom)* of the indicated protein levels in PC12 cells that were treated with Salubrinal (Sal; 75 μM) for 2 h prior to exposure to tunicamycin (Tuni; 20 μg/ml). Cells were collected at the indicated time points for immunoblotting. Values represent the mean ± SEM of three independent experiments. *p<0.01, compared between the indicated groups. (B) Representative immunoblots *(top)* and results of densitometric analysis *(bottom)* of the indicated protein levels in PC12 cells expressing empty vector (VT), wild-type (WT) or mutant (A53T) αSyn after treatment with Sal (+) or vehicle alone (-). Cells were

collected 24 h after Sal treatment. Values represent the mean ± SEM of three independent experiments. *p<0.01, compared between the indicated groups. (C) qRT-PCR analysis of the relative expression of the indicated ER Ca^{2+} release channels in PC12 cells that were treated with Sal for 2 h prior to exposure to Tuni for the indicated time points.

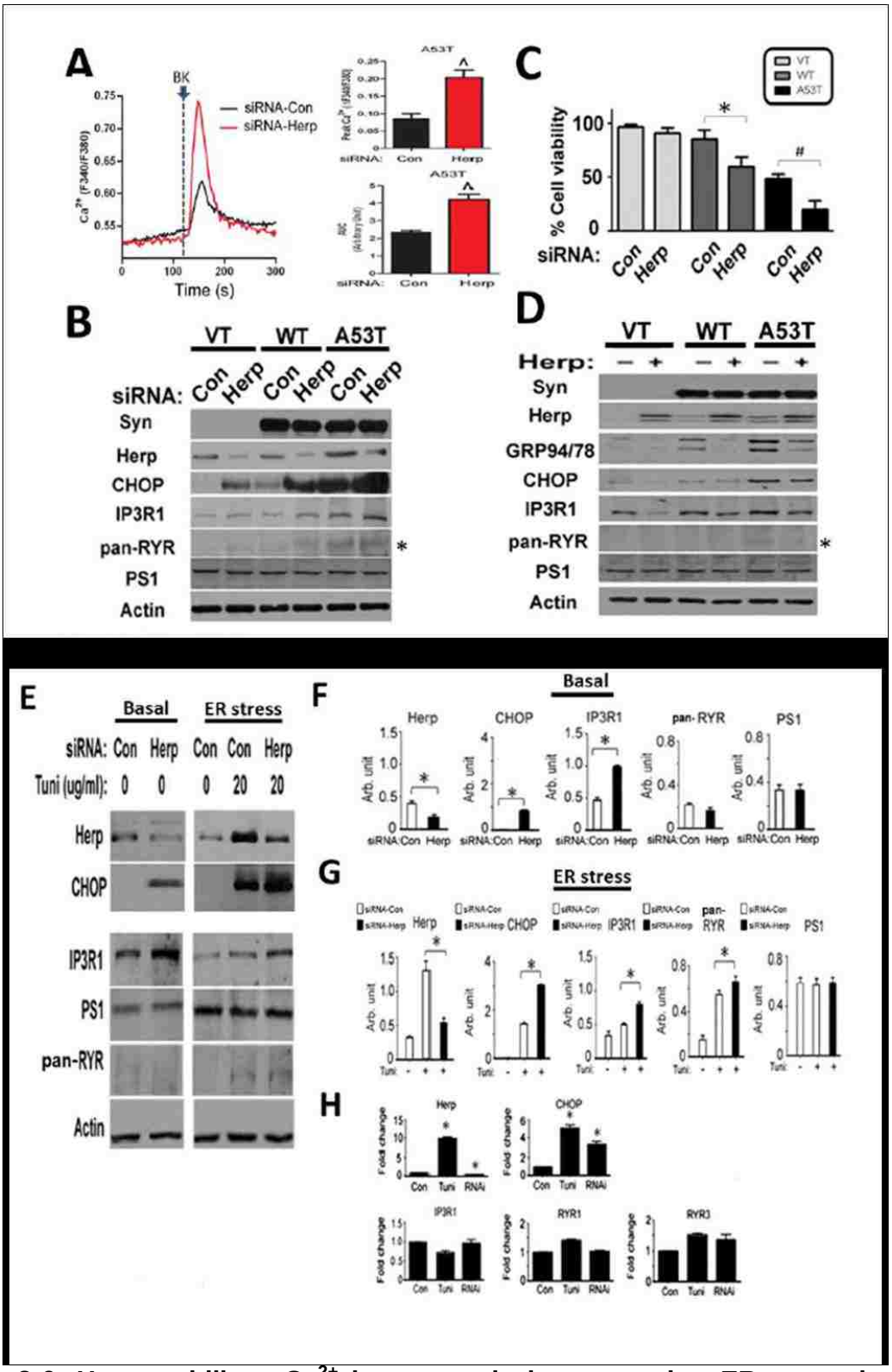

Figure 2-6. Herp stabilizes Ca^{2+} homeostasis by preventing ER stress-induced accumulation of ER-resident Ca^{2+} release channels

(A) Representative recordings of the bradykinin (BK)-evoked increase of intracellular Ca2+ ([Ca2+]i) in PC12 cells expressing mutant (A53T) αSyn 24 h after transfection with siRNA-Con or siRNA-Herp (100 nM). Arrow indicates the time of BK addition. Cells were loaded with fura-2 and [Ca2+]i was recorded in Ca2+ free medium as described under “Materials and Methods”. Histograms show Ca2+ peak values (change from baseline) and AUC (area under the curve). Values are the mean ± SEM of determinations made in 4 to 6 separate cultures (15-20 cells assessed/culture). ^p<0.001, compared to siRNA-Con. (B) Representative immunoblots of ER stress proteins and Ca2+ release channels in PC12 cells expressing VT, WT or A53T 24 h after transfection with siRNA-Con and siRNA-Herp (100 nM). Asterisk indicates the protein band corresponding to pan-RYR. The level of actin is not affected by siRNA treatment. (C) Histograms showing the viability of PC12 cells expressing VT, WT or A53T 24 h after transfection with siRNA-Con or siRNA-Herp (100 nM). Values represent the mean ± SEM of three independent experiments. #p<0.05; *p<0.01, compared to the siRNA-Con treated groups. (D) Representative immunoblots of levels of ER stress proteins and Ca2+ release channels in PC12 cells expressing VT, WT or A53T after transfection with empty vector (-) or vector expressing Herp (+) for 48 h. Asterisk indicates the protein band corresponding to pan-RYR. (E-G) Representative immunoblots and results of densitometric analysis of the indicated protein levels in PC12 cells that were either transfected with the indicated siRNAs and collected 24 h after (Basal condition; left panels) or transfected with the siRNAs 8 h prior to incubation with tunicamycin (Tuni; 20 μg/ml)) for 24 h (ER stress condition; right panels). *p<0.01, compared to the siRNA-Con treated groups. (H) qRT-PCR analysis of the relative

expression of the indicated proteins in PC12 cells that were treated with vehicle control (Con), Tuni (20 μg/ml) or siRNA-Herp (100 nM) for 24 h. Values represent the mean ± SEM of three independent experiments. The mRNA level in Con was set at 1. *p<0.01, compared to Con.

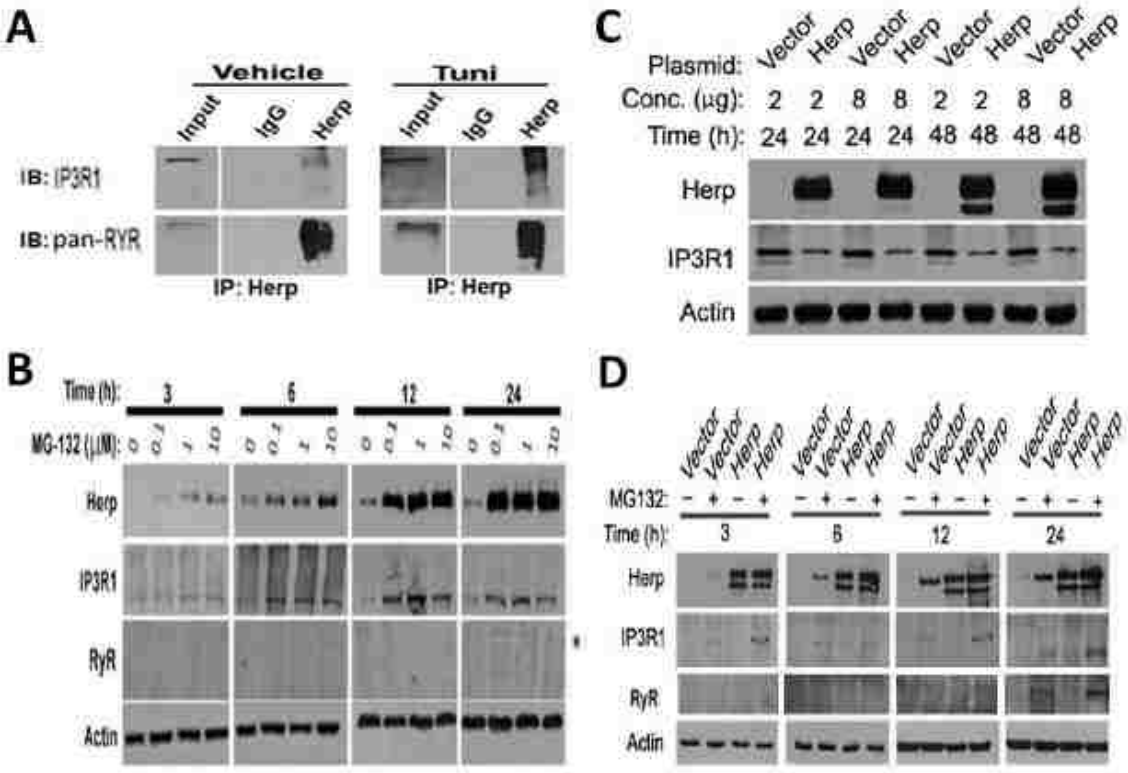

Figure 2-7. Herp interacts with and facilitates proteasomal-mediated degradation of ER-resident Ca^{2+} release channels

(A) Representative immunoblots of the indicated ER Ca^{2+} release channels immunoprecipitated (IP) by anti-Herp antibody from lysates of PC12 that were treated with either tunicamycin (Tuni; 20 μg/ml) or vehicle for 16 h. The pre-immune normal IgG used as the negative control failed to yield an immunopositive band for IP3R or RYR. Input verifies the presence of these ER Ca^{2+} release channel protein in cell lysates. (B) Representative immunoblots of Herp, IP3R1 and pan-RYR protein levels in

PC12 cells that were treated with the indicated doses of the proteasomal inhibitor MG-132 for 3, 6, 12, and 24 h. (C) Representative immunoblots of Herp and IP_3R1 protein levels in HEK293 cells that were transiently transfected with the indicated concentrations of an empty plasmid (Vector) or a plasmid expressing Herp for 24 and 48 h. pan-RYR was undetectable in HEK293 cells. (D) Representative immunoblots of Herp, IP_3R, and pan-RYR protein levels in PC12 cells that were transfected with either an empty plasmid (Vector) or a plasmid expressing Herp 24 h prior to the addition of 1 μM MG-132. Cells were collected at the indicated time points after MG-132 addition.

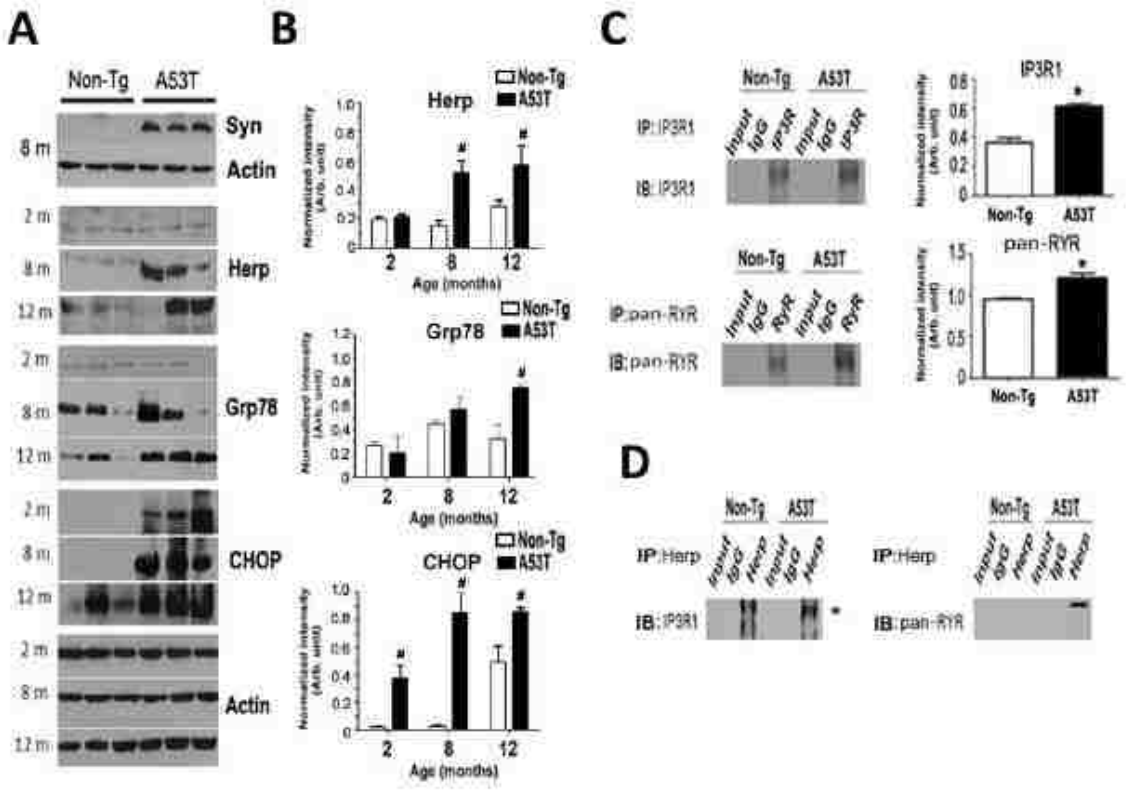

Figure 2-8. Elevation of ER stress markers and ER-resident Ca^{2+} release channels in A53T αSyn mice

(A, B) Representative immunoblots *(A)* and results of densitometric analysis *(B)* of the indicated ER stress proteins in lumbar spinal cords from age-matched non-transgenic (Non-Tg) and mutant αSyn (A53T) mice. A representative immunoblot confirming the

expression of human αSyn in spinal cords of A53T is shown *(upper panel).* All immunoblots were reprobed for actin to control for equal protein loading *(bottom panels).* Values represent the mean ± SEM of four mice per group. $^{\#}p<0.05$; $*p<0.01$, compared to Non-Tg mice. (C) Immunoprecipitation to quantify protein levels of IP3R1 *(top)* and pan-RYR *(bottom)* in lumbar spinal cords of 8 months-old Non-Tg and A53T mice. Each ER Ca^{2+} release channel protein was immunoprecipitated (IP) and immunoblotted (IB) with the respective antibodies. Pre-immune normal IgG was used as a negative control for IP. Histograms show the densitometric analysis of the band corresponding to each ER Ca^{2+} release channel protein. Values represent the mean ± SEM of four mice per group.$*p< 0.01$ compared to Non-Tg mice**.** (D) Representative immunoblots of IP_3R1 *(left)* and pan-RYR *(right)* in protein complexes IP with anti-Herp antibody from lumbar spinal cord homogenates of 8 months-old Non-Tg and A53T mice. Pre-immune normal IgG was used as a negative control for IP. Asterisk denotes the specific band.

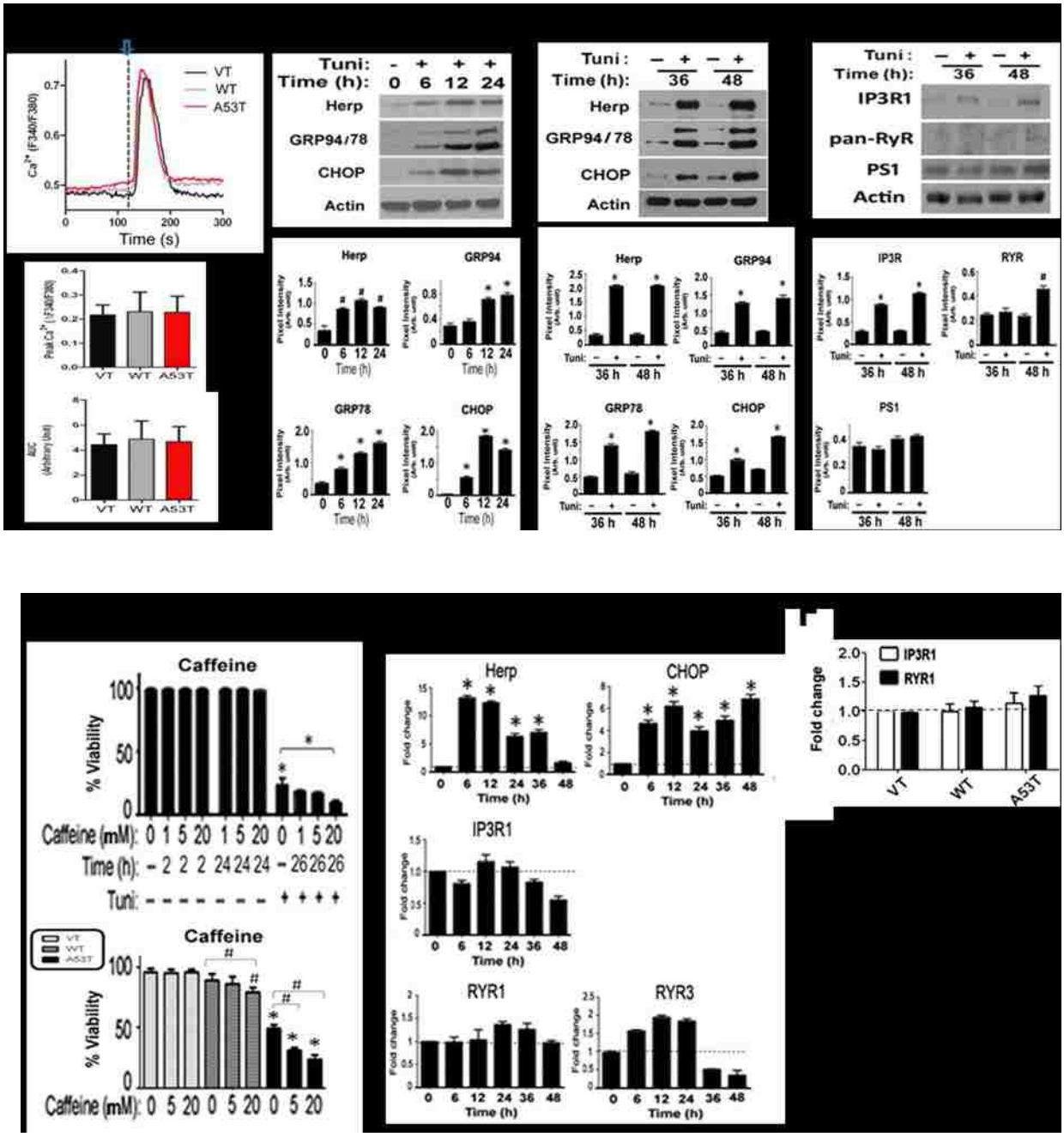

Supplementary Figure 2-1. Effects of tunicamycin and mutant αSyn on ER luminal Ca^{2+} levels, ER stress protein expression and cell survival

(A) Representative recordings of the thapsigargin (Thap; 1 μM)-induced elevation of intracellular Ca^{2+} ($[Ca^{2+}]i$) in PC12 cells expressing wild-type (WT) or mutant (A53T) α-Syn. PC12 cells transfected with empty vector (VT) were included as controls. Arrow indicates time of Thap addition. Cells were loaded with fura-2 and $[Ca^{2+}]_i$ was recorded in Ca^{2+} free medium as described under "Materials and Methods". Histograms show Ca^{2+} peak values (change from baseline) and AUC (area under the curve). Values are the mean ± SEM of determinations made in 4 to 6 separate cultures (15-20 cells assessed/culture). (B) Representative immunoblots *(top)* and results of densitometric analysis *(bottom)* showing time course of Herp, Grp94, Grp78 and CHOP protein levels in PC12 cells treated with either tunicamycin (Tuni; 20 μg/ml) (+) or vehicle alone (-). Values represent the mean ± SEM of three independent experiments. $^{\#}p<0.05$; *p< 0.01, compared to vehicle**.** (C) Representative immunoblots *(top)* and results of densitometric analysis *(bottom)* of IP_3R1, pan-RYR, and PS1 protein levels in PC12 cells at the indicated time points after the addition of Tuni (+) or vehicle alone (-). Values represent the mean ± SEM of three independent experiments. $^{\#}p<0.05$; *p< 0.01, compared to vehicle**.** (D) Histograms show the percent of viable cells after treatment of PC12-Tuni *(top)* and PC12-A53TαSyn *(bottom)* with the indicated doses of caffeine. PC12 cells were treated with caffeine either in vehicle for 2 or 24 h or in combination with Tuni for 26 h. In PC12 cells expressing VT, WT and A53T, caffeine was added 24 h after induction and then left incubated for another 24 h. Cell viability was determined by trypan blue exclusion. Values represent the mean ± SEM of three separate experiments. *p<0.01, $^{\#}p<0.05$, compared to vehicle control or VT at each time point and between the indicated groups. (E) qRT-PCR analysis of the relative

expression of ER-stress proteins and Ca^{2+} release channels in PC12 cells treated with Tuni (+) for the indicated time points. Values represent the mean ± SEM of nine separate experiments. #p<0.05; *p< 0.01, compared to vehicle. (F) qRT-PCR analysis of the relative expression of IP_3R1 and RYR1 in the indicated PC12 cells ectopically expressing empty vector (VT), wild-type (WT) or mutant (A53T) αSyn. Cells were harvested 48 h after expression. Values represent the mean ± SEM of three separate experiments. #p<0.05; *p< 0.01, compared to VT.

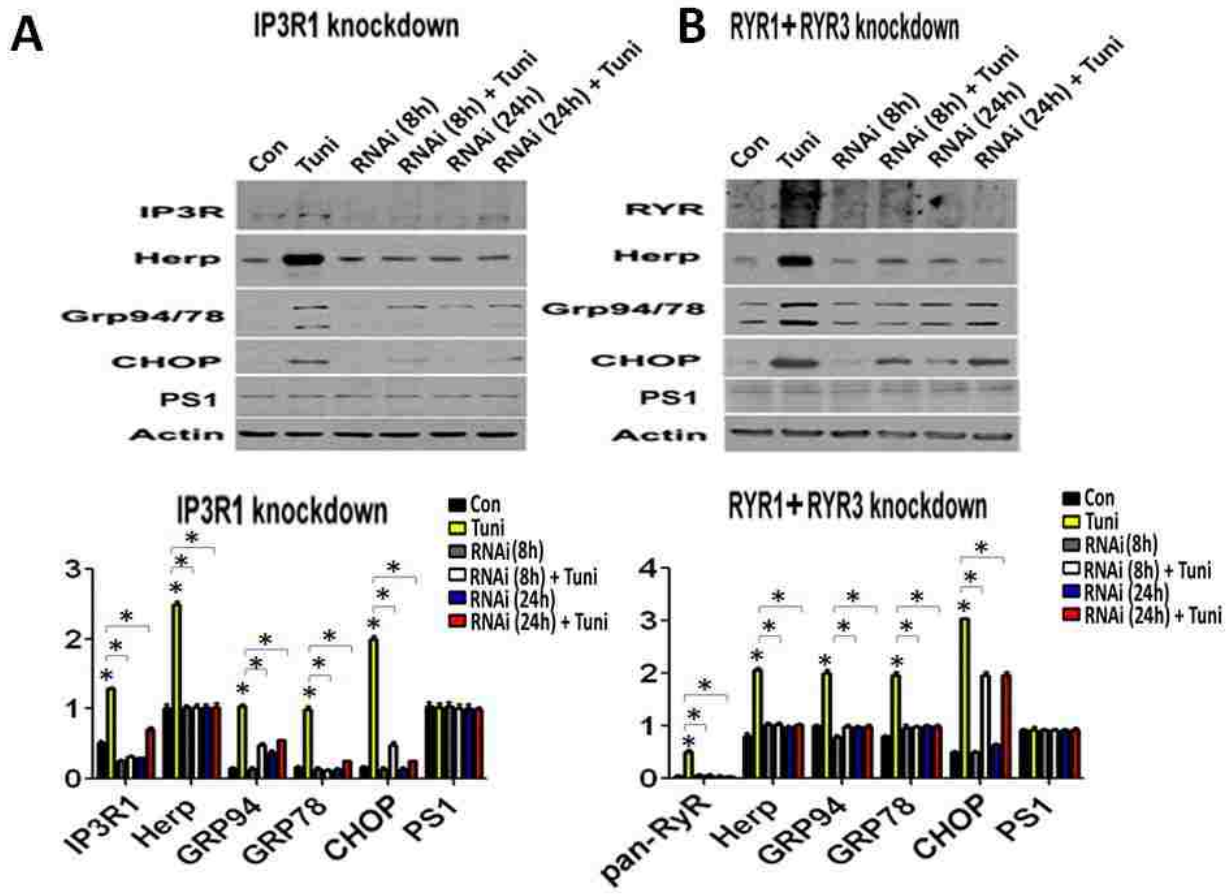

Supplementary Figure 2-2. Knockdown of ER Ca^{2+} release channel expression ameliorates ER stress

(A, B) Representative immunoblots *(top)* and results of densitometric analysis *(bottom)* of Herp, Grp94/78, CHOP, and PS1 protein levels in PC12 cells that were transfected

with siRNA-IP3R1 (250 nM) *(A)* or a combination of siRNA-RYR1 and siRNA-RYR3 (100 nM each) *(B)* for either 8 and 24 h prior to the addition of tunicamycin (Tuni; 20 μg/ml) or vehicle alone (Con). Values represent the mean ± SEM of three independent experiments. *p< 0.01, compared to Con and between the indicated groups.

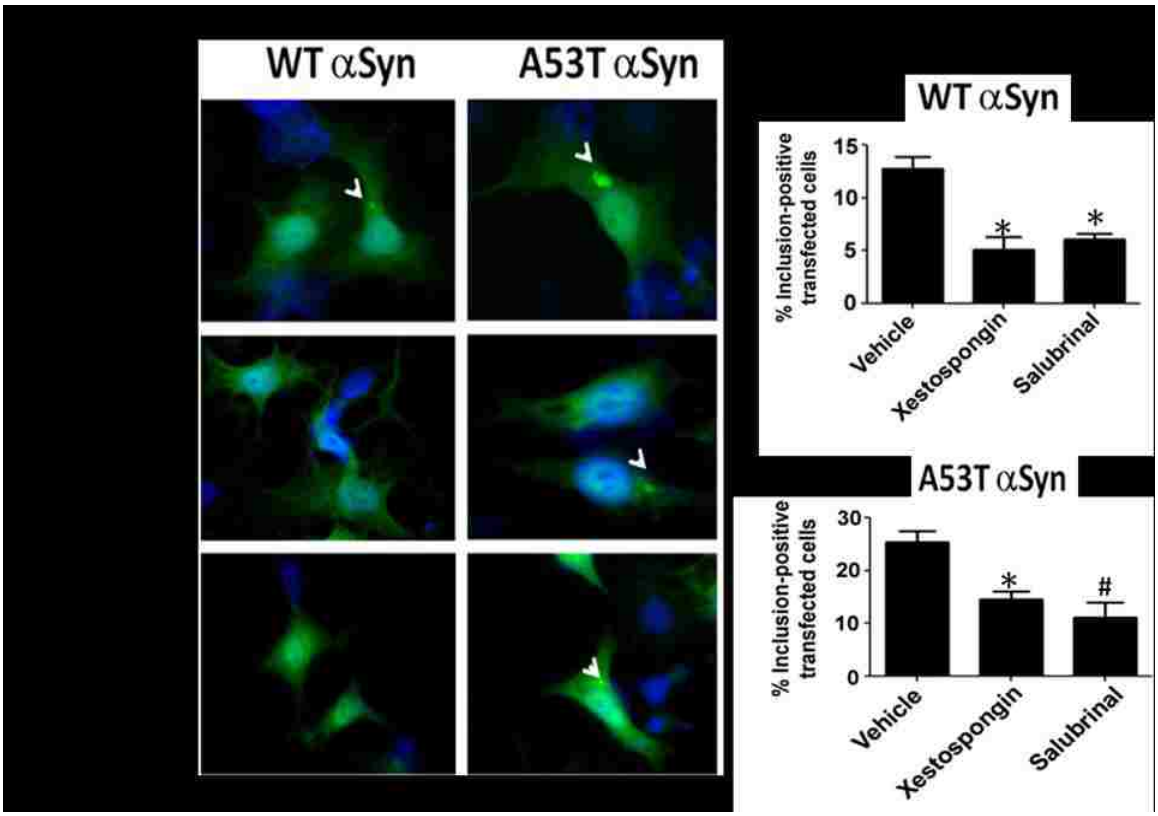

Supplementary Figure 2-3. Inhibition of ER Ca^{2+} release reduces αSyn inclusions formation

(A) Representative images of αSyn inclusions (indicated by arrowhead) in PC12 cells transfected with either the GFP-tagged WTαSyn or GFP-tagged mutant (A53T) αSyn construct. Twenty four hours after transfection, PC12 cells were treated with Xestospongin (5 μM), Salubrinal (Sal; 75 μM) or the respective vehicles for another 24 h, fixed, and counterstained with the nuclear dye 4',6-diamidino-2-phenylindole (DAPI; blue). (B) Histograms show the percentage of the indicated transfected PC12 cells with

cytoplasmic αSyn protein inclusions. Values represent the mean ± SEM of three cultures in triplicate. #p< 0.05; *p< 0.01, compared to vehicle controls.

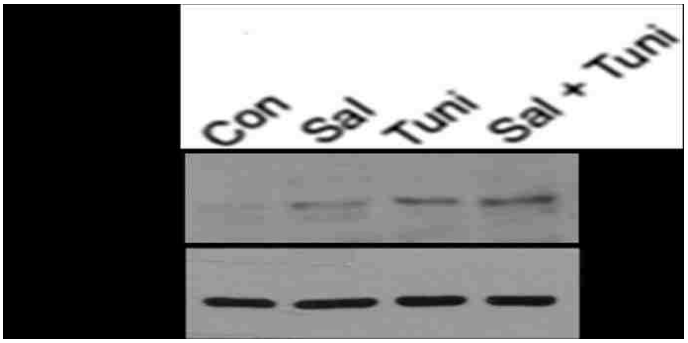

Supplementary Figure 2-4. Levels of phospho-eIF2α and total eIF2α following tunicamycin and/or salubrinal treatments

A representative blot of phospho-eIF2α and total eIF2α in PC12 cells that were treated with either salubrinal (Sal; 75 μM) or tunicamycin (Tuni; 20 μg/ml) alone, or in combination. Cells were harvested 12 h after treatments.

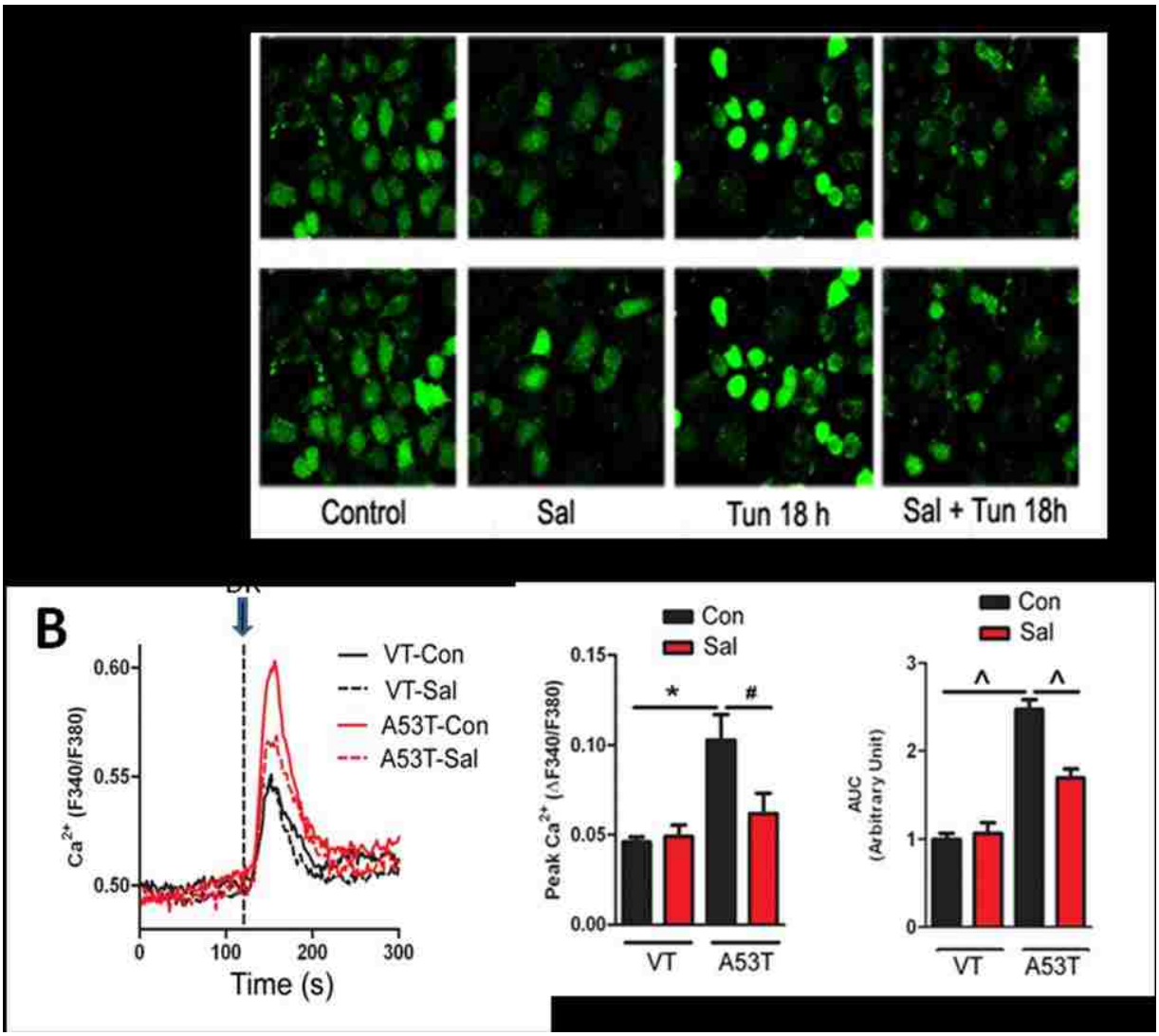

Supplementary Figure 2-5. Salubrinal reduces bradykinin-evoked Ca^{2+} transients in PC12-Tuni and PC12-α A53TSyn cells

(A) Representative images of the bradykinin-induced changes in the fluo-4 fluorescence intensity in PC12 cells that were treated with tunicamycin (Tuni; 20 μg/ml) for 18 h in the presence of salubrinal (Sal; 75 μM) or vehicle control (Con). (B) Representative recordings of the bradykinin (BK; 10 μM)-induced elevation of intracellular Ca^{2+} ($[Ca^{2+}]i$) in PC12 cells after expression of mutant (A53T) α-Syn in the presence of Sal or Con. PC12 cells transfected with the empty vector (VT) were

included as controls. Cells were loaded with fura-2 and $[Ca^{2+}]_i$ was recorded in Ca^{2+} free medium as described under "Materials and Methods". Arrow indicates time of BK addition. Histograms show Ca^{2+} peak values (change from baseline) and AUC (area under the curve). Values are the mean ± SEM of determinations made in 4 to 6 separate cultures (15-20 cells assessed/culture). #p<0.05,*p<0.01, ^p<0.001, compared to VT.

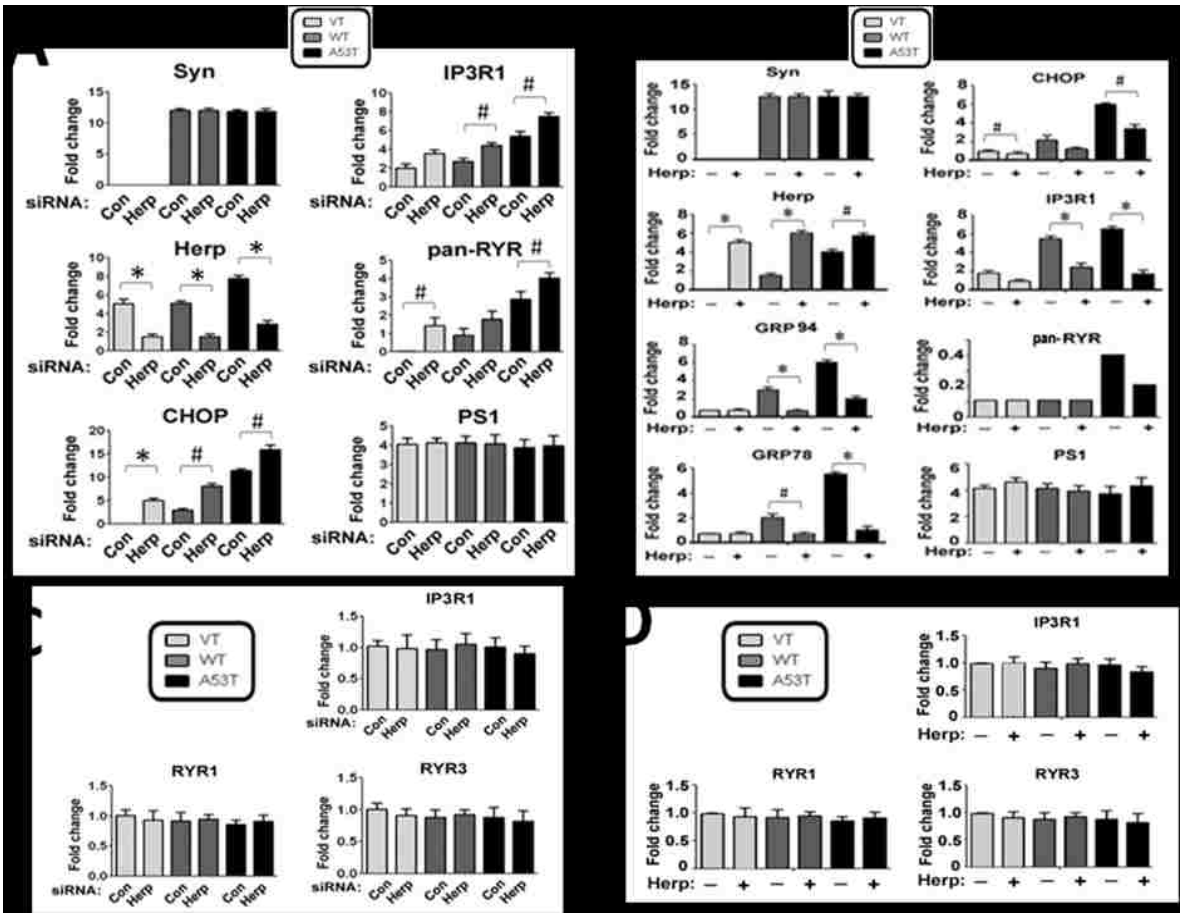

Supplementary Figure 2-6. Densitometric and qRT-PCR analyses of ER stress proteins and ER-resident Ca^{2+} release channel levels

(A, B) Results of densitometric analysis of ER stress proteins and ER Ca^{2+} release channels in the indicated PC12 cells 24 h after transfection with siRNA-Con or siRNA-

Herp (100 nM). Values represent the mean ± SEM of three independent experiments. #p< 0.05; *p< 0.01, compared between the indicated groups. (B) Results of densitometric analysis of ER stress proteins and ER Ca^{2+} release channels in the indicated PC12 cells 48 h after ectopic expression of Herp. Values represent the mean ± SEM of three independent experiments. #p< 0.05; *p< 0.01, compared between the indicated groups. (C, D) qRT-PCR analysis of the relative expression of ER-resident Ca^{2+} release channels in the indicated PC12 cells 24 h after addition of siRNAs or ectopic expression of Herp. Values are the mean ± SEM of three independent experiments. #p< 0.05; *p< 0.01, compared between the indicated groups.

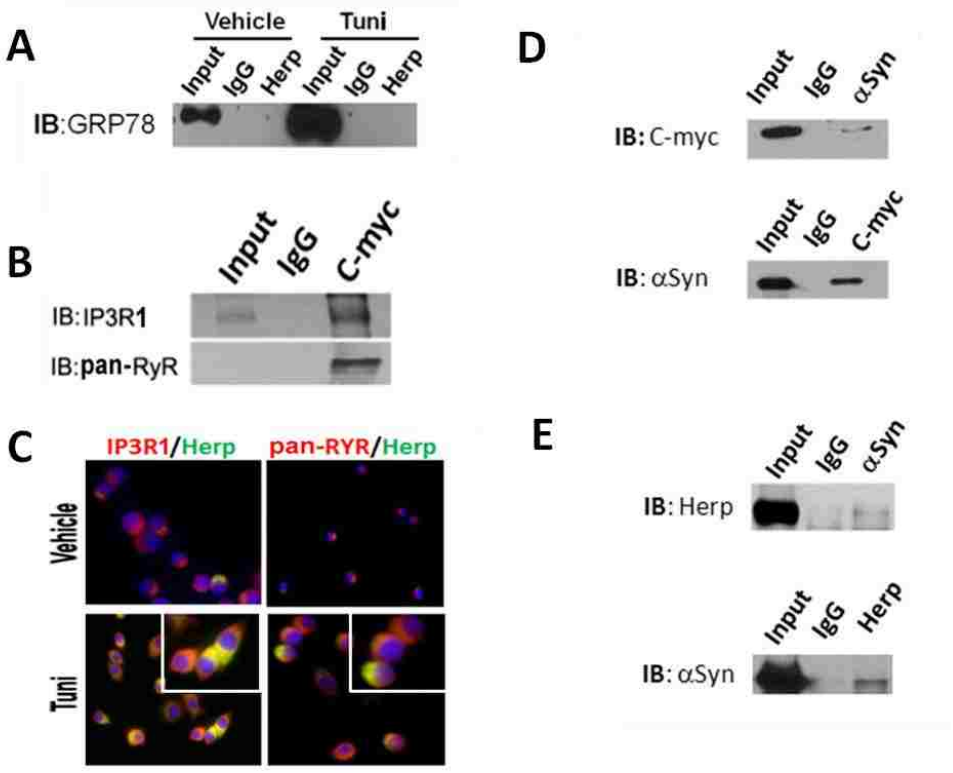

Supplementary Figure 2-7. Herp interacts with ER-resident Ca^{2+} release channels and A53TαSyn

(A) A representative immunoblot shows absence of Grp78 in the protein complex immunoprecipitated (IP) by anti-Herp antibody from total lysates of PC12 cells treated

with tunicamycin (Tuni; 20 μg/ml) or vehicle for 16 h. Input shows Grp78 in total lysates. The pre-immune normal IgG used as control for IP. (B) A representative immunoblot shows the presence of IP3R *(top)* and pan-RYR *(bottom)* in protein complexes IP by anti-c-Myc antibody from total lysates of HEK293 cells that were transiently transfected with the c-myc-tagged Herp for 24 h. The pre-immune normal IgG was used as the negative control for IP. Note that IP3R1 but not pan-RYR was readily detected in the inputs. (C) Representative immunofluorescence micrographs show co-localization of Herp (green) with IP3R (red) and pan-RYR (red) in PC12 cells that were treated with either vehicle *(top)* or Tuni *(bottom)* for 24 h. (D) Representative immunoblots show the presence of Herp or αSyn in protein complexes IP by anti- αSyn or anti-c-myc antibody, respectively, from total lysates of PC12 cells that were transiently transfected with both A53TαSyn and c-myc-tagged Herp for 24 h. The pre-immune normal IgG was used as the negative control for IP. Inputs verify the presence of c-myc-tagged Herp or αSyn in lysates**.** (E) Representative immunoblots show the presence of Herp or αSyn in protein complexes IP by anti- αSyn *(top)* or anti-Herp *(bottom)* antibody, respectively, from total lysates of PC12 cells that were transiently transfected with either Herp *(top)* or A53TαSyn *(bottom)* for 24 h. The pre-immune normal IgG was used as the negative control for IP. Inputs verify the presence of c-myc-tagged Herp or αSyn in lysates**.**

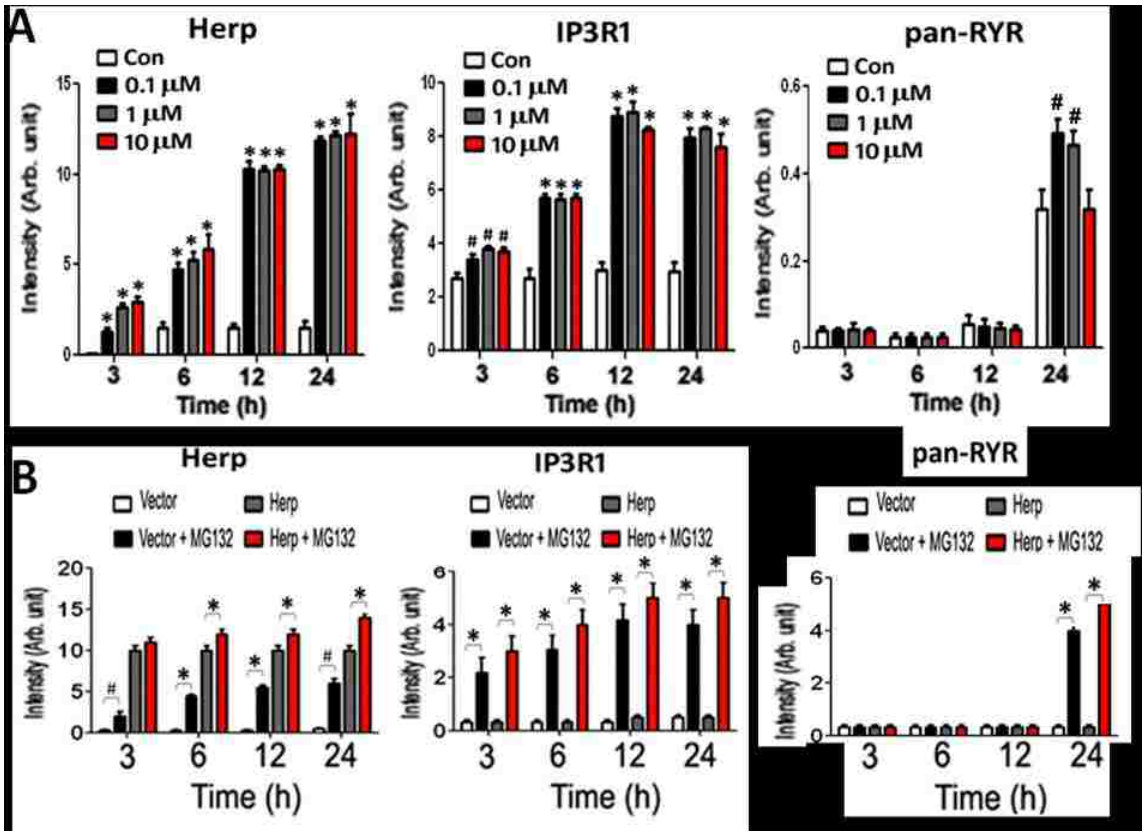

Supplementary Figure 2-8. Blockade of proteasome inhibits Herp- induced degradation of ER-resident Ca^{2+} release channels

(A) Results of densitometric analysis of Herp, IP3R1 and pan-RYR protein levels in PC12 cells that were treated with the indicated doses of the proteasomal inhibitor MG-132 or vehicle as control (Con) for 3, 6, 12, and 24 h. Values are the mean ± SEM of three independent experiments. $^{\#}p<0.05$; $*p<0.01$, compared to Con. (B) Results of densitometric analysis of Herp, IP3R1, and pan-RYR protein levels in PC12 cells transfected with either a plasmid expressing Herp or an empty plasmid (Vector) 24 h prior to the addition of 1 μM MG-132. Cells were collected at the indicated time points after MG-132 addition. Values are the mean ± SEM of three independent experiments. $^{\#}p<0.05$; $*p<0.01$, compared between the indicated groups.

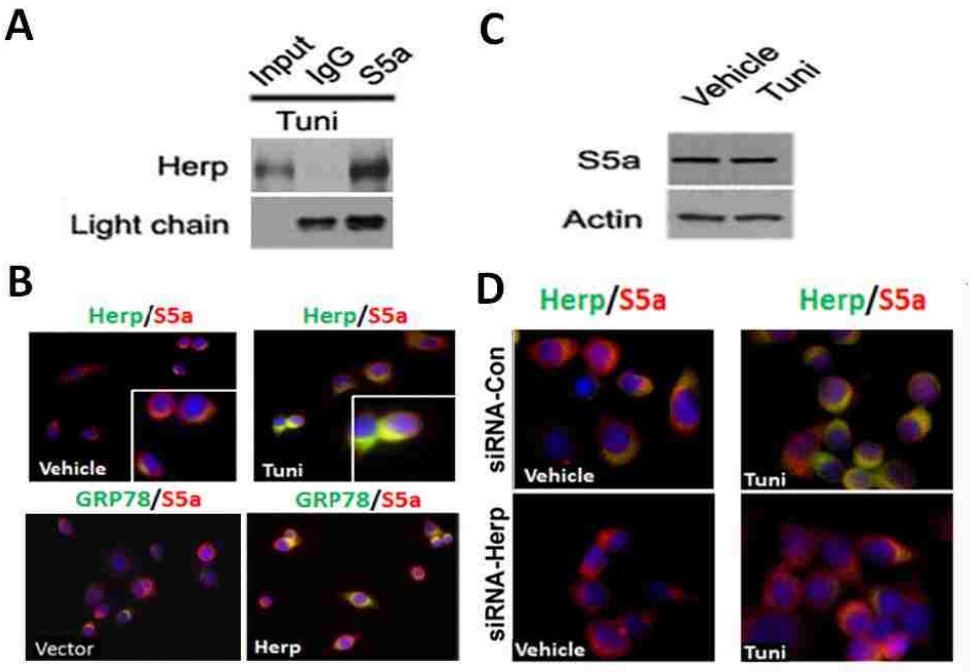

Supplementary Figure 2-9. Herp interacts and co-localizes with the ubiquitin-interacting S5a subunit of the proteasome

(A) A representative immunoblot of Herp immunoprecipitated (IP) by anti-S5a antibody from total lyates of PC12 cells that were treated with Tuni (20 μg/ml) for 16 h. Pre-immune normal IgG was used as a negative control for IP. Inputs verify the amounts of Herp in lysates. Light chain indicates equal amounts of normal IgG and anti-S5a IgG in the protein complexes. (B) Representative immunofluorescence micrographs showing the co-localization of S5a (red) with either Herp or Grp78 (green) in PC12 cells exposed to Tuni or vehicle for 12 h. (C) A representative immunoblot of S5a protein in PC12 cells exposed to Tuni or vehicle for 16 h. (D) Representative immunofluorescence micrographs showing the co-localization of S5a (red) with Herp (green) in PC12 cells

transfected with siRNA-Con or siRNA-Herp 24 h prior to exposure to Tuni for another 14 h.

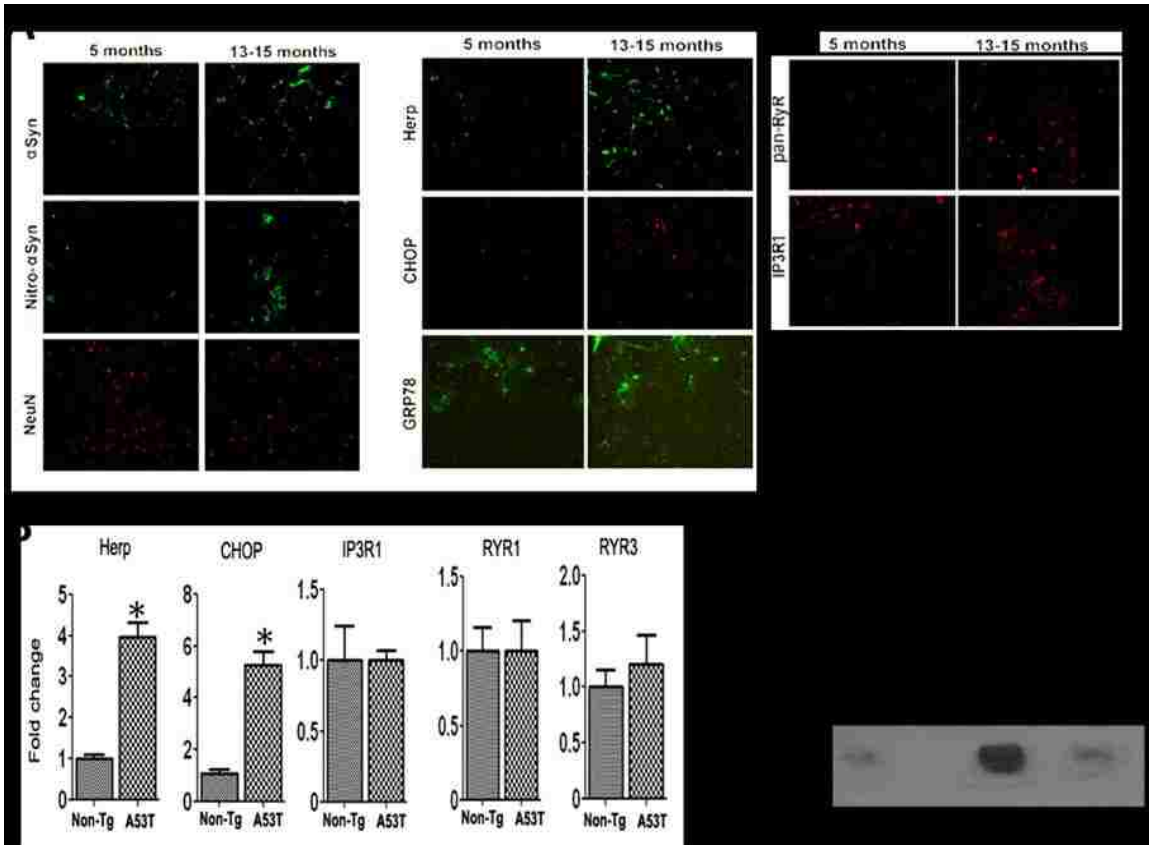

Supplementary Figure 2-10. Accumulation of ER stress markers and of ER-resident Ca^{2+} channels in A53TαSyn transgenic mice

(A) Representative immunofluorescence micrographs showing the immunoreactivities of antibodies directed to the indicated proteins in the lumbar spinal cords from pre-symptomatic (5 months) and symptomatic (13-15 months) A53T mice. (B) mRNA levels of the indicated proteins in the lumbar spinal cords from 13-15 months old non-transgenic (Non-Tg) and mutant αSyn (A53T) mice**.** Values are the mean ± SEM of four mice per group. *p<0.01, compared to Non-Tg. (C) A representative immunoblot of αSyn in protein complexes immunoprecipitated (IP) with anti-Herp antibody from lumbar spinal cord homogenates of 13-15 months old Non-Tg and A53T mice**.** Pre-immune

normal IgG was used as a negative control for IP. Inputs verify the amounts of αSyn in spinal cord extract as determined by immunoblotting using an antibody to mouse and human αSyn.

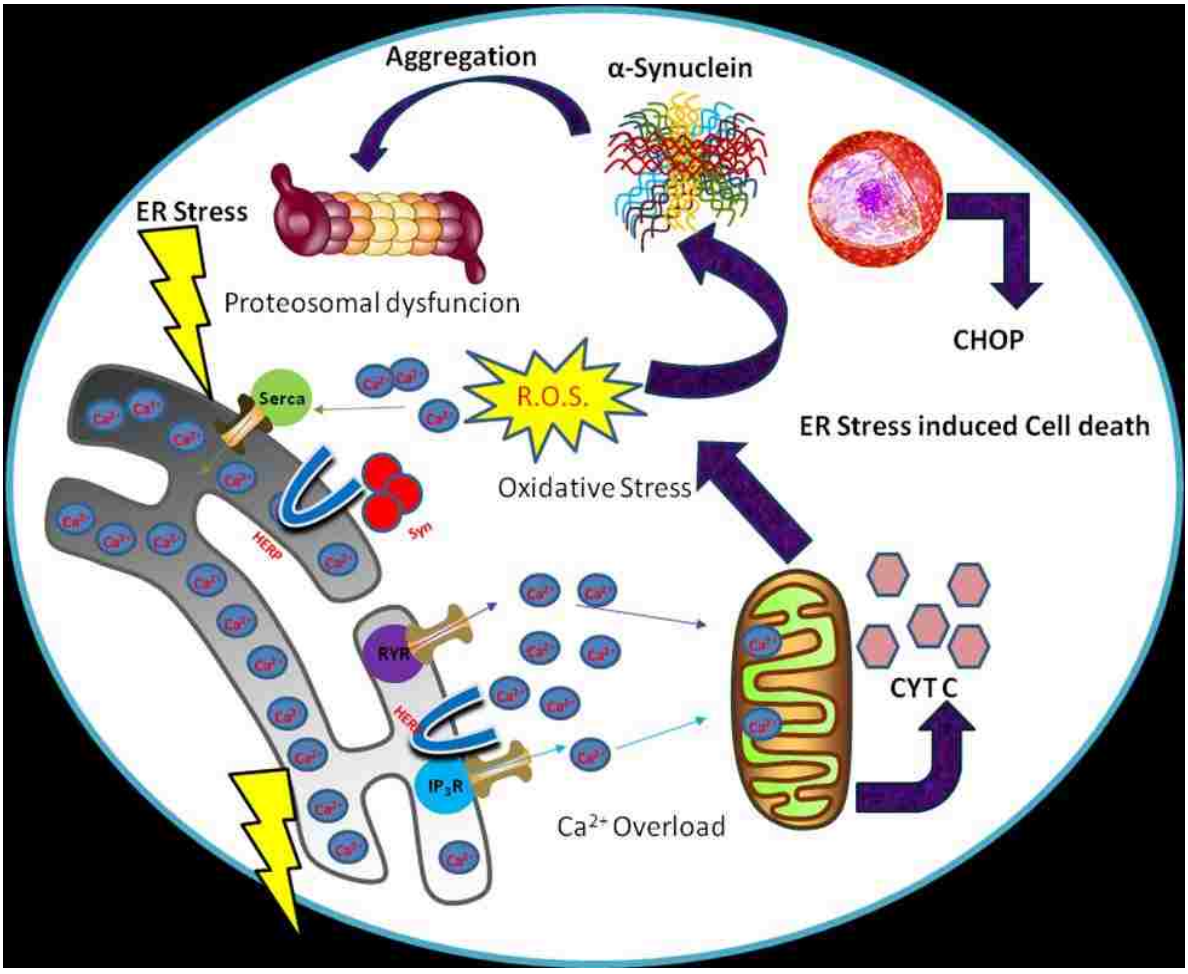

Summary Diagram 2-1. Schematic representation summarizing the mechanisms involved in αSyn-induced activation of ER stress-associated apoptosis

Tables

Table 2-1. Target sequences of siRNA duplexes

Gene	Species	Forward Sequence	
HERP	Rat	GUUAUUCUGAAGAGCUUUA	UAAAGCUCUUCAGAAUAAC
IP3R1	Rat	GUAGCAAGAGUGUUAGGGA	UCCCUAACACUCUUGCUAC
RYR1	Rat	CCUCUAUUCUUACGGCUUU	AAAGCCGUAAGAAUAGAGG
RYR3	Rat	GGACUAUUUAGAUACUAGA	UCUAGUAUCUAAAUAGUCC

Table 2-2. Primer sets used for the detection of transcripts by semi-quantitative PCR

Gene	Species	Forward Sequence	Reverse Sequence
Herp	Rat	CCACTACCACAACTACCACTG	CCTCTCTTTGGCTTTCTGGAA
Grp78	Rat	CTGGGTACATTTGATCTGACTGG	GCATCCTGGTGGCTTTCCAGCCATTC
CHOP	Rat	AAGGTCTACGAAGGTGAACGACCCC	GACCCCAAGACACGTGAGCAACTGC
Syn	Human	CGACGACAGTGTGGTGTAAAGGAA	TGGGCACATTGGAACTGAGCACTT
Beta actin	Rat	GAGAGGGAAATCGTGCGTGAC	CATCTGCTGGAAGGTGGACA

Table 2-3. Primer sets used for the detection of transcripts by quantitative real-time PCR (qRT-PCR).

Gene	Species	Forward Sequence	Reverse Sequence
IP3R1	Rat/Mouse	GAGAGAAAGCGCACGCCGAGA	GCAATCCCATGTCCGCGAAGAG
IP3R2	Rat	TCTTGGTGGATATGGCAAGGGTCT	AGTTGAAGAAGCCGCTCACGATGT
IP3R2	Rat/Mouse	AGACACCTCAGATCGACAGCAACA	GCACACAGAGCTTACTCAGCCTAA
IP3R3	Rat/Mouse	CAGAACGACCGCAGGTTTGTCAT	TTCTGCCCATTGTTGGGAACATCG
RYR1	Mouse	CCGGCGATGAATATGAACTT	TGATAGCCAGCAGAATGACG
RYR2	Mouse	CATGGACAGCTTCCCCTGAA	GTGTGACTGCCGTGCTTGG
RYR3	Mouse	CTGGCCATCATTCAAGGTCT	GTCTCCATGTCTTCCCGTA
RYR1	Rat	CTTGAACTACTTGTCGAGGAACTT	TGGCGGAGAGTCTGAAACC
RYR2	Rat	ACAACCCAAATGCTGGTCTC	TCCGGTTCAGACTTGGTTTC
RYR3	Rat	CTGGCCATCATTCAAGGTCT	GTCTCCATGTCTTCCCGTA
Herp	Mouse	ACAGAGCAGCCGGACAACTCTAAT	TACGTTGTGTAGCCAGAGAAGCCA
Herp	Rat	TCGGGTGGTTTCCATTCAGACAGA	GGGTCTTCCATTTCAGGGTCCAAA
CHOP	Mouse	GTCCCTAGCTTGGCTGACAGA	TGGAGAGCGAGGGCTTTG
CHOP	Rat	TCTCTGCCTTTCGCCTTTGAGACA	TGCAGGGTCAAGAGTAGTGAAGGT
Beta actin	Mouse	CTTCCTTCTTGGCTATGGAATCC	CGTAAAGACCTCTATGCCAACACA
Beta actin	Rat	AGCCATGTACGTAGCCATCC	ACCCTCATAGATGGGCACAG
18S	Rat/Mouse	GTAACCCGTTGAACCCCATT	CCATCCAATCGGTAGTAGCG

References

1. Spillantini MG, Crowther RA, Jakes R, Hasegawa M, Goedert M. Alpha-Synuclein in filamentous inclusions of Lewy bodies from Parkinson's disease and dementia with lewy bodies. Proc Natl Acad Sci U S A. 1998;95:469-73.

2. Conway KA, Harper JD, Lansbury PT. Accelerated in vitro fibril formation by a mutant alpha-synuclein linked to early-onset Parkinson disease. Nat Med. 1998;4:1318-20.

3. Singleton AB, Farrer M, Johnson J, Singleton A, Hague, S, Kachergus J, et al. Alpha-Synuclein locus triplication causes Parkinson's disease. Science 2003;302: 841.

4. Bellucci A, Navarria L, Zaltieri M, Falarti E, Bodei S, Sigala S, et al. Induction of the unfolded protein response by α-synuclein in experimental models of Parkinson's disease. J Neurochem. 2011;116:588-605.

5. Cooper AA, Gitler AD, Cashikar A, Haynes CM, Hill KJ, Bhullar B, et al. Alpha-synuclein blocks ER-Golgi traffic and Rab1 rescues neuron loss in Parkinson's models. Science. 2006;313:324-28.

6. Kaufman RJ. Stress signaling from the lumen of the endoplasmic reticulum: coordination of gene transcriptional and translational controls. Genes Dev. 1999;13:1211-33.

7. Harding HP, Calfon M, Urano F, Novoa I, Ron D. Transcriptional and translational control in the Mammalian unfolded protein response. Annu Rev Cell Dev Biol. 2002;18:575-99.

8. Holtz WA, O'Malley KL. Parkinsonian mimetics induce aspects of unfolded protein response in death of dopaminergic neurons. J Biol Chem. 2003;278:19367-77.

9. Ryu EJ, Harding HP, Angelastro JM, Vitolo OV, Ron D, Greene LA. Endoplasmic reticulum stress and the unfolded protein response in cellular models of Parkinson's disease. J Neurosci. 2002;22:10690-8.

10. Hoozemans JJ, van Haastert ES, Eikelenboom P, De Vos RA, Rozemuller JM, Scheper W. Activation of the unfolded protein response in Parkinson's disease. Biochem Biophys Res Commun. 2007;354:707-11.

11. Smith WW, Jiang H, Pei Z, Tanaka Y, Morita H, Sawa A, et al. Endoplasmic reticulum stress and mitochondrial cell death pathways mediate A53T mutant alpha-synuclein-induced toxicity. Hum Mol Genet. 2005;14:3801-11.

12. Oyadomari S, Mori M. Roles of CHOP/CHOP in endoplasmic reticulum stress. Cell Death Differ. 2004;11:381-89.

13. Silva RM, Ries V, Oo TF, Yarygina O, Jackson-Lewis V, Ryu EJ, et al. CHOP/GADD153 is a mediator of apoptotic death in substantia nigra dopamine neurons in an in vivo neurotoxin model of parkinsonism. J Neurochem. 2005;95:974-86.

14. Kokame, K, Agarwala, KL, Kato, H and Miyata, T. (2000) Herp, a new ubiquitin-like membrane protein induced by endoplasmic reticulum stress. J Biol Chem., 275, 32846-32853.

15. Hori O, Ichinoda F, Yamaguchi A, Tamatani T, Taniguchi M, Koyama Y, et al. Role of Herp in the endoplasmic reticulum stress response. Genes Cells. 2004;9:457-69.

16. Chan SL, Fu W, Zhang P, Cheng A, Lee J, Kokame K, et al. Herp stabilizes neuronal Ca2+ homeostasis and mitochondrial function during endoplasmic reticulum stress. J Biol Chem. 2004;279:28733-43.

17. Schulze A, Standera S, Buerger E, Kikkert M, Van Voorden S, Wiertz E, et al. The ubiquitin-domain protein HERP forms a complex with components of the endoplasmic reticulum associated degradation pathway. J Mol Biol. 2005;354:1021-7.

18. Slodzinski H, Moran LB, Michael GJ, Wang B, Novoselov S, Cheetham ME, et al. Homocysteine-induced endoplasmic reticulum protein (herp) is up-regulated in parkinsonian substantia nigra and present in the core of Lewy bodies. Clin Neuropathol. 2009;28:333-43.

19. Chigurupati S, Wei Z, Belal C, Vandermey M, Kyriazis GA, Arumugam TV, et al. The homocysteine-inducible endoplasmic reticulum stress protein counteracts calcium store depletion and induction of CCAAT enhancer-binding protein homologous protein in a neurotoxin model of Parkinson disease. J Biol Chem. 2009;284:18323-33.

20. Chan SL, Culmsee C, Haughey N, Klapper W, Mattson, MP. Presenilin-1 mutations sensitize neurons to DNA damage-induced death by a mechanism involving perturbed calcium homeostasis and activation of calpains and caspase-12. Neurobiol Dis. 2002;11:2-19.

21. Chan SL, Mayne M, Holden CP, Geiger JD, Mattson, MP. Presenilin-1 mutations increase levels of ryanodine receptors and calcium release in PC12 cells and cortical neurons. J Biol Chem. 2000;275:18195-200.

22. Kyriazis GA, Belal C, Madan M, Taylor DG, Wang J, Wei Z, et al. Stress-induced switch in Numb isoforms enhances Notch-dependent expression of subtype-specific transient receptor potential channel. J Biol Chem. 2010;285:6811-25.

23. Mikoshiba K. The IP3 receptor/Ca2+ channel and its cellular function. Biochem Soc Symp. 2007;74:9-22.

24. Patterson RL, Boehning D, Snyder SH. Inositol 1, 4, 5-trisphosphate receptors as signal integrators. Annu Rev Biochem. 2004;73:437-65.

25. Tu H, Nelson O, Bezprozvanny A, Wang Z, Lee SF, Hao YH, et al. Presenilins form ER Ca2+ leak channels, a function disrupted by familial Alzheimer's disease-linked mutations. Cell. 2006;8:981-93.

26. Nath S, Goodwin J, Engelborghs Y, Pountney DL. Raised calcium promotes α-synuclein aggregate formation. Mol Cell Neurosci. 2011;46:516-26.

27. Lee B, Gai W, Laychock SG. Proteasomal activation mediates down-regulation of Inositol 1,4,5-Trisphosphate receptor and calcium mobilization in rat pancreatic islets. Endocrinology. 2001;142:1744-51.

28. Mackrill JJ. Possible regulation of the skeletal muscle ryanodine receptor by a polyubiquitin binding subunit of the 26S proteasome. Biochem Biophys Res Commun. 1998;245:428-9.

29. Sai X, Kokame K, Shiraishi H, Kawamura Y, Miyata T, Yanagisawa K, et al. The ubiquitin-like domain of Herp is involved in Herp degradation, but not necessary for its enhancement of amyloid beta-protein generation. FEBS Lett. 2003;553:151-6.

30. Giasson BI, Duda JE, Quinn SM, Zhang B, Trojanowski JQ, Lee VM. Neuronal alpha-synucleinopathy with severe movement disorder in mice expressing A53T human alpha-synuclein. Neuron. 2002;34:521-33.

31. Hajnoczky G, Csordas G, Madesh M, Pacher P. Control of apoptosis by IP(3) and ryanodine receptor driven calcium signals. Cell Calcium. 2000;28:349-63.

32. Mattson, MP. Calcium and neurodegeneration. Aging Cell. 2007;6:337-50.

33. Frandsen A, Schousboe A. Dantrolene prevents glutamate cytotoxicity and Ca2+ release from intracellular stores in cultured cerebral cortical neurons. J Neurochem. 1991;56:1075-8.

34. Guo Q, Sopher BL, Furukawa K, Pham DG, Robinson N, Martin GM, et al. Alzheimer's presenilin mutation sensitizes neural cells to apoptosis induced by trophic factor withdrawal and amyloid beta-peptide: involvement of calcium and oxyradicals. J Neurosci. 1997;17:4212-22.

35. Kim, TY, Kim, E, Yoon, SK and Yoon, JB. (2008) Herp enhances ER-associated protein degradation by recruiting ubiquilins. Biochem Biophys Res Commun., 369, 741-746.

36. Madesh M, Hawkins BJ, Milovanova T, Bhanumathy CD, Joseph SK, Ramachandrarao SP, et al. Selective role for superoxide in InsP3 receptor-mediated mitochondrial dysfunction and endothelial apoptosis. J Cell Biol. 2005;170:1079-90.

37. Deniaud A, Sharaf el dein O, Maillier E, Poncet D, Kroemer G, Lemaire C, et al. Endoplasmic reticulum stress induces calcium-dependent permeability transition, mitochondrial outer membrane permeabilization and apoptosis. Oncogene. 2008;27:285-99.

38. Jiang P, Gan M, Ebrahim AS, Lin WL, Melrose HL, Yen, SH. ER stress response plays an important role in aggregation of α-synuclein. Mol Neurodegener. 2010;5:56.

39. Mouatt-Prigent A, Agid Y, Hirsch EC. Does the calcium binding protein calretinin protect dopaminergic neurons against degeneration in Parkinson's disease? Brain Res. 1994;668:62-70.

40. Von Lewinski F, Fuchs J, Vanselow BK, Keller BU. Low Ca2+ buffering in hypoglossal motoneurons of mutant SOD1 (G93A) mice. Neurosci Lett. 2008;445:224-28.

41. Kikuchi H, Almer G, Yamashita S, Guégan C, Nagai M, Xu Z, et al. Spinal cord endoplasmic reticulum stress associated with a microsomal accumulation of mutant superoxide dismutase-1 in an ALS model. Proc Natl Acad Sci U S A. 2006;103:6025-30.

42. Saxenam S, Cabuy E, Caroni P. A role for motoneuron subtype-selective ER stress in disease manifestations of FALS mice. Nat Neurosci. 2009;12:627-36.

43. Okuda-Shimizu Y, Hendershot LM. Characterization of an ERAD pathway for nonglycosylated BiP substrates, which require Herp. Mol Cell. 2007;28(4):544-54. PMCID: 2149893.

CHAPTER THREE: THE HOMOCYSTEINE-INDUCIBLE ENDOPLASMIC RETICULUM STRESS PROTEIN COUNTERACTS CALCIUM STORE DEPLETION AND INDUCTION OF CCAAT ENHANCER-BINDING PROTEIN HOMOLOGOUS PROTEIN IN A NEUROTOXIN MODEL OF PARKINSON DISEASE

This research was originally published in Journal of Biological Chemistry. Srinivasulu Chigurupati, Zelan Wei, Cherine Belal, Myriam Vandermey, George A Kyriazis, Thiruma V Arumugam, and Sic L Chan. The homocysteine-inducible endoplasmic reticulum stress protein counteracts calcium store depletion and induction of CCAAT enhancer-binding protein homologous protein in a neurotoxin model of Parkinson Disease. *Journal of Biological Chemistry*. 2009; 284(27):18323–18333.

Introduction

Parkinson disease (PD) is the second most common age-related neurodegenerative disorder that results in the selective degeneration of dopaminergic neurons of the substantia nigra pars compacta (1, 2). The proximate cause of selective degeneration of dopaminergic neurons in PD has not been clearly elucidated. Several mechanisms are inferred to play a role in the pathogenesis of PD based on studies from animals or *in vitro* studies using dopaminergic neurotoxins. These include mitochondrial dysfunction, oxidative stress, and impairment of the ubiquitin-proteasomal pathway (UPP) (1–3). It has been shown that several genes that are mutated in familial PD encode for proteins that have functions linked to UPP and mitochondria (1–3). The UPP plays a critical role in ER-associated protein degradation (ERAD), a protein quality control system of the ER that eliminates misfolded proteins in the ER lumen (4). UPP dysfunction

results in the accumulation of misfolded or unfolded proteins within the ER, which induces ER stress (5).

Important roles for ER stress and ER stress-induced cell death have been reported in a broad spectrum of pathological conditions (6). To alleviate ER stress and enhances cell survival, cells launch the unfolded protein response (UPR), an adaptive response to minimize accumulation of misfolded proteins that would otherwise be toxic to the cell (7). The biological objectives of the UPR are to reduce the overall protein translation, increase the production of ER localized chaperones, and increase the clearance of unfolded proteins by UPP (7). Although short time UPR activation serves to reduce the unfolded protein load, a protracted activation of UPR, as the result of either severe or prolonged ER dysfunction, activates the cell death program (7). Important mediators of ER stress-associated death include the activation of the ER-associated procaspase-12 (in mouse) or procaspase-4 (in human) and increased expression of the pro-apoptotic transcription factor CCAAT enhancer-binding protein homologous protein (CHOP, also termed as growth arrest-DNA damage response protein or Gadd153) (8).

Recent studies have demonstrated hallmarks of ER stress in several experimental models of PD (9–12) and in dopaminergic neurons in the substantia nigra of PD subjects (13). Although these studies indicate that ER stress is closely associated with PD, it is yet not clear whether and how ER stress contributes to the degenerative cascades in PD. Cells that fail to respond to ER stress are more sensitive to neurotoxin-induced death (9), suggesting that up-regulation of ER stress proteins, at least during the early phase of the ER stress response, is important to

restore ER homeostasis and to prevent activation of the ER stress-induced apoptotic program. Consistent with this notion, preconditioning with a sublethal level of ER stress has been shown to protect cells, in part through up-regulation of ER stress proteins. Hence, understanding the molecular mechanisms by which ER stress proteins overcome ER stress may help to uncover novel approaches to block the ER stress-associated pathological processes in cell culture and animal models of PD (9–12).

Herp (homocysteine-inducible ER stress protein) is a membrane-bound, ubiquitin-like protein that is located in the ER (14). Herp expression is strongly up-regulated in cultured primary neurons exposed to proteasomal inhibitors or pharmacological agents that selectively induce ER dysfunction (14–16). We previously reported that overexpression of Herp promotes neuronal survival, whereas knockdown of Herp protein by small interference RNA enhances vulnerability to ER stress- and amyloid β-peptide-induced apoptosis (16). The ability of Herp to prevent ER stress-induced death was correlated with its ability to stabilize cellular Ca^{2+} homeostasis (16, 17). Here, we investigated the role of Herp in the cellular response to 1-methyl-4-phenylpyridinium (MPP^+), a neurotoxicant commonly used to elicit experimental models of PD (18). Because disturbances in intracellular Ca^{2+} homeostasis have been implicated in oxidative cell injury (19), we test the hypothesis of whether Herp may play a role in counteracting MPP^+-induced disturbances in intracellular Ca^{2+} homeostasis. Our results indicate that knockdown of Herp increases MPP^+-induced CHOP expression, ER Ca^{2+} leakage, and

vulnerability to MPP^+-induced cytotoxic cell death, suggesting that Herp is critical for survival adaptation to this PD neurotoxin.

Materials and Methods

Materials

1-methyl-4-phenylpyridinium (MPP^+) and tunicamycin were purchased from Sigma Chemical. Lactacystin and LLVY-AMC were obtained from BioMol. The antibodies for Herp and CHOP were obtained from BioMol and Santa Cruz Biotechnology. The antibody for ERK1 was obtained from Cell Signaling. The antibodies to Grp78 and Bcl-2 were purchased from Stressgen and Millipore, respectively. Secondary antibodies conjugated to horseradish peroxidase (HRP) were from Jackson Immunoresearch, respectively. 7-dichloro-dihydrofluorescein diacetate (DCF-DA) was obtained from Molecular Probes.

Generation of DNA Constructs

Plasmids containing the full-length or mutant deletion human Herp cDNA were constructed as described previously (16). Site-directed mutagenesis was performed to generate by a PCR-based primer overlap extension method. In brief, the same pair of flanking primers and two different mutant overlapping primers were synthesized as described (16). The PCR products that contained the mutant sequence were subcloned into the PCR4 TOPO TA cloning vector (Stratagene), which was then amplified and digested with BamHI and EcoRII and subcloned into the pcDNA3.1 vector. The mutation was confirmed by automated DNA sequencing.

Generation of Stably Transfected Cell Lines

Transfection of PC12 cells was carried out using the Lipofectamine reagent (Invitrogen) as previously described (16). Stably expressing clones were obtained after selection for growth in the presence of geneticin (500 mg/liter) and characterized for Herp expression by immunoblot analysis. For experiments, PC12 cells were plated onto glass coverslips and used between 18 and 48h after plating. Cells stably transfected with the empty vector were used as controls.

Experimental Treatments

PC12 and MN9D cells were treated with MPP^+ (1 mM), tunicamycin (5 μg/ml), and lactacystin (5 μM) in OPTI-MEM (Invitrogen). Each of these compounds was prepared in Me_2SO immediately before applying them to the cultures. When Me_2SO was used as the solvent, their final concentration did not exceed 0.1%. At the end of each treatment, the cultures were processed for immunoblotting and for evaluating the extent of cell death.

RNA Interference

Herp and CHOP siRNA duplexes are designed to specifically target the 21-nucleotide region 5'-CGC-AACAAATAGTCGGAACATC-3' of the Herp gene (NM_004562.1) and 5'-CTCTTGACCCTGCATCCCTA-3' of the CHOP gene (nucleotides 270 –291; NM_024134). These target sequences were chosen based on previous experiments testing the gene-silencing effectiveness of three to four siRNA duplexes (16, 20). Blast searches confirmed that these sequences were not homologous to any genes. A previously described scrambled sequence (20) is used

as siRNA-Control. The cells were transfected with the siRNA duplexes using Lipofectamine 2000 (Invitrogen) in Opti-MEM according to manufacturer's protocol. After overnight incubation, the cultures were washed and replaced with 2 ml of fresh serum containing Dulbecco's modified Eagle's medium to allow recovery for 24 h. To monitor knockdown, the cells were harvested and processed for RT-PCR and/or Western blot analyses.

Quantification of Cell Survival

Cell viability was assessed by the trypan blue exclusion method and the lactate dehydrogenase release assay as described previously (16, 20). Cell viability was evaluated in triplicates for each treatment. All of the experiments were repeated at least three times.

RNA Isolation and RT-PCR

Total RNA from cells grown on 100-mm dishes was isolated with TRIzol (Invitrogen), and 2 μg of RNA was reverse transcribed with Superscript II reverse transcriptase and an oligo(dT) primer (Invitrogen). Semi-quantitative RT-PCR analyses of Herp, CHOP, and glyceraldehyde-3-phosphate dehydrogenase were performed using the following pairs of primers:

rat Herp, 5'-CCACTACCACAACTACCA-CTG-3' (forward) and 5'-CCTCTCTTTGGCTTTCTGGAA-3' (reverse); rat glyceraldehyde-3-phosphate dehydrogenase, 5'-TGTGATGGACTCCGGTGACGG-3' (forward) and 5'-ACAGCTTCTCTTTGATGTCACGC-3' (reverse); rat CHOP, 5'-AAGGTCTACGAAGGTGAACGACCCC-3 (forward) and 5'-

GACCCCAAGACACGTGAGCAACTGC-3' (reverse); rat Grp78/Bip,5'-CCACAAGGATGCAGACATTG-3' (forward) and 5'-AGGGCCTCCACTTCCATAGA-3' (reverse); and rat glyceraldehyde-3-phosphate dehydrogenase (which served as an internal control), 5'-CCACAAGGATGCAGACATTG-3' (forward) and 5'-AGGGCCTCCACTTCCATAGA-3' (reverse).

Measurement of ER and Mitochondrial Ca^{2+} Concentrations

Free Ca^{2+} levels in the ER ($[Ca^{2+}]_{ER}$) will be evaluated using the ER-targeted YC4 (YC4-ER; gift of Dr. W. F. Graier, University of Graz), a low affinity ratiometric "cameleon" indicator with a KDEL sequence and a calreticulin signal peptide, as previously described (21). For measurement of mitochondria Ca^{2+} level ($[Ca^{2+}]_M$), the mitochondria-targeted ratiometric-pericam (RP-mt; gift of Dr. A. Miyawaki, RIKEN Brain Science Institute) was used as described previously (22). Briefly, cells plated at 60% confluency on glass coverslips were transiently transfected with 2 μg of p-BudCR4.1-YC4-ER or pcDNA3-Rp-mt using Lipofectamine. Twenty-four hours after transfection, the cells were incubated with MPP^+, and changes in $[Ca^{2+}]_{ER}$ and $[Ca^{2+}]_M$ were monitored by confocal laser scanning imaging system with excitation set at 440 nm (for YC4-ER) or at 433 and 485 nm (for Rp-mt). Emission was monitored at 485 and 535 nm (for YC4-ER) or at 539 nm (for Rp-mt). Measurements were performed in Locke's buffer containing: 154 mM NaCl, 5.6 mM KCl, 2.3 mM $CaCl_2$, 1.0 mM $MgCl_2$, 3.6 mM $NaHCO_3$, 5 mM HEPES, and 10 mM D-glucose, pH 7.2 (16, 20).

The data were expressed as the ratios of the fluorescence in treated relative to untreated cultures.

Protein extraction, immunoprecipitation, and Western blotting

Cell lysates for Western blotting were prepared in T-PER lysis buffer (Pierce). In all experiments, the same amount of total protein was loaded for each sample. The membranes were probed with the primary antibodies: Herp, Grp78/Bip, CHOP and ERK1, followed by horseradish peroxidase conjugated secondary antibody and developed with the Super Signal West Pico Chemiluminescent substrate (Pierce). For immunoprepitation, aliquots of cell lysates containing 300 µg of protein were incubated with rabbit polyclonal Herp antibody in immunoprecipitation buffer (150 mM NaCl, 2 mM EDTA, 1% Nonidet P-40, 5 µg/ml leupeptin, 5 µg/ml aprotinin, 2 µg/ml pepstatin A, 0.25 mM phenylmethylsulfonyl fluoride, 50 mM Tris, pH 7.6). Antigen-antibody complexes were precipitated with immobilized protein A, washed three times in immunoprecipitation buffer, and solubilized by heating in Laemmli buffer containing 2-mercaptoethanol at 100 °C for 4 min. The solubilized proteins were separated by SDS-polyacrylamide gel and then immunoblotted with a polyclonal antibody to Bcl-2.

Proteasomal activity

Chymotrypsin-like activity of proteasome was assayed using the fluorogenic peptide Suc-Leu-Leu-Val-Tyr-7-amino-4-methylcoumarin (LLVY-AMC) according to the method reported previously (15). Briefly, after the treatment with MG132 or lactacystin for 30 min, cultures were harvested, lysed in proteasome buffer (10 mmol/L Tris–HCl, pH 7.5, 1 mmol/L ethylene diamine tetraacetic acid (EDTA), 2 mmol/L adenosine-5'-

triphosphate, 20% glycerol, and 4 mmol/L dithiothreitol), and centrifuged at 13, 000 g at 4 °C for 10 min. The supernatant (20 µg of protein) was then incubated with proteasome activity assay buffer (0.05 mol/L Tris–HCl, pH 8.0, 0.5 mmol/L EDTA, 40 µmol/L LLVY-AMC) for 1 h at 37 °C. The reaction was stopped by adding 0.9 mL of cold water and placing the reaction mixture on ice for at least 10 min. Subsequently, the fluorescence of the solution was measured by Fluorescence Microplate Reader with excitation at 380 nm (Ex) and emission at 440 nm (Em). All readings were standardized relative to the fluorescence intensity of an equal volume of free 7-amino-4-methylcoumarin solution.

Statistical analysis

Comparison between two groups was performed using Student's t-test, whereas multiple comparisons between more than two groups were analyzed by one-way ANOVA and post hoc tests. The data evaluated for the effects of two variables were analyzed using two-way ANOVA. The results are presented by mean ± standard deviation. For all analyses, statistical significance is defined as p-value of ≤0.05.

Results

Herp Is Required for Survival Adaptation to MPP^+-induced ER Stress

Several ER stress inducible proteins such as Grp78 and Herp are constitutively expressed. To address the role of Herp in the MPP^+-induced cell death model, we used RNA interference to knockdown endogenous Herp expression. Transfection of PC12 cells with a siRNA that targets Herp (siRNA-Herp) resulted in a substantial reduction in the level Herp protein (**Fig. 1*A***). To evaluate

the effect of Herp knockdown on neuronal vulnerability to MPP^+ toxicity, we assessed cell viability by using the trypan blue exclusion (**Fig. 1*B***) and lactate dehydrogenase release (not shown). Exposure of cultures to 0.5 mM MPP^+ induced~ 45–50% cell death within 24 h. Depletion of Herp protein markedly enhanced the vulnerability of PC12 cells to MPP^+ toxicity. Compared with cultures transfected with a scramble control siRNA (siRNA-Con), there were significantly more dead cells in cultures treated with siRNA-Herp, indicating that down-regulation of Herp sensitizes PC12 cells to MPP^+-induced death (**Fig. 1*B***). Similar results were obtained in MN9D, a midbrain-derived dopaminergic neuronal cell line (**Fig. 1*B***). Next, we determined whether PC12 cells stably overexpressing Herp (PC12-Herp) are resistant to MPP^+-induced death. Herp protein overexpression was confirmed in three independent clones by immunoblotting (**Fig. 1*C***). Compared with PC12-VT, PC12-Herp cells were significantly more resistant to 0.5 mM MPP^+ (**Fig. 1*D***), a dose that yielded ~50% cell death 24 h post-treatment (**Fig. 1*B***). Collectively, the results indicate that survival adaptation to MPP^+ is dependent on Herp function.

Given that Herp expression is responsive to ER stress (14 –16) and that ER stress has been shown to accompany neurotoxin-induced death (9 –11), we next evaluated whether MPP^+ may induce the expression of Herp. Levels of Herp mRNA and protein in PC12 cells were not markedly increased after exposure to MPP^+ (**Fig. 2*A***). The same dose of MPP^+ also failed to robustly increase Herp protein expression in MN9D cells (**Fig.2*B***), thus excluding the possibility that the observed anomaly in Herp induction was cell type-specific. By contrast, the protein level of Grp78, a marker of ER stress, was transiently up-regulated in PC12 and MN9D cells by MPP^+

(**Fig. 2, *A*** and ***B***), indicating activation of the ER stress response by MPP^+. For comparison, we treated sister cultures with tunicamycin, a known pharmacological ER stressor that causes protein accumulation in the ER by inhibiting protein glycosylation (16). Levels of both Herp and Grp78 protein were robustly up-regulated in both PC12 and MN9D cells after treatment with tunicamycin (**Fig. 2*C***). Taken together, the above results suggest that cells are unable to induce Herp protein expression in response to MPP^+.

Herp Counteracts MPP^+-induced Perturbation of ER Ca^{2+} Homeostasis

Oxidative stress is an important factor implicated in the disruption of neuronal Ca^{2+} homeostasis (23). Consistent with previous reports (24, 25), MPP^+ increased the intracellular accumulation of hydroxyl and peroxynitrite in PC12 and MN9D cells (**Supplemental Fig. S1**). Given that perturbations of intracellular Ca^{2+} homeostasis have been implicated in oxidative stress-induced cell death (19), we next examined the effects of MPP^+ on ER Ca^{2+} handling. To this end, we monitor changes in the Ca^{2+} concentration in the ER lumen ($[Ca^{2+}]_{ER}$) of PC12 and MND9D cells at various time points after treatment with MPP^+. The early rise in $[Ca^{2+}]_{ER}$ was quickly followed by a gradual and progressive decline in MPP^+-treated cells (**Fig. 3*A***), suggesting that MPP^+ increased Ca^{2+} leakage from the ER.

Because Herp functions to stabilize ER Ca^{2+} homeostasis during ER stress (16, 17), we next evaluated whether overexpression of Herp prevents MPP^+-induced perturbations of $[Ca^{2+}]_{ER}$. Compared with PC12-VT cells, PC12-Herp cells exhibited reduced ER Ca^{2+} leakage and were able to maintain $[Ca^{2+}]_{ER}$ (**Fig. 3*B***). Because uncontrolled ER Ca^{2+} release can lead to protracted rise in the Ca^{2+} concentration

of the mitochondria ($[Ca^{2+}]_M$) (8, 29) and because aberrant mitochondrial Ca^{2+} handling has been shown to be involved in MPP^+-induced toxicity (30, 31), we next assessed changes in $[Ca^{2+}]_M$ in PC12 and MN9D cells at various time points after treatment with MPP^+. The decrease of $[Ca^{2+}]_{ER}$ was accompanied by an increase in $[Ca^{2+}]_M$ in MPP^+-treated cells (**Fig. 3*C***), indicating that MPP^+ induces Ca^{2+} mobilization from the ER to mitochondria. As expected, the magnitude of the increase in $[Ca^{2+}]_M$ was significantly attenuated in PC12-Herp (**Fig. 3*D***), suggesting that Herp likely inhibits the toxic Ca^{2+} transfer from the ER to mitochondria under oxidant-induced ER stress. Representative pseudocolored images of the indicated PC12 clones expressing the fluorescent Ca^{2+} indicators, YC4-ER and pericam-mt, are shown in **Fig. 3** (***B*** and ***D***), respectively. Co-localization studies confirmed that the indicated fluorescent indicators are properly targeted and expressed either in the ER (YC4-ER) or in the mitochondria (pericam-mt) (**Supplemental Fig. S3**).

Herp Blocks MPP^+-induced Activation of CHOP

CHOP has been implicated as a mediator of apoptosis in the context of ER and oxidative stress (32, 33). ER stress-induced cell death in cultures occurs only when CHOP is permanently up-regulated but not when the increase in CHOP is transient, suggesting that CHOP contributes to the activation of ER-initiated apoptosis signaling (31–34). Given that store depletion has been associated with CHOP up-regulation (20, 35) and that overexpression of Herp counteracts MPP^+-induced ER Ca^{2+} store depletion (**Fig. 3*B***), we next evaluate whether CHOP is differentially induced by MPP^+ in PC12-VT and PC12-Herp clones. The magnitude of the MPP^+ induced increase in CHOP protein level was significantly lower in PC12-

Herp when compared with PC12-VT (**Fig. 4*A***). The Herp-mediated suppression of CHOP was also associated with reduced Grp78 induction (**Fig. 4*A***), suggesting that Herp restores ER homeostasis in MPP^+-treated cells by inhibiting downstream events caused by CHOP.

By contrast, suppression of endogenous Herp by RNA interference potentiates CHOP induction in MPP^+-treated PC12 cells (**Fig. 4*B***). Treatment with siRNA-Con, which had no effect on Herp expression (**Fig. 1*A***), did not enhance MPP^+-induced CHOP up-regulation (**Fig. 4*B***). These data are consistent with a previous study showing that Herp null cells displayed aberrant ER stress signaling with increased level of CHOP transcript when compared with wild-type control cells (15).

Next, we determined whether suppression of CHOP induction by RNA interference is sufficient to inhibit MPP^+ toxicity. siRNA targeting CHOP (siRNA-CHOP) (20) was used to inhibit the MPP^+-induced CHOP expression in PC12 cells (**Fig. 4*C***). Cell viability assessed by trypan blue exclusion assay showed that siRNA-induced silencing of CHOP provided significant protection against MPP^+ toxicity (**Fig. 4*D***). By contrast, the siRNA-Con did not rescu PC12 cells from MPP^+ toxicity (**Fig. 4*D***). Interestingly, knockdown of CHOP did not further rescue PC12-Herp cells from MPP^+-induced toxicity (**Supplemental Fig. S2**), suggesting that Herp promotes cell survival in large by suppressing CHOP-dependent pro-apoptotic signaling. Collectively, the above results indicate that Herp attenuates MPP^+-induced cell death by inhibiting CHOP up-regulation.

CHOP Contributes to MPP^+-induced Perturbation of ER Ca^{2+} Homeostasis

To determine whether CHOP up-regulation in MPP^+-treated cells is causally linked to ER Ca^{2+} store depletion, we measured the MPP^+-induced perturbation in ER Ca^{2+} homeostasis in PC12 cells transfected with siRNA-CHOP. Compared with siRNA-Control, siRNA-CHOP substantially reduced ER Ca^{2+} leakage in MPP^+-treated PC12 cells. CHOP knockdown also attenuates MPP^+-induced ER Ca^{2+} store depletion (**Fig. 5*A***). Because Herp suppressed CHOP induction in MPP^+-treated PC12 cells, we examined whether knockdown of Herp expression exacerbated MPP^+-induced ER Ca^{2+} store depletion. As expected, knockdown of Herp exacerbated ER Ca^{2+} leakage (**Fig. 5*B***) in MPP^+-treated PC12 cells (**Fig. 5*C***). These data indicate that Herp prevents CHOP-mediated ER Ca^{2+} store depletion in MPP^+-treated PC12 cells.

The Herp-dependent Protective Mechanism Is Not Mediated by the Anti-apoptotic Bcl-2 Protein

Because CHOP has been shown to down-regulate the expression of Bcl-2 protein (36) and because overexpression of Bcl-2 affects Ca^{2+} handling by the ER (8, 37), we next determined whether Bcl-2 protein may be acting downstream of Herp to maintain ER Ca^{2+} homeostasis in MPP^+-treated PC12 cells. Levels of Bcl-2 protein in PC12-VT and PC12-Herp were not significantly different before and after exposure to MPP^+ (**Supplemental Fig. S4**). To rule out the possibility that Herp might interact with Bcl-2 and therefore facilitated Bcl-2 association with the ER membrane, we measured the amounts of Bcl-2 protein in isolated microsomes. Levels of Bcl-2 protein in the microsomes prepared from PC12-Herp were comparable with those

from PC12-VT and were nearly unchanged following exposure to MPP^+ (**Supplemental Fig. S4**). No interaction between Bcl-2 and Herp was detected by co-immunoprecipitation analysis (**Supplemental Fig. S4**). All in all, although Herp affects Ca^{2+} handling by the ER in a manner resembling the effects of Bcl-2 overexpression, data from these experiments excluded a role for Bcl-2 in the Herp-dependent stabilization of ER Ca^{2+} homeostasis in MPP^+-treated cells.

The Ubiquitin-like (UBL) Domain Is Essential for Herp-mediated ER Ca^{2+} Stabilization and Protection from MPP^+-induced Toxicity

Previous studies established a critical role of the N-terminal UBL domain in the cytoprotective action of Herp (15–17). Overexpression of a mutant Herp deletion construct lacking the UBL domain (ΔUBL-Herp; **Fig. 6*A***) failed to protect PC12 cells from ER stress-induced cell death (15–17). To determine whether the Herp-dependent protection against MPP^+ toxicity may also require the UBL domain, we generated PC12 clones stably overexpressing ΔUBL-Herp. Stable transfection inducing overexpression of ΔUBL-Herp was verified by immunoblotting (**Fig. 6*A***). Compared with PC12-VT, PC12-ΔUBL -Herp clones were not more resistant to MPP^+-induced cell death (**Fig. 6*B***), suggesting that the UBL domain is required for Herp-dependent cytoprotective action.

To determine whether the UBL domain is essential for the stabilization of ER Ca^{2+} homeostasis, we measured $[Ca^{2+}]_{ER}$ in PC12-ΔUBL -Herp. The magnitude of the MPP^+-induced ER Ca^{2+} leakage was indistinguishable in PC12-VT and PC12-ΔUBL -Herp, suggesting that the UBL domain is required for the ability of Herp to maintain ER Ca^{2+} homeostasis (**Fig. 6*C***). We also found that CHOP mRNA and

protein levels in PC12-VT clones are not significantly different in PC12-ΔUBL - Herp clones (**Fig. 6*D***), which further supports the notion that a functional Herp protein is required to suppress CHOP induction and to stabilize ER Ca^{2+} homeostasis.

Herp-dependent Stabilization of ER Ca^{2+} Homeostasis Requires a Functional UPP

Herp has recently been implicated in the regulation of ERAD (38, 39), a protein quality control system of the ER, which eliminates misfolded proteins by UPP-dependent degradation (4). To determine whether ERAD is involved in the Herp-dependent stabilization of ER Ca^{2+} homeostasis, we blocked ERAD with the proteasomal inhibitor lactacystin. Treatment of PC12 cells with lactacystin for 12 and 24 h significantly reduced proteasomal activity (**Supplemental Fig. S5**). Inhibition of proteasome function reversed the Herp-dependent suppression of CHOP induction (**Fig. 7*A***) and accelerates ER Ca^{2+} depletion (**Fig. 7*B***), suggesting that proteosomal activity is required for Herp-dependent stabilization of ER Ca^{2+} homeostasis. Consistent with the notion that the proteasomal function is required for the neuroprotective action of Herp, we found that lactacystin not only increased the vulnerability of PC12 cells (**Fig. 7*C***) but also restores the sensitivity of PC12-Herp clones to MPP^+ toxicity (**Fig. 7*D***).

Discussion

Elucidating the specific and sequential molecular events induced by MPP^+ will provide a better understanding of the molecular basis of dopaminergic cell death. MPP^+ is selectively toxic to dopaminergic neurons and has been studied extensively

as an etiologic model of PD because mitochondrial dysfunction is implicated in both MPP^+ toxicity and the pathogenesis of PD. MPP^+ toxicity has been attributed to the generation of reactive oxygen species (ROS) (24, 25). ROS generated from mitochondrial appear to be a main contributor of oxidative stress-mediated neurodegeneration in PD models (40).

Oxidative stress is an important factor implicated in the disruption of neuronal Ca^{2+} homeostasis (19). In this study we showed that MPP^+ induces the deregulation of ER Ca^{2+} homeostasis. There is a growing body of evidence that the ER can play pivotal roles in regulating cell survival and apoptosis in a variety of cell types including neurons. The ER serves many specialized functions in the cells including the biosynthesis of membrane and secretory proteins (7) and maintenance of neuronal Ca^{2+} homeostasis (41). Dysregulation of ER Ca^{2+} homeostasis occurs as an early event during many forms of apoptosis and has been implicated in the pathophysiology of several acute and chronic neurodegenerative diseases, including ischemic injury, trauma, and Alzheimer, Huntington, and prion diseases (41– 43). Uncontrolled Ca^{2+} release from the ER is a key proapoptotic event, as indicated by the ability of blockers of ER Ca^{2+} release to reduce the extent of ischemic injury (44) and to protect cultured neurons against cell death induced by glutamate, mutant huntingtin, Aβ, and prion peptides (21, 45). Whether dysregulation of ER Ca^{2+} homeostasis contributes to PD initiation and progression has not yet been established.

Disturbances in intracellular Ca^{2+} homeostasis could play a role in dopaminergic degeneration because treatment with various PD neurotoxins has

been shown to perturb intracellular Ca^{2+} homeostasis (26–28). The MPP^+-induced cell death was inhibited by co-expression of calbindin-D28K or co-treatment with BAPTA (1,2-bis-(*o*-aminophenoxy)-ethane-*N*,*N*,*N*',*N*'-tetracidic acid), suggesting a critical role for intracellular Ca^{2+} loads in MPP^+-induced toxicity (46). The pertinent mechanism whereby neurotoxins disrupt intracellular Ca^{2+} homeostasis remains poorly understood. Antagonists of glutamate and Ca^{2+} channels (47) have been reported ineffective in preventing MPP^+ toxicity, suggesting that the Ca^{2+} perturbations induced by MPP^+ are likely attributed to deregulated ER Ca^{2+} release. Consistent with the latter notion, inhibition of ER Ca^{2+} release prevents the MPP^+-induced perturbations of intracellular Ca^{2+} (47).

Various pathological conditions that induce ER stress have been shown to perturb ER Ca^{2+} homeostasis (8, 16, 29), but the underlying mechanisms remain poorly characterized. Oxidative damage to the ER can lead to perturbations in ER Ca^{2+} homeostasis. Protein folding in the ER can generate ROS, which in turn may exacerbate ER stress by perturbing the function of ER foldases and/or chaperones (48). ROS could also sensitize ryanodine receptor- and inositol triphosphate receptor-mediated ER Ca^{2+} release (49, 50) or block sarcoplasmic/endoplasmic reticulum Ca^{2+}-ATPase-mediated Ca^{2+} sequestration by the ER (51). During ER stress, increased Ca^{2+} transfer from the ER to mitochondria leads to mitochondria Ca^{2+} overload and generation of mitochondrial-derived ROS, which could further disrupt protein folding in the ER and potentiate ER Ca^{2+} release through a positive feed-forward mechanism (52, 53).

Recent studies show that neurotoxins induce ER stress via the generation of ROS (54, 55), suggesting that ER stress may be involved downstream of ROS. The biological relevance of the neurotoxin induced-ER stress is still unknown. Given that ER is an important regulator of intracellular Ca^{2+} homeostasis, oxidant-induced deregulation of ER Ca^{2+} homeostasis could contribute to dopaminergic degeneration.

Induction of ER stress proteins during oxidative and ER stress seems to be important to remedy the perturbations of ER Ca^{2+} homeostasis. We previously reported that Herp is essential for cell survival in response to ER stress (16). Here, we found that Herp is critical for cellular stress adaptation in response to MPP^+. Consistent with this notion, we found that overexpression of Herp attenuated MPP^+-induced toxicity, whereas knockdown of Herp increased not only CHOP expression but also ER Ca^{2+} leakage and mitochondrial Ca^{2+} accumulation, resulting in cell death (**Fig. 1**). Notably, we found that MPP^+ failed to up-regulate Herp expression in dopaminergic cells *in vitro* (**Fig. 2, *A*** and ***B***). Failure to induce a compensatory increase in Herp expression may deteriorate ER function in MPP^+-treated cells. Hence, exploring ways to increase Herp expression can increase the ability of dopaminergic cells to cope with ER stress and to protect from MPP^+ toxicity.

Given that Herp plays a crucial role in stabilizing ER Ca^{2+} homeostasis (16, 17), we determined whether stable expression of Herp counteracts MPP^+-induced toxicity by inhibiting Ca^{2+} transfer for ER to mitochondria. Time course analysis of the of the MPP^+-induced alterations in $[Ca^{2+}]_{ER}$ and $[Ca^{2+}]_M$ revealed that knockdown of Herp

accelerates ER Ca^{2+} store depletion with a time course that parallels $[Ca^{2+}]_M$ accumulation (**Fig. 3*B***) and that overexpression of Herp reversed the toxic Ca^{2+} transfer between the ER and mitochondria (**Fig. 3, *A*** and ***B***). The mitochondrial apoptotic pathway is an integral part of MPP^+-induced apoptosis (24, 25). Excessive accumulation of $[Ca^{2+}]_M$ causes collapse of the mitochondria membrane potential, which results in mitochondrial transition pore opening and release of pro-apoptogenic factors including cytochrome *c* that promotes downstream caspase activation (53). Because mitochondria are linked to the ER both by proximity and through Ca^{2+} signaling (52, 56), various pathological conditions that perturb ER Ca^{2+} homeostasis could adversely impact the function of the mitochondria. Hence, oxidant-induced damage to the ER could cause a protracted elevation in $[Ca^{2+}]_M$ that could enhance generation of mitochondrial-derived ROS that through a feed forward mechanism exacerbates the loss of Ca^{2+} from the ER (53).

The underlying molecular and cellular mechanisms whereby Herp stabilizes ER Ca^{2+} homeostasis and preserves mitochondrial function in MPP^+-treated cells remain to be established. It is unlikely that the ER membrane-associated Herp functions as a calcium-binding chaperone analogous to Grp78 and calreticulin (14). We excluded a role for Bcl-2 in the Herp-mediated stabilization of ER Ca^{2+} homeostasis based on the findings that Herp fails to bind to Bcl-2 and that total levels of Bcl-2 in the microsome fractions were not significantly different in PC12-VT and PC12-Herp cells (**Supplemental Fig. S4**). Hence, the mechanism by which Herp maintains ER Ca^{2+} homeostasis appears to be different from the proposed anti-apoptotic action of Bcl-2 (37). Because the UBL domain is essential for Herp-

mediated protection against neurotoxins (**Fig. 7*B***), we determined that the UBL domain is essential for the ability of Herp to maintain ER Ca^{2+} homeostasis. Expression of Herp lacking the UBL domain fails to stabilize intracellular Ca^{2+} and to suppress the induction of CHOP in MPP^{+}-treated cells (**Fig. 7, *C*** and ***D***), indicating that UBL is critical for the cytoprotective function of Herp.

How the UBL domain is involved in the protective function of Herp is not clear. The presence of the UBL domain, which faces into the cytosol (14), suggests that Herp may function as a proteasome-interacting domain, as has recently been demonstrated for Parkin (57). Several recent studies support a role of Herp in ERAD (38, 39). Herp interacts with Hrd1p, a membrane-anchored E3 ligase (38), and with ubiquilin, a shuttle protein that delivers ubiquitinated substrates to the proteasome for degradation (58). Overexpression of Herp enhances the degradation of the ERAD substrate CD3o, whereas siRNA-mediated reduction of Herp expression stabilized the ERAD substrate CD3γ but did not alter or increased degradation of non-ERAD substrates tested (38). It is possible that Herp may target yet to be identified CHOP-regulated ERAD substrates whose accumulation results in perturbations in ER Ca^{2+} homeostasis. Hence, elucidating the precise role of Herp in ERAD and the identity of the ERAD substrates that accumulate in Herp knockdown cells will likely provide clues to the mechanisms of Herp-mediated ER Ca^{2+} stabilization and protection from MPP^{+}-induced toxicity.

Funding

This work was supported by funds from the American Federation on Aging Research to Dr. Sic L. Chan.

Figures

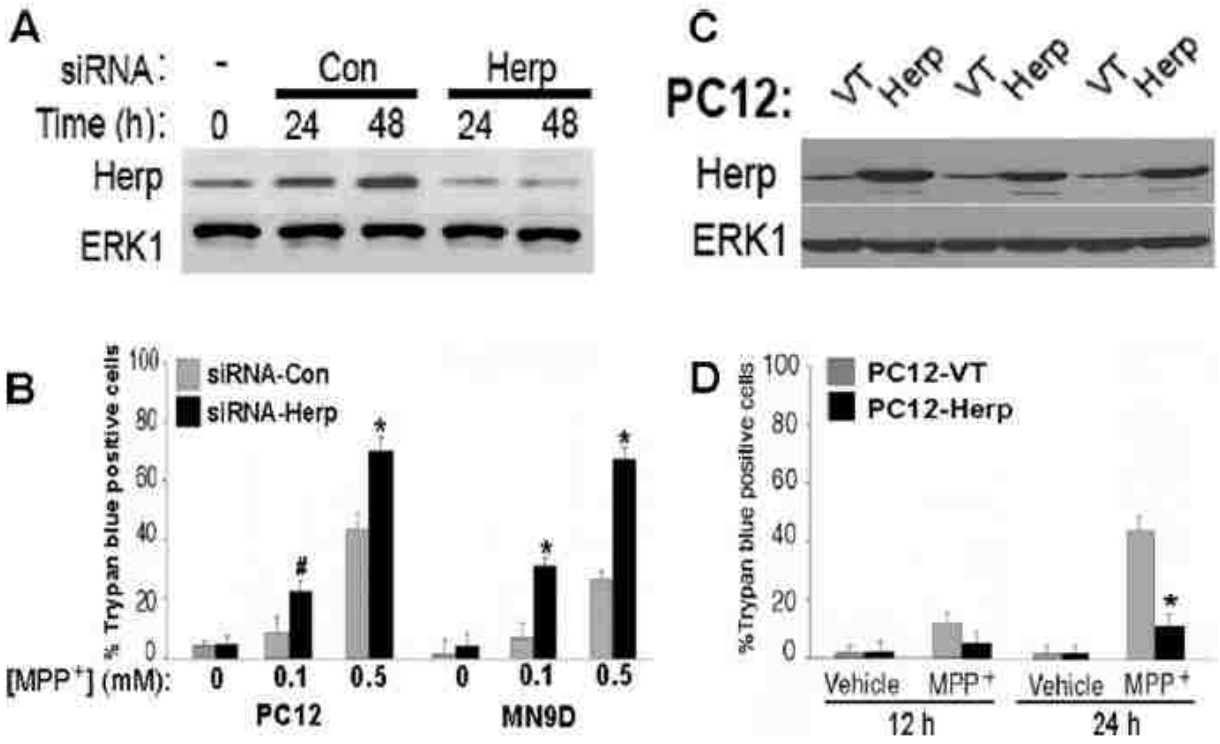

Figure 3-1. Herp protects from MPP^+ toxicity

(A) PC12 cells were transfected with siRNA targeting Herp (Herp;100 nM) or nonsilencing control siRNA (Con;100 nM) for 24 and 48 h. For sequences of each siRNA-Herp or siRNA-Con, see "Materials and Methods". Total protein lysates were prepared and analyzed by immunoblotting using an anti-Herp antibody. Equal protein loading was confirmed by reprobing immunoblots with an anti-ERK1 antibody. (B) PC12 cells and MN9D were transfected with siRNA-Herp or siRNA-Con (100 nM) for 24 h prior to exposure to 0.5 mM MPP^+ or vehicle. At the indicated time points, the percentage of Trypan blue-positive cells in each culture was quantified. The values are the means and S.D. of three independent experiments, *$p<0.01$, #$p<0.05$ (ANOVA with Scheffe post-hoc tests) compared with vehicle-treated cultures. (C) PC12 clones were

stably transfected with plasmid containing Herp (Herp) or the empty plasmid (VT). Total protein lysates were analyzed in three independent clones by Western blotting using an anti-Herp antibody. Equal protein loading was confirmed by reprobing the immunoblots with an anti-ERK1 antibody. (D) Cultures of PC12-VT and PC12-Herp were left untreated or treated for the indicated time points with 0.5 mM MPP^+ or vehicle, and cell viability was assessed. These results were expressed as percentage of Trypan blue-positive cells in each culture, normalized to untreated cultures. The values represent mean $\pm$ SD of 3 independent experiments, *$p<0.01$(ANOVA with Scheffe post-hoc tests).

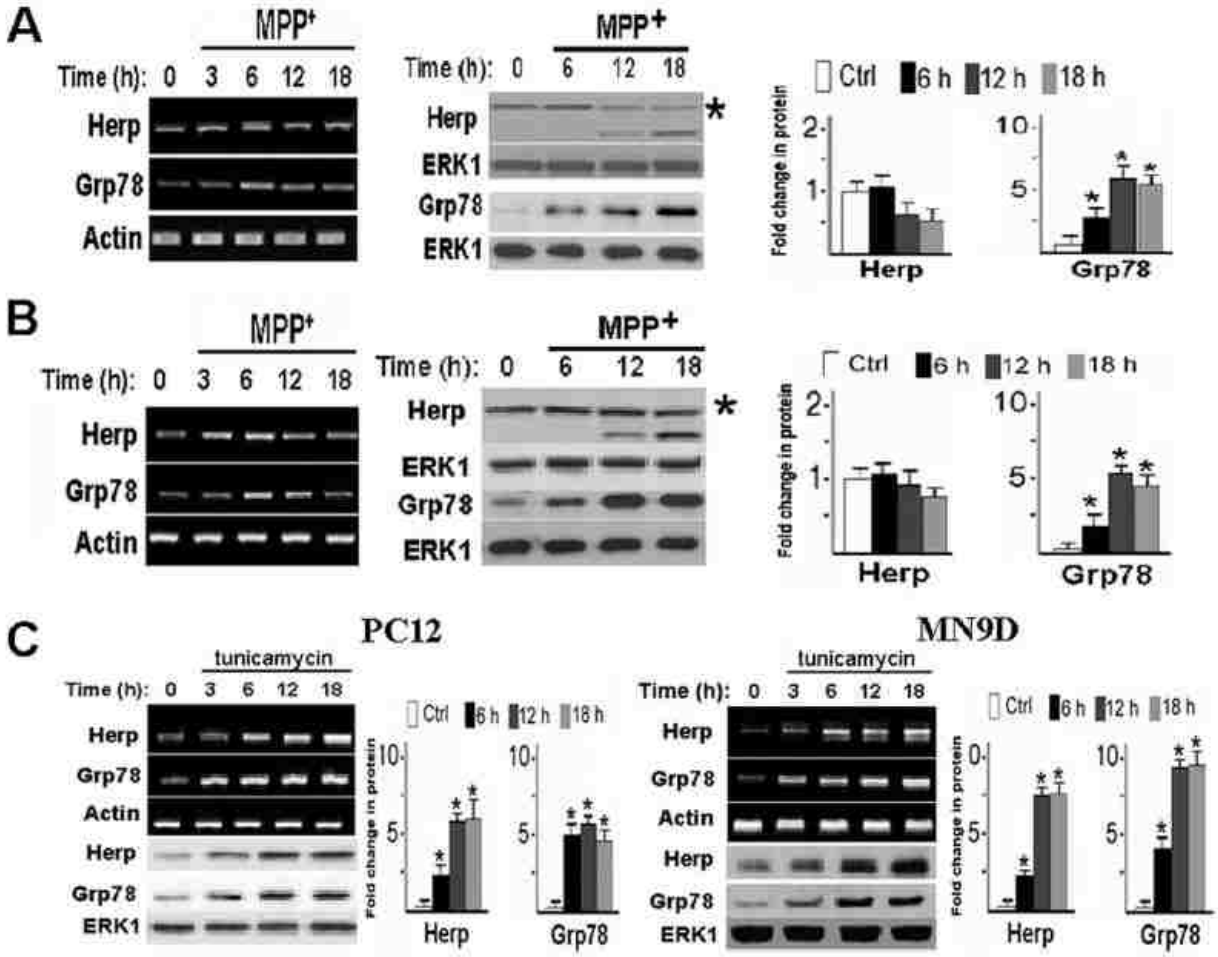

Figure 3-2. MPP$^+$ and tunicamycin induce Herp and CHOP expression with different kinetics

PC12 (A) and MN9D (B) cells were treated with 0.5 mM MPP$^+$ for the indicated time points. Total RNA and cell lysates were prepared and analyzed by semi-quantitative RT-PCR and immunoblotting for Herp and Grp78, respectively. As control (Ctrl) for equal loading, actin mRNA and ERK1 protein were determined. Densitometric analyses of protein bands are shown next to each panel. *p<0.01 (ANOVA with Scheffe post-hoc tests) compared to untreated cultures. Asterisks indicated the full-length Herp protein. (C) PC12 and MN9D cells were treated with 5 µg/ ml tunicamycin for the indicated time points. Total lysates were prepared and analyzed by by semi-quantitative RT-PCR and

immunoblotting for Herp and Grp78, respectively. Quantitation of the density of the protein bandsis shown next to each panel, *p<0.01, (ANOVA with Scheffe post-hoc tests) compared to untreated cells.

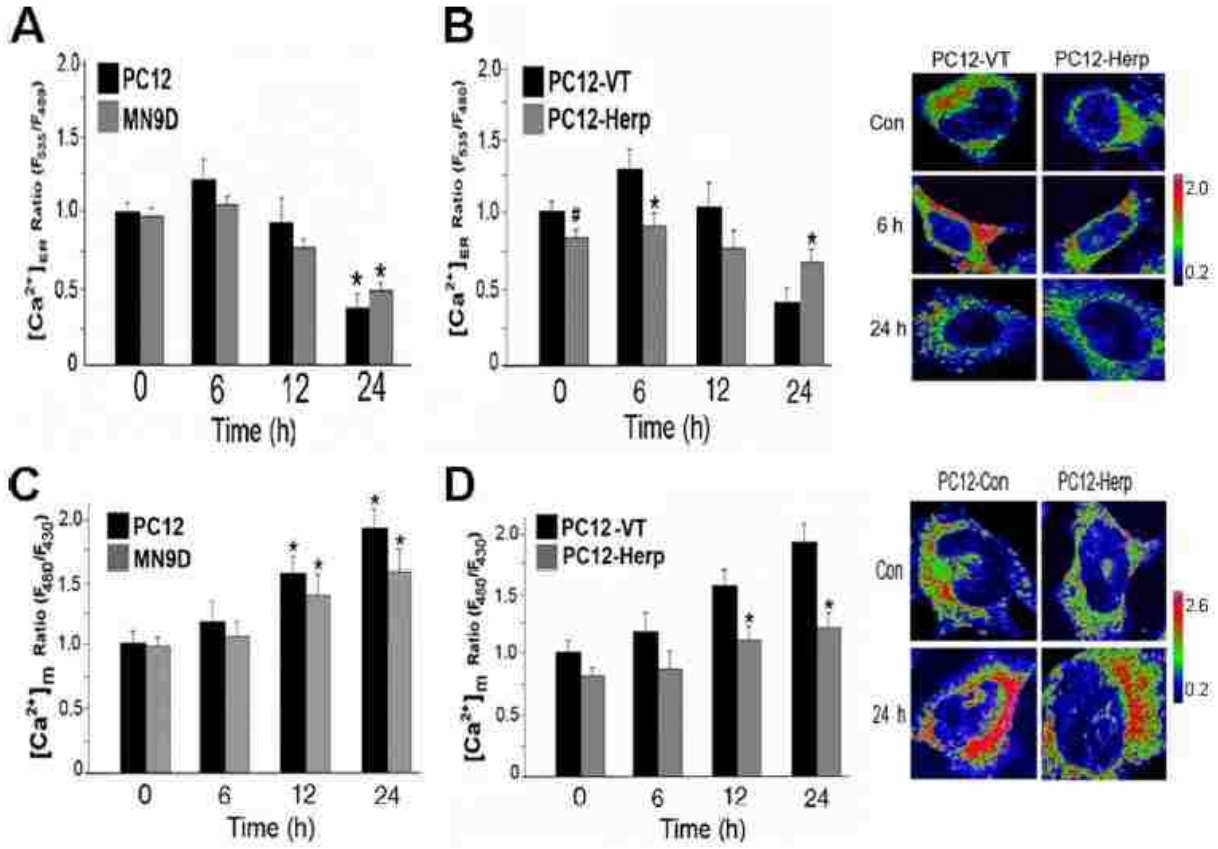

Figure 3-3. Herp counteracts MPP^+-induced depletion of ER Ca^{2+} store

Statistical evaluations of the changes in the Ca^{2+} concentration in the ER ($[Ca^{2+}]_{ER}$) (A and B) and mitochondria ($[Ca^{2+}]_m$) (C and D) in PC12 and MN9D cells (A and C) and in the indicated stably tranfected PC12 clones (B and D) after treatment with MPP^+. The indicated cultures were transiently transfected with 2 µg YC4-ER or RP-mt for 24 h prior to incubation with 0.5 mM MPP^+. At the indicated time points, $[Ca^{2+}]_{ER}$ and $[Ca^{2+}]_m$ were measured as described in Materials and Methods. The results were expressed as the ratio of the YC4-ER or RP-mt fluorescence signals in MPP^+-treated relative to untreated

cultures. Values are mean and S.D. of measurements made in three or four cultures (n=4 dishes, 4-6 microscopic fields per dish, 25-30 cells per field), *$p<0.01$, $^{\#}p<0.05$ (ANOVA with Scheffe post-hoc tests) compared to either untreated cultures or PC12-VT cultures. Representative pseudocolored images of the indicated PC12 clones at baseline and after exposure to MPP^+ are shown in B and D. The pseudocolor bar shows the ratio range. Con, control.

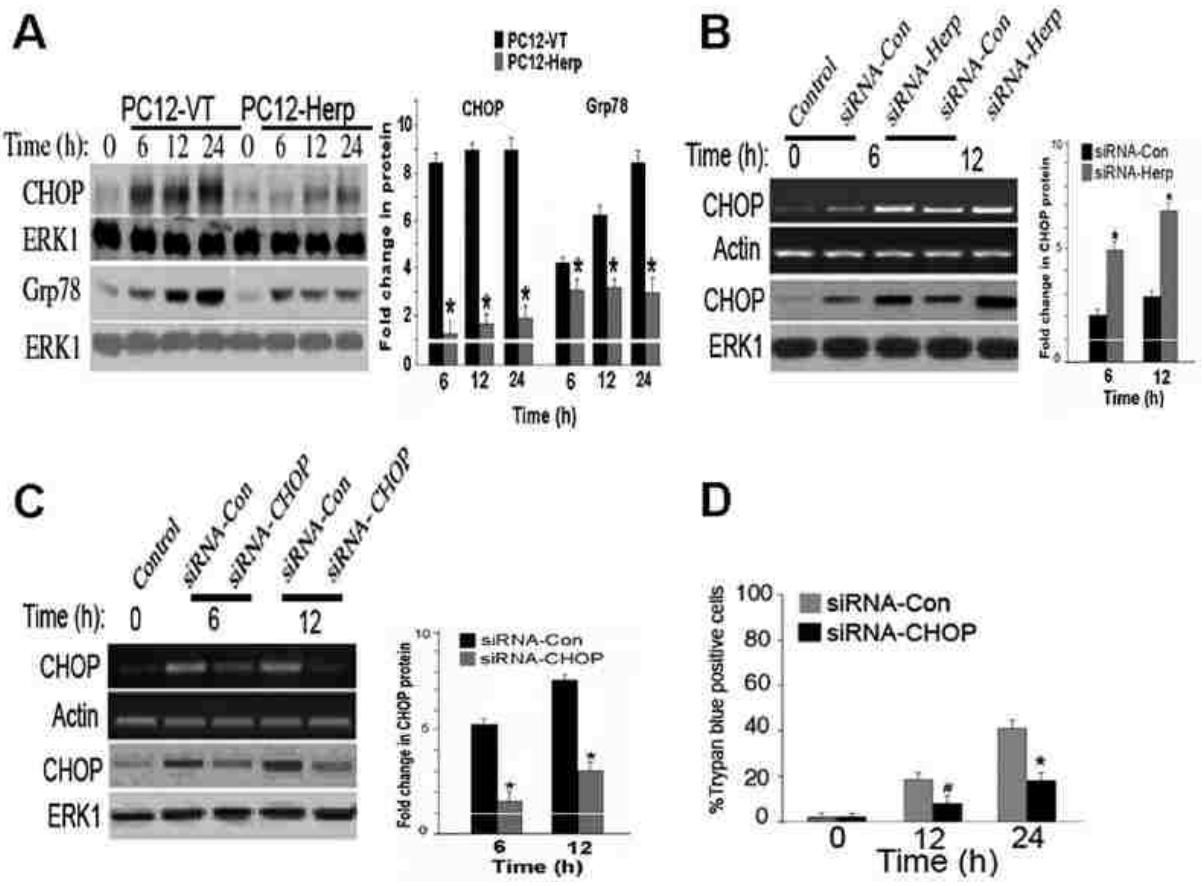

Figure 3-4. Herp counteracts MPP^+-induced upregulation of CHOP

(A) Time course of CHOP and Grp78 protein levels in cultures of PC12-VT and PC12-Herp before and after incubation with 0.5 mM MPP^+. As control for equal loading, immunoblots were reprobed with an antibody to ERK1. Densitometric analysis of protein bands normalized to untreated control cultures is shown in the right panel. *p<0.01 (ANOVA with Scheffe post-hoc tests), compared to PC12-VT (B) Time course of MPP^+-induced CHOP mRNA and protein levels in cultures of PC12 cells transfected with siRNA-Herp or siRNA-Con (100 nM). The cultures were incubated with 0.5 mM MPP^+ 24h after transfection. Actin and ERK1 were used as loading controls. Densitometric analyses of protein bands normalized to untreated control cultures are shown in the right panel. *p<0.01 (ANOVA with Scheffe post-hoc tests), compared to cultures

transfected with siRNA-Con. (C and D) PC12 cells were transfected with siRNA-CHOP or siRNA-Con (100 nM). One day after transfection, PC12 cells were exposed to 0.5 mM MPP^+ or vehicle for the indicated time points and subsequently harvested for detection of Herp mRNA and protein (C) or fixed for quantitation of cell death (D). Actin and ERK1 were used as loading controls. Densitometric analyses of protein bands normalized to untreated control cultures is shown in the right panel, *p<0.01 (ANOVA with Scheffe post-hoc tests), compared with cultures transfected with siRNA-Con. For quantitation of cell death, the percentages of Trypan blue-positive cells in each treated culture, normalized to vehicle-treated cultures, were shown. The values are the means and S.D. of three dishes per group for each time point, $^{*}p < 0.01$, $^{\#}p < 0.05$ (ANOVA with Scheffe post-hoc tests) compared to cultures transfected with siRNA-Con.

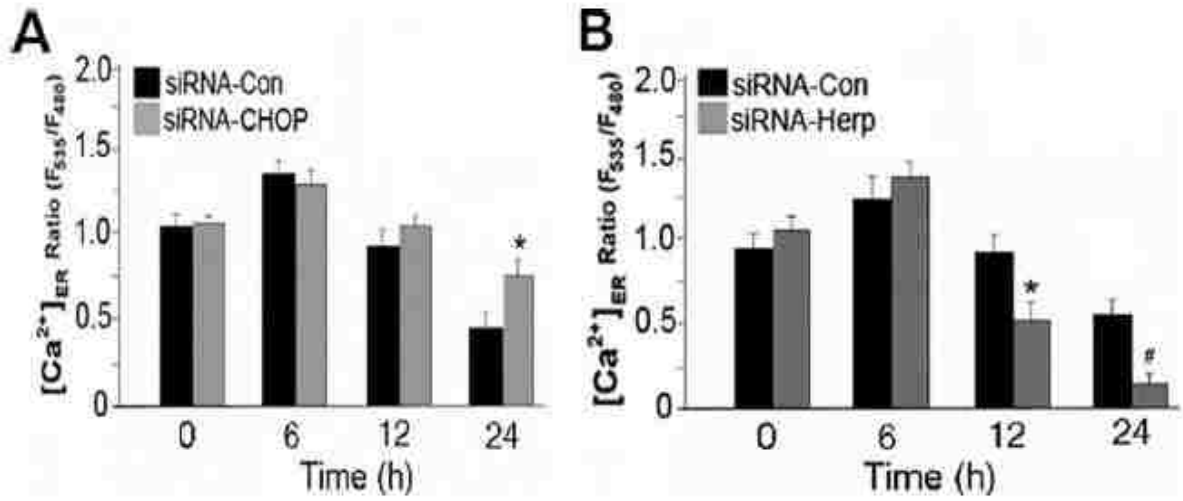

Figure 3-5. CHOP and Herp modulates ER Ca^{2+} homeostasis in MPP^+-treated cells

Knockdown of CHOP (A) and Herp (B) alters ER Ca^{2+} store contents in MPP^+-treated PC12 cells. Twenty-four hours after co-transfection with 2 µg pBudCE4.1-YC4-ER with the indicated siRNA duplexes (100 nM), cultures were incubated with 0.5 mM MPP^+ or vehicle control (Con). Changes in ER Ca^{2+} concentration ($[Ca^{2+}]_{ER}$) were recorded at the indicated time points as described in Materials and Methods and presented as the ratios of the YC4-ER fluorescence signal in MPP^+-treated relative to untreated cultures. The values are mean and S.D. of measurements made in three separate cultures (n=4 dishes, 4-6 microscopic fields per dish, 25-30 cells per field), *$p<0.01$, #$p<0.05$ (ANOVA with Scheffe post-hoc tests), compared to cultures treated with siRNA-Con.

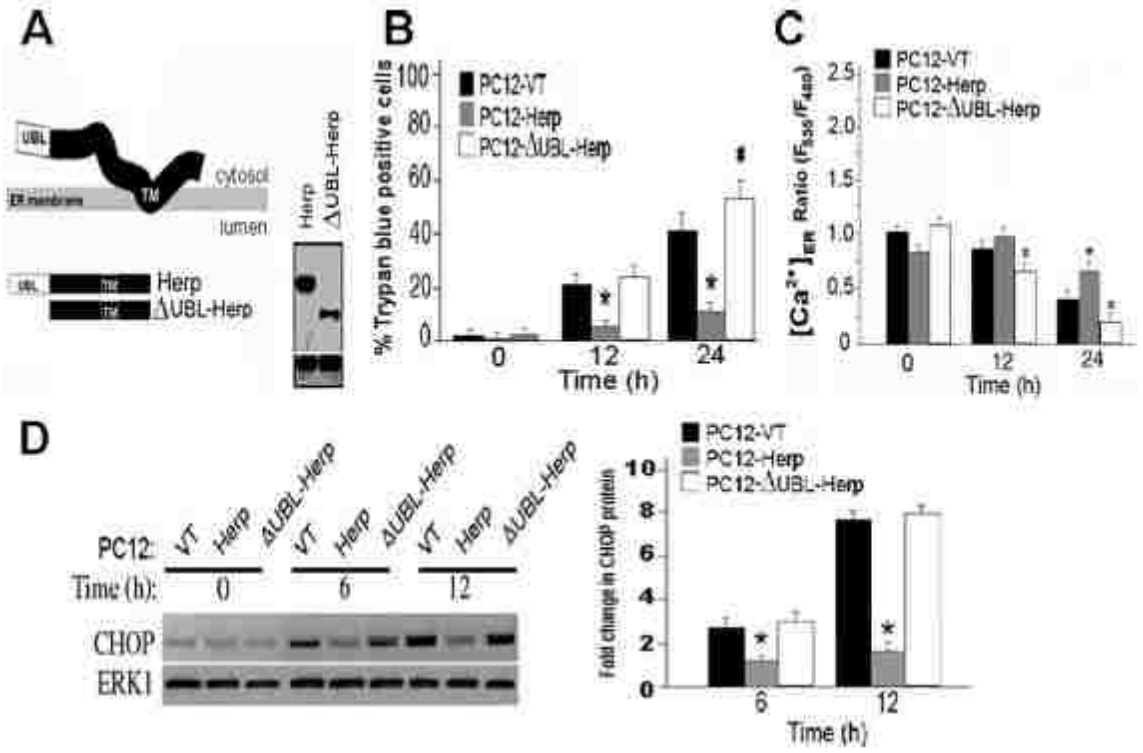

Figure 3-6. The ubiquitin-like (UBL)-domain is essential for Herp-mediated stabilization of ER Ca^{2+} homeostasis and rescue from MPP^+ toxicity

(A) Schematic diagram of full-length Herp protein and a deletion mutant lacking the amino-terminal ubiquitin-like (UBL) domain (ΔUBL-Herp). Expression of Herp and ΔUBL-Herp protein in stably transfected PC12 clones is shown in the inset. ERK1 was used as the loading control. (B) ΔUBL-Herp fails to rescue PC12 cells from MPP^+ toxicity. The indicated PC12 clones were exposed to 0.5 mM MPP^+ for the indicated time points. The results were expressed as percentage of Trypan blue-positive cells in each culture, normalized to vehicle-treated cultures, from three independent experiments, *$p<0.01$, $^{\#}p<0.05$ (ANOVA with Scheffe post-hoc tests). $^{\#}p<0.05$, (ANOVA with Scheffe post-hoc tests), compared to PC12-VT. (C) ΔUBL-Herp fails to stabilize ER Ca^{2+} homeostasis. Twenty-four hours after transfection of pBudCE4.1-YC4-ER, the indicated PC12 clones were incubated with 0.5 mM MPP^+. Changes in ER Ca^{2+}

concentration ($[Ca^{2+}]_{ER}$) were recorded at the indicated time points as described in Materials and Methods and presented as the ratio of the fluorescence signals in MPP^+-treated relative to untreated cultures. The values are mean and S.D. of measurements made in three or four cultures (n=4 dishes, 4-6 microscopic fields per dish, 25-30 cells per field), *$p<0.01$, (ANOVA with Scheffe post-hoc tests) compared to PC12-VT and PC12-ΔUBL-Herp. #$p<0.05$, (ANOVA with Scheffe post-hoc tests), compared to PC12-VT. (D) ΔUBL-Herp fails to suppress MPP^+ induced upregulation of CHOP. Time course of MPP^+-induced increase in CHOP protein level in the indicated stably-transfected PC12 clones. As control for equal loading, immunoblots were reprobed with an antibody to ERK1. Densitometric analysis of protein bands normalized to untreated control cultures is shown in the right panel. *$p<0.01$ (ANOVA with Scheffe post-hoc tests), compared to PC12-VT and PC12-ΔUBL-Herp.

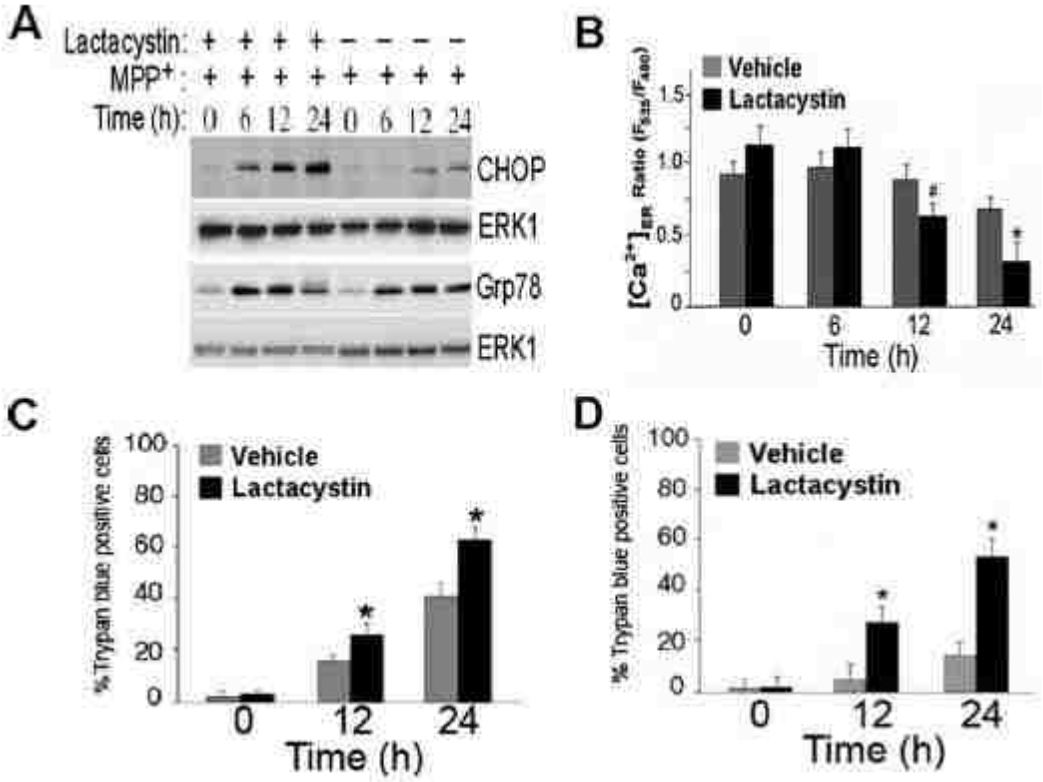

Figure 3-7. Proteasomal-mediated degradation is essential for Herp-dependent stabilization of ER Ca^{2+} homeostasis and rescue from MPP^+ toxicity

(A) The proteasomal inhibitor lactacystin abolishes Herp-mediated suppression of CHOP in MPP^+-treated PC12 cells. Time course of CHOP and Grp78 protein levels in PC12-Herp cultures incubated with 0.5 mM MPP^+ in the presence or absence of lactacystin (5 μM). As control for equal loading, immunoblots were reprobed with an antibody to ERK1. (B) Lactacystin abolishes the Herp-dependent suppression of ER Ca^{2+} store depletion in MPP^+-treated PC12 cells. Twenty-four hours after transfection with 2 μg pBudCE4.1-YC4-ER, the cultures of PC12-Herp were incubated with 0.5 mM MPP^+ in the presence of lactacystin (5 μM) or its vehicle control. Changes in ER Ca^{2+} concentration ($[Ca^{2+}]_{ER}$) were recorded at the indicated time points as described in Materials and Methods and presented as the ratio of the YC4-ER fluorescence signal in

MPP^+-treated relative to untreated cultures. The values are the means and S.D. of measurements made in three or four cultures (n=4 dishes, 4-6 microscopic fields per dish, 25-30 cells per field), *p<0.01, (ANOVA with Scheffe post-hoc tests). (C and D) Lactacystin enhances MPP^+ toxicity (C) and reverses the Herp-dependent cell death rescue from MPP^+-toxicity (D). Cultures of PC12 (C) and PC12-Herp clones (D) were exposed to 0.5 mM MPP^+ in the presence of lactacystin (5 μM) or vehicle control for the indicated time points. Shown is the percentage of Trypan blue-positive cells in each culture, normalized to untreated cultures, from three independent experiments, *p<0.01, (ANOVA with Scheffe post-hoc tests) compared to vehicle-treated cultures.

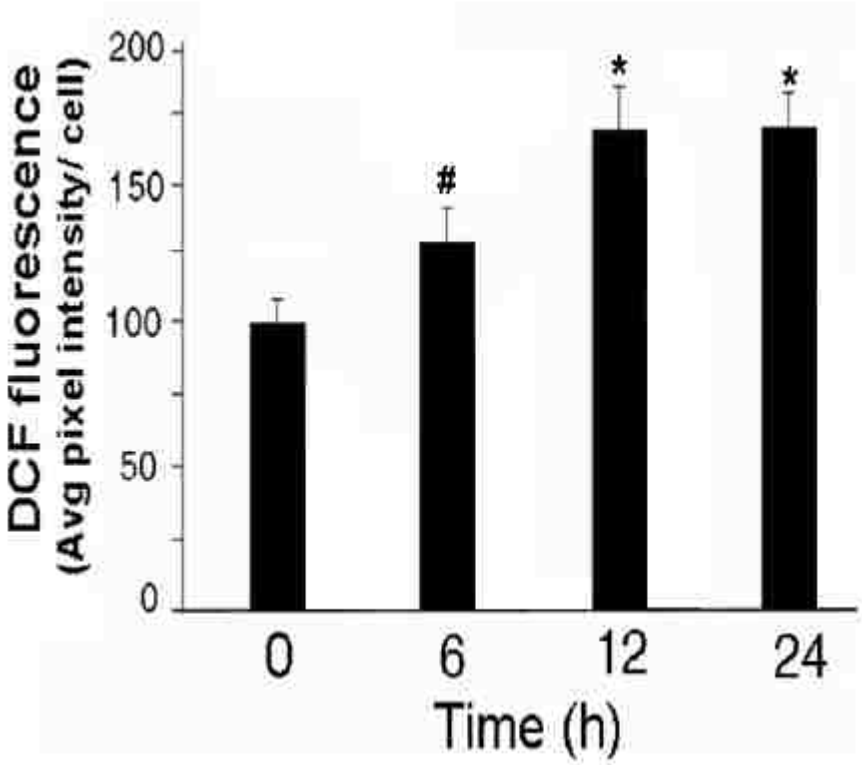

Supplementary Figure 3-1. MPP^+ increases ROS accumulation

PC12 cells were loaded with the fluorescence probe, 7-dichlorodihydrofluorescein diacetate (10 μM DCF-DA, Molecular Probes). Fluorescence images were acquired using a confocal microscope and quantified (20). Values are the average DCF

fluorescence pixel intensity per cell before and after exposure to 0.5 mM MPP^+ at the indicated time periods. Values are mean ± S.D. of determinations made in four to five cultures; 30–40 cells assessed in each culture, *p<0.01, #p<0.05 (ANOVA with Scheffe post-hoc tests), compared to untreated cultures.

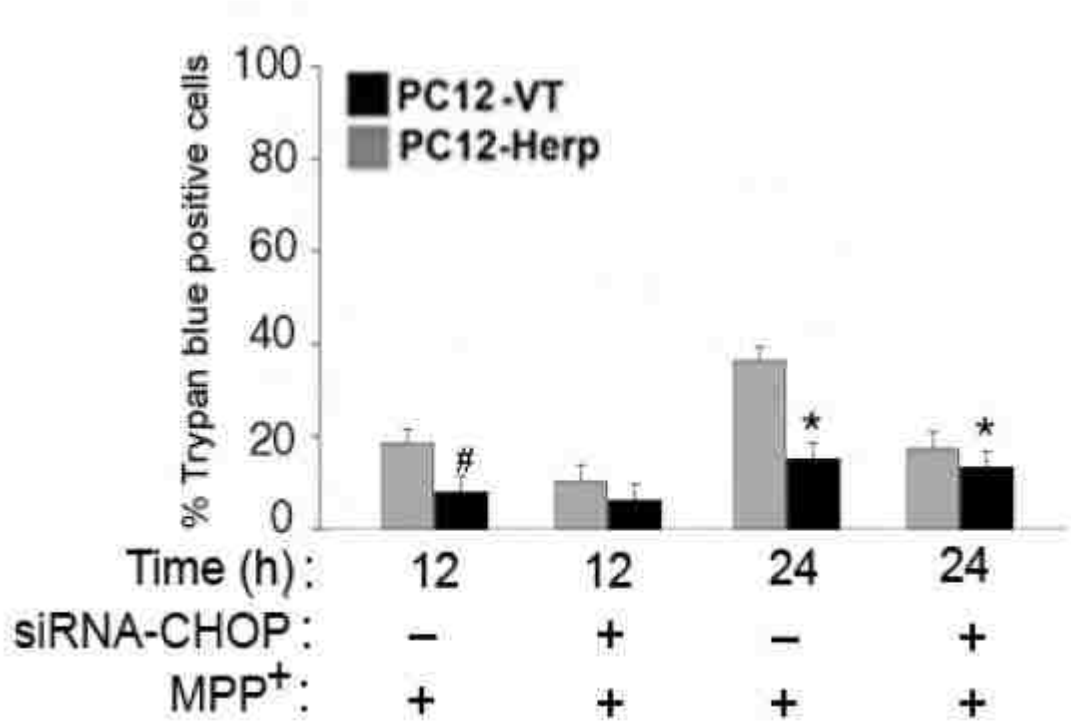

Supplementary Figure 3-2. Effect of CHOP knockdown on the survival of PC12-Herp clones

The indicated PC12 clones were transfected with siRNA-CHOP or siRNA-Con (100 nM). One day after transfection, PC12 cells were exposed to 0.5 mM MPP^+ for the indicated time points and fixed for quantitation of cell death. Results were expressed as percentage of Trypan blue-positive cells in each culture, normalized to untreated cultures. Values represent mean ± SD of determinations made in four separate cultures, *p<0.01, #p<0.05 (ANOVA with Scheffe post-hoc tests), compared to PC12-VT cultures.

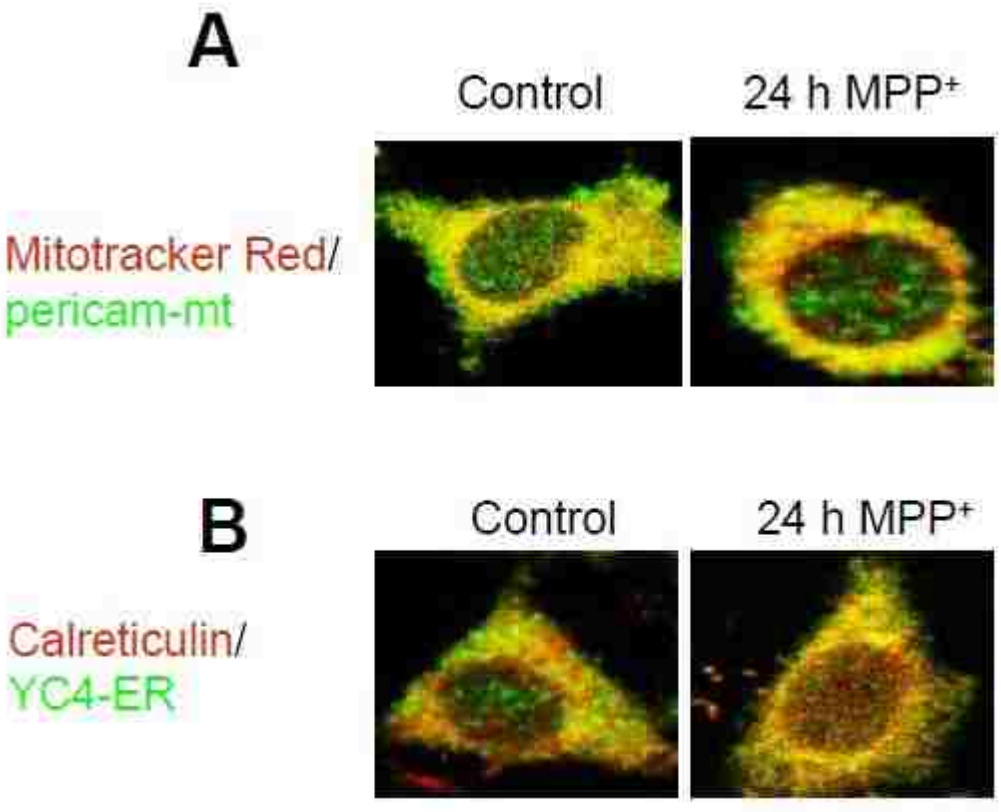

Supplementary Figure 3-3. The fluorescent indicators are properly targeted and expressed in their respective organelles

(A) YC4-ER co-localizes with the ER marker calnexin before and after exposure to MPP+ (0.5 mM). PC12 cells were transfected with YC4-ER, fixed and immunostained with the calnexin antibody. Fluorescence images were acquired using a confocal microscope. (B) Pericam-mt co-localizes with the vital dye MitoTracker red in PC12 cells before and after exposure to MPP+ (0.5 mM). Pericam-mt transfected PC12 cells were loaded with MitoTracker red and imaged using a confocal microscope.

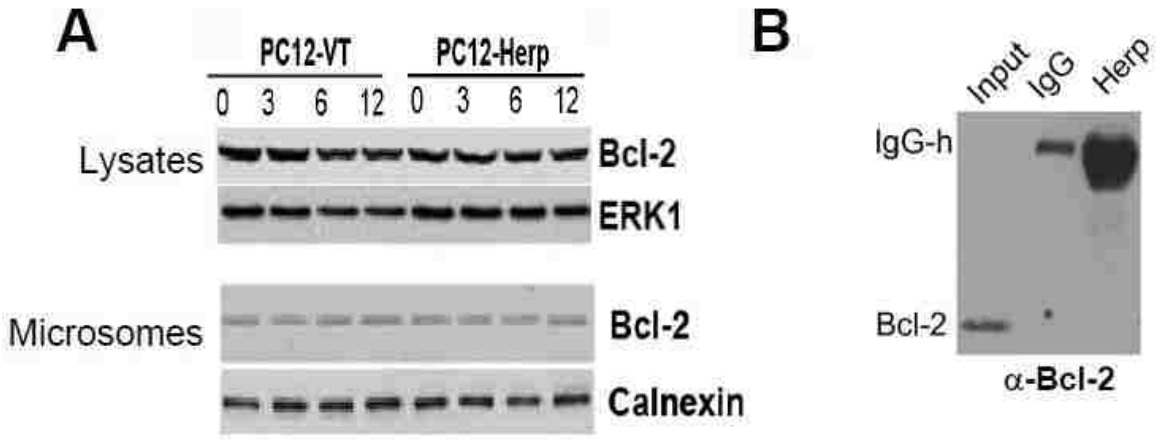

Supplementary Figure 3-4. The Herp-dependent protective mechanism is not mediated by Bcl-2

(A) Time course of Bcl-2 protein in total cell lysates (upper panels) and microsomes (lower panels) harvested from PC12-VT and PC12-Herp after incubation with 0.5 mM MPP+. Microsomal fractions were isolated by differential centrifugation as described previously (16). Equal protein loading was confirmed by reprobing the immunoblots for ERK1 and calnexin (an ER-resident protein), respectively. (B). Herp fails to interact with Bcl-2. A polyclonal mouse anti-Herp antibody was used for immunoprecipitation as described in Materials and Methods. The Bcl-2 protein is detected in the input (whole lysates) but not in the immune complexes bound to control IgG or Herp antibody. The heavy chain of IgG is indicated as IgG-h.

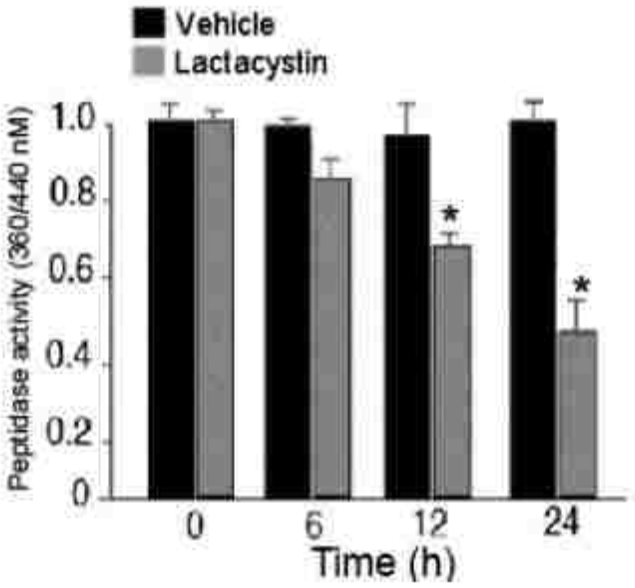

Supplementary Figure 3-5. Lactacystin treatment reduces proteasomal activity

PC12 cells were treated with 5 μM lactacystin or vehicle control. At the indicated time points, chymotrypsin-like activity of the proteasome were assessed in whole cell lysates using the fluorogenic peptide Suc-Leu-Leu-Val-Tyr-7-amino-4-methylcoumarin (LLVY-AMC) according to the method reported previously (15). Values are the average fluorescence intensity (360/440 nM) before and after exposure to 0.5 mM MPP+ at the indicated time points. Values are mean ± S.D. of determinations made in four to five dishes, *$p<0.01$ (ANOVA with Scheffe post-hoc tests), compared to vehicle-treated cultures.

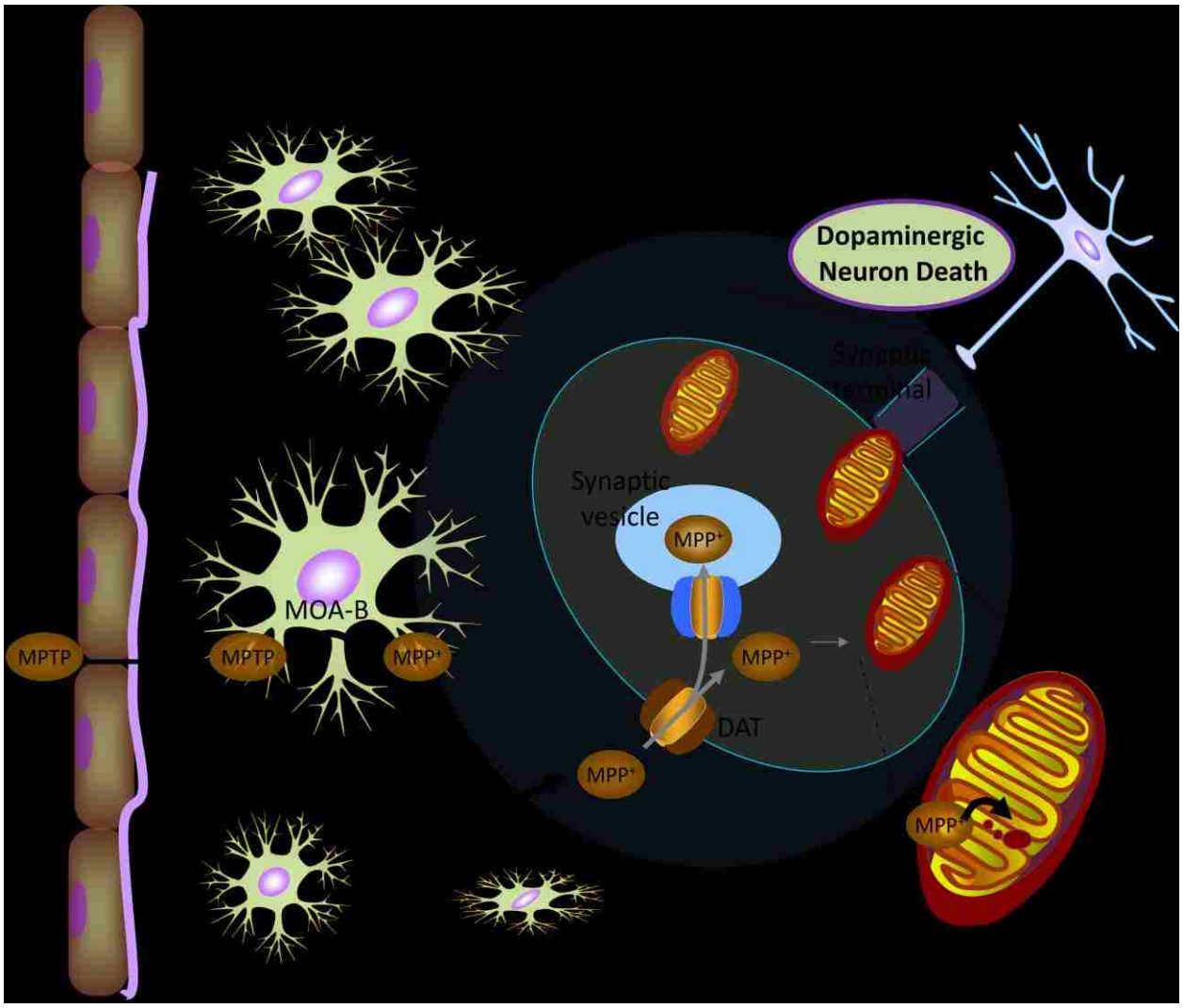

Summary Diagram 3-1. Part 1. Schematic representation of MPTP entry into dopaminergic nerurons

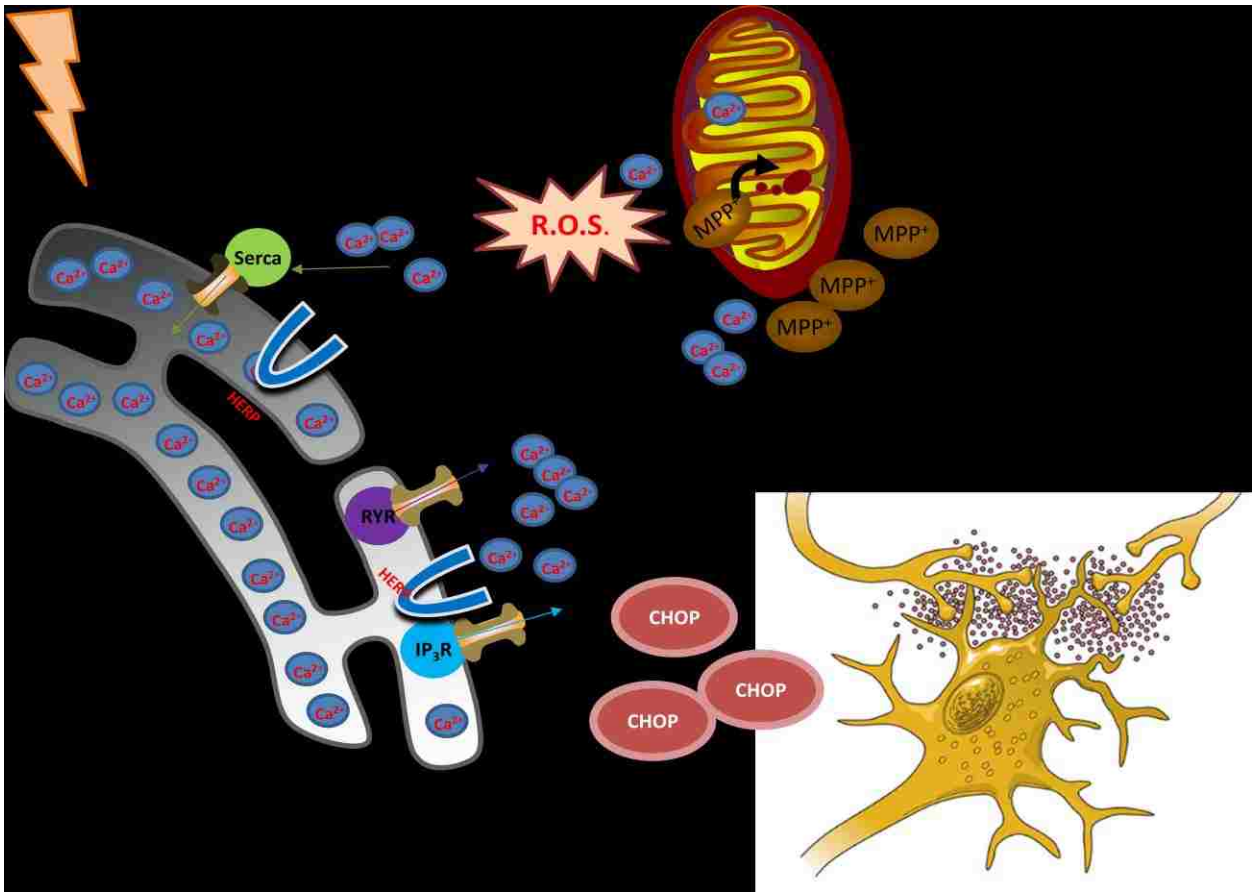

Summary Diagram 3-2. Part 2. Schematic representation of the mechanisms involved in toxicity of MPTP

References

1. Dawson TM, Dawson VL. Molecular pathways of neurodegeneration in Parkinson's disease. Science. 2003;302:819–22.

2. Cookson MR. The biochemistry of Parkinson's disease. Annu. Rev. Biochem. 2005;74:29–52.

3. McNaught KS, Olanow CW, Halliwell B, Isacson O, Jenner P. Failure of the ubiquitin-proteasome system in Parkinson's disease.Nat. Rev. Neurosci. 2001;2:589-94.

4. Hiller MM, Finger A, Schweiger M, Wolf DH. ER degradation of a misfolded luminal protein by the cytosolic ubiquitin-proteasome pathway. Science. 1996;273:1725-28.

5. Boyce M, Yuan J. Cellular response to endoplasmic reticulum stress: a matter of life or death. Cell Death Differ. 2006;13:363–73.

6. Lindholm D, Wootz H, Korhonen L. ER stress and neurodegenerative diseases. Cell Death Differ. 2006;13:385–92.

7. Harding HP, Calfon M, Urano F, Novoa I, Ron D. Transcriptional and translational control in the Mammalian unfolded protein response. Annu.Rev. Cell Dev. Biol. 2002;18:575–99.

8. Breckenridge DG, Germain M, Mathai JP, Nguyen M, Shore GC. Regulation of apoptosis by endoplasmic reticulum pathways. Oncogene. 2003;22:8608–18.

9. Ryu EJ, Harding HP, Angelastro JM, Vitolo OV, Ron D, Greene LA. Endoplasmic reticulum stress and the unfolded protein response in cellular models of Parkinson's disease J. Neurosci. 2002;22:10690-8.

10. Holtz WA, O'Malley KL. Parkinsonian mimetics induce aspects of unfolded protein response in death of dopaminergic neurons. J. Biol. Chem. 2003;278:19367–77.

11. Yamamuro A, Yoshioka Y, Ogita K, Maeda S. Involvement of endoplasmic reticulum stress on the cell death induced by 6-hydroxydopamine in human neuroblastoma SH-SY5Y cells. Neurochem. Res. 2006l31:657–64.

12. Smith WW, Jiang H, Pei Z, Tanaka Y, Morita H, Sawa A, et al. Endoplasmic reticulum stress and mitochondrial cell death pathways mediate A53T mutant alpha-synuclein-induced toxicity. Hum. Mol. Genet. 2005;14:3801–11.

13. Hoozemans JJ, van Haastert ES, Eikelenboom P, de Vos RA, Rozemuller JM, Scheper W. Activation of the unfolded protein response in Parkinson's disease. Biochem. Biophys. Res. Commun. 2007;354:707–11.

14. Kokame K, Agarwala KL, Kato H, Miyata T. Herp, a new ubiquitin-like membrane protein induced by endoplasmic reticulum stress. J. Biol. Chem. 2000;275:32846–53.

15. Hori O, Ichinoda F, Yamaguchi A, Tamatani T, Taniguchi M, Koyama Y, et al. Role of Herp in the endoplasmic reticulum stress response. Genes Cells. 2004;9:457–69.

16. Chan SL, Fu W, Zhang P, Cheng A, Lee J, Kokame K, et al. Herp stabilizes neuronal Ca2+ homeostasis and mitochondrial function during endoplasmic reticulum stress. J. Biol. Chem. 2004;279:28733–43.

17. Tuvia S, Taglicht D, Erez O, Alroy I, Alchanati I, Bicoviski V, et al. The ubiquitin E3 ligase POSH regulates calcium homeostasis through spatial control of Herp. J. Cell Biol. 2007;177:51-61.

18. Dauer W, Przedborski S. Parkinson's disease: mechanisms and models. Neuron. 2003;39:889–909.

19. Kim J, Choi TG, Ding Y, Kim Y, Ha KS, Lee, KH., et al. Overexpressed cyclophilin B suppresses apoptosis associated with ROS and Ca2+ homeostasis after ER stress. J. Cell Sci. 2008;121:3636–48.

20. Chan SL, Liu D, Kyriazis GA, Ouyang X, Mattson MP. Mitochondrial uncoupling protein-4 regulates calcium homeostasis and sensitivity to store depletion-induced apoptosis in neural cells. J. Biol. Chem. 2006;281:37391–403.

21. Malli R, Frieden M, Osibow K, Mayer M, Demaurex N, Graier WF. Sustained Ca2+ transfer across mitochondria is essential for mitochondrial Ca2+ buffering, store-operated Ca2+ entry, and Ca2+ store refilling. J. Biol. Chem. 2003;278:44769-79.

22. Nagai T, Sawano A, Park ES, Miyawaki A. Circularly permuted green fluorescent proteins engineered to sense Ca2+. Proc. Natl. Acad. Sci. U.S.A. 2001;98:3197–202.

23. Mattson MP, Chan SL. Dysregulation of cellular calcium homeostasis in Alzheimer's disease: bad genes and bad habits. J. Mol. Neurosci. 2001;17:205–24.

24. Cassarino DS, Fall CP, Swerdlow, RH., Smith, TS., Halvorsen, EM., Miller, SW., et al. Elevated reactive oxygen species and antioxidant enzyme activities in animal and cellular models of Parkinson's disease. Biochim. Biophys. Acta. 1997;1362:77–86.

25. Kalivendi SV, Kotamraju S, Cunningham S, Shang T, Hillard CJ, Kalyanaraman B. 1-Methyl-4-phenylpyridinium (MPP+)-induced apoptosis and mitochondrial oxidant generation: role of transferrin-receptor-dependent iron and hydrogen peroxide. Biochem. J. 2003;371:151–64.

26. Lee DH, Han YS, Han ES, Bang H, Lee CS. Differential involvement of intracellular Ca2+ in 1-methyl-4-phenylpyridinium- or 6-hydroxydopamine-induced cell viability loss in PC12 cells. Neurochem. Res. 2006;31:851–60.

27. Lee CS, Park SY, Ko HH, Song JH, Shin, YK, and Han ES. Inhibition of MPP+-induced mitochondrial damage and cell death by trifluoperazine and W-7 in PC12 cells. Neurochem. Int. 2005;46:169–78.

28. Kass GE, Wright JM, Nicotera P, Orrenius S. The mechanism of 1-methyl-4-phenyl-1,2,3,6-tetrahydropyridine toxicity: role of intracellular calcium. Arch. Biochem. Biophys. 1988;260:789–97.

29. Deniaud A, Sharaf el dein O, Maillier E, Poncet D, Kroemer, G., Lemaire, C, et al. Endoplasmic reticulum stress induces calcium-dependent permeability transition, mitochondrial outer membrane permeabilization and apoptosis. Oncogene. 2008;27:285–99.

30. Lee CS, Song EH, Park SY, Han ES. Combined effect of dopamine and MPP+ on membrane permeability in mitochondria and cell viability in PC12 cells. Neurochem. Int. 2003;43:147–54.

31. Packer MA, Miesel R, Murphy MP. Exposure to the parkinsonian neurotoxin 1-methyl-4-phenylpyridinium (MPP+) and nitric oxide simultaneously causes cyclosporin A-sensitive mitochondrial calcium efflux and depolarization. Biochem. Pharmacol. 1996;51:267–73.

32. Oyadomari S, Mori M. Roles of CHOP/GADD153 in endoplasmic reticulum stress. Cell Death Differ. 2004;11:381–89.

33. Wang XZ, Lawson B, Brewer JW, Zinszner H, Sanjay A, Mi LJ, et al. Signals from the stressed endoplasmic reticulum induce C/EBP-homologous protein (CHOP/GADD153). Mol. Cell Biol. 1996;16:4273-80.

34. Benavides A, Pastor D, Santos P, Tranque P, Calvo S. CHOP plays a pivotal role in the astrocyte death induced by oxygen and glucose deprivation. Glia. 2005;52:261–75.

35. Copanaki, E., Schürmann, T., Eckert, A., Leuner, K., Müller, WE., Prehn, JH., et al. The amyloid precursor protein potentiates CHOP induction and cell death in response to ER Ca2+ depletion. Biochim. Biophys. Acta. 2007;1773:157–65.

36. McCullough KD, Martindale JL, Klotz LO, Aw TY, Holbrook NJ, Gadd 153 sensitizes cells to endoplasmic reticulum stress by down-regulating Bcl2 and perturbing the cellular redox state. Mol. Cell Biol. 2001;21:1249–59.

37. Pinton P, Ferrari D, Rapizzi E, Di Virgilio F, Pozzan T, Rizzuto R. The Ca2+ concentration of the endoplasmic reticulum is a key determinant of ceramide-induced apoptosis: significance for the molecular mechanism of Bcl-2 action , (2001) EMBO J. 20, 2690–701.

38. Schulze A, Standera S, Buerger E, Kikkert M, van Voorden S, Wiertz E, et al. The ubiquitin-domain protein HERP forms a complex with components of the endoplasmic reticulum associated degradation pathway. J. Mol. Biol. 2005;354:1021–7.

39. Okuda-Shimizu Y, Hendershot LM. Characterization of an ERAD pathway for nonglycosylated BiP substrates, which require Herp. Mol. Cell. 2007;28:544–54.

40. Jenner P. Oxidative stress in Parkinson's disease. Ann. Neurol. 2003;53:S26–38.

41. Mattson MP, LaFerla FM, Chan SL, Leissring MA, Shepel PN, Geiger JD. Calcium signaling in the ER: its role in neuronal plasticity and neurodegenerative disorders. Trends Neurosci. 2000;23:222–9.

42. Tang TS, Tu H, Chan EY, Maximov A, Wang Z, Wellington CL, et al. Huntingtin and huntingtin-associated protein 1 influence neuronal calcium signaling mediated by inositol-(1,4,5) triphosphate receptor type 1, Neuron. 2003;39:227–39.

43. Hetz C, Russelakis-Carneiro M, Maundrell K, Castilla J, Soto C. Caspase-12 and endoplasmic reticulum stress mediate neurotoxicity of pathological prion protein. EMBO J. 2003;22:5435–45.

44. Wei H, Perry DC. Dantrolene is cytoprotective in two models of neuronal cell death. J. Neurochem. 1996;67:2390–8.

45. Ferreiro E, Resende R, Costa R, Oliveira CR, Pereira CM. An endoplasmic-reticulum-specific apoptotic pathway is involved in prion and amyloid-beta peptides neurotoxicity. Neurobiol. Dis. 2006;23:669–78.

46. Choi WS, Lee E, Lim J, Oh YJ. Calbindin-D28K prevents drug-induced dopaminergic neuronal death by inhibiting caspase and calpain activity. Biochem. Biophys. Res. Commun. 2008;371:127–31.

47. Lotharius J, Dugan LL, O'Malley KL. Distinct mechanisms underlie neurotoxin-mediated cell death in cultured dopaminergic neurons. J. Neurosci. 1999;19:1284–93.

48. Haynes CM, Titus EA, Cooper AA. Degradation of misfolded proteins prevents ER-derived oxidative stress and cell death. Mol. Cell. 2004;15:767–76.

49. Suzuki YJ, Ford GD. Superoxide stimulates IP3-induced Ca2+ release from vascular smooth muscle sarcoplasmic reticulum. Am. J. Physiol. 1992;262:H114 –6.

50. Madesh M, Hawkins BJ, Milovanova T, Bhanumathy CD, Joseph SK, Ramachandrarao SP, et al. Selective role for superoxide in InsP3 receptor-mediated mitochondrial dysfunction and endothelial apoptosis. J. Cell Biol. 2005;170:1079–90.

51. Boraso A, Williams AJ. Modification of the gating of the cardiac sarcoplasmic reticulum Ca(2+)-release channel by H2O2 and dithiothreitol. Am. J. Physiol. 1994;267: H1010–16.

52. Hajnóczky G, Csordás G, Madesh M, Pacher P. Control of apoptosis by IP3and ryanodine receptor driven calcium signals. Cell Calcium. 2000;28:349–63.

53. Jacobson J, Duchen MR. Mitochondrial oxidative stress and cell death in astrocytes--requirement for stored Ca2+ and sustained opening of the permeability transition pore. J. Cell Sci. 2002;115:1175–88.

54. Holtz WA, Turetzky JM, Jong YJ, O'Malley KL. Oxidative stress-triggered unfolded protein response is upstream of intrinsic cell death evoked by parkinsonian mimetics. J. Neurochem. 2006;99:54–69.

55. Yokouchi M, Hiramatsu N, Hayakawa K, Okamura M. Du S, Kasai A, et al. Involvement of selective reactive oxygen species upstream of proapoptotic branches of unfolded protein response. J. Biol. Chem. 2008;283:4252–60.

56. Pinton P, Giorgi C, Siviero R, Zecchini E, Rizzuto R. Calcium and apoptosis: ER-mitochondria Ca2+ transfer in the control of apoptosis. Oncogene. 2008;27:6407–18.

57. Kahns S, Kalai M, Jakobsen LD, Clark BF, Vandenabeele P, Jensen PH. Caspase-1 and caspase-8 cleave and inactivate cellular parkin. J. Biol. Chem. 2003;278:23376–80.

58. Kim TY, Kim E, Yoon SK, Yoon JB. Herp enhances ER-associated protein degradation by recruiting ubiquilins. Biochem. Biophys. Res. Commun. 2008;369:741–46.

CHAPTER FOUR: ABERRANT ACCUMULATION OF α-SYNUCLEIN WORSENS ISCHEMIA-INDUCED BRAIN DAMAGE BY INCAPACITATING DJ-1–MEDIATED NEUROPROTECTIVE RESPONSES

Introduction

Brain injury following cerebral ischemia or stroke results from the complex interplay of multiple pathways including ionic imbalance and excitotoxicity, oxidative and nitrative stress, and inflammation (1). Reactive oxygen species (ROS) are produced in excess during the course of cerebral ischemia reperfusion (I/R) by a variety of mechanisms such as aberrant electron transport in injured mitochondria, calcium influx and inflammatory reactions (2). A growing body of evidence supports the essential role of oxidative and nitrative stress in the initiation and progression of the injury process after I/R (3). Reoxygenation during reperfusion activates nitric oxide synthase and increases the generation of nitric oxide, which combines with superoxide to produce peroxynitrite, a potent oxidant that can modify cellular targets (proteins, lipids, and DNA) and participate in signaling mechanisms that result in exacerbation of infarct (4). Oxidation-modified proteins have been shown to accumulate and participate in the generation of protein aggregates (5).

Protein aggregation is part of the etiology of many chronic neurodegenerative diseases such as Alzheimer's (AD), Parkinson’s (PD) and Huntington's (HD) diseases although the causes of protein aggregation vary among the diseases (6). Abnormal accumulation of protein aggregates also occurs after acute brain injury such as ischemic stroke and has been detected in vulnerable neurons from the onset of I/R until

delayed neuronal death (7, 8). The protein aggregates formed after cerebral ischemia are detergent-resistant (7), consistent with the nature of irreversible protein aggregation in other pathologic conditions. The role of protein aggregation in neuronal pathology after brain ischemia is not clear. It is believed that protein aggregation may contribute to delayed neuronal death as induction or transgenic overexpression of heat shock protein 70 (Hsp70) and other molecular chaperones before ischemia reduces evidence of protein aggregation under conditions where neuronal survival is increased (9, 10).

PD is the second most prevalent neurodegenerative disorder and is characterized pathologically by the relatively selective degeneration of midbrain dopaminergic neurons and the accumulation of insoluble α-Syn containing intracytoplasmic inclusions called Lewy bodies (11, 12). α-Syn was the first gene identified whose mutations cause autosomal dominant forms of familial PD (13). Overexpression of PD-causing mutant α-Syn in animal models leads to α-Syn aggregation and neurodegeneration (14). Genetic and biochemical studies implicate protein misfolding and aggregation, aberrant expression and degradation in α-Syn-induced pathology (15, 16). α-Syn is a small 140 amino acid presynaptic protein that is intrinsically unfolded and assembles under pathological conditions into characteristic Lewy inclusion bodies that typify PD and other Lewy body-containing neurodegenerative diseases termed synucleinopathies (16). Familial PD mutants of α-Syn have increased propensity to aggregate. (17). Furthermore, exposure to oxidizing conditions has been shown to accelerate α-Syn aggregation (16). Specifically, nitration of α-Syn protein accelerates its rate of fibrillization (16). Triplication of its gene locus has also been identified in early onset familial PD suggesting that aberrant accumulation of

α-Syn can play a crucial role in PD pathogenesis (18). While the normal function of α-Syn continues to be characterized, multiple lines of evidence suggest that PD pathogenesis is closely linked with a toxic gain of function associated with misfolded α-Syn.

DJ-1 is another PD gene linked to early onset disease with autosomal recessive inheritance (12, 19). DJ-1 is a small 189 amino acid protein that is ubiquitously expressed and exhibits anti-oxidant and chaperone-like activities (20-23). The DJ-1-mediated protective actions have been demonstrated in several pathological disease models both *in vitro* and *in vivo* (20-23). Consequently, PD-causing mutations that result in loss of DJ-1 function expose dopaminergic neurons to endogenous and exogenous stressors (19). Consistent with this notion, DJ-1 knockdown cells and DJ-1 null mice or flies are highly susceptible to PD-inducing neurotoxins such as paraquat, 6-hydroxydopamine, rotenone and 1-methyl-4-phenyl-1,2,3,6-tetrahydropyridine (MPTP) (20-23). DJ-1 null mice also display larger infarcts as compared to wild-type mice in a rodent model of ischemic stroke (24) suggesting that DJ-1 deficiency may concur in exacerbating oxidative damage. Conversely, overexpression of DJ-1 correlated positively with survival outcome (25).

Given that oxidative stress is an established mediator of ischemia-induced neuronal injury and plays a critical role in mediating α-Syn aggregate formation and toxicity, and the recent findings that DJ-1 inhibits α-Syn aggregate formation and protects from ischemic brain damage (24), we explored the pathological interactions between these two PD-associated proteins in the context of oxidative stress, protein aggregation, and neuronal survival under ischemic conditions.

Materials and Methods

Transient Middle Cerebral Artery (MCA) Occlusion

C57BL/6, α-Syn$^{-/-}$ transgenic (B6;129X-SncatmlRosl, Stock #3692) and non-transgenic control (129/Sv x C57BL/6; Jackson Labs, Bar Harbor) mice were housed in a pathogen free facility, about 4-5 animals per cage in a temperature controlled room with a 12 hour light/dark cycle and with food and water ad libitum. The generation of α-Syn$^{-/-}$ mice was previously described (56). Male mice (10-12 weeks old) weighing 22–26 g were anaesthetized with 1.5% halothane in 70% N_2O and 30% O_2, and focal cerebral ischemia was induced by occluding the left MCA by using the thread occlusion technique, essentially as described (57). Briefly, a 5-0 nylon filament, with its tip rounded by heating near a flame, was inserted through the external carotid artery stump and advanced into the right internal carotid artery until it blocked the MCA blood flow. Arterial blood pressure and cerebral blood flow were monitored during ischemia and the first 20 min of reperfusion as described previously (57). Sixty min. after occlusion, the filament was gently withdrawn to restore blood flow. Rectal temperature was monitored and maintained at 37 ± 0.5 °C with a thermostatic blanket throughout the entire duration of the surgical procedure and in the recovery period until the animals regained full consciousness. Sham-operated animals were subjected to similar surgical procedures without occlusion of the MCA. At 3-72 h post-ischemic reperfusion, the animals were anesthesized with 5% halothane and sacrificed. The α-Syn$^{-/-}$ mice were compared to their own non-transgenic controls in the 129 x C57BL/6 genetic background (F10-F12). Morphological studies revealed no fundamental abnormalities in the adult brain thereby excluding the possibility that germ line deficiency would bias stroke outcome. All

procedures and animal handling were approved by and conformed to the guidelines of the Institutional Animal Care and Use Committee of the University of Central Florida.

Cerebral Infarct Volume Measurement

After cerebral ischemia reperfusion (I/R), mice were sacrificed and brains removed. Two millimeter coronal sliced were made with a rodent brain matrix (Kent Scientific Corp) and stained for 20 min at 37 °C with 2% 2,3,5-triphenyltetrazoliun chloride monohydrate (TTC; Sigma) for detecting infarcted tissue (57) The total infarct volume was obtained from integrating infarcted areas and correcting for brain edema. Briefly, the sections were scanned and the infarcted area in each section was calculated by subtracting the non-infarct area of the ipsilateral hemisphere from the area of the contralateral hemisphere with NIH Image analysis software (Scion Image). Infarction areas in each section were summed and multiplied by section thickness to give total infarction volume.

Neurological Evaluation

The functional outcome of the stroke injury was determined blinded to the treatment history of the mice using a 5 grade neurological deficit score (0, no deficit; 1, failure to extend right paw; 2, circling to the right; 3, falling to the right; 4, lacking spontaneous locomotion) as described previously (57). Mice were evaluated before MCA occlusion to establish a baseline and at 24 h after I/R.

Primary Cultures

Cultures of dissociated neocortical cells were prepared from brains of 18-d-old mouse embryos as previously described (58). Briefly, cerebral hemispheres were removed and incubated for 15 min in Ca^{2+}- and Mg^{2+}-free Hank's Buffered Salt Solution (Invitrogen) containing 0.2% trypsin. Cells were dissociated by trituration and plated into polyethyleneimine-coated plastic or glass-bottomed culture dishes containing Minimum Essential Medium with Earle's salts supplemented with 10% heat-inactivated fetal bovine serum and (in mM): 2 L-glutamine, 1 pyruvate, 20 potassium chloride, 10 sodium bicarbonate, and 1 HEPES, pH 7.2. After cell attachment (3-6 h after plating), the culture medium was replaced with maintenance medium (Neurobasal Medium containing 2% B27 supplement and 0.5 µM glutamine, Invitrogen). Thereafter, maintenance medium was changed every 3 days. Experiments were performed in 12-14-days old cultures.

Production of Lentivirus Particles and Infection of Neuron Cultures

The DJ-1 cDNA was amplified by PCR from its pcDNA3-based expression vector and cloned into a Gateway entry vector (pENTR4; Invitrogen). The viral constructs were obtained through homologous recombination between pENTR4-DJ-1 and the lentiviral destination vector pLenti6/V5-DEST (ViralPowerTM Lentiviral Expression System; Invitrogen). Cortical neurons in 48-well at around 70% confluence were infected with 10^5 genomic particles / cell of pLenti6-DJ1 or pLenti6-LacZ (lactosidase) and then kept in regular complete medium.

RNA Interference

Cortical cultures were transfected with prevalidated siRNA duplexes targeting mouse DJ-1 and αSyn (Dharmacon), or a scramble control siRNA (siRNA-Con; Ambion) using Oligofectamine 2000 (Invitrogen) in Opti-MEM (Invitrogen) according to manufacturer's protocol. To monitor knockdown, neurons were harvested and processed for RT-PCR and Western blot analyses.

Oxygen Glucose Deprivation (OGD) Treatment

Cortical neuronal cultures were rinsed and incubated in glucose-free Locke's buffer (in mM: NaCl, 154; KCl, 5.6; $CaCl_2$, 2.3; $MgCl_2$, 1.0; $NaHCO_3$, 5; and HEPES, 5 mM; pH 7.2) in an anaerobic chamber (Billups-Rothenberg) containing 94% N_2/ 5% CO_2/ 1% O_2 (59). Control cultures not deprived of oxygen and glucose were placed in Locke's containing 5.5 mM glucose under a 95% air / 5% CO_2 atmosphere. To terminate OGD, cultures were removed from the anaerobic chamber and incubated in the normal growth medium in the normoxic incubator. At various time points following reoxygenation, cell lysates were prepared. In knockdown experiments, cultures were trasnfected with siRNAs 12 h prior to OGD. In some experiments, the JNK (c-Jun N-terminal kinase) and p53 inhibitors, SP600125 (Calbiochem) and pifithrin-α, were added to cultures 2 h prior to OGD.

Immunoprecipitation

Tissues were solubilized in binding buffer containing 50 mM Tris–HCl (pH 7.4), 150 mM NaCl, 1 mM EDTA, 1 mM DTT, 0.2 mM phenylmethanesulfonyl fluoride, and 1.0% NP-40 as described previously (60). The homogenate was centrifuged at 20,000 ×

g for 10 min. Solubilized proteins were adjusted to 0.1% NP-40 and incubated for 12 h at 4 °C with normal pre-immune IgG or antibody to mouse DJ-1 and αSyn. After an additional incubation with protein A conjugated beads, the immune complexes were then recovered by low speed centrifugation and washed extensively with the binding buffer containing 0.1% NP-40. Immunoprecipitated proteins were eluted by boiling in SDS-PAGE sampling buffer and analyzed by immunoblotting.

Immunoblotting

Detergent-soluble and -insoluble fractions were prepared from dissected hemispheres by homogenization of samples with a Dounce homogenizer (50 strokes) in 8 volumes of ice-cold homogenization buffer [10 mM Tris HCl (pH 7.4), 150 mM NaCl, 5 mM EDTA, 0.5% Nonidet P-40, 10 mM Na-ß-glycerophosphate, and complete protease inhibitor mixture (Roche). After homogenization, samples were rotated at 4 °C for 30 min for complete lysis, then the homogenate centrifuged (10,000 *g*, 4 °C, 20 min.) and the resulting pellet and supernatant fractions were collected. The pellet fractions were washed t in lysis buffer containing 1% Triton X-100 on a shaker for 1 hour at 4°C, and then centrifuged at 20,000 *g* at 4 °C for 10 minutes to obtain Triton X-100 -soluble and -insoluble fractions. The resulting pellet was solubilized in lysis buffer containing 1% SDS. Protein amounts in the obtained fractions were determined using the BCA kit (Pierce). Protein samples were separated by sodium dodecyl sulfate-polyacrylamide gel electrophoresis and blotted to nitrocellulose membranes (BioRad) as described (61). All membranes were blocked with 5% non-fat dry milk in Tris-buffered saline (TBS) containing 0.1% Tween-20 and incubated with the following primary antibodies: DJ-1 (Abcam or Chemicon); α-Syn (Abcam or Millipore); ERK1/2 (Santa Cruz); phospho-

JNK1/2 and total JNK1/2 (Santa Cruz); p53 (Cell Signaling); PARP (Cell Signaling); beta-Actin (Sigma). Protein bands were then detected using horseradish peroxidase conjugated secondary antibodies (Jackson Immunoreseacrh) and visualized using the enhanced chemiluminescent substrate kit (Pierce). The protein levels were quantified using NIH Image analysis software (Scion Image).

Semi-Quantitative Reverse Transcriptase-PCR (RT-PCR)

Abundance of mRNAs was examined by RT-PCR. After indicated time points, total RNA was extracted from dissected ipsilateral and contralateral hemispheres of sham-operated and ischemic brains using the RNeasy Mini kit (Qiagen). To prevent genomic DNA contamination, the isolated total RNA samples were treated with DNAse. Complementary DNA was synthesized from 2.5 µg of total RNA using the Superscript III system with oligo-dT primer (Invitrogen). The primer used were as follows: α-Syn (NM_009221) forward 5'-GTGGAGCAAAAATACATCTTT AG-3' and reverse: 5'-TGTACGCCATGGA AGAGCA GC-3' ; DJ-1 (NM_007262.3.) forward 5'GCTTCCAAAAGAGCTCTGGTCA-3′ and reverse 5′-GCTCTAGTCTTTGAGAACAAGC-3′ ; p53 (NM_011640) forward 5'-CACGTACTCTC CTCCCCTCAAT-3' and reverse 5'-AACT GCACAGGGCACGTCTT-3′ ; beta-Actin (NM_007393): forward 5′-CCTAGGCACCAGGG TGTGAT-3′ and reverse 5′-GCTCGAAGTCTA GAGCAACA-3′; 18S rRNA (NM_X00686): forward 5'-AGGGGAGAGCGGGTAAGAGA-3'-and reverse 5'-GGACAGGACTAGGCGGA ACA-3'; GADPH (NM M32599): forward 5'-AGGCCGGTGCTGAGTATGTC-3' and reverse 5'-TGCCTGCTTCACCACCTTCT-3'. All reactions were performed in triplicate using GADPH or 18S as internal controls. RT-PCR products were resolved on agarose gels

stained with ethidium bromide. Relative quantification of gene expression was performed by normalizing the fluorescence intensities of each band to those of internal controls.

Immununohistochemistry

Ischemia-induced changes cellular distribution of α-Syn and DJ-1 proteins were evaluated by immunohisto-chemistry. Mice were anesthetized with sodium pentobarbital (120 mg/kg, i.p) and perfused transcardially with 4% paraformaldehyde in saline. Brains were removed and post-fixed overnight, and placed in 30% sucrose for 24 h (62). Coronal sections (25 µm) were cut in a Leica cryostat and mounted on Superfrost slides (VWR). Sections were incubated with phosphate buffered saline (PBS) containing 0.2% (v/v) Triton X-100 and 5% goat or horse serum for 1 h. Subsequently, sections were incubated overnight at 4 °C with a monoclonal antibody against mouse α-Syn (Syn102; EMD Millipore) or nitrated (Tyr39) α-Syn (nSyn14; EMD Milipore), or a polyclonal antibody against DJ-1 (Chemicon). Antibody binding was visualized with a secondary anti-rabbit antibody conjugated to either fluorescein isothiocyanate (FITC) or anti-mouse conjugated to Texas Red (Invitrogen). To stain the nuclei, sections or coverslips were further incubated with the nucleic acid stain 4',6-diamidino-2-phenylindole (DAPI) in PBS containing 1% RNase and 0.2% Triton X-100 for 10 min, and then mounted in FluorSave aqueous mounting medium (Calbiochem). The immunofluorescent staining was analyzed and documented using a Nikon Eclipse 80i microscope equipped with a DXR1200C color digital camera. All images were acquired using the same laser intensity and photodetector gain to allow quantitative comparisons of relative levels of

immunoreactivity. For double immune-fluorescence staining, the primary antibodies were incubated sequentially and processed further as described above.

Quantification of Cell Death

Cell death was assessed by using a lactate dehydrogenase (LDH) Cytotoxicity Detection Kit (Roche) or by trypan blue exclusion. The LDH method quantifies cell death in culture based on the measurement of LDH released into the growth medium when cell membrane integrity is lost. Trypan blue stains only the cells with disrupted plasma membrane integrity so these cells were considered dead. Dead cells were counted in four microscopic fields per dish, with a minimum of 100 cells per field and results were expressed as a percentage of the total number of cells. All of the experiments were repeated at least three times without knowledge of treatment history.

Statistical Analysis

Values were expressed as mean ± SEM and comparisons between two groups were statistically evaluated by the Student's *t* test using the GraphPad Instut software. The bonferroni correction was used when more than two groups were present. Results are presented as means ± SEM. P-value of less than 0.05 was considered to be statistical significance.

Supplementary Methods

Primary glial cultures

Enriched primary glial cultures were prepared from whole brains of 1-day old mice. After reaching confluence, microglia were isolated by shaking the flasks

containing mixed glia for 5 h at 150 rpm. Enriched microglia were maintained in DMEM containing 10% FBS and 1 mm sodium pyruvate. To obtain astroglia, the mixed glial cultures, after the separation of microglia, were detached with trypsin-EDTA and seeded in the same culture medium used for microglia. After at least six consecutive passages, highly enriched astroglia were used for experiments. The purity of glial cultures was routinely verified at >95% by Iba1 (microglia) and GFAP (astrocytes) immunoreactivity.

Proteasomal Activity Assay

Freshly prepared cortical homogenates (20 µg of protein) were diluted in 1x assay buffer (5x reaction buffer: 250 mmol/L Tris–HCL pH 7.6, 5 mmol/L dithiothreitol, 50 mmol/L $MgCl_2$, and 10 mmol/L ATP) with 10 µg of substrate III (Calbiochem) in a 96-well plate. Reactions were carried out for 30 min. at 37°C and stopped by adding 5% SDS. Chymotrypsin-like proteasomal activity was measured with a spectrofluorometer via substrate consumption at 440 nm with an excitation wavelength of 380 nm. Three independent reactions were performed for each sample in the presence or absence of the selective proteasomal inhibitor lactacystin (1 µmol/L; BioMol). Proteasome activity was calculated by subtracting the lactacystin-insensitive (or non-proteasome) peptidase activity from total peptidase activity.

Results

Cerebral Ischemia Reperfusion (I/R) Alters α-Syn Protein Level and Solubility

Given that mouse α-Syn shares similar primary and secondary structures with human α-Syn and that the mouse protein forms amyloid fibrils *in vitro* (27), we

determined whether α-Syn constitutes a component of the protein aggregates in ischemic brains. As aggregate-prone proteins accumulate in the insoluble pellet (P)-fraction as the result of decreased detergent-solubility, we monitored the chronological changes of α-Syn protein in the detergent soluble (S)- and P-fractions obtained from the cortices of mice. Sham-operated mice subjected to the same surgical procedures but without induction of I/R were used as controls. Immunoblot analysis revealed a marked and sustained accumulation of α-Syn protein in the P-fractions prepared from the ipsilateral ischemic cortices when compared to those from the contralateral nonischemic cortices. Insoluble α-Syn monomers and oligomers were detected as early as 3 h post-I/R and their levels increase progressively up to 72 h post-I/R (**Fig 1A**). Though the monoclonal α-Syn antibody detected the α-Syn dimer as the prominent oligomeric form in the P-fractions, high molecular oligomers were also present though at substantially lower levels (data not show). Levels of α-Syn are not significantly altered in the S- and P- fractions obtained from the cortices of sham-operated mice (data not shown).

Next, we examined the alterations in α-Syn subcellular localization in the ischemic lesions by immunohistochemistry. The diffuse neurophilic α-Syn staining observed in the contralateral non-ischemic neurons was replaced by discrete circumscribed clumps of intense immunolabeling in both the neurophil and somata of neurons in the ischemic lesions (**Fig 1B**). The observed somatic accumulation of α-Syn has also been described in MPTP-intoxicated mice (27) suggesting that the aberrant accumulation and subsequent aggregation of α-Syn in the somata is likely attributed to impaired axonal transport resulting from ATP deficits in the ischemic neurons.

Application of the preabsorbed or omission of the α-Syn antibody yields no appreciable labeling (data not shown).

Because the nitratively modified form α-Syn is less soluble and accumulates in human Lewy bodies and other α-Syn containing inclusions (16), we stained ischemic brain sections with an antibody that recognizes the nitrated form of mouse α-Syn (nSyn14). nSyn14 immunoreactivity was detected in the ipsilateral but not contralateral cortices (**Fig 1C**) suggesting that α-Syn modifications resulting from I/R-associated oxidative and nitrative stress play a critical role in facilitating α-Syn aggregation. No appreciable Syn14 immunoreactivity was detected in the cortices of sham-operated mice (data not shown). Collectively, these data suggest that abnormal cellular accumulation of α-Syn protein that can promote its self-aggregation is a pathological event initiated after I/R.

α-Syn is Upregulated in Neurons Subjected to Ischemic Insults In Vitro

The aberrant accumulation of α-Syn in the S-and P-fractions (**Fig 1A**) suggests that α-Syn expression might be increased in ischemic neurons. As predicted, α-Syn mRNA levels were elevated in the ipsilateral but not contralateral cortices after I/R (**Suppl Fig 1A**). Both α-Syn mRNA and protein levels were increased in the primary mouse cortical cultures after OGD (**Suppl Fig 1B**), an *in vitro* model of I/R. The OGD-induced upregulation of α-Syn was more robust in neurons when compared to astrocytes and microglia (**Suppl Fig 1B**) and this may account for the relatively much weaker α-Syn immunostaining of glial cells in ischemic brains (data not show). Collectively, these data indicate that α-Syn expression is induced specifically in the

ischemic neurons and that α-Syn upregulation may play a precipitating role in I/R-induced neuronal injury.

Accumulation of Insoluble α-Syn in the Ischemic Lesions is Independent of Parkin and Proteasome Activity

Parkin is an ubiquitin ligase controlling the degradation of some protein substrates by the proteasomes (28). Loss of function mutations in *parkin* gene cause early-onset PD with autosomal recessive inheritance (35). In sporadic form of PD, parkin has been shown to accumulate in the insoluble fraction (29). Recently, it has been shown that parkin mitigates α-Syn-induced neuronal cell death in animal and tissue culture models (30), suggesting a functional relationship between these two PD-associated proteins. Although the mechanism by which parkin protects from α-Syn-induced cytotoxicity is not completely understood, parkin may regulate the normal metabolism of α-Syn or the clearance of pre-formed α-Syn aggregates (30). To determine whether the appearance of α-Syn-positive inclusions in the ischemic brains might be a consequence of decreased parkin solubility, we monitored the chronological changes of α-Syn protein in the S- and P-fractions of lesioned and non-lesioned cortices. Parkin levels in the S-fractions were not markedly altered up to 12 h after I/R (Suppl Fig 2; upper panel) suggesting that the appearance of insoluble α-Syn in the ischemic cortices at 3 h post-I/R (shown in Fig 1A) could not be attributed to decreased parkin solubility. Prolonged reperfusion (>12h) appears to impact parkin solubility as evidenced by the subtle changes in the amount of parkin in the S- and P-fractions (**Suppl Fig 2**; lower panel). Because proteosomal alterations are often found in patients with sporadic PD (11, 12) and may play a role in α-Syn accumulation, we measured

proteasome activity in the S-fractions obtained from the ischemic and non-ischemic cortices (shown in **Fig 1A**). Though proteasome activity decreases progressively in the ischemic cortices (**Suppl Fig 2B**), α-Syn aggregate formation precedes the significant reduction in proteasome activity indicating that α-Syn accumulation and aggregation may not be attributed to altered proteasome activity. Taken together, these results suggest that under ischemic stress conditions decreased α-Syn solubility may be attributed to the robust expression of α-Syn that self-aggregates in a pro-oxidant environment.

Cerebral I/R Alters DJ-1 Solubility and Localization

Consistent with the notion that oxidative stress induces the expression of DJ-1 (20), we found that DJ-1 mRNA levels in the ipsilateral cortices increased markedly and peaked at 18 h post-I/R (**Fig 2A**). By 24 h after reperfusion, mRNA levels of DJ-1 returned close to those seen in the cortices of sham-operated mice (**Fig 2A**). The corresponding DJ-1 protein decreased in the S–fractions (**Fig 2B,C**) and accumulated time-dependently in the α-Syn containing P-fractions (**Figs 1 and 2B,C**) suggesting that I/R decreases the solubility of these two PD-associated proteins and that accumulation of insoluble DJ-1 parallels that of insoluble α-Syn. By contrast, DJ-1 mRNA and protein levels were not markedly altered in the contralateral cortices of I/R-treated mice when compared to the cortices of sham-operated mice (**Fig 2A-C**). The increase of DJ-1 protein in the ipsilateral but not contralateral cortices was confirmed by immunofluorescent staining (**Fig 2D**).

DJ-1 is Recruited into Pathological α-Syn-Containing Inclusions in the Ischemic Lesions

Next, we determined whether the observed decrease in DJ-1 solubility after I/R might be related to its interaction with α-Syn in vulnerable neurons. First, we evaluated the cellular localization of DJ-1 and α-Syn in the ischemic brains by immunohistochemistry. After I/R, DJ-1 immunolabeling pattern changes from a relatively even distribution to a heterogenous granular pattern in the ipsilateral but not contralateral cortices (**Fig 3A**). Double immunofluorescence labeling confirmed that DJ-1 immunopositive granules were co-localized with the somatic α-Syn inclusions in the ischemic neurons (**Fig 3A**). The specificity of DJ-1 labeling was confirmed by omission or preadsorption of the primary antibody (data not shown).

Next, we performed co-immunoprecipitation assay to determine whether the interaction of DJ-1 with α-Syn accounts for the observed altered subcellular localization of DJ-1. Both proteins were readily detected in protein complexes immunoprecipitated from the nonfractionated homogenates of the ipsilateral cortices but not those of the contralateral cortices of ischemic brains (**Fig 3B**). Furthermore, nSyn14 was also detected in the DJ-1 containing protein complexes (data not show) indicating the association of DJ-1 with the less soluble modified form of α-Syn. The specificity of the observed interaction was verified in the samples incubated with pre-immune IgG or no antibody (Con).

Knockdown of α-Syn Prevents the Ischemia-Induced Decrease of DJ-1 Solubility

To further delineate the relationship between α-Syn accumulation and decreased DJ-1 solubility in ischemic neurons, siRNA experiments were performed to block the

OGD-induced upregulation of α-Syn in cultured mouse cortical neurons. Transfection with siRNA targeting α-Syn mRNA (α-Syn siRNA) markedly suppressed the OGD–induced accumulation of α-Syn mRNA and protein (**Fig 4A**). Fluorescein-labeled control siRNA (Con siRNA) with a scrambled sequence was used to determine the specificity of knockdown and to confirm siRNA delivery to > 90% neurons (data not shown). As DJ-1 appears to function as a broad-spectrum neuroprotectant, it is conceivable that removal of DJ-1 from the soluble cellular compartment where it normally exerts its actions results in decreased amount of functional DJ-1 and thereby unfavorably impacts neuronal survival. Consistent with this notion, we found that knockdown of α-Syn not only inhibits the accumulation of DJ-1 in the P-fraction (**Fig 4B**) but also improved the survival of transfected neurons under ischemic stress conditions (**Fig 4C**). Knockdown of α-Syn did not increase DJ-1 mRNA levels suggesting that the increase in soluble DJ-1 protein could not be attributed to the compensatory increase of DJ-1 expression (**Fig 4D**). Collectively, these results indicate that the ischemia-induced upregulation of α-Syn drives the abnormal accumulation of DJ-1 in pathological inclusions and that protection from ischemic stress is dependent on the sustained increase of DJ-1 in the soluble cellular compartment.

DJ-1 Suppresses α-Syn Accumulation and Aggregate Formation in Ischemic Neurons

Because DJ-1 has been shown to inhibit the generation of α-Syn aggregates (31, 32), we next examined the impact of DJ-1 knockdown on α-Syn solubility in mouse cortical neurons under ischemic stress conditions. Treatment with the DJ-1 siRNA markedly suppressed the OGD-induced increase of DJ-1 mRNA and protein levels in

cortical cultures by 70 to 80% relative to those treated with the Con siRNA (**Fig 5A**). Consequently, knockdown of DJ-1 resulted in the accumulation of insoluble α-Syn (**Fig 5B**) and decreased neuronal survival after OGD (**Fig 5C**). To further determine whether α-Syn aggregate formation was facilitated as the result of decreased DJ-1 function, we ectopically expressed DJ-1 in cortical neurons. Overexpression of DJ-1 inhibited the accumulation of α-Syn (**Fig 5D**) and protected neurons from OGD-induced death (**Fig 5E**) suggesting that DJ-1 increases the threshold of ischemic neuronal death by suppressing the accumulation of α-Syn and its subsequent self-aggregation. Hence, decreased DJ-1 solubility may concur in triggering the accumulation of insoluble α-Syn that in turn accelerates the depletion of DJ-1 from the soluble cellular compartment.

DJ-1 Counteracts Ischemia-Induced Activation of the p53 Pathway

Next, we determined the mechanism(s) through which the effects of α-Syn on DJ-1 function might aggravate neuronal damage. Considering the critical role of DJ-1 in reducing cellular oxidative stress, we reasoned that the tumor suppressor protein p53 might be an important downstream target of DJ-1 to counteract ischemic neuronal death. p53 is a transcription factor that is known to propagate oxidant-induced death signaling cascades as chemical inhibitors of p53 can rescue vulnerable neurons from ischemic insults *in vivo* and *in vitro* (32, 33). Normally, p53 exists at a very low level but is rapidly increased in response to a range of insults including oxidative stress and DNA damage (33). The Jun N-terminal kinase 1/2 (JNK1/2) is known to be activated by oxidative stress and increases p53 protein stability by phosphorylation (35). Knockdown of DJ-1 promotes p53 activation in part through the activation of JNK1/2 (**Fig 6A**). The OGD-induced increase of p53 was associated with apoptosis as evident by the

cleavage of poly (ADP-ribose) polymerase (PARP), a substrate of caspase-3 (**Fig 6A**). Pharmacological inhibition of JNK and p53 activation using SP600125 and pifitrin-α, respectively, significantly rescued DJ-1 siRNA transfected neurons from OGD-induced death (**Fig 6B**) without significantly altering the expression of p53 (**Fig 6C**). Our results therefore strengthen the notion that DJ-1 counteracts ischemia-induced apoptotic signaling through the inhibition of redox-dependent p53 activation.

α-Syn Deficiency Ameliorates Cerebral I/R Injury

If α-Syn upregulation was indeed important in promoting ischemic brain damage, we hypothesize that α-Syn deficiency would ameliorate the extent of anatomical and functional brain damage after cerebral ischemia. Accordingly, we evaluated lesion development in mice with targeted disruption of the *α-Syn* gene 24 h following I/R by quantifying cerebral infarction and evaluating neurological function. α-Syn$^{-/-}$ mice developed smaller infarct compared to α-Syn$^{+/+}$ mice (**Fig 7B**). The smaller infarct was associated with a faster recovery after stroke as measured by a neurological score (**Fig 7B**). These data indicate that α-Syn$^{-/-}$ mice are less susceptible to I/R brain injury.

To confirm that α-Syn accumulation negatively impacts neuronal survival after I/R, cortical neurons from α-Syn$^{-/-}$ and α-Syn$^{+/+}$ embryos were subjected to OGD. In line with the α-Syn knockdown studies, we observed that α-Syn$^{-/-}$ cortical neurons were significantly less vulnerable to OGD-induced cell death (**Fig 7C**).

Because α-Syn aggregation interferes with DJ-1 solubility, we next examined DJ-1 accumulation in the S- and P-fractions obtained from α-Syn$^{-/-}$ and α-Syn$^{+/+}$ cortical cultures under ischemic conditions. The amounts of DJ-1 in the P-fractions were

substantially lower in α-Syn$^{-/-}$ when compared with α-Syn$^{+/+}$ neurons after OGD (**Fig 7D**). Consistent with the finding that DJ-1 negatively modulates the p53 pathway under ischemic stress, we found that the accumulation of p53 protein was markedly lower in α-Syn$^{-/-}$ when compared to α-Syn$^{+/+}$ neurons (**Fig 7D**).

Discussion

The development of effective protective strategies requires a comprehensive understanding of the diverse mechanisms of ischemic brain damage. Pathophysiological processes associated with neuronal death in stroke and chronic neurodegenerative diseases are usually investigated independently. However, stroke and degenerative diseases may have common links as disease mechanisms or genes defined for one neurodegenerative condition might also be central in stroke. Stroke can either instigate or accelerate latent or progressive neurodegenerative events and is a known epidemiologic risk factor for Alzheimer's disease (AD) (36). Whether stroke also increases the risk of developing PD or vice versa is still controversial due to the relatively small-scale studies and the confounding factors associated with PD medications that can influence stroke susceptibility and outcome (37). As PD patients also have symptoms not classically associated with movement such as cognitive defects, it is possible that, small "silent" strokes may predispose PD patients to cognitive impairments later in life (38). Because α-Syn accumulates in neurons with age, it is likely that a similar mechanism may contribute to the progressive susceptibility to stroke-induced neuronal injury.

α-Syn toxicity is generally considered a consequence of its aggregation (11, 12). It has been reported that both human and mouse α-Syn proteins are natively unfolded and that, at higher doses or following exposure to oxidizing conditions, the mouse protein adopts fibrillar amyloid structures resembling those comprising human wild-type and PD-linked (A53T and A30P) mutant α-Syn (26). Supporting the notion that *SNCA* gene amplifications or polymorphisms with resultant relatively higher levels of the protein increase the risk for developing PD (18, 39), we found that the ischemia-induced upregulation of endogenous α-Syn and its subsequent aggregation in the presence of an oxidative environment plays an important role in the initiation of α-Syn driven perturbations that negatively impact neuronal survival. Genetic ablation of α-Syn reduces brain damage and improves functional outcome in a mouse model of focal ischemic stroke. Ablation or knockdown of α-Syn also improves neuronal survival to an ischemic challenge *in vitro.* The endangering consequence of α-Syn accumulation has also been demonstrated in complex I-induced death of dopaminergic neurons (27) and α-Syn$^{-/-}$ mice are resistant to the toxic effects of MPTP (40). Furthermore, α-Syn pathologies following traumatic brain injury were also prevented in α-Syn$^{-/-}$ mice (41). Hence, elucidating the factor(s) responsible for driving the robust expression of α-Syn in ischemic neurons could lead to a feasible therapeutic strategy aimed at inhibiting α-Syn accumulation and the associated neurons loss not only after I/R but also in traumatic brain injury, AD, PD and related disorders.

Although the underlying mechanisms remain to be determined, soluble oligomers and insoluble inclusions formed in different neurodegenerative diseases have been shown to inactivate cellular protective mechanisms (42). Biochemical and

immunohistochemical data support a scenario where the ischemic stress-induced accumulation of α-Syn aggregates recruits DJ-1 into the insoluble inclusions and thereby interferes with DJ-1 solubility and subcellular distribution, and hence, its ability to execute broad-spectrum neuroprotective functions. Several studies provided evidence that DJ-1 forms high molecular weight complexes with α-Syn in brain tissues from patients with PD and related disorders (43-46). Decreased DJ-1 solubility has been demonstrated in human brain tissues of patients inflicted with PD-related diseases but not normal control subjects (44).

Though the interaction between DJ-1 and α-Syn has been explored previously as a possible mechanism for DJ-1 accumulation into pathological inclusions in cellular models of α-Syn overexpression (38, 39) and in human brain tissues (44), our data concurs with the interaction accounting for the altered DJ-1 solubility in ischemic neurons. We cannot exclude the possibilities that the interaction between these two PD-associated proteins may be indirect and that the presence of accessory factors in the ischemic neurons may be required for the observed interaction *in vivo*. It is noteworthy that the DJ-1 chaperone activity is redox-dependent (31, 32) and thereby its interaction with α-Syn may be regulated in the context of oxidative stress under ischemic conditions.

Decreased DJ-1 solubility leads to impaired cellular anti-oxidant responses resulting in the aggravation of oxidative damage after I/R. DJ-1 can directly scavenge radicals and becomes more acidic in the presence of an oxidative environment (20, 47). The resulting acidic form of the molecule is present at significantly higher level in PD and AD brains when compared to control subjects (47). DJ-1 has been demonstrated to

redistribute to the mitochondria wherein it regulates the activity of complex I and protects against mitochondria damage (20). Consistent with this notion, DJ-1 overexpression has been shown to confer neuronal resistance towards stimuli that promote mitochondria-dependent apoptosis (21-23). Hence, reduced DJ-1 solubility may promote mitochondrial dysfunction and aggravate ROS production resulting in the subsequent activation of p53, a redox-regulated transcription factor that propagates death responses to oxidative stress**.** Support for a pivotal role of p53 in PD is provided by the recent findings that mice that are either deficient in p53 (48) or treated with pifithrin-α resist MPTP neurotoxicity (49). Activation of p53 is also essential for neuronal death in cerebral ischemia as mice given pifithrin-α exhibited increased resistance of neurons to ischemic injury and excitotoxic damage (34). Consistent with the notion that α-Syn aggregation (50) and DJ-1 deficiency (51) lead to the activation of the p53 pathway**,** we found that α-Syn$^{-/-}$ neurons exhibit less p53 accumulation following OGD and that the OGD-induced increase of p53 was substantially suppressed after ectopic expression of DJ-1. We demonstrated that the ischemic stress-induced α-Syn accumulation contributes in part to the increase of p53 through the activation of JNK which in turn phosphorylates and stabilizes the p53 protein. Hence, DJ-1 likely suppresses p53 activation by ameliorating oxidative stress under ischemic conditions. Our data do not exclude the possible involvement of other DJ-1-mediated antioxidant mechanisms responsible for increasing the threshold for ischemia-induced neuronal death. DJ-1 has been reported to function as a co-activator required for the induction of neuroprotective and detoxifying genes likely through the interaction with NF-E2-related

factor (Nrf2), a transcription factor that coordinates the expression of a variety of antioxidant enzymes (52).

DJ-1 has chaperone activity and can inhibit α-Syn aggregate formation through the induction of heat shock protein 70 (Hsp70) (53), a stress inducible chaperone that protects the brain from ischemic injury (9, 10). Ectopic expression of Hsp70 has been shown to inhibit α-Syn fibril formation (54, 55). Consequently, decreased DJ-1 solubility and diminished protein function not only aggravates oxidative stress but also facilitates α-Syn aggregation that is accelerated by the pro-oxidant environment within ischemic neurons. Although oxidation of DJ-1 is necessary for its chaperone activity, excessive oxidation can lead to impaired activity and protein aggregation. Hence, we cannot exclude the possibility that compromised DJ-1 function could be attributed to additional mechanisms independent of the interaction with α-Syn. However, the differential solubility and localization of DJ-1 in α-Syn$^{-/-}$ and α-Syn$^{+/+}$ neurons under ischemic stress provides compelling evidence that α-Syn accumulation plays an essential role in compromising DJ-1 function either directly by physical interaction or indirectly through the generation of oxidants. In conclusion, although ischemic stroke has different causes than the slowly progressive neurodegenerative disorders, many of the common disease mechanisms may come into play after cerebral I/R. Biochemical characterization of the insoluble fractions from the ischemic lesions provides evidence for α-Syn and DJ-1 co-aggregation which unfavorably impacts neuronal survival by interfering with DJ-1-mediated neuroprotective responses resulting in lowered threshold for oxidative stress-induced death. Our results not only provide a novel perspective on the potential pathogenic role of α-Syn in cerebral I/R but also suggest that the

mechanism of neuronal death in ischemic stroke might have similar features with those of PD and related disorders.

Funding

This study was supported by a grant from the National Institute of Health (1R21NS066265-01) to SLC.

Figures

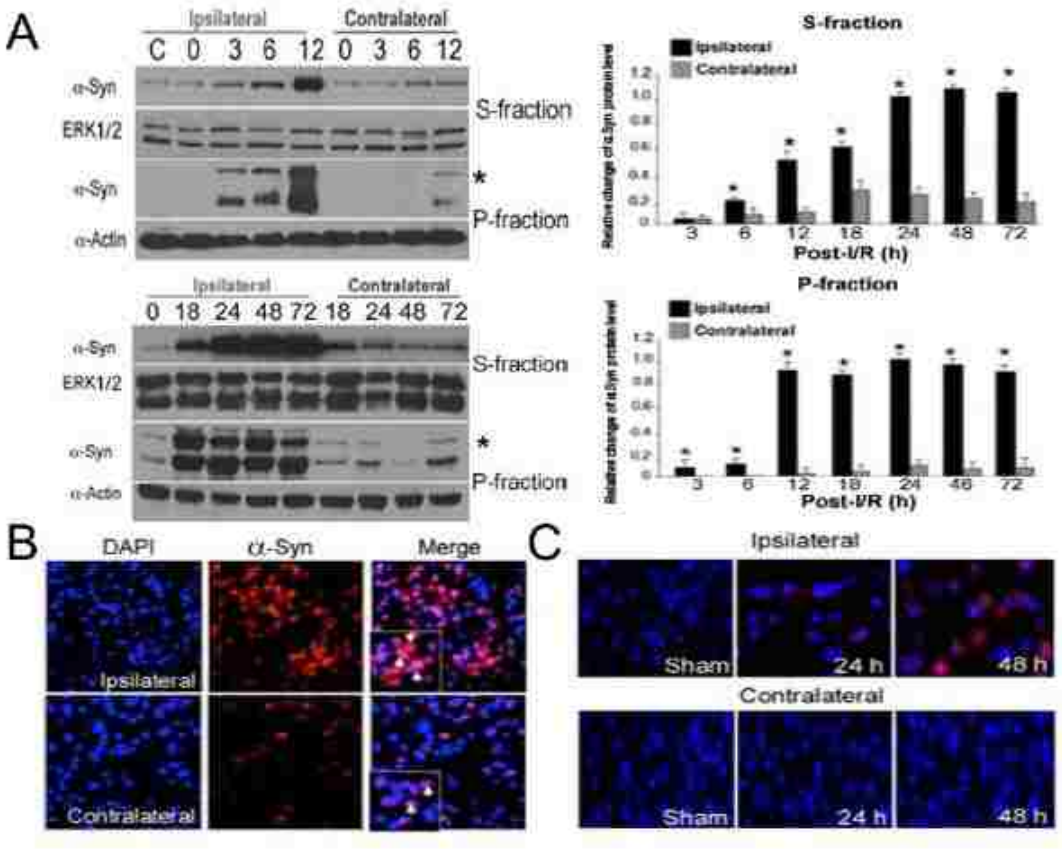

Figure 4-1. Impact of cerebral ischemia reperfusion (I/R) on α-Syn protein level and solubility

(A) Representative immunoblots *(left)* and results of densitometric analysis *(right)* of α-Syn protein levels in the detergent-soluble (S) and -insoluble (pellet; P) fractions

obtained from the ipislateral and contralateral cortices of mice 3, 6, 12 *(upper panels)* and 18, 24, 48, 72 h *(lower panels)* after I/R. Total protein loading in the S- and P-fractions was confirmed by reprobing the immunoblots for ERK1/2 or actin, respectively. The ipsilateral cortex of sham-treated mice sacrificed 24 h after was included as control (C). Asterisk indicates the detergent-resistant α-Syn dimer. Values are the mean ± SEM. n=4-6 mice; *p < 0.01 versus ipsilateral. *(B, C)* Representative immunofluorescence images of sections from the ipsilateral and contralateral cortices labeled with antibodies against *(B)* α-Syn and *(C)* nitrated α-Syn. Both α-Syn and nitrated α-Syn immunoreactivities are shown in red and DAPI staining of the nuclei in blue.

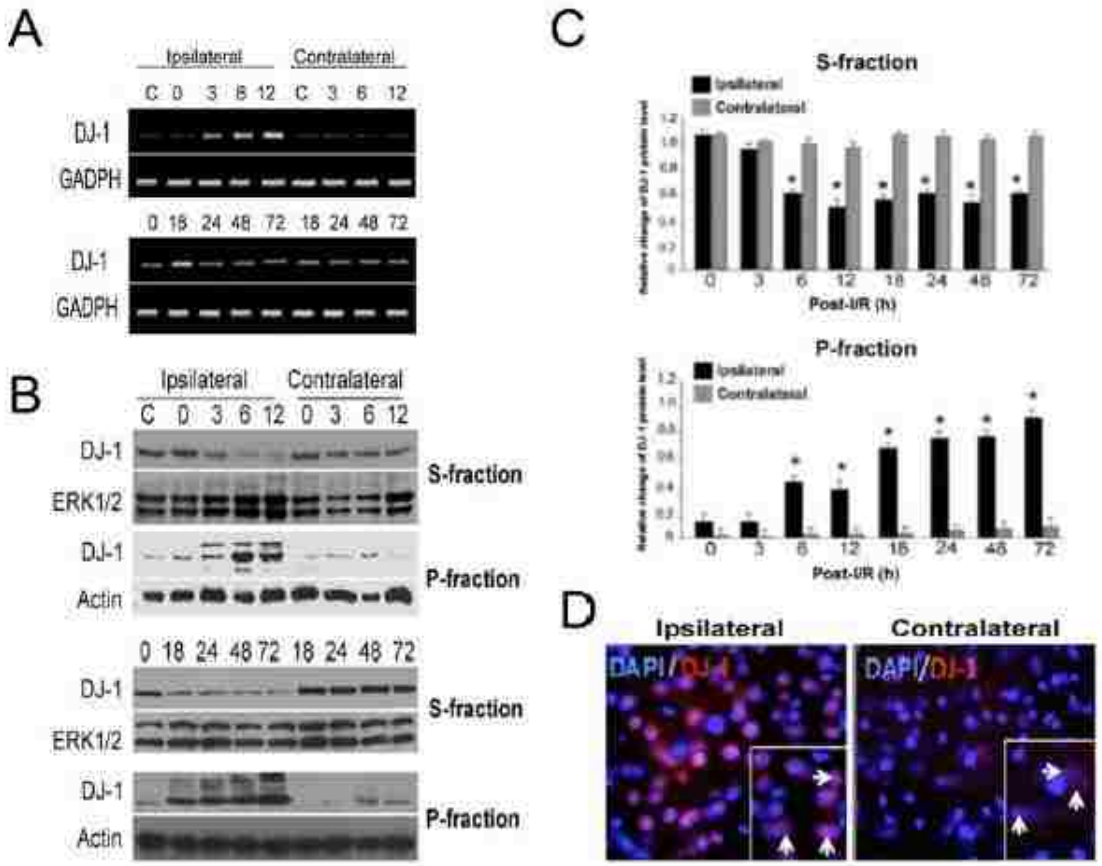

Figure 4-2. Impact of cerebral ischemia reperfusion (I/R) on DJ-1 protein level and solubility

(A) Representative gel images of DJ-1 and GADPH mRNA levels in the ipsilateral and contralateral cortices of mice 3, 6, 12 (top) and 18, 24, 48, 72 h (bottom) after I/R. The ipsilateral cortex of sham-treated mice sacrificed 24 h after was included as control (C). GADPH is used as an internal control. PCR products amplified were separated on ethidium bromide stained agarose gels. (B, C) Representative immunoblots (B) and results of densitometric analysis (C) of DJ-1 protein in the detergent-soluble (S) and -insoluble (pellet; P) fractions obtained from the ipsilateral and contralateral cortices of mice 3, 6, 12 (top) and 18, 24, 48, 72 h (bottom) after I/R. Blots were stripped and reprobed for ERK1/2 or actin to confirm equal protein loading. The ipsilateral cortex of sham-treated mice sacrificed 24 h after was included as control (C). Values are the

mean ± SEM. n=4-6 mice; *p < 0.01. (D) Representative fluorescence images of DJ-1 immunostained sections of the ipsilateral and contralateral cortices 12 h after I/R. Note that the uniform cytoplasmic staining (indicated by arrows in the inserts) in the contralateral cortex differs from the heterogenous inclusion-like staining in the ipsilateral cortex.

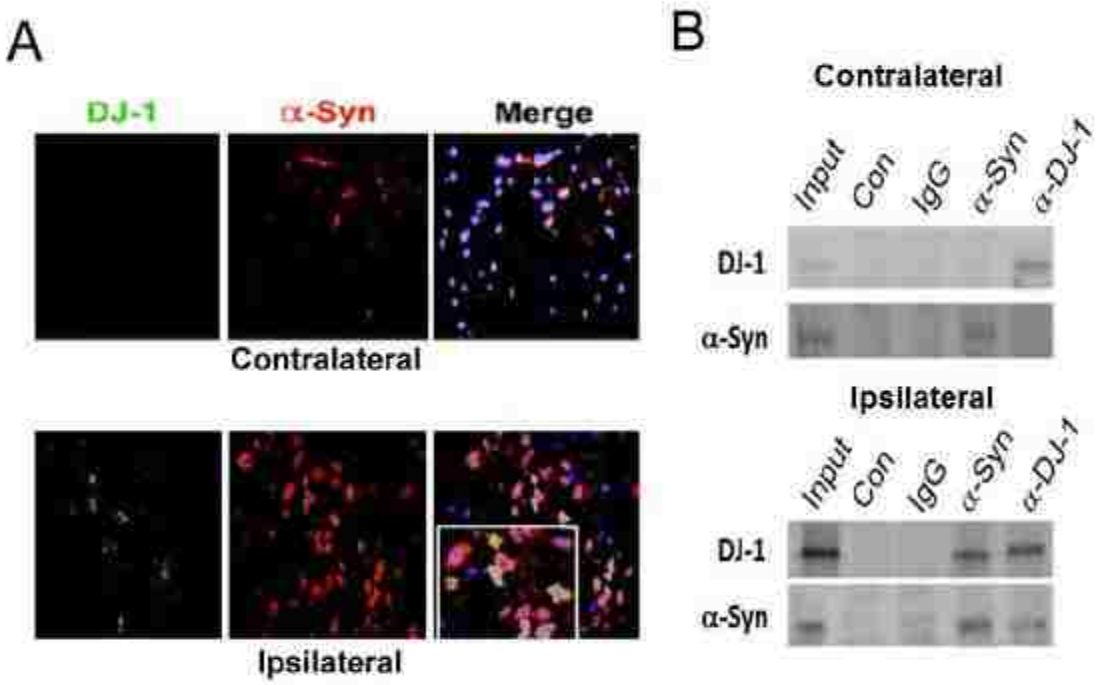

Figure 4-3. DJ-1 interacts and colocalizes with α-Syn after cerebral ischemia reperfusion (I/R)

(A) Representative fluorescence images of sections from the ipsilateral (top) and contralateral cortices (bottom) doubly immunostained for DJ-1 (green) and α-Syn (red). Co-localization of both signals (yellow) is displayed in a merged image. DAPI (blue) was used to stain the nuclei. (B) Co-immunoprecipitation analysis of the interaction of DJ-1 and α-Syn in Triton X-100 soluble homogenates (100 µg total protein) of contralateral

(top) and ipsilateral (bottom) cortices 24 h after I/R. Samples were pre-cleared and subjected to immunoprecipitation with preimmune IgG and antibodies to DJ-1 and α-Syn. As an additional control (Con), the antibody was left out. Immune complexes were subjected to immunblot analysis with antibodies to DJ-1 and α-Syn.

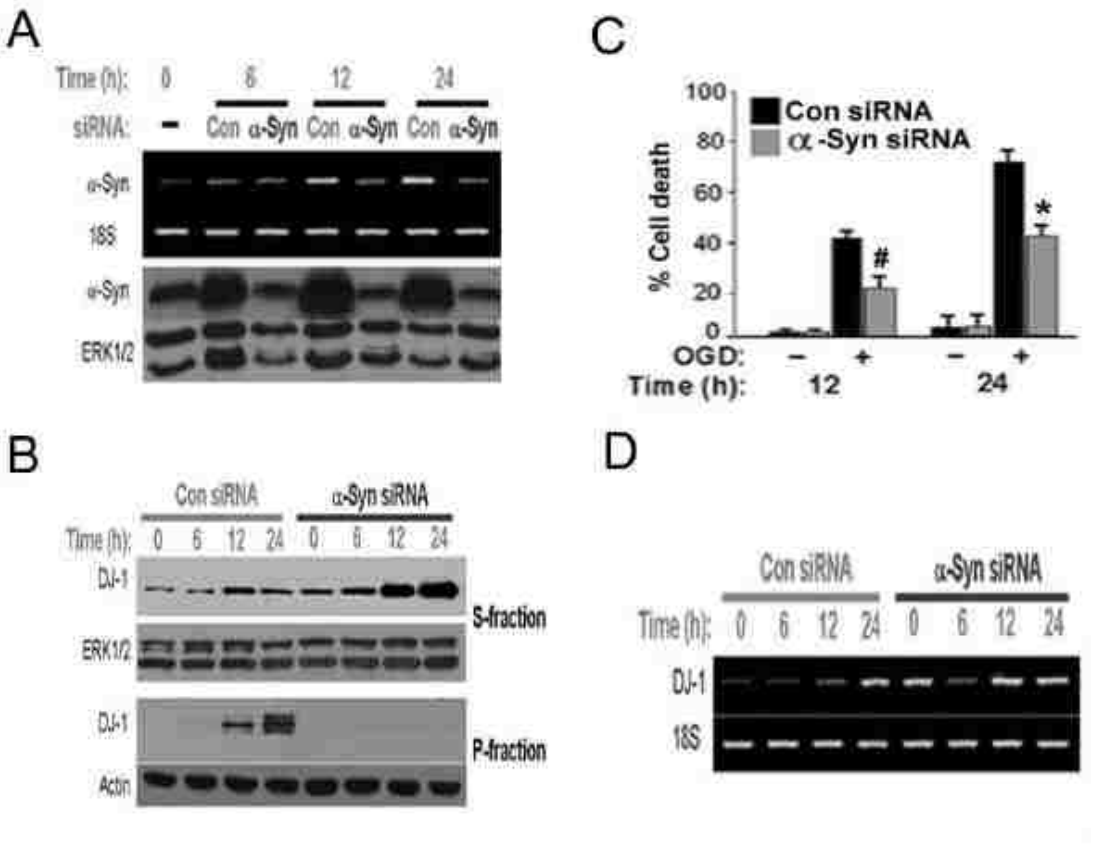

Figure 4-4. Impact of α-Syn knockdown on DJ-1 protein solubility and neuronal vulnerability to oxygen-glucose deprivation (OGD)

(A) RT-PCR (top) and immunoblot (bottom) analyses of α-Syn mRNA and protein levels in primary mouse cortical neurons that were transfected with either a siRNA targeting α-Syn (α-Syn siRNA; 5 nM) or nontargeting control siRNA (Con siRNA; 5 nM) 18 h prior to OGD. Neurons were collected at the indicated time points during reoxygenation. 18S rRNA and ERK were used as internal controls. (B) Representative immunoblots of DJ-1

protein levels in the detergent-soluble (S) and -insoluble (pellet; P) fractions obtained from cortical neurons that were transfected with the indicated siRNAs 18 h prior to OGD. Neurons were collected at the indicated time points during reoxygenation. Blots were stripped and reprobed for ERK1/2 or actin to confirm equal protein loading. (C) Histogram shows the viability of cortical neurons transfected with the indicated siRNAs after OGD. Cell death was quantified 12 and 24 h during reoxygenation. Values represent the mean ± SEM of three separate experiments. #p<0.05, *p<0.01 versus Con-siRNA. (D) Representative gel images of DJ-1 and 18S rRNA mRNA levels in cortical neurons that were transfected with the indicated siRNAs 18 h prior to OGD. Neurons were collected at the indicated time points during reoxygenation.

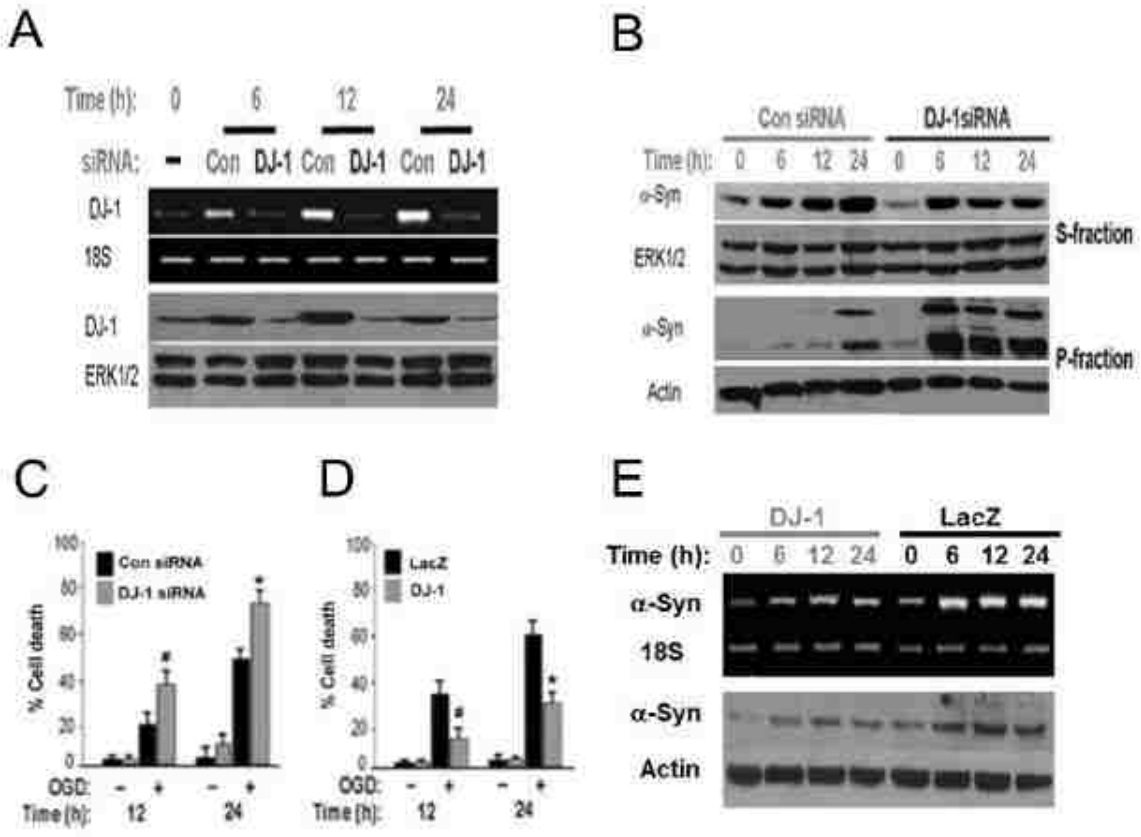

Figure 4-5. Impact of DJ-1 knockdown on α-Syn solubility and neuronal vulnerability to oxygen-glucose deprivation (OGD)

(A) RT-PCR (top) and immunoblot (bottom) analyses of DJ-1 mRNA and protein levels in primary mouse cortical neurons that were transfected with either a siRNA targeting DJ-1 (DJ-1 siRNA; 5 nM) or nontargeting control siRNA (Con siRNA; 5 nM) 12 h prior to OGD. Neurons were collected at the indicated time points during reoxygenation. 18S rRNA and ERK were used as internal controls. (B) Representative immunoblots of α-Syn protein levels in the detergent-soluble (S) and -insoluble (pellet; P) fractions obtained from cortical neurons that were transfected with the indicated siRNAs 12 h prior to OGD. Neurons were collected at the indicated time points during reoxygenation. Blots were stripped and reprobed for ERK1/2 or actin to confirm equal protein loading. (C, D) Histogram shows the impact of DJ-1 knockdown (C) or overexpression (D) on neuronal vulnerability to OGD. Cortical neurons were transfected with the indicated siRNAs or infected with pLenti6-DJ-1 or pLenti-LacZ. Eight hours after siRNA transfection or forty eight hours after infection, neurons were subjected to OGD. Cell death was quantified 12 and 24 h during reoxygenation. The values are the mean ± SEM of three-independent experiments. #$p<0.05$, *$p<0.01$ versus the respective controls. (E) RT-PCR (top) and immunoblot (bottom) analyses of DJ-1 mRNA and protein levels in cortical neurons that were infected with pLenti6-DJ-1 or pLenti6-LacZ 48 h prior to OGD. Neurons were collected at the indicated time points during reoxygenation. 18S rRNA and actin were used as internal controls.

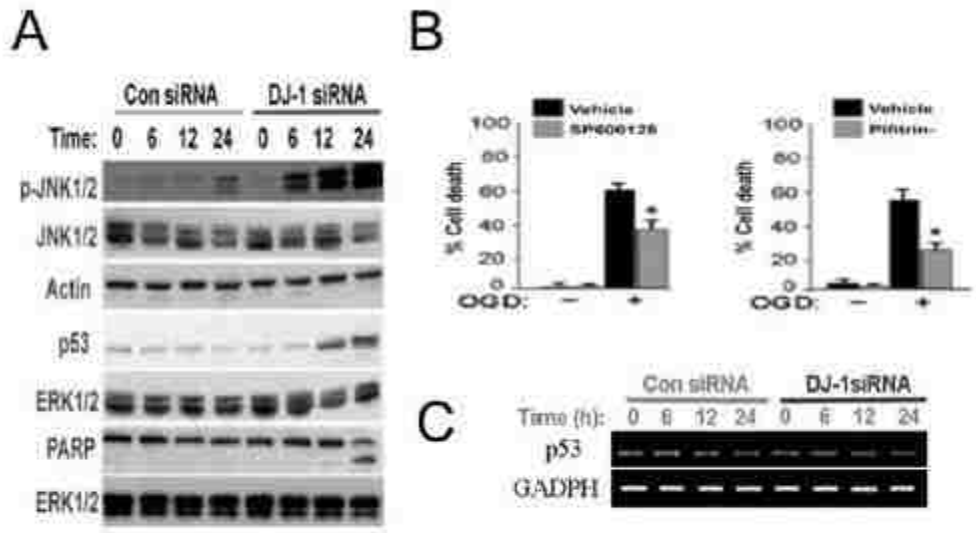

Figure 4-6. DJ-1 suppresses p53 activation in neurons subjected to oxygen-glucose deprivation (OGD)

(A) Representative immunoblots of phospho-JNK1/2, total JNK1, p53 and PARP protein levels in cortical neurons that were transfected with either a siRNA targeting DJ-1 (DJ-1 siRNA; 5 nM) or non-targeting control siRNA (Con siRNA; 5 nM) 12 h prior to OGD. Neurons were collected at the indicated time points during reoxygenation. Blots were stripped and reprobed for ERK1/2 or actin to confirm equal protein loading. (B) Histogram shows the impact of pharmacological inhibition of JNK1 and p53 on neuronal vulnerability to OGD-induced death. Cortical neurons were treated with SP6001 (10 μM) or pifitrin-α (200 μM) 2 h prior to OGD. Cell death was quantified 24 h during reoxygenation. The values are the mean ± SEM of three-independent experiments. *$p<0.01$ versus respective vehicle controls. (C) Representative gel images of p53 and GADPH mRNA levels in cortical neurons that were transfected with the indicated siRNAs 12 h prior to OGD. Neurons were collected at the indicated time points during reoxygenation.

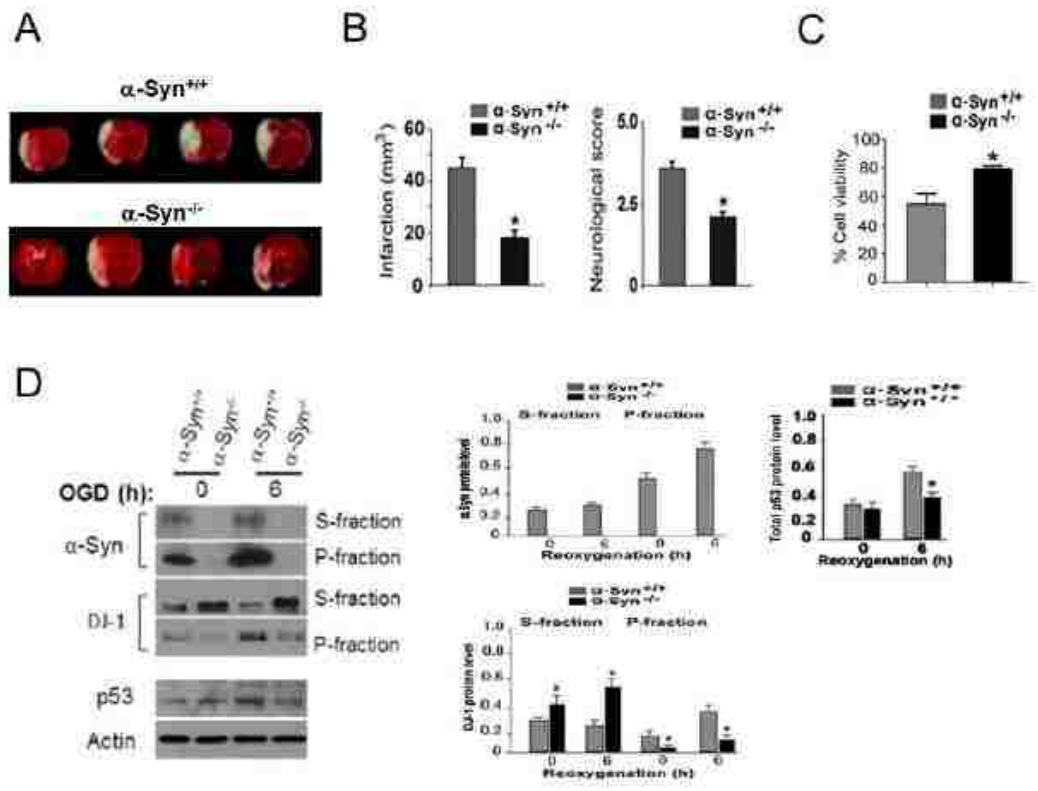

Figure 4-7. Syn gene ablation ameliorates cerebral ischemia reperfusion (I/R) injury

(A) Representative images of brain sections from α-Syn-/- and α-Syn+/+ mice 48 h after I/R that were stained with 2,3,5-triphenyltetrazoliun chloride monohydrate (TTC). (B) Bar graphs show the infarct volume (left) and neurological scores (right). The values are the mean ± SEM of 6-8 mice. *p<0.01 versus α-Syn+/+. (C) Histogram shows the impact of Syn gene ablation on neuronal vulnerability to oxygen-glucose deprivation (OGD)-induced death. Cell viability was quantified 24 and 48 h during reoxygenation. The values are the mean ± SEM of three-independent experiments. *p<0.01 versus α-Syn+/+. (D) Representative immunoblots (left) and results of densitometric analysis (right) of protein levels of α-Syn and DJ-1 in the detergent-soluble (S) and -insoluble (pellet; P) fractions obtained from α-Syn-/- and α-Syn+/+ cortical neurons after OGD.

Neurons were collected at 6 h during reoxygenation. Total p53 protein level in total lysates is shown in the lower panel. The values are the mean ± SEM of three-independent experiments. #p<0.05,*p<0.01 versus α-Syn+/+.

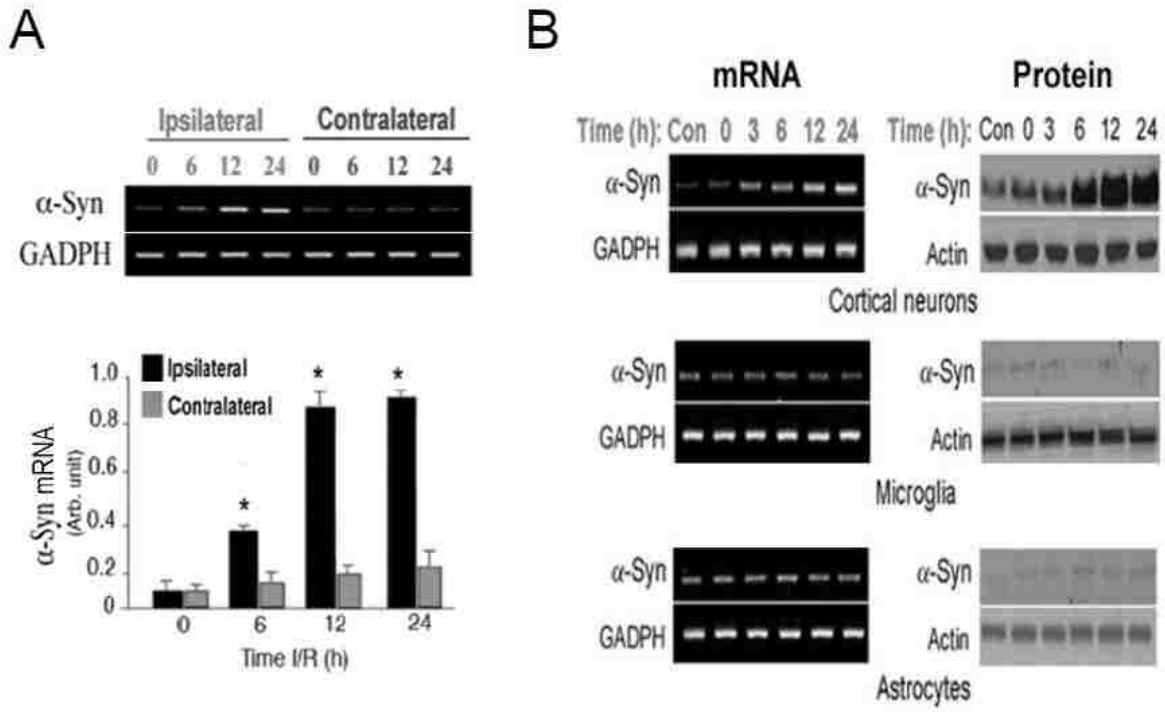

Supplementary Figure 4-1. α-Syn is up-regulated in brains and cultured neurons under ischemic stress

(A) RT-PCR analysis of α-Syn mRNA expression in the ipsilateral and contralateral cortices after cerebral ischemia reperfusion at the indicated time points. Histogram shows the relative change in α-Syn mRNA levels. Data were normalized on the basis of GADPH mRNA levels. Values represent mean ± SEM. n=4-6 mice, *p < 0.01 versus contralateral. (B) Time course of α-Syn mRNA (left) and protein (right) levels in cultured cortical neurons, microglia and astrocytes subjected to oxygen-glucose deprivation followed by reoxygenation for the indicated time points. Control cultures (Con) were left at 21% of O2 and in medium containing 25 mM of glucose.

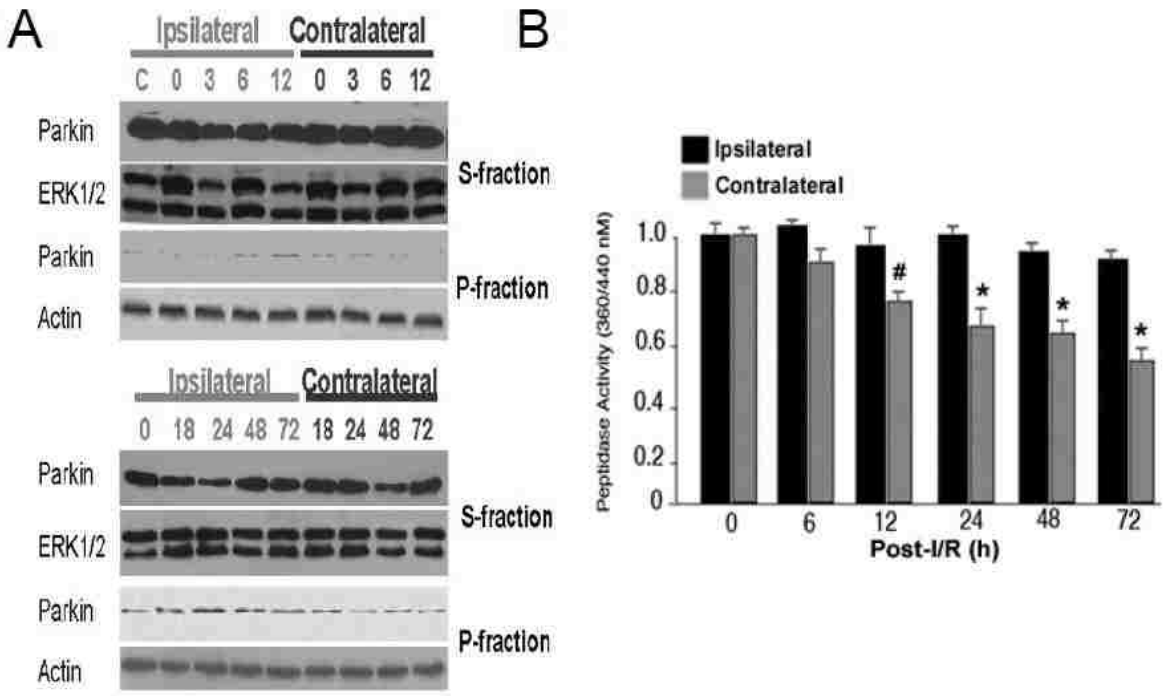

Supplementary Figure 4-2. Effects of ischemia on parkin protein level and proteasome activity

(A) Representative immunoblots of the time course of parkin protein in the detergent-soluble (S) and -insoluble (pellet; P) fractions obtained from the ipsilateral and contralateral cortices of mice (n=4-6) subjected to cerebral ischemia reperfusion at the indicated time points. Blots were stripped and reprobed for ERK1/2 or actin to confirm equal protein loading. The ipsilateral cortex of sham-treated mice was included as control (C). (B) Proteasome activity in whole cortical homogenates was assayed with 50 µM succinyl-LLVY-AMC substrate in the presence or absence of 20 µM lactacystin. Release of fluorescent AMC was measured by at λ=460 nm using a spectral fluorimeter and proteasome activity was calculated by subtracting the lactacystin-insensitive (or nonproteasome) peptidase activity from total peptidase activity. Data are mean ± SEM. N=4-6 mice. #$p<0.05$, *$p<0.01$ versus contralateral.

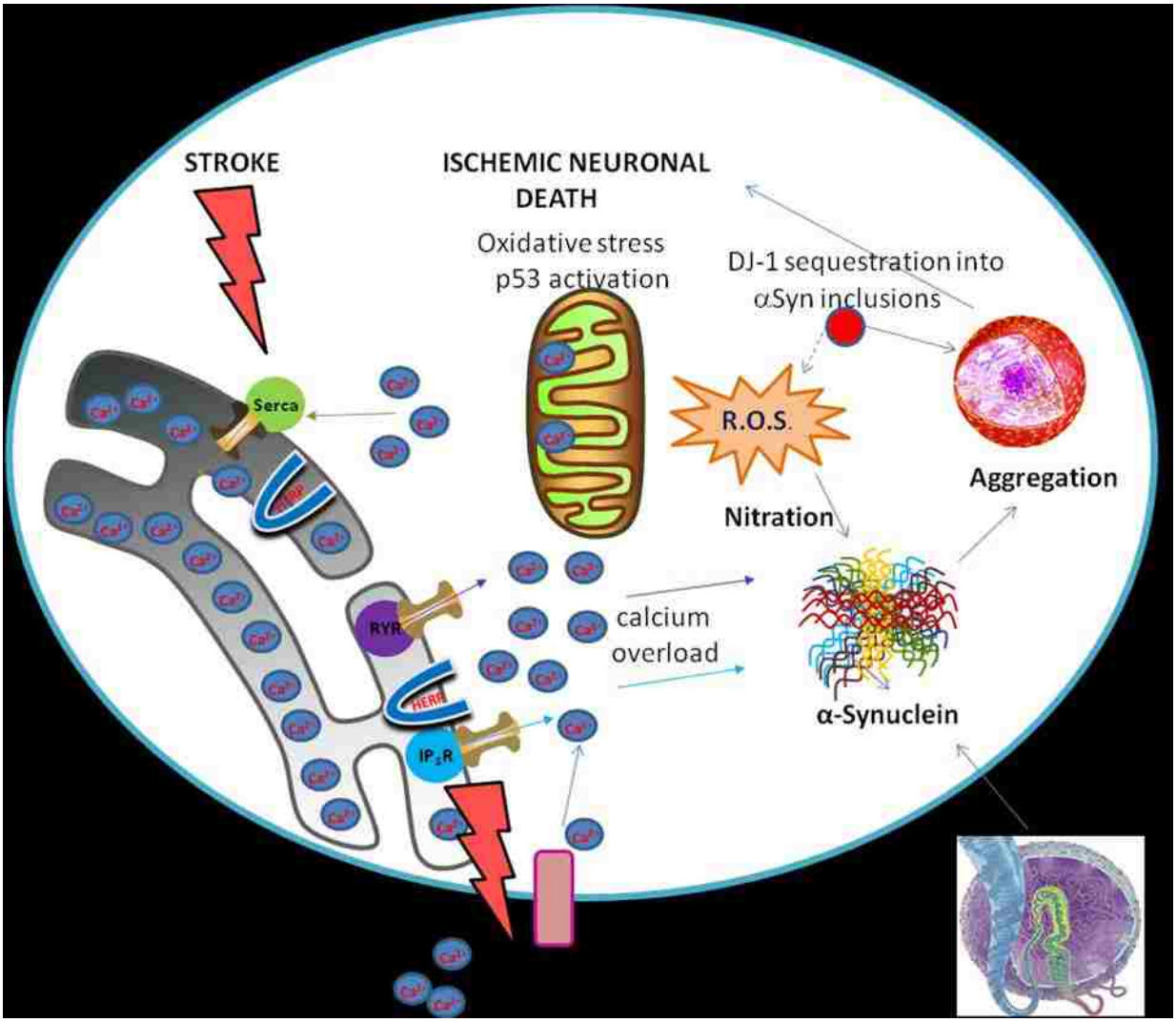

Summary Diagram 4-1. Schematic representation of the pathological processes involved in ischemic brain injury

References

1. Doyle KP, Simon RP, Stenzel-Poore MP. Mechanisms of ischemic brain damage. Neuropharmacology. 2008;55:310-8.

2. Chan PH. Reactive oxygen radicals in signaling and damage in the ischemic brain. J Cereb Blood Flow Metab. 2001;21:2-14.

3. Piantadosi CA, Zhang J. Mitochondrial generation of reactive oxygen species after brain ischemia in the rat. Stroke. 1996;27:327-31; discussion 332.

4. Schaller B, Graf R. Cerebral ischemia and reperfusion: the pathophysiologic concept as a basis for clinical therapy. J Cereb Blood Flow Metab. 2004;24:351-71.

5. Giasson BI, Ischiropoulos H, Lee VM, Trojanowski JQ. The relationship between oxidative/nitrative stress and pathological inclusions in Alzheimer's and Parkinson's diseases. Free Radic Biol Med. 2002;32:1264-75.

6. Koo EH, Lansbury PT Jr, Kelly JW. Amyloid diseases: abnormal protein aggregation in neurodegeneration. Proc Natl Acad Sci U S A.1999;96:9989-90.

7. Hu BR, Janelidze S, Ginsberg MD, Busto R, Perez-Pinzon M, Sick TJ, et al. Protein aggregation after focal brain ischemia and reperfusion. J Cereb Blood Flow Metab. 2001;21:865-75.

8. Hu BR, Martone ME, Jones YZ, Liu CL. Protein aggregation after transient cerebral ischemia. J Neurosci. 2000;20:3191-9.

9. Hutter JJ, Mestril R, Tam EK, Sievers RE, Dillmann WH, Wolfe CL. Overexpression of heat shock protein 72 in transgenic mice decreases infarct size in vivo. Circulation. 1996;94:1408-11.

10. Plumier JC, Krueger AM, Currie RW, Kontoyiannis D, Kollias G, Pagoulatos GN. Transgenic mice expressing the human inducible Hsp70 have hippocampal neurons resistant to ischemic injury. Cell Stress Chaperones. 1997;2:162-7.

11. Cookson MR. The biochemistry of Parkinson's disease. Annu Rev Biochem. 2005;74:29-52.

12. Dawson TM, Dawson VL. Molecular pathways of neurodegeneration in Parkinson's disease. Science. 2003;302:819-22.

13. Polymeropoulos MH, Lavedan C, Leroy E, Ide SE, Dehejia A, Dutra A, et al. Mutation in the alpha-synuclein gene identified in families with Parkinson's disease. Science. 1997;276:2045-7.

14. Masliah E, Rockenstein E, Veinbergs I, Mallory M, Hashimoto M, Takeda A, et al. Dopaminergic loss and inclusion body formation in alpha-synuclein mice: implications for neurodegenerative disorders. Science. 2000;287:1265-9.

15. Conway KA, Harper JD, Lansbury PT. Accelerated in vitro fibril formation by a mutant alpha-synuclein linked to early-onset Parkinson disease. Nat Med. 1998;4:1318-20.

16. Giasson BI, Duda JE, Murray IV, Chen Q, Souza JM, Hurtig HI, et al. Oxidative damage linked to neurodegeneration by selective alpha-synuclein nitration in synucleinopathy lesions. Science. 2000;290:985-9.

17. Li J, Uversky VN, Fink AL. Effect of familial Parkinson's disease point mutations A30P and A53T on the structural properties, aggregation, and fibrillation of human alpha-synuclein. Biochemistry. 2001;40:11604-13.

18. Singleton AB, Farrer M, Johnson J, Singleton A, Hague S, Kachergus J, et al. alpha-Synuclein locus triplication causes Parkinson's disease. Science. 2003;302:841.

19. Bonifati V, Rizzu P, van Baren MJ, Schaap O, Breedveld GJ, Krieger E, et al. Mutations in the DJ-1 gene associated with autosomal recessive early-onset parkinsonism. Science. 2003;299:256-9.

20. Canet-Aviles RM, Wilson MA, Miller DW, Ahmad R, McLendon C, Bandyopadhyay S, et al. The Parkinson's disease protein DJ-1 is neuroprotective due to cysteine-sulfinic acid-driven mitochondrial localization. Proc Natl Acad Sci U S A. 2004;101:9103-8.

21. Kim RH, Smith PD, Aleyasin H, Hayley S, Mount MP, Pownall S, et al. Hypersensitivity of DJ-1-deficient mice to 1-methyl-4-phenyl-1,2,3,6-tetrahydropyrindine (MPTP) and oxidative stress. Proc Natl Acad Sci U S A. 2005;102:5215-20.

22. Martinat C, Shendelman S, Jonason A, Leete T, Beal MF, Yang L, et al. Sensitivity to oxidative stress in DJ-1-deficient dopamine neurons: an ES-derived cell model of primary Parkinsonism. PLoS Biol. 2004;2:e327.

23. Meulener M, Whitworth AJ, Armstrong-Gold CE, Rizzu P, Heutink P, Wes PD, et al. Drosophila DJ-1 mutants are selectively sensitive to environmental toxins associated with Parkinson's disease. Curr Biol. 2005;15:1572-7.

24. Aleyasin H, Rousseaux MW, Phillips M, Kim RH, Bland RJ, Callaghan S, et al. The Parkinson's disease gene DJ-1 is also a key regulator of stroke-induced damage. Proc Natl Acad Sci U S A. 2007;104:18748-53.

25. Zhou W, Freed CR. DJ-1 up-regulates glutathione synthesis during oxidative stress and inhibits A53T alpha-synuclein toxicity. J Biol Chem. 2005;280:43150-8.

26. Rochet JC, Conway KA, Lansbury PT Jr. Inhibition of fibrillization and accumulation of prefibrillar oligomers in mixtures of human and mouse alpha-synuclein. Biochemistry. 2000;39:10619-26.

27. Vila M, Vukosavic S, Jackson-Lewis V, Neystat M, Jakowec M, Przedborski S. Alpha-synuclein up-regulation in substantia nigra dopaminergic neurons following administration of the parkinsonian toxin MPTP. J Neurochem. 2000;74:721-9.

28. Shimura H, Hattori N, Kubo S, Mizuno Y, Asakawa S, Minoshima S, et al. Familial Parkinson disease gene product, parkin, is a ubiquitin-protein ligase. Nat Genet. 2000;25:302-5.

29. Kawahara K, Hashimoto M, Bar-On P, Ho GJ, Crews L, Mizuno H, et al. alpha-Synuclein aggregates interfere with Parkin solubility and distribution: role in the pathogenesis of Parkinson disease. J Biol Chem. 2008;283:6979-87.

30. Petrucelli L, O'Farrell C, Lockhart PJ, Baptista M, Kehoe K, Vink L, et al. Parkin protects against the toxicity associated with mutant alpha-synuclein: proteasome dysfunction selectively affects catecholaminergic neurons. Neuron. 2002;36:1007-19.

31. Shendelman S, Jonason A, Martinat C, Leete T, Abeliovich A. DJ-1 is a redox-dependent molecular chaperone that inhibits alpha-synuclein aggregate formation. PLoS Biol. 2004;2:e362.

32. Zhou W, Zhu M, Wilson MA, Petsko GA, Fink AL. The oxidation state of DJ-1 regulates its chaperone activity toward alpha-synuclein. J Mol Biol. 2006;356:1036-48.

33. Culmsee C, Mattson MP. p53 in neuronal apoptosis. Biochem Biophys Res Commun. 2005;331:761-77.

34. Culmsee C, Zhu X, Yu QS, Chan SL, Camandola S, Guo Z, et al. A synthetic inhibitor of p53 protects neurons against death induced by ischemic and excitotoxic insults, and amyloid beta-peptide. J Neurochem. 2001;77:220-8.

35. Milne DM, Campbell LE, Campbell DG, Meek DW. p53 is phosphorylated in vitro and in vivo by an ultraviolet radiation-induced protein kinase characteristic of the c-Jun kinase, JNK1. J Biol Chem. 1995;270:5511-8.

36. Qiu C, Xu W, Winblad B, Fratiglioni L. Vascular risk profiles for dementia and Alzheimer's disease in very old people: a population-based longitudinal study. J Alzheimers Dis. 2010;20:293-300.

37. Jellinger KA. Prevalence of cerebrovascular lesions in Parkinson's disease. A postmortem study. Acta Neuropathol. 2003;105:415-9.

38. Nataraj A, Rajput, AH. Parkinson's disease, stroke, and related epidemiology. Mov Disord. 2005;20:1476-80.

39. Mata IF, Shi M, Agarwal P, Chung KA, Edwards KL, Factor SA, et al. SNCA variant associated with Parkinson disease and plasma alpha-synuclein level. Arch Neurol. 2010;67:1350-6.

40. Dauer W, Kholodilov N, Vila M, Trillat AC, Goodchild R, Larsen KE, et al. Resistance of alpha -synuclein null mice to the parkinsonian neurotoxin MPTP. Proc Natl Acad Sci U S A. 2002;99:14524-9.

41. Uryu K, Giasson BI, Longhi L, Martinez D, Murray I, Conte V, et al. Age-dependent synuclein pathology following traumatic brain injury in mice. Exp Neurol. 2003;184:214-24.

42. Mattson MP, Sherman M. Perturbed signal transduction in neurodegenerative disorders involving aberrant protein aggregation. Neuromolecular Med. 2003;4:109-32.

43. Baulac S, LaVoie MJ, Strahle J, Schlossmacher MG, Xia W. Dimerization of Parkinson's disease-causing DJ-1 and formation of high molecular weight complexes in human brain. Mol Cell Neurosci. 2004;27:236-46.

44. Meulener MC, Graves CL, Sampathu DM, Armstrong-Gold CE, Bonini NM, Giasson BI. DJ-1 is present in a large molecular complex in human brain tissue and interacts with alpha-synuclein. J Neurochem. 2005;93:1524-32.

45. Bandopadhyay R, Kingsbury AE, Cookson MR, Reid AR, Evans IM, Hope AD, et al. The expression of DJ-1 (PARK7) in normal human CNS and idiopathic Parkinson's disease. Brain. 2004;127:420-30.

46. Neumann M, Muller V, Gorner K, Kretzschmar HA, Haass C, Kahle PJ. Pathological properties of the Parkinson's disease-associated protein DJ-1 in alpha-synucleinopathies and tauopathies: relevance for multiple system atrophy and Pick's disease. Acta Neuropathol. 2004;107:489-96.

47. Choi J, Sullards MC, Olzmann JA, Rees HD, Weintraub ST, Bostwick DE, et al. Oxidative damage of DJ-1 is linked to sporadic Parkinson and Alzheimer diseases. J Biol Chem. 2006;281:10816-24.

48. Trimmer PA, Smith TS, Jung AB, Bennett, JP Jr. Dopamine neurons from transgenic mice with a knockout of the p53 gene resist MPTP neurotoxicity. Neurodegeneration. 1996;5:233-9.

49. Duan W, Zhu X, Ladenheim B, Yu QS, Guo Z, Oyler J, et al. p53 inhibitors preserve dopamine neurons and motor function in experimental parkinsonism. Ann Neurol. 2002;52:597-606.

50. Martin LJ, Pan Y, Price AC, Sterling W, Copeland NG, Jenkins NA, et al. Parkinson's disease alpha-synuclein transgenic mice develop neuronal mitochondrial degeneration and cell death. J Neurosci. 2006;26:41-50.

51. Bretaud S, Allen C, Ingham PW, Bandmann O. p53-dependent neuronal cell death in a DJ-1-deficient zebrafish model of Parkinson's disease. J Neurochem. 2007;100:1626-35.

52. Clements CM, McNally RS, Conti BJ, Mak TW, Ting JP. DJ-1, a cancer- and Parkinson's disease-associated protein, stabilizes the antioxidant transcriptional master regulator Nrf2. Proc Natl Acad Sci U S A. 2006;103:15091-6.

53. Batelli S, Albani D, Rametta R, Polito L, Prato F, Pesaresi M, et al. DJ-1 modulates alpha-synuclein aggregation state in a cellular model of oxidative stress: relevance for Parkinson's disease and involvement of HSP70. PLoS One. 2008;3:e1884.

54. Luk KC, Mills IP, Trojanowski JQ, Lee VM. Interactions between Hsp70 and the hydrophobic core of alpha-synuclein inhibit fibril assembly. Biochemistry. 2008;47:12614-25.

55. Dedmon MM, Christodoulou J, Wilson MR, Dobson CM. Heat shock protein 70 inhibits alpha-synuclein fibril formation via preferential binding to prefibrillar species. J Biol Chem. 2005;280:14733-40.

56. Abeliovich A, Schmitz Y, Farinas I, Choi-Lundberg D, Ho WH, Castillo PE, et al. Mice lacking alpha-synuclein display functional deficits in the nigrostriatal dopamine system. Neuron. 2000;25:239-52.

57. Arumugam TV, Chan SL, Jo DG, Yilmaz G, Tang SC, Cheng A, et al. Gamma secretase-mediated Notch signaling worsens brain damage and functional outcome in ischemic stroke. Nat Med. 2006;12:621-3.

58. Kyriazis GA, Wei Z, Vandermey M, Jo DG, Xin O, Mattson MP, et al. Numb endocytic adapter proteins regulate the transport and processing of the amyloid precursor protein in an isoform-dependent manner: implications for Alzheimer disease pathogenesis. J Biol Chem. 2008;283:25492-502.

59. Wei Z, Chigurupati S, Arumugam TV, Jo DG, Li H, Chan SL. Notch activation enhances the microglia-mediated inflammatory response associated with focal cerebral ischemia. stroke. Stroke. 2011;42: 2589-94.

60. Chan SL, Mayne M, Holden CP, Geiger JD, Mattson, MP. Presenilin-1 mutations increase levels of ryanodine receptors and calcium release in PC12 cells and cortical neurons. J Biol Chem. 2000;275:18195-200.

61. Kyriazis GA, Belal C, Madan M, Taylor DG, Wang J, Wei Z, et al. Stress-induced switch in Numb isoforms enhances Notch-dependent expression of subtype-specific transient receptor potential channel. J Biol Chem. 2010; 285:6811-25.

62. Chigurupati, S, Madan, M, Okun, E, Wei, Z, Pattisapu, JV, Mughal, MR, et al. Evidence for altered Numb isoform levels in Alzheimer's disease patients and a triple transgenic mouse model. J Alzheimers Dis. 2011; 24:349-61.

APPENDIX
COPYRIGHT PERMISSION

Copyright Permission Policy

These guidelines apply to the reuse of articles, figures, charts and photos in the *Journal of Biological Chemistry*, *Molecular & Cellular Proteomics* and the *Journal of Lipid Research*.

For authors reusing their own material:

Authors need **NOT** contact the journal to obtain rights to reuse their own material. They are automatically granted permission to do the following:

Reuse the article in print collections of their own writing.
Present a work orally in its entirety.
Use an article in a thesis and/or dissertation.
Reproduce an article for use in the author's courses. (If the author is employed by an academic institution, that institution also may reproduce the article for teaching purposes.)
Reuse a figure, photo and/or table in future commercial and noncommercial works.
Post a copy of the paper in PDF that you submitted via BenchPress.

Only authors who published their papers under the "Author's Choice" option may post the final edited PDFs created by the publisher to their own/departmental/university Web sites.
All authors may link to the journal site containing the final edited PDFs created by the publisher.

Please note that authors must include the following citation when using material that appeared in an ASBMB journal:

"This research was originally published in Journal Name. Author(s). Title. *Journal Name*. Year; Vol:pp–pp. © the American Society for Biochemistry and Molecular Biology."

For other parties using material for noncommercial use:

Other parties are welcome to copy, distribute, transmit and adapt the work — at no cost and without permission — for noncommercial use as long as they attribute the work to the original source using the citation above.

Examples of noncommercial use include:

Reproducing a figure for educational purposes, such as schoolwork or lecture presentations, with attribution.
Appending a reprinted article to a Ph.D. dissertation, with attribution.

For other parties using material for commercial use:

Navigate to the article of interest and click the "Request Permissions" button on the middle navigation bar. (See diagram at right.) It will walk you through the steps for obtaining permission for reuse.

Examples of commercial use by parties other than authors include:

Reproducing a figure in a book published by a commercial publisher.

http://www.jbc.org/site/misc/Copyright_Permission.xhtml

Copyright policy: *Human Molecular Genetics*

COPYRIGHT

Copyright of any article published in HMG will belong to the author or their designee. However, it is a condition of publication in the journal that authors grant an exclusive licence to publish to Oxford University Press. This ensures that requests from third parties to reproduce articles are handled efficiently and consistently and allows the article to be as widely disseminated as possible. As part of the licence agreement, authors may use their own material in other publications provided that the Journal is acknowledged as the original place of publication and Oxford University Press as the Publisher. Upon receipt of accepted manuscripts at Oxford Journals authors will be invited to complete an online copyright licence to publish form.

Authors are reminded that it is their responsibility to comply with copyright laws. It is essential to ensure that no part of the text or illustrations have appeared or are due to appear in other publications, without prior permission from the copyright holder. Signed patient consent forms must be obtained for recognizable photographs. Submission of the manuscript will be taken to indicate the authors compliance with these conditions.

Quoted from http://www.oxfordjournals.org/our_journals/hmg/for_authors/general.html